SEISMIC DESIGN PROCEDURE FOR THE BOTTOM PLATE CORNER CONNECTION OF FLAT-BOTTOM CYLINDRICAL TANKS DUE TO UPLIFT RESPONSE OF THE BOTTOM PLATE DURING EARTHQUAKES

January, 2019

SHOICHIRO HAYASHI

SEISMIC DESIGN PROCEDURE FOR THE BOTTOM PLATE CORNER CONNECTION OF FLAT-BOTTOM CYLINDRICAL TANKS DUE TO UPLIFT RESPONSE OF THE BOTTOM PLATE DURING EARTHQUAKES

CHAPTER 1 INTRODUCTION

1-1 OUTLINE OF THIS PAPER ・・・・・・・・・・・・・・・・・・・・・・・・1
1-2 BACKGROUND OF THIS STUDY ・・・・・・・・・・・・・・・・・・・・・4
1-2-1 Type of above ground cylindrical tanks for refrigerated liquefied flammable gas service ・・・・・・4
1-2-2 Seismic design of tanks ・・・・・・・・・・・・・・・・・・・・・8
1-2-3 Factors affecting the current seismic design of LNG tanks ・・・・・・13
1-3 CONCEPT AND ORGANIZATION OF THIS PAPER ・・・・・・・・・・・16
1-3-1 Concept of this Paper ・・・・・・・・・・・・・・・・・・・・・・16
1-3-2 Organization of this Paper ・・・・・・・・・・・・・・・・・・・・16
1-3-3 Tank used in this Paper ・・・・・・・・・・・・・・・・・・・・・17
REFERENCES ・・・・・・・・・・・・・・・・・・・・・・・・・・・・・20

CHAPTER 2 PREVIOUS STUDIES ON UPLIFT OF BOTTOM PLATE DURING EARTHQUAKE FOR ABOVE GROUND CYLINDRICAL TANKS

2-1 PREVIOUS STUDIES REGARDING DYNAMIC PRESSURE INDUCED BY BULGING RESPONSE ・・・・21
2-2 PREVIOUS STUDIES REGARDING ROCKING RESPONSE ・・・・・23
2-2-1 Previous studies regarding rocking behavior of tanks ・・・・・・・・23
2-2-2 Previous studies about modeling of axial force in a sidewall ・・・・・24
2-2-3 Previous studies regarding rocking response and dynamic pressure ・・27
REFERENCES ・・・・・・・・・・・・・・・・・・・・・・・・・・・・・29

CHAPTER 3 DYNAMIC RESPONSE BEHAVIOR DURING EARTHQUAKES

3-1 TIME-HISTORY FE ANALYSIS MODEL OF TANK ・・・・・・・・・・・32
3-1-1 Specifications of the tank and FE analysis model ・・・・・・・・・32
3-1-2 Applied seismic wave ・・・・・・・・・・・・・・・・・・・・・・34
3-1-3 Analysis case ・・・・・・・・・・・・・・・・・・・・・・・・・35
3-2 ANALYSIS RESULTS ・・・・・・・・・・・・・・・・・・・・・・・37
3-2-1 Response acceleration ・・・・・・・・・・・・・・・・・・・・・37
3-2-2 Base shear ・・・・・・・・・・・・・・・・・・・・・・・・・・39
3-2-3 Dynamic pressure ・・・・・・・・・・・・・・・・・・・・・・・41

3-2-4 Uplift height ・・・・・・・・・・・・・・・・・・・・・・・・・・・・44
3-2-5 Uplift width and height ・・・・・・・・・・・・・・・・・・・・・47
3-2-6 Axial force in the sidewall ・・・・・・・・・・・・・・・・・・・50
3-2-7 Sidewall deformation ・・・・・・・・・・・・・・・・・・・・・・56
3-2-8 FFT analysis of base shear and sidewall displacement ・・・・・・・・58
3-2-9 Angular acceleration at the bottom of the sidewall
and uplift induced dynamic pressure ・・・・60
3-3 CONCEPT OF INTRODUCING DYNAMIC EFFECT
TO A STATIC ANALYSIS ・・・・64
3-4 FINDINGS ・・・・・・・・・・・・・・・・・・・・・・・・・・・・・67
REFERENCES ・・・・・・・・・・・・・・・・・・・・・・・・・・・・・69

CHAPTER 4 MODELING OF UPLIFT BEHAVIOR AT BOTTOM PLATE

4-1 MODELING OF THE BOTTOM PLATE ・・・・・・・・・・・・・・・・70
4-1-1 Modeling of the bottom plate ・・・・・・・・・・・・・・・・・・70
4-1-2 Modeling of the uplift part ・・・・・・・・・・・・・・・・・・・71
4-1-3 Modeling of the supported part ・・・・・・・・・・・・・・・・・74
4-1-4 Connection of the uplift and the supported part ・・・・・・・・・・77
4-1-5 Trial calculation of the bottom plate model ・・・・・・・・・・・79
4-2 MODELING OF THE SIDEWALL ・・・・・・・・・・・・・・・・・・82
4-2-1 Modeling of the sidewall ・・・・・・・・・・・・・・・・・・・・82
4-2-2 Introducing the equivalent stiffness ・・・・・・・・・・・・・・・86
4-2-3 Trial calculation of the bottom plate and the sidewall model ・・・・88
4-3 CASE STUDY ・・・・・・・・・・・・・・・・・・・・・・・・・・・92
4-3-1 Case study of the uplift ・・・・・・・・・・・・・・・・・・・・・92
4-3-2 Influence of the uplift on dynamic pressure ・・・・・・・・・・・・93
4-4 FINDINGS ・・・・・・・・・・・・・・・・・・・・・・・・・・・・・96
REFERENCES ・・・・・・・・・・・・・・・・・・・・・・・・・・・・・97

CHAPTER 5 MODELING OF AXIAL FORCE DISTRIBUTION AT BOTTOM OF SIDEWALL WHEN UPLIFT OF BOTTOM PLATE OCCURS

5-1 MODELING OF THE EXTENT OF THE UPLIFT AREA
DUE TO SUBSIDENCE OF THE TANK'S BOTTOM PLATE ・・98
5-1-1 Modeling of the extent of the uplift area ・・・・・・・・・・・・・98
5-1-2 Modeling of force couple and axial force at compression area ・・・105
5-1-3 Modeling of force couple and axial force at tensile area ・・・・・・107
5-1-4 Formula of angle indicating the location of neutral axis ・・・・・・・113

5-2 MODELING OF RELATIONSHIP BETWEEN OUT OF ROUND DEFORMATION OF SIDEWALL AND UPLIFT HEIGHT ・・・・116
5-2-1 Modeling of deformation of sidewall and uplift height ・・・・・・・116
5-2-2 Comparison of the calculation result with the FE analysis ・・・・・・118
5-2-3 Reflect the effect of sidewall deformation to the formula of angle indicating the location of neutral axis ・・・・121
5-3 CALCULATION OF UPLIFT AREA AND AXIAL FORCE OF SIDEWALL ・・・・・122
5-3-1 Conditions of calculation by proposed model ・・・・・・・・・・122
5-3-2 Result of calculation ・・・・・・・・・・・・・・・・・・・・125
5-4 FINDINGS ・・・・・・・・・・・・・・・・・・・・・・・・・・128
REFERENCES ・・・・・・・・・・・・・・・・・・・・・・・・・・129

CHAPTER 6 PROPOSAL OF DESIGN PROCEDURE FOR TANK BOTTOM PLATE

6-1 DESIGN PROCEDURE FOR TANK BOTTOM PLATE ・・・・・・・・130
6-2 CALCULATION METHOD FOR ANGULAR ACCELERATION AND REDUCTION RATIO IN RESPONSE ACCELERATION ・・・・134
6-3 SAMPLE CALCULATION OF DEFORMATION AND STRESS OF THE BOTTOM CORNER CONNECTION ・・・・136
6-3-1 Sample calculation of subject tank ・・・・・・・・・・・・・136
6-3-2 Applicability to other dimensional tanks ・・・・・・・・・・148
6-4 FINDINGS AND SUGGESTED ITEMS TO BE STUDIED IN THE NEXT STEP ・・・・156
REFERENCES ・・・・・・・・・・・・・・・・・・・・・・・・・・157

CHAPTER 7 CONCLUSION ・・・・・・・・・・・・・・・・・・・・・・158

ACKNOWLEDGEMENT ・・・・・・・・・・・・・・・・・・・・・・・162

PAPERS PUBLISHED BY THE AUTHOR IN PREPARING THIS PAPER ・・・・163

APPENDIX
APPENDIX A ・・・・・・・・・・・・・・・・・・・・・・・・・・165
APPENDIX B ・・・・・・・・・・・・・・・・・・・・・・・・・・171
APPENDIX C ・・・・・・・・・・・・・・・・・・・・・・・・・・174

NOMENCLATURE ・・・・・・・・・・・・・・・・・・・・・・・・・176

CHAPTER 1

INTRODUCTION

CHAPTER 1
INTRODUCTION

1-1 OUTLINE OF THIS PAPER

In recent years, owners of above ground refrigerated liquefied flammable gas storage tanks, such as LNG storage tanks, have been requiring higher seismic design conditions for their tanks.

Under severe seismic design conditions, detailed verification of a soundness of structures including uplift behavior of a tank bottom plate has been required.

In most current seismic design procedures specified in standards, dynamic pressure for a design is typically calculated statically as if the maximum dynamic pressure represents an oscillation pressure during the earthquake. Besides, these do not consider effects of dynamic uplift behavior when calculating stress in a bottom plate. These procedures result in a more conservative design approach.

However, previous studies confirmed that static analysis fails to calculate dynamic response behavior including the uplift of bottom plates, correctly. This is because in most cases, effects of dynamic oscillation including the uplift of a tank bottom plate during earthquakes based on outcomes from actual dynamic experiments or theories are not taken into account. In this paper, to find a more accurate design procedure, the following steps are followed.

Firstly, a finite element (FE) analysis method, being a fluid-structure coupled 3-dimensional time-history FE analysis, hereinafter called ‘the FE analysis’, is used to specific tank for studying a tank response. It studies dynamic response behavior parameters such as response acceleration, base shear, dynamic pressure, uplift of a tank bottom plate, deformation of a sidewall, distribution of an axial force at a bottom of a sidewall and so on.

Secondly, two mathematical models are developed to approximate results achieved by a more complex and time-consuming finite element analysis. Besides, a seismic design procedure is developed. This consists of these two mathematical models which use as inputs, outputs of previous studies for deriving dynamic pressure.

Finally, the results obtained from the seismic design procedure are compared to the results obtained from the FE analysis.

The FE analysis revealed that the tank response such as the response acceleration, the dynamic pressure, the base shear and the uplift height of the tank bottom plate are significantly smaller than that due to static conditions. It implies reviewing dynamical behavior of tanks during earthquakes.

The FE analysis also shows that undulating deformation occurs at the top of a sidewall. This deformation has not been observed previously under static conditions typical of experimental

laboratory studies. The magnitude of this deformation is affected by the stiffness of stiffener rings installed on the sidewall. By applying the FE analysis, it is discovered that this deformation has a relationship with the response acceleration, the dynamic pressure, the base shear and the uplift height.

Next, a new seismic design procedure referred to as 'Simplified Seismic Design Procedure' is developed to provide a more accurate evaluation for design of a connection between a bottom plate and a sidewall of inner tanks. This procedure takes into account the uplift behavior of a tank bottom plate by using the findings of the dynamic response of the tank including the uplift obtained from the FE analysis.

The proposed Simplified Seismic Design Procedure is established from a comprehensive application of;

- theories of bulging and rocking motion to calculate dynamic pressure,
- two proposed mathematical models to calculate displacement and stress of a connection between a bottom plate and a sidewall of inner tanks,
- parameters for the models obtained from the FE analysis.

The first mathematical model for design of a connection between a bottom plate and a sidewall of inner tanks is referred to as the 'Structural Mathematical Model'. This model takes into account the uplift of the outer edge of the tank bottom plate due to earthquake forces, subsidence of the bottom insulation and bulging deformation of the sidewall. The proposed model can be used instead of a more commonly used finite element analysis methods which are generally used for design of a connection between a bottom plate and a sidewall.

In finite element analysis methods, several properties are considered, including tank dimensions and plate thickness of each part, magnitude and distribution of dynamic liquid pressure that is affected by width and height of the uplift of a bottom plate, elasticity of a bottom insulation, and displacement of a tank sidewall due to a bulging mode during earthquakes.

This paper includes these important properties in the Structural Mathematical Model to estimate the uplift height and the stress distribution accurately. The bottom plate part of the model is developed based on a theory of elastic bearing beam. To increase accuracy but maintain practicality, a thin cylindrical theory is introduced in conjunction with the bottom plate part for considering influences of the bulging displacement of the tank sidewall on the bottom plate. From the case study by the proposed model, it is found that the bulging displacement of the sidewall has a significant effect on the uplift height of the bottom plate.

In establishing the procedure, secondary mathematical model is presented. This model is referred to as the 'Force Coupling Mathematical Model'. This additional mathematical model provides the axial force distribution at the bottom of the sidewall from the dynamic pressure induced by the bulging and rocking motion, which are an essential factor for the calculation process by the Structural Mathematical Model.

The proposed procedure is an alternative design method for a corner connection of tanks instead of current design standards or more complicated commonly used time-history finite element analysis. However, this procedure has been developed successfully only for the standardized specific tank. Therefore, further work is required to verify its suitability to tanks with alternative dimensions in detail. In addition there are several items, as specified in Chapter 7, to be solved to improve the procedure.

1-2 BACKGROUND OF THIS STUDY

1-2-1 Type of above ground cylindrical tanks for refrigerated liquefied flammable gas service

There are several types of above ground cylindrical tanks for refrigerated liquefied flammable gas service. Each tank type is classified by the relevant guideline. For example, API 625 [1] specifies as follows.

(a) Single Containment Tank System

This system incorporates a liquid-tight container and a vapor-tight container. It can be a liquid and vapor-tight single-wall tank or a tank system comprised of an inner and outer container, designed and constructed so that only the inner container is required to be liquid-tight and contain the liquid product.

The outer container, if any, is primarily for the retention and protection of the insulation system from moisture and may hold the product vapor pressure, but is not designed to contain the refrigerated liquid in the event of leakage from the inner container.

The outer tank (if any) shall be vapor-tight.

A single containment tank system is surrounded by a secondary containment (normally a dike wall) which is designed to retain liquid in the event of leakage.

(b) Double Containment Tank System

This consists of a liquid and vapor tight primary tank system, which is itself a single containment tank system, built inside a liquid tight secondary liquid container.

The secondary liquid container is designed to hold all the liquid contents of the primary container in the event of leaks from the primary container, but it is not intended to contain or control any vapor resulting from product leakage from the primary container. The annular space between the primary container and the secondary container shall not be more than 6 m (20 ft).

(c) Full Containment Tank System

This consists of a liquid tight primary container and a liquid and vapor tight secondary container. Both are capable of independently containing the product stored.

The secondary container shall be capable of both containing the liquid product and controlling the vapor release in the event of product leakage from the primary liquid container.

Vapor tightness of the tank system during normal service is required. Under inner tank leakage (emergency) conditions, tank system product losses due to container permeability are acceptable.

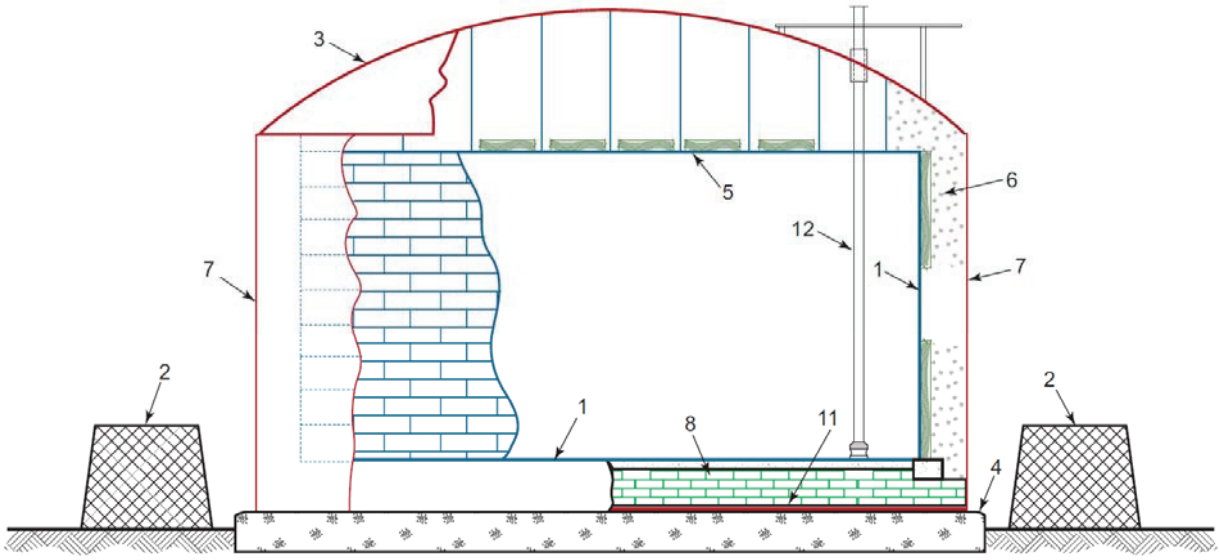

Key

1 primary liquid container (low temp steel)
2 secondary liquid container (dike)
3 warm vapor container (roof)
4 concrete foundation
5 suspended deck with insulation
6 insulation (annular space)
7 warm vapor container (outer shell)
8 bottom insulation
11 warm vapor container (outer bottom)
12 pump column

FIGURE 1-1: SINGLE CONTAINMENT TANK SYSTEM
DOUBLE WALL WITH STEEL PRIMARY CONTAINER AND STEEL VAPOR CONTAINER

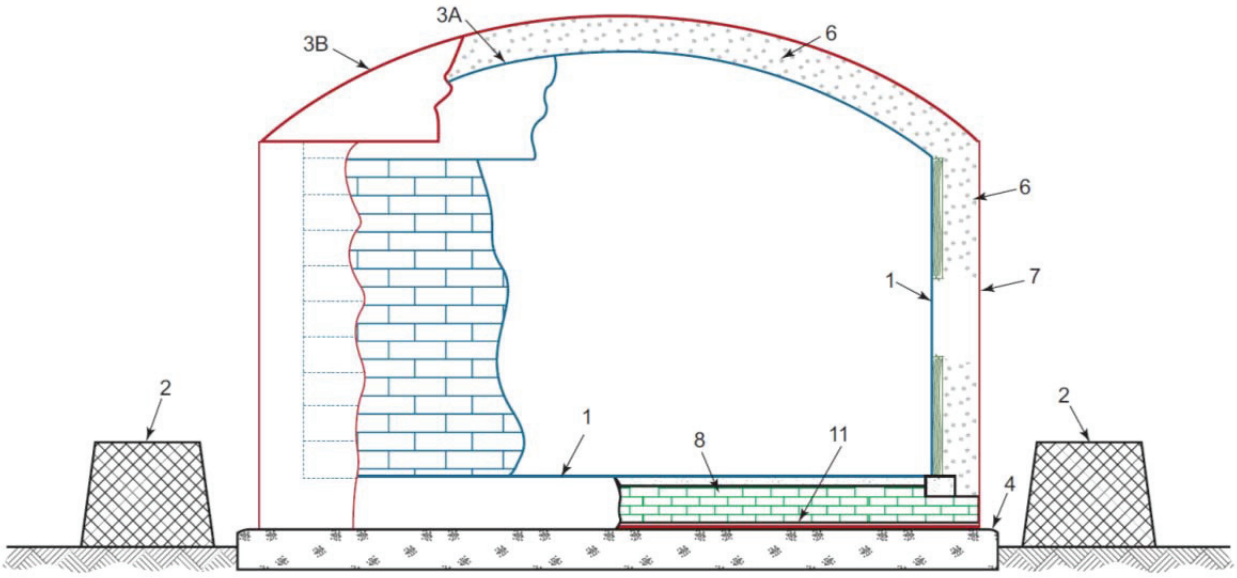

Key

1 primary liquid container (low temp steel)
2 secondary liquid container (dike)
3A refrigerated temp roof
3B purge gas container (roof)
4 concrete foundation
6 insulation (annular and roof space)
7 purge gas container (outer shell)
8 bottom insulation
11 purge gas container (outer bottom)

FIGURE 1-2: SINGLE CONTAINMENT TANK SYSTEM
DOUBLE WALL WITH STEEL PRIMARY CONTAINER AND STEEL PURGE GAS CONTAINER

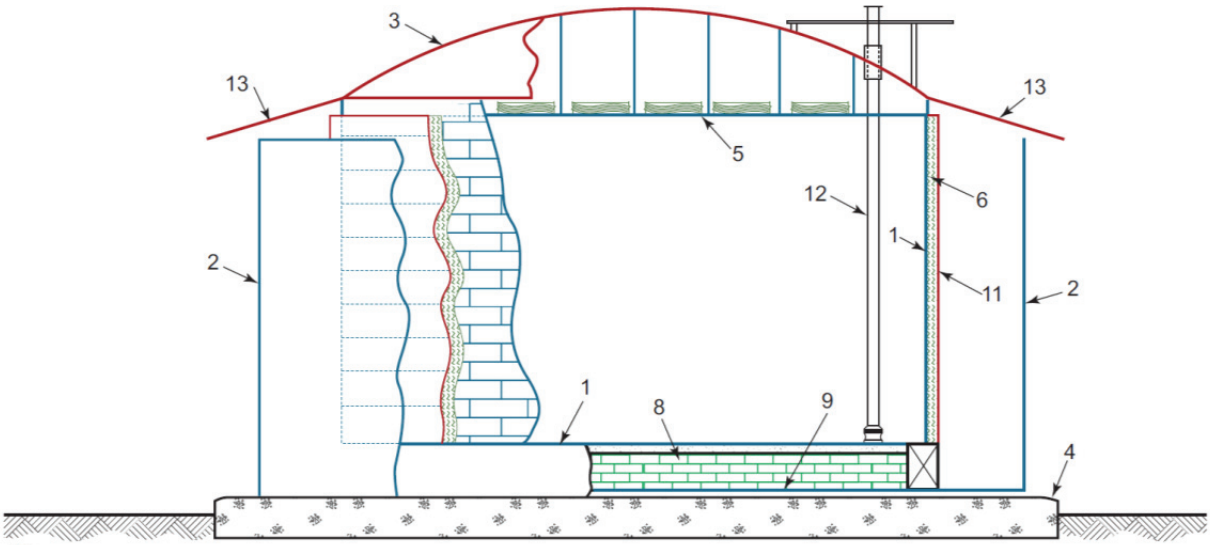

Key

1 primary liquid container (low temp steel)
2 secondary liquid container (low temp steel)
3 warm vapor container (roof)
4 concrete foundation
5 suspended deck with insulation
6 insulation
8 bottom insulation
9 secondary liquid container (low temp steel)
11 moisture vapor barrier
12 pump column
13 rain shield

FIGURE 1-3: DOUBLE CONTAINMENT TANK SYSTEM
STEEL PRIMARY CONTAINER AND STEEL SECONDARY CONTAINER

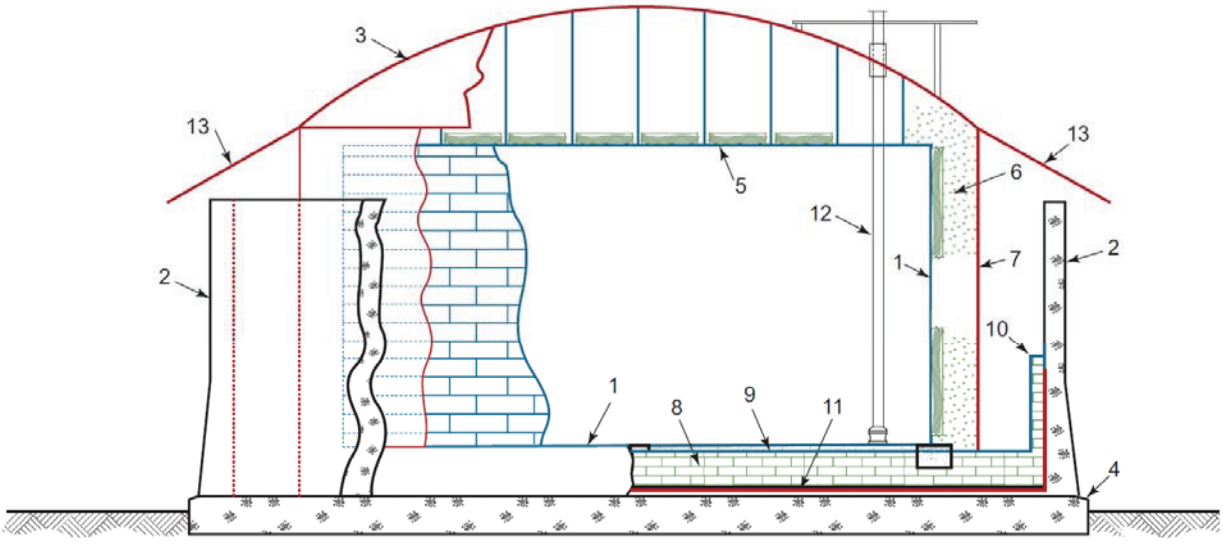

Key

1 primary liquid container (low temp steel)
2 secondary liquid container (concrete)
3 warm vapor container (roof)
4 concrete foundation
5 suspended deck with insulation
6 insulation (annular space)
7 warm vapor container (outer shell)
8 bottom insulation
9 secondary liquid container (low temp steel)
10 thermal corner protection
11 moisture vapor barrier
12 pump column
13 rain shield

FIGURE 1-4: DOUBLE CONTAINMENT TANK SYSTEM
STEEL PRIMARY CONTAINER, STEEL VAPOR CONTAINER, AND CONCRETE SECONDARY CONTAINER

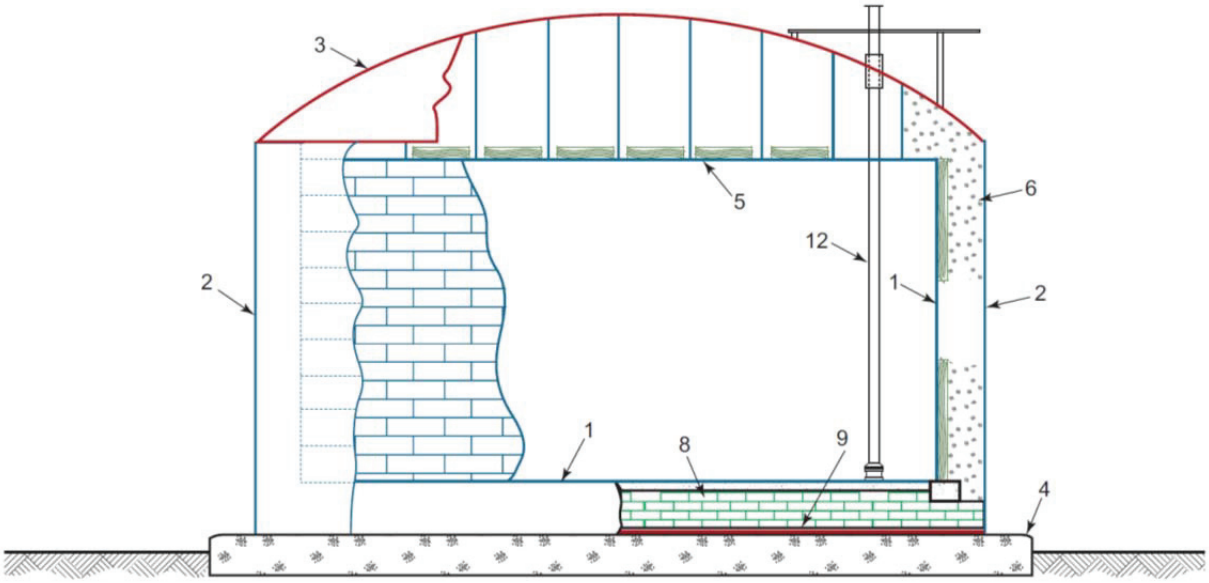

Key

1 primary liquid container (low temp steel)
2 secondary liquid container (low temp steel)
3 warm vapor container (roof)
4 concrete foundation
5 suspended deck with insulation
6 insulation (annular space)
8 bottom insulation
9 secondary liquid container (low temp steel)
12 pump column

FIGURE 1-5: FULL CONTAINMENT TANK SYSTEM
STEEL PRIMARY CONTAINER, STEEL SECONDARY CONTAINER, AND STEEL ROOF

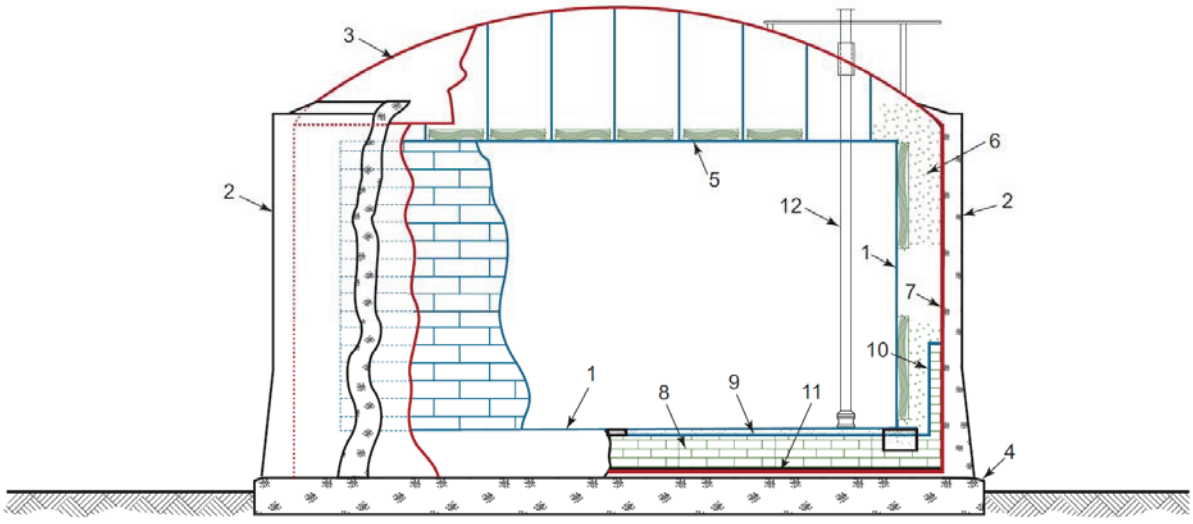

Key

1 primary liquid container (low temp steel)
2 secondary liquid container (concrete)
3 warm vapor container (roof)
4 concrete foundation
5 suspended deck with insulation
6 insulation (annular space)
7 product vapor container (liner)
8 bottom insulation
9 secondary liquid container (low temp steel)
10 Thermal corner protection
11 moisture vapor barrier
12 pump column

FIGURE 1-6: FULL CONTAINMENT TANK SYSTEM
STEEL PRIMARY CONTAINER, CONCRETE SECONDARY CONTAINER, AND STEEL ROOF

Recently, ‘Full Containment’ tanks are beginning to become more popular because of their minimum footprint and a safer containment they offer. In the international guide lines, it is assumed that a seismic event which would lead to a large-scale sloshing incident unlikely occurs, then “open top” design is usually selected for a primary liquid container. This type of tank has a roof formed by a suspended deck with insulation, due to lower construction cost.

‘Open top’ tanks have the advantage that the bottom plate corner connection is not affected by gas pressure. Hence, uplift of the bottom plate does not occur during normal operation. If the seismic design process confirms that there will be a limited amount of uplift from an earthquake event, then anchor straps are not installed. However, for tanks located in Japan, legislation requires that the primary liquid container is fully contained. These tanks are the dome roofed type and require anchor straps.

1-2-2 Seismic design of tanks

As specified below, several major regulations or guidelines for seismic design of tanks have been established. Such regulations or guidelines are selected and applied, depending on the country of construction of tanks, area of use and client requirements.

Japanese guidelines

a. High Pressure Gas Law (高圧ガス保安法) and related guide lines.
b. Recommended practice for LNG above ground storage. (LNG 地上式貯槽指針)
c. Recommended practice for LNG in ground storage. (LNG 地下式貯槽指針)
d. JIS B 8501. (鋼製石油貯槽の構造)

International guidelines

e. API 620 Design and Construction of Large, Welded, Low-pressure Storage Tanks.
f. API 625 Tank Systems for Refrigerated Liquefied Gas Storage.
g. API 650 Welded Steel Tanks for Oil Storage.
h. EN 14620 1-5 Design and manufacture of site built, vertical, cylindrical, flat-bottomed steel tanks for the storage of refrigerated, liquefied gases with operating temperatures between 0℃ and -165℃.

Guideline ‘a’ is widely applied for seismic design of tanks in Japan and provides philosophy and policy for seismic design in Japan. This regulation has been revised when an incident or disaster occurred in Japan. Guidelines ‘b’, ‘c’, ‘d’, are the most common design guide lines for large scale LNG above ground tanks, in ground tanks and oil tanks.

API is major guideline and applied for many projects in the world. API625 specifies outline and general items, concept and classification of type of tanks and requirements for seismic design. API 620 and API 650 specify detailed design guidelines including a specific procedure of

seismic design. EN 14620 is also a major guideline, especially for projects in Europe and in countries which adopt European standards.

Part 1 of standard EN14620 summaries a outline, general items, concepts and classification of types of tanks and policy of requirement of seismic design. A detailed design guideline and a specific procedure for seismic design are stated in Part 2.

The guideline requires an assessment of the soundness of a tank for earthquake from two aspects. The first aspect is a short period seismic wave component. If this wave has a natural period close to that of tank structure, it will induce a dynamic pressure in contents, which will act on tanks as a pressure load during an earthquake. The second aspect is a relatively long period seismic wave component. This wave introduces sloshing, which affects tanks as a wave pressure or overflow from a sidewall of open top tanks.

In the assessment of the short period seismic wave component, two different earthquake levels are applied, as specified below.

Japanese guidelines

Level 1

Earthquake that is likely to occur during life cycle of tank.
Tank shall maintain its operating functions.

Level 2

High level earthquake, whose probability is relatively low during life cycle of tank.
Tank shall maintain its structural integrity to avoid a leakage occurring.

International guidelines (API / EN 14620)

Operating Basis Earthquake (OBE)

The OBE is also referred to as Operating Level Earthquake (OLE) in API 620.
Tank shall maintain their operating functions.

Safe Shutdown Earthquake (SSE)

The SSE is also referred to as Contingency Level Earthquake (CLE) in API 620.
Tank shall maintain its structural integrity to allow for a safe shutdown.

International guidelines specify that the assessment procedure for judging necessity of anchor straps for preventing failure of tanks for each seismic level. This is because open top design is one option in international guidelines for when earthquake risk is low and does not cause large uplift to lead to failure of tanks. In this situation, a design without anchor strap is acceptable.

The Japanese and international guidelines lists above specify a procedure for tank seismic design. The procedures in JIS B 8501 and international guidelines consider uplift phenomenon, however, that is established based on outcomes of static base previous studies. In addition,

dynamic pressure, which is used for the design of un-anchored tanks, calculated by the guidelines does not include a dynamic effect of the uplift of a tank bottom plate. Because the quoted theory is based on the assumption of a fixed tank bottom plate (i.e. no-uplift of the tank bottom plate).

The several design procedures specified in international guidelines are outlined below.

API620 Appendix L Seismic Design of Storage Tanks

In the Appendix L of API620, the design procedure for tanks which experience uplift is provided based on the model of Wozniak and Mitchell [2]. For tanks, compression force b can be determined from the value of the compressive force parameter obtained from Figure 1-7 as a function of the overturning moment parameter. The curve in Figure 1-7 is derived from the assumed load distribution around the shell of a tank as in Figure 1-5. When $M/[D^2(W_t + W_L)]$ is greater than 0.785 but less than or equal to 1.5, b is computed from the formula of $(b + W_L)/(W_t + W_L)$ and the value obtained from the curve in Figure 1-7.

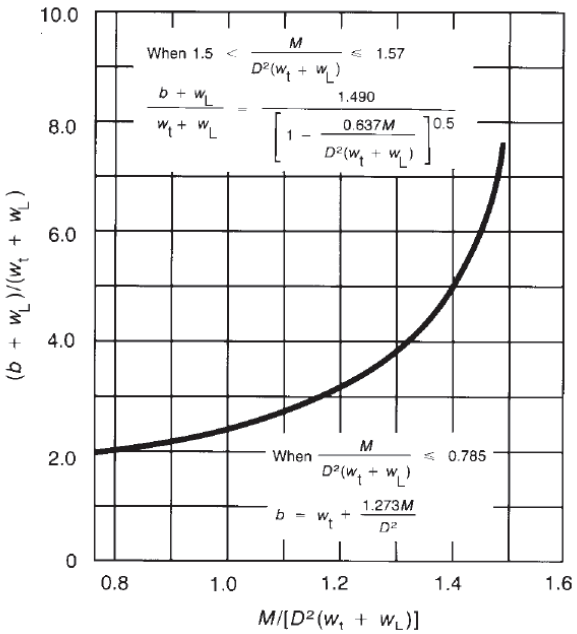

FIGURE 1-7: CURVE FOR OBTAINING THE VALUE OF b WHEN $M/[D^2(W_t + W_L)]$ EXCEEDS 0.785

When $M/[D^2(W_t + W_L)]$ is greater than 1.5 but less than or equal to 1.57, b is computed by following equation.

$$\frac{b + W_L}{W_t + W_L} = \frac{1.490}{\left[1 - \dfrac{0.637M}{D^2(W_t + W_L)}\right]^{0.5}}$$

While $M/[D^2(W_t + W_L)]$ is less than 0.785, b is computed by following equation.

$$b = W_t + \frac{1.273M}{D^2}$$

The variables used in the previous equations are defined as follows.

D : Diameter of the tank, in ft.

M : Overturning moment applied to the bottom of the tank shell, in ft-lbs.

W_L : Maximum weight of the tank contents that may be utilized to resist the shell overturning moment, in lb/ft of shell circumference. W_L shall not exceed $1.25GHD$.

$$W_L = 7.9t_b\sqrt{F_{by}GH}$$

t_b : Thickness of bottom plate under the shell, in in.

F_{by} : Minimum specified yield strength of the bottom plate under the shell, in lbf/in^2, gauge

G : Design specific gravity of the product to be stored, as specified by the Purchaser.

H : Maximum design product height, in ft.

b : Maximum longitudinal shell compressive force, in lb/ft of shell circumference.

W_t : Weight of the tank shell and the portion of the fixed roof and insulation, if any, supported by the shell, in lb/ft of shell circumference.

Finally, compression stress of bottom shell is given by following formula.

$$\text{Compression stress} = b/(12t)$$

Eurocode8: Design of structures for earthquake resistance- Part4: Silos, tanks and pipelines

According to EN 1998-4:2006, the vertical uplift at the edge of the base, w, as derived from a parametric study with finite element models of un-anchored cylindrical steel tanks above ground of commonly used geometry and fixed, fairly heavily loaded roof, is given in Figure 1-8 as a function of the normalized overturning moment M/WH, for different values of the aspect ratio H/R.

For the estimation of radial membrane stress in the plate, the length L of the uplift part of the tank bottom is necessary. Results from [3] for fixed-roof tanks are shown in Figure 1-9. Once uplift occurs, the dependence of L on the vertical uplift w is almost linear.

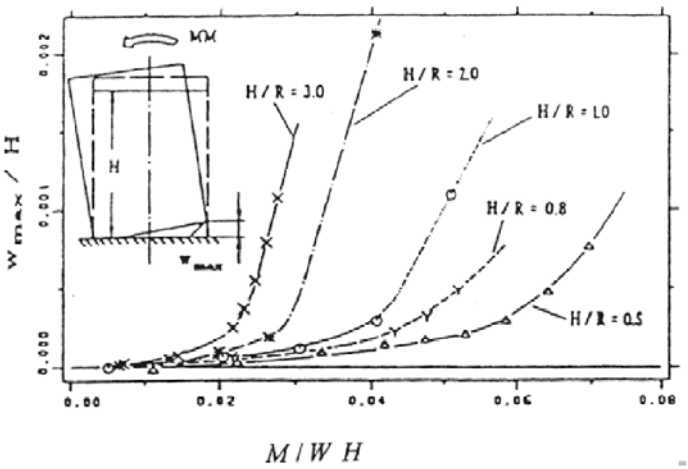

FIGURE 1-8: MAXIMUM VERTICAL UPLIFT OF FIXED-ROOF UNANCHORED CYLINDRICAL TANKS ON GROUND VERSUS OVERTURNING MOMENT M/WH [3]

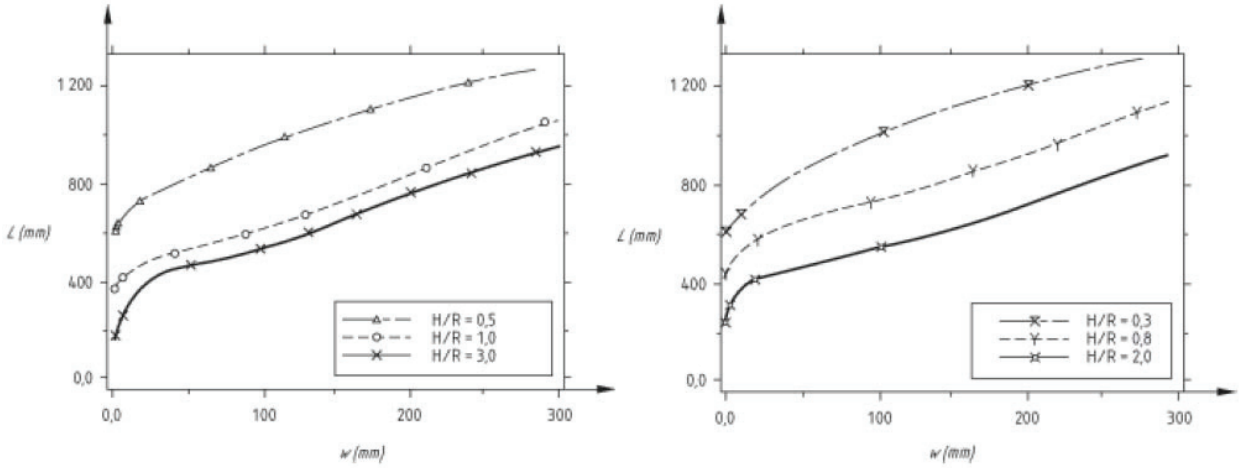

FIGURE 1-9: LENGTH OF UPLIFTED PART OF THE BASE IN FIXED-ROOF UNANCHORED CYLINDRICAL TANKS ON GROUND AS A FUNCTION OF THE VERTICAL UPLIFT AT THE EDGE [3]

An estimate of the membrane stress σ_{rb} in the base plate due to the uplift is given in [4].

$$\sigma_{rb} = \frac{1}{s}\left(\frac{2}{3}\frac{E}{1-\nu^2} sp^2 R^2 (1-\mu)^2\right)^{1/3}$$

Where,

R : Radius of the tank

s : Thickness of the base plate

E : Modulus of elasticity of tank material

p :Pressure on the base

μ :1-L/(2R), with L=uplifted part of the base

1-2-3 Factors affecting the current seismic design of LNG tanks

Demand for LNG is growing worldwide because of the changeover from oil to LNG as a fuel source. This is due to concerns over global warming and environmental problems. Expansion of existing LNG terminals and construction of new ones are planned in many countries, and some of such projects are already in progress. This trend is expected to continue because of lower transportation and infrastructure costs. These costs are dropping due to progress in LNG technology, broadening of LNG demand and the expectation of increasing shale gas production.

Sites for LNG terminals are selected by assessment of environmental impact and possible hazards to the locality. Since it is difficult to find a perfect location which satisfies all requirements, sites selected for construction may occasionally have unfavorable soil conditions from the viewpoint of earthquake response. Design requirements tend to be higher for LNG storage tanks to be built on such sites, as they have severe seismic conditions listed in their specifications.

Severe seismic conditions result in a large response of tanks. This response can cause large uplift of the bottom plate which induces failure of the bottom plate and the sidewall. To deal with increased seismic design requirements, it is necessary to implement one or more of the following measures.

(1) Rearrange of tank dimensions such as increasing of thickness of a sidewall and an annular plate, which is installed at periphery part of a bottom plate, widening of an annular plate.
(2) Install anchor straps (Figure 1-10)
(3) Install seismic isolators (Figure 1-11)
(4) Change a tank proportion to being shorter and broader

Figure 1-10 shows an installation example of anchor straps for uplift restraint of an annular part of a tank. Anchor straps measuring 15 to 20 cm wide and several centimeters thickness are installed at intervals of about 1 m, depending on a magnitude of design overturning moment during an earthquake. The anchor straps penetrate the annular part of the secondary barrier which protects the concrete outer tank from contact with LNG in an event of leakage from an inner tank. When LNG leaks, it cools the secondary barrier and causes contraction displacement, which generates large stress around the penetrations. Therefore, adequate design consideration must be given to protect the weak points.

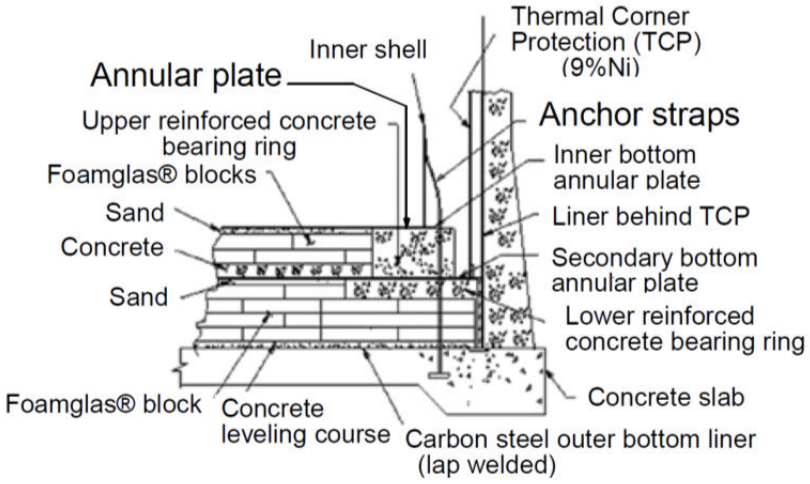

FIGURE 1-10: EXAMPLE OF CONFIGURATION OF THE BOTTOM PLATE WITH ANCHOR STRAPS [5]

Figure 1-11 shows an installation example of pendulum seismic isolators [6]. Depending on a tank size, about 200 to 300 units of such device need to be installed between a concrete slab and a tank foundation.

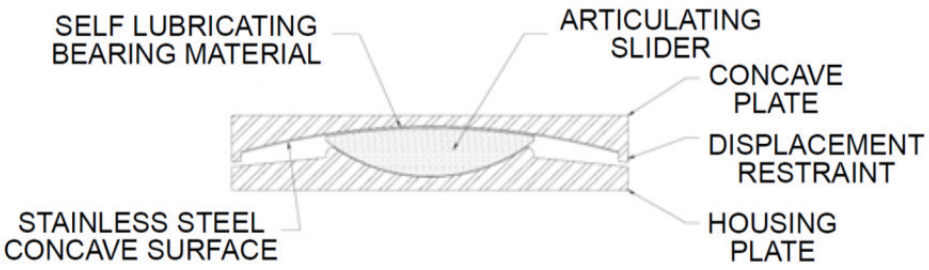

Example of seismic isolator [6]

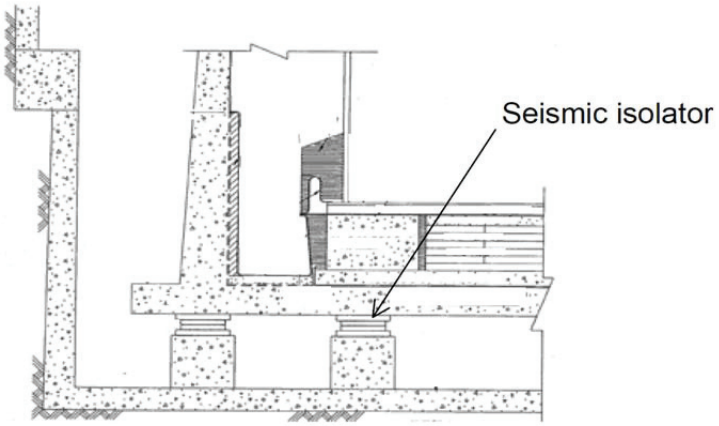

FIGURE 1-11: INSTALLATION EXAMPLE OF SEISMIC ISOLATORS

Measures (1), (2) and (3) mentioned above directly affect a construction cost, while (4) may be impossible depending on a layout plan of a terminal or for some other reasons.

Current situation of seismic design for tanks summarizes as follows.

- Many previous studies, based on static conditions, were conducted on tanks with a bottom plate fixed to a foundation (i.e. cases with no-uplift or cases with anchor straps). The results from these studies are quoted in existing seismic design standards, including equations for estimation of dynamic pressure and verification of stress of a bottom plate and a sidewall.
- Similarly, some previous studies, based on static conditions, were also conducted on tanks with an unfixed bottom. The results from these studies as well as tilt tests using scale models are quoted in existing seismic design standards.
- Tanks regulated by API or Euro Codes usually are not required to be equipped with anchor straps in case uplift height during earthquakes is acceptably small. This is because these tanks do not have a inner roof. Hence, there is no uplifting force due to gas pressure acting on a bottom plate. However, anchor straps may be required, when uplift height due to an earthquake is beyond acceptable level. There is an increasing demand for adding an FE analysis which incorporates tank uplift to take into account verification of the design that is obtained by standard seismic design methods.
- There are a few previous studies which examine the effect of dynamic behavior on tank uplift. These studies typically conduct by theoretically or use time-history finite element analysis. It has been revealed in some fundamental studies that uplift is smaller under dynamic conditions than in static conditions [7], [8].
- LNG tanks in Japan usually have an inner roof to sustain the pressure of tanks and are thus equipped with anchor straps. Therefore, finite element analysis based on static conditions is commonly used with fixed conditions applied to the bottom corner part and with the maximum dynamic pressure loaded statically.

Seismic design conditions are anticipated to be more severe in future. Hence, it is desirable to avoid unnecessarily excessive specifications and establish a rationalized tank design, with construction costs and other economic factors taken into account. Consequently, it is essential to understand the tank dynamic behavior during uplift of a bottom plate corner connection. In addition, establishing a simplified standard design procedure is desirable for tank engineers rather than to using a complicated time-history finite element analysis. This procedure should take into account an interaction of dynamic pressure and uplift of a tank bottom plate.

1-3 CONCEPT AND ORGANIZATION OF THIS PAPER

1-3-1 Concept of this Paper

This paper proposes a simplified design procedure for tank bottom plate corner connections based on the understanding of dynamic response behavior through the FE analysis, with the following assumptions:

- Tanks are un-anchored.
- Yield of a bottom plate or a sidewall and an occurrence of a plastic hinge are not discussed. This is because in the design process, the dimensions and thickness of each part are selected to be within the allowable stress level or, if there is no other option, anchors are installed.
- Effect by membrane force in a tank bottom plate due to large deformation is not considered, because large deformation that generates high stress is not accepted by stress limitation of design standard.
- The theoretical models of dynamic pressure due to bulging motion of Housner [9] and rocking motion of Taniguchi and Segawa (rectangular tank model) [7], which are the basis of this study, are established with the assumption of a rigid sidewall and tank bottom. Therefore, there are several differences compared with actual phenomena or the FE analysis. For example, the rocking motion model of Taniguchi and Segawa [7] is assumed as single point contact with tank bottom insulation.
- The undulating local deformation of the sidewall observed in the FE analysis is not considered, its expected effect on uplift is discussed.

1-3-2 Organization of this Paper

This paper consists of seven chapters.

Chapter 1, presents an outline and background including current design concepts and seismic design of tanks. Factors affecting the current seismic design of tanks and the concepts of this paper also specified.

Chapter 2, reviews previous studies involving dynamic pressure, rocking response, uplift behavior of a bottom plate and characteristics of an axial force at a bottom of a sidewall and summarizes these.

Chapter 3, researches in the detail dynamic response behavior including the uplift of the tank bottom plate for specific tank by applying fluid-structural coupled 3-dimensional time-history FE analysis.

Chapter 4, develops the integrated Structural Mathematical Model of the tank's sidewall, bottom plate and the tank bottom (bottom insulation). It's effectiveness is then verified.

Chapter 5, develops the Force Coupling Mathematical Model for determining an extent of uplift and axial force distribution at the bottom of the sidewall. The Force Coupling

Mathematical Model is an essential part of the Structural Mathematical Model. This is because the Force Coupling Mathematical Model calculates the value of the axial force which is a required input to the Structural Mathematical Model.

Chapter 6, proposes the Simplified Seismic Design Procedure for a tank bottom plate corner connection, based from previous studies and both the Structural Mathematic Model and the Force Coupling Mathematical Model. It also summarizes the items to be studied in the future.

Chapter 7, summaries the outcomes of this paper.

1-3-3 Tank used in this Paper

In this paper, the subject tank is shown in Figures 1-12 and 1-13. Its major dimensions and properties are as follows.

D:	Tank diameter	74,400 mm
H:	Tank height	36,820 mm
h:	Liquid height	36,250 mm
t_s:	Thickness of bottom of the sidewall	29.6mm
k:	Reaction coefficient of the tank bottom	25.5 N/mm^2
E:	Modulus of elasticity of steel	191,000 MPa
W_b:	Width of the annular plate	1,900 mm
t_b:	Thickness of the bottom plate (annular plate)	18.7mm
ρ:	Fluid density	480 kg/m^3
g:	Gravity acceleration	9.8 m/s^2

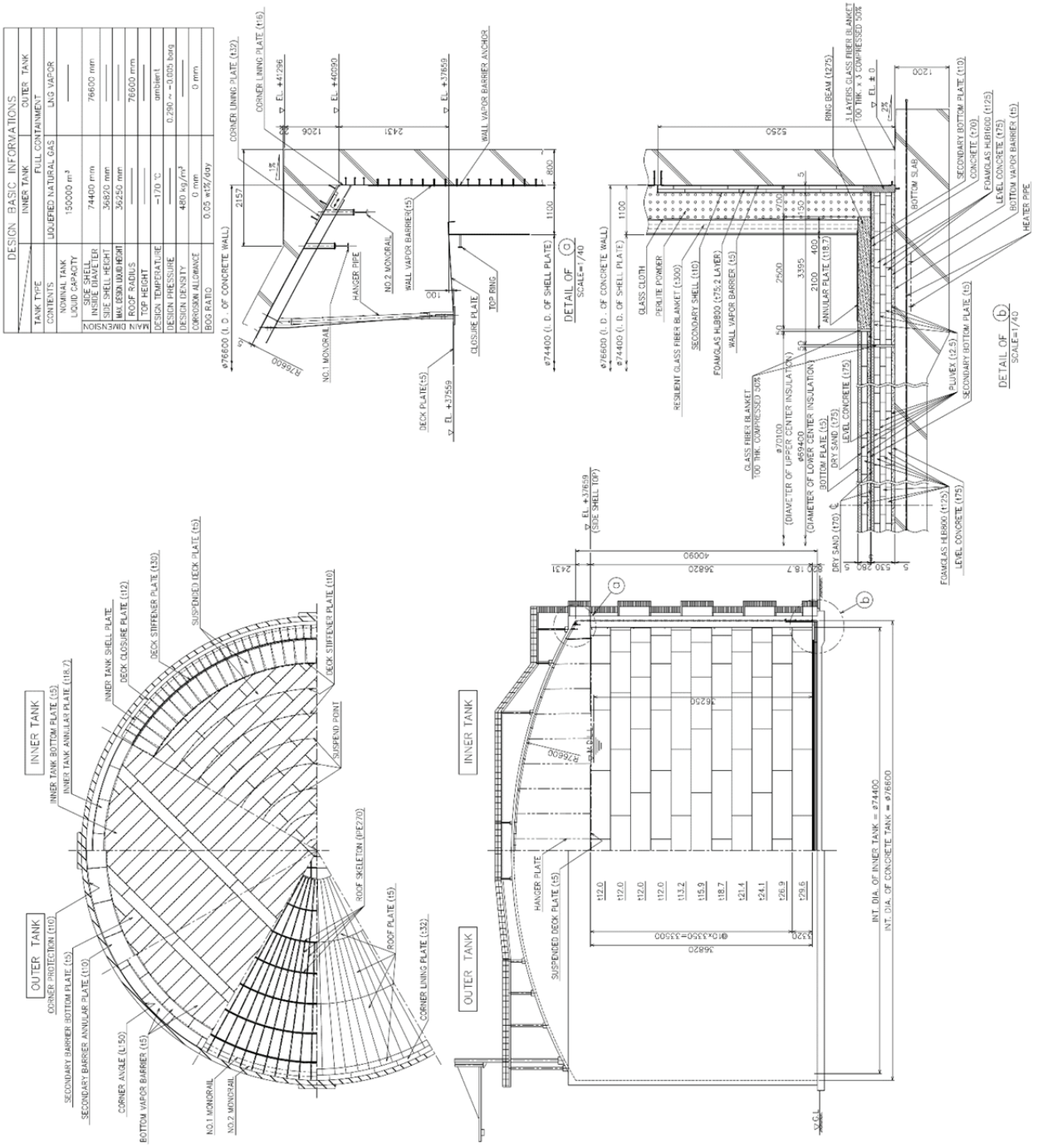

FIGURE 1-12: TANK USED IN THIS PAPER

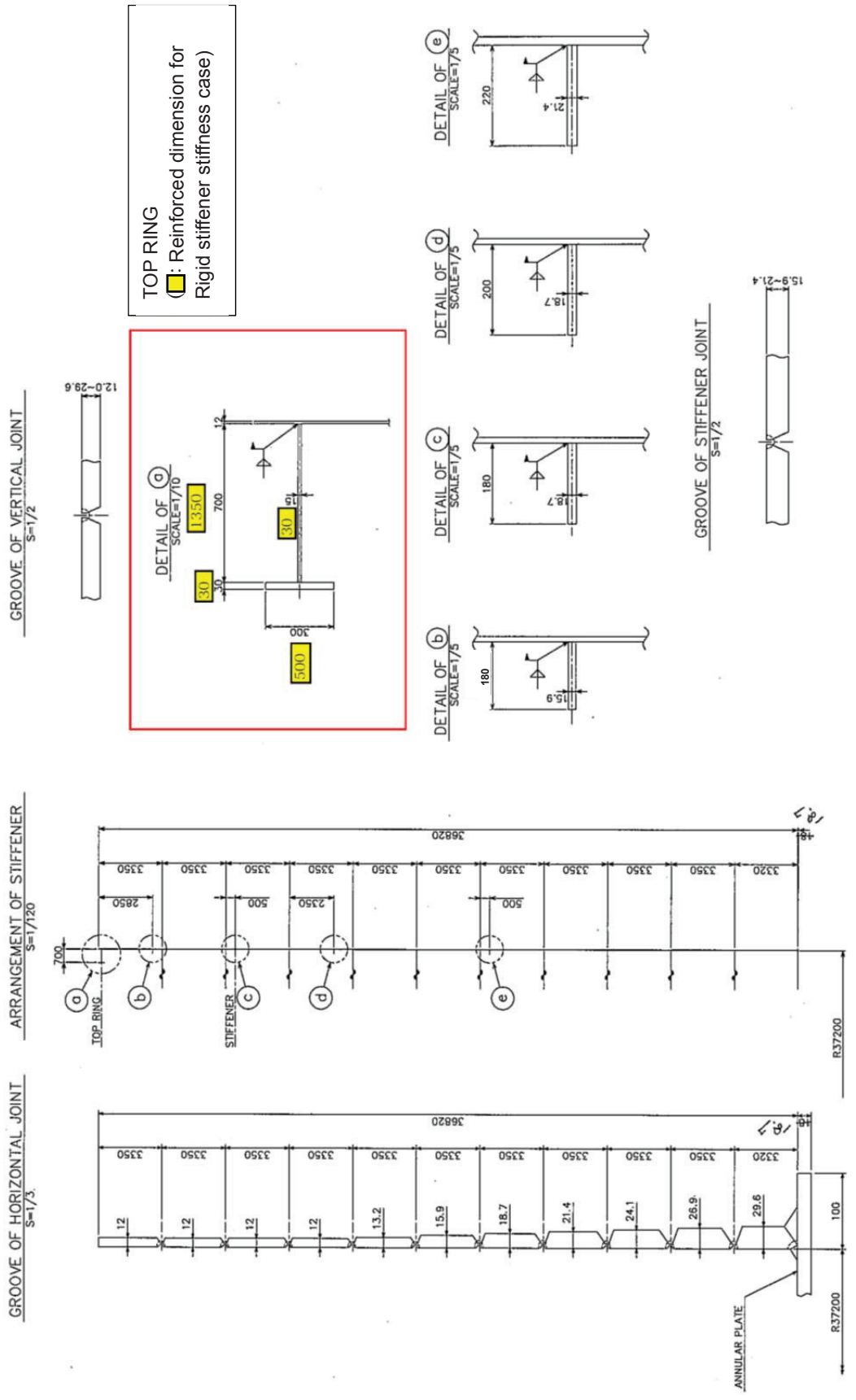

FIGURE 1-13: CONFIGURATION OF STIFFENER

REFERENCES

[1] API STANDARD 625, August 2010, “Tank Systems for Refrigerated Liquefied Gas Storage”.

[2] Wozniak, R. S. and Mitchell, W. W., 1978, “Basis of Seismic Design Provisions for Welded Steel Oil Storage Tanks”, API Refining Dept. 43rd Midyear Meeting, Toronto.

[3] Scharf, K., 1990, “Beiträge zur Erfassung des Verhaltens von erdbebenerregten, oberirdischen Tankbauwerken,” Fortschritt-Berichte VDI, Reihe 4. Bauingenieurwesen, Nr. 97, VDI Verlag, Düsseldorf.

[4] Cambra F.J., 1982, “Earthquake response considerations of broad liquid storage tanks” Report EERC 82/25.

[5] LNG Journal, January / February 2005.

[6] Earthquake Protection Systems, Inc., September 2003, “Technical Characteristics of Friction PENDULUM^{TM} Bearings”.

[7] Taniguchi T. and Segawa T., July 2008, “Fluid Pressure on Rectangular Tank Consisting of Rigid Side Walls and Rectilinearly Deforming Bottom Plate Due to Uplift Motion”, Proceedings of ASME PVP Conference, PVP2008-61166.

[8] Hayashi, S. and Taniguchi, T., et al., 2011, “A Study of Fluid-Structure Coupled Analysis for Large LNG Storage Tanks in Consideration of Uplift”, Proceedings of ASME PVP Conference, PVP2011-57925.

[9] Housner, G. W., 1957, “Dynamic Pressure on Accelerated Fluid Containers”, Bulletin of the Seismological Society of America, Vol. 47, pp. 15-35.

CHAPTER 2

PREVIOUS STUDIES ON UPLIFT OF BOTTOM PLATE DURING EARTHQUAKE FOR ABOVE GROUND CYLINDRICAL TANKS

CHAPTER 2
PREVIOUS STUDIES ON UPLIFT OF BOTTOM PLATE DURING EARTHQUAKE FOR ABOVE GROUND CYLINDRICAL TANKS

As specified in Chapter 1, seismic design of tanks is generally categorized into (a) tank structure vibration response caused by the short period seismic wave component of earthquakes which has a frequency close to a natural period of a tank, and (b) sloshing of liquid caused by sympathetic vibration with the relatively long period seismic wave component of earthquakes.

This paper focuses on response behavior of tanks due to the short period seismic wave component. In the previous studies, response behavior has been studied from viewpoint of both of bulging and rocking motion.

2-1 PREVIOUS STUDIES REGARDING DYNAMIC PRESSURE INDUCED BY BULGING RESPONSE

In the studies regarding dynamic pressure caused by earthquake, theoretical research of Housner [1], which was subjected to dynamic pressure induced by translation of a tank (called "bulging pressure") based on the assumption of a fixed base and a rigid wall tank, was widely recognized. This theory is established with the conception that dynamic pressure is consist of impulsive pressure due to inertia force and convective pressure by sloshing of liquid. While the effect of coupling of sidewall and liquid is not considered.

Jacobsen [2], Senda and Nakagawa [3] performed a research from the same viewpoint as Housner. They applied a potential theory to vibration of liquid at free surface and they arrived at similar achievement as Housner from a macroscopic viewpoint.

Baron and Shalak [4], Bauer [5] and other researchers [6]-[10] studied a problem assuming an elastic tank. These studies model a sidewall as a beam structure. However, the outcome of their research does not provide a guideline for designing tanks subject to earthquake conditions.

Veletsos at al. [11] proposed a procedure for obtaining dynamic pressure with a consideration of fluid-tank interaction, which approximates the vibration mode by using a simplified function and beam structure to model a sidewall.

Okada at al. [12] conducted finite element interaction analysis with a coupling model of fluid-elastic shell system, then, Sakai at al. [13] proposed a procedure for obtaining dynamic pressure from an eigenmode and its simplified method. These results take into account an effect of deformation of a sidewall and how it affects dynamic pressure.

The dynamic pressure proposed by Housner [1], Veletsos at al. [11] and Sakai at al. [13] are applied to the current seismic design of tanks.

In a Japanese guideline of above ground LNG tank [16], other several examples of calculation of dynamic pressure are presented [14], [15].

Calculation conditions
計算条件

		75,000kℓ
Inner dia. of inner tank	内槽内径 D mm	57,600
Sidewall height	側板高さ H mm (H/D)	28,820(0.50)
Inner tank material	内槽材料	9%ニッケル鋼
Material properties	材料定数 縦弾性係数 kgf/cm²	2.1×10^{6}
	材料定数 ポアソン比	0.3
	材料定数 単位体積重量 kgf/cm³	7.85×10^{-3}
Average thickness of sidewall	側板平均板厚 cm	1.73
Acceleration at bottom	底板面入力加速度 Gal	100
Damping ratio of tank	貯槽減衰定数 %	5
Soil conditions	地盤条件	第4種地盤

9% Ni steel
Modulus of elasticity
Poisson's ratio
Density
Class 4

Sidewall height (m)
側板高さ(m)

Dynamic pressure on the sidewall (seismic wave downstream side)
側板動液圧分布(地震方向下手側)

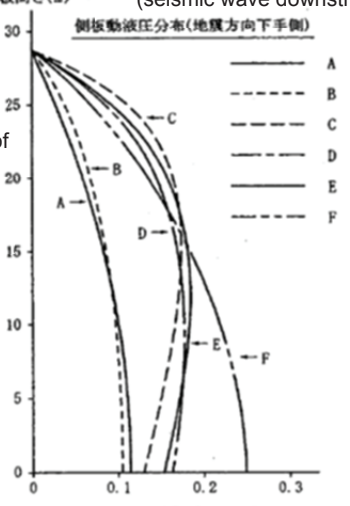

Table 4.6(a) Analysis example of 75,000 kL tank
解図4.6(a) 75,000kℓ貯槽の解析例 [3]

	[1]	[3]	[11]			[14]	[12]	[15]
Items 項目 / Method 計算法	A [1] (Housner 理論) (応答倍率 1.0 と仮定)	B [2] (速度ポテンシャル理論) (応答倍率 1.0 と仮定)	C [4] (Veletsos)	D [5] 剛体移動分	D [5] 相対変形分	D [5] 合計	E [6] (有限要素法)	F [3]
Natural period 固有周期 (S)	—	—	0.37	—	0.37	—	0.35	0.37
Maximum response acceleration 最大応答加速度 (Gal)	100	100	338	—	—	258	270	210
Base shear due to dynamic pressure 動液圧によるベースシャー (tf)	1,980 (0.98)	2,030 (1.00)	3,710 (1.83)	2,030	1,711	3,741 (1.84)	3,870 (1.91)	4,158 (2.06)
Overturning moment of sidewall due to dynamic pressure 動液圧による側板転倒モーメント (tf·m)	21,400 (0.91)	23,600 (1.00)	50,400 (2.14)	23,600	23,050	46,650 (1.98)	49,100 (2.08)	44,940 (1.91)

〔備 考〕[1] Eの有限要素法ではシェルを17要素、液体を12要素に分割している。
[2] 表中( )内の数値はBによるものを1として比較したものである。
[3] Fの値は、Aの結果にDより求められる固有周期に対する応答倍率を乗じたものである。

A : Housner theory (Assumed amplification ratio of response acceleration as 1.0)
B : Velocity potential theory (Assumed amplification ratio of response acceleration as 1.0)
C : Veletosos theory
D : This value consist of component due to rigid movement and relative deformation.
E : Finite element method

〔Note〕
[1] In case E, sidewall consists of 17 elements and liquid part consists of 12 elements.
[2] () values in the table are ratio against B.
[3] The value of F is obtained by multiplying the result of A by amplification ratio due to natural period which is calculated by D.

FIGURE 2-1:
EXAMPLE OF CALCULATION RESULTS FOR DYNAMIC PRESSURE [16]

2-2 PREVIOUS STUDIES REGARDING ROCKING RESPONSE

2-2-1 Previous studies regarding rocking behavior of tanks

There are various studies about rocking and uplifting of a bottom plate of tanks. Tani and Hori [17] investigated rocking due to soil-tank interaction analytically and obtained the result that flexibility of foundation has an effect to reduce dynamic pressure. Clough [18] performed static-tilt tests and dynamic shaking table tests in their series of studies and reported that deformation and stress of sidewall became large under unanchored conditions, while with roof conditions 30-40% axial stress decreased. Isoe [19] conducted large scale static-tilt tests in which were geometrically similar to actual tanks and reported that restriction of sidewall deformation by a roof contributed to reduction of uplift height of a bottom plate.

	Model	Prototype		
	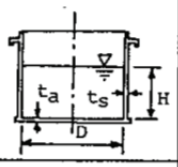	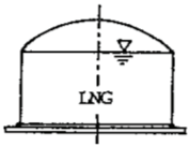	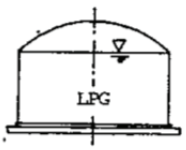	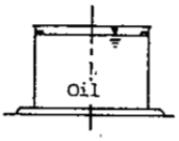
W (m^3)	333 - 427	80,000	60,000	25,000
γ_1(kN/ m^3)	9.8 (water)	4.75	5.68	7.84
E (kN/mm^2)	68.6 (aluminum alloy)	206	206	206
L_m / L_p	———	1/6	1/5	1/4
H (mm)	4,600 - 5,900	28,800	29,600	19,800
D (mm)	9,600	59,500	50,000	40,000
t_a,t_s (mm)	3 , 5	18 , 30.5	18 , 28	12 , 20

Dimension and properties of the Tilt model and actual tanks

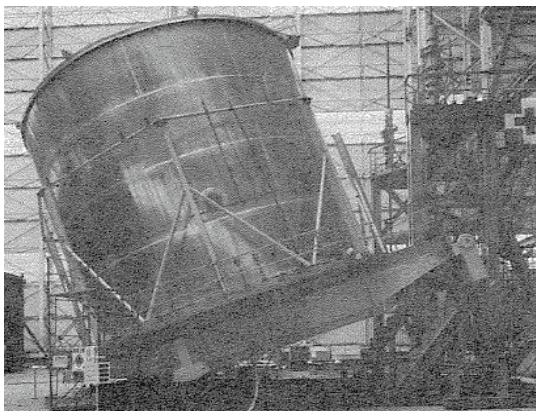

Photo of Tilt test

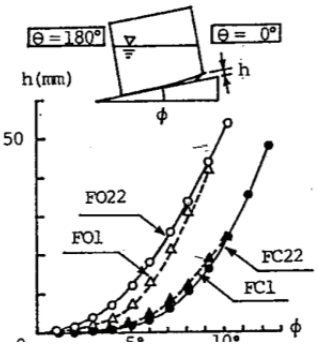

Case	Roof	Foundation
FO1	no	plywood
FC1	exist	plywood
FO22	no	rubber
FC22	exist	rubber

Historical record of uplift height in the Tilt test

FIGURE 2-2: DETAILS OF LARGE SCALE, STATIC-TILT TEST [19]

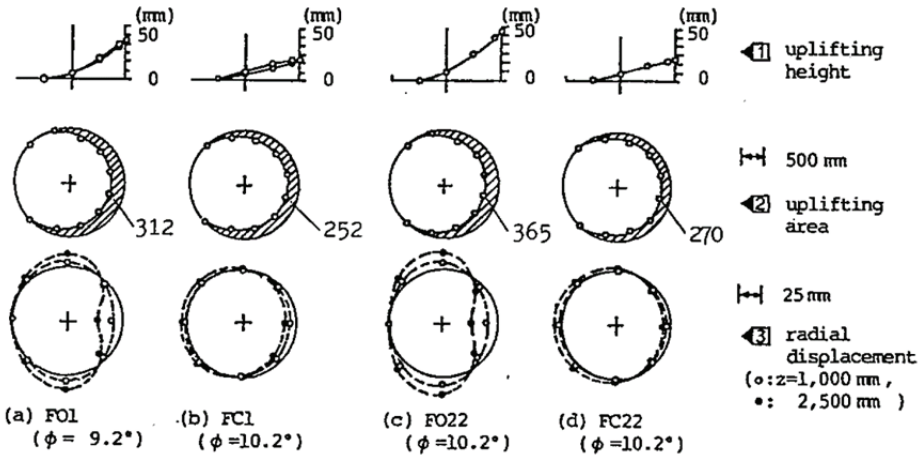

Displacement of tanks in the Tilt test

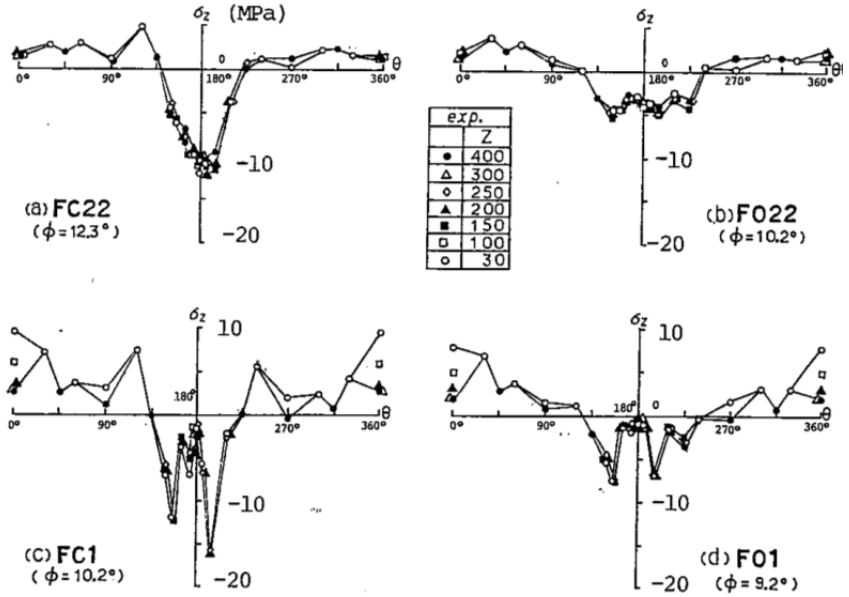

Axial stress of side wall in the Tilt test

FIGURE 2-3:
GRAPHICAL RESULTS FROM LARGE SCALE STATIC-TILT TEST [19]

Maekawa et al. [20-22] studied experimentally and analytically by explicit finite element method, seismic characteristics of water storage tanks. They reported that an oval-type vibration occurred at a sidewall. They also insisted that this vibration effects on a tank natural period for changing to long period by decreasing of stiffness of tank structure.

2-2-2 Previous studies about modeling of axial force in a sidewall

Clough [18], Wozniak and Mitchell [23] and Kobayashi and Ishida et al. [24] each proposed an analytical model for estimating an axial force in sidewall when uplift occurs, using different approaches. These models are based on equilibrium between a vertical force (i.e. an axial force in a sidewall) and a overturning moment. Their details are outlined and discussed below.

Clough Model

Clough developed a formula for calculating compressive stress in a sidewall which is dependent on a extent of uplift, which corresponds to the amount of overturning moment and the axial force on a bottom plate. His theory was developed from:

- assuming a triangle shape distribution of a compressive force along a sidewall, from the result of experiment (see a red line in Figure 2-4) ,
- defining uplift area as between a tank radius R and a radius of r,
- applying the relation of (a) liquid weight of crescent shape uplift area equal to (b) a force couple of overturning moment equal to (c) total of an assumed compressive force, as follows.

$$F_h = W_f \times (R - r) + W_s \times k_R$$
$$W = W_f + W_s$$

Then, the maximum compressive force f_{max} is obtained from k_R (center of reaction force along sidewall).

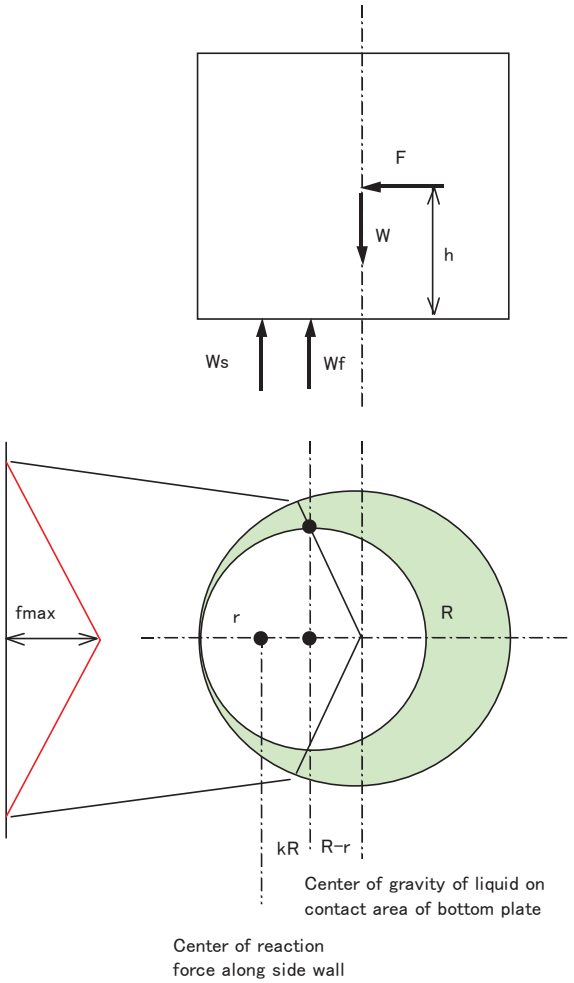

R : Radius of container
r : Radius of portion remains in contact
h : Height of F
F : Effective lateral seismic force
W : Total weight of shell and contents
W_s : Reaction at the point of contact between shell and foundation
W_f : Weight of contents within r
f_{max} : Peak compressive shell force
k : Dimensionless constant

FIGURE 2-4: AXIAL FORCE IN SIDEWALL OF CLOUGH MODEL [18]

Wozniak, Mitchell Model

Wozniak and Mitchell proposed a method for safety assessment of tanks against an overturning moment. This method is quoted by API650 and API620.

Their theory was developed by:

- modelling the bottom plate as a beam with two plastic hinges and assumes a vertical tensile axial force in the sidewall which has no relationship with uplift height,
- assuming that vertical tensile axial force distribution along a sidewall is constant, while the downward acting, compressive axial force distribution is a cosine curve,
- obtaining (a) the maximum tensile force (N_{umax}), (b) the maximum compressive force (N_{cmax}), and (c) the start point of uplifting (β), by establishing equilibrium between the vertical axial force and the overturning moment, and establishing continuity of the vertical axial forces at β .

This model ignores the tensile force in the radial direction in the bottom plate of uplift area.

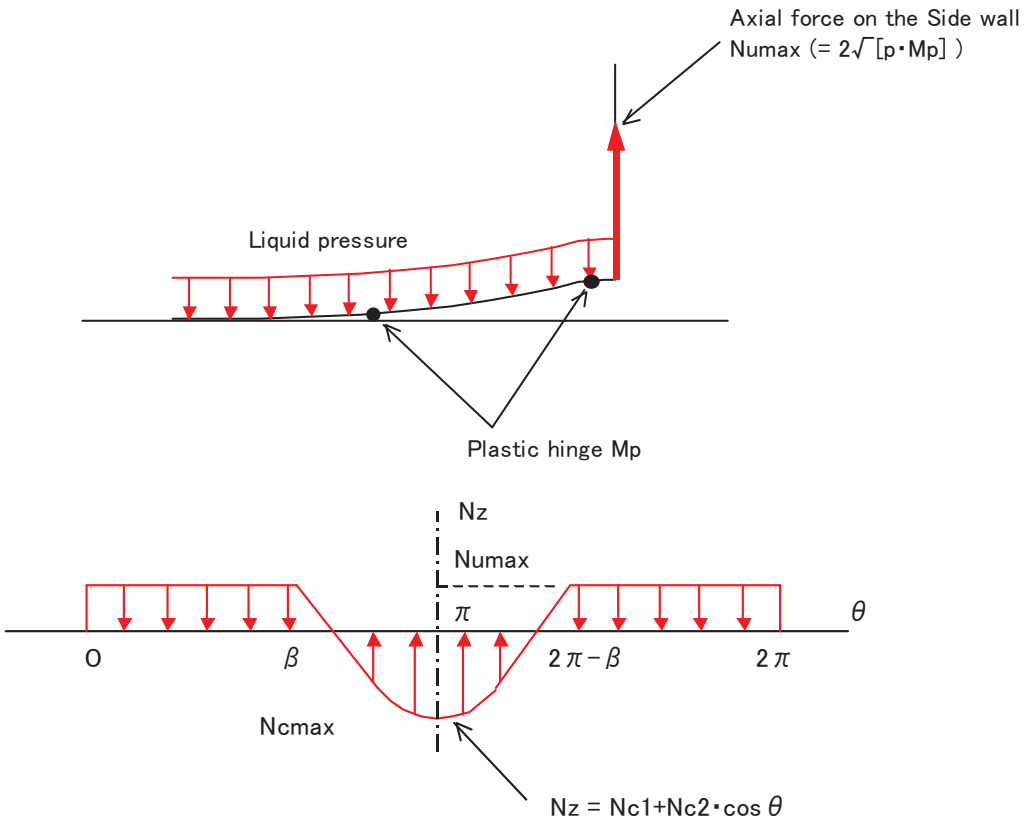

FIGURE 2-5: AXIAL FORCE IN SIDEWALL OF WOZNIAK MITCHELL MODEL [23]

Kobayashi, Ishida Model

Kobayashi and Ishida et al. proposed a method for estimating a axial force along a sidewall based on the assumption that the vertical axial force followed distribution as shown in Figure 2-6. Their theory was developed by:

- modeling the bottom plate as a beam and considering a tensile force in area of uplift in the bottom plate,
- confirming by undertaking a small scale (1m radius) tilt test,

They expanded their theory to dynamic rocking analysis.

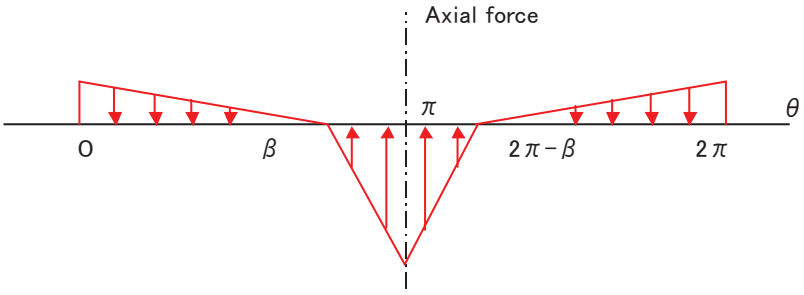

FIGURE 2-6: AXIAL FORCE IN SIDEWALL OF KOBAYSHI & ISHIDA MODEL [24]

The Kobayshi and Ishida's analytical studies of uplift behavior had been developed with an innovative geometric non-linearity, material yielding, a membrane force in a bottom plate, flexibility of foundation, effects of dynamic shaking, etc.

2-2-3 Previous studies regarding rocking response and dynamic pressure

By focusing on a phenomenon of rocking of tanks due to an earthquake, Taniguchi et al. [25-28] investigated the interaction between the rocking motion of a tank and the effective mass of fluid being rocked and the its inertia, which effects on oscillation of a tank.

Taniguchi and Segawa [29], Taniguchi and Sirasaki [30] focused on the dynamic pressure induced by uplift of a bottom plate and proposed a theoretical model based on the assumption of a rigid sidewall and bottom plate. In that fundamental study, it was revealed that the uplift behavior under dynamic cyclic loading has the possibility of reducing the dynamic pressure induced by translation of tank compared to no-uplift (i.e. fixed base) conditions which are generally used for seismic design of most tanks.

Taniguchi and Katayama [31] considered a model of a cylindrical tank with partial uplift of a bottom plate by assuming that it consists of a set of thin rectangular tanks. By using of this model, they established the theoretical equations of the effective mass of fluid for rocking

motion, rocking-bulging interaction and effective moment inertia of fluid for rocking motion, and their centroid.

Taniguchi and Okui [32], [33] proposed a model for estimating an angular acceleration of a bottom plate due to horizontal acceleration. The angular acceleration is one of principal factors for magnitude of the dynamic pressure induced by uplift of a bottom plate. In this model, the response acceleration and the base shear under uplift condition are also obtained. D'Amico at al. [34] improved Taniguchi and Okui's model for increasing the accuracy by investigating the effectiveness of terms of original model and modifying the model.

Nakashima [35] developed an FE analysis model of tanks by applying a semi-analytical finite ring element. This model consists of shell elements for a sidewall, non-liner ring elements for a bottom plate and spring elements for under a bottom plate. He performed static finite displacement analysis by the model for estimating amount of uplift of the bottom plate under a rocking motion. Then verified an uplift mechanism and related physical quantity, and examined reliability of current seismic design guidelines and suggested the items to be considered.

TABLE 2-1: ESTIMATION OF ANGULAR ACCELERATION [32]

表 3.2.2 解析条件
Analysis conditions

Analysis conditions	Uplift conditions	Ratio of uplift area	Amplification ratio of response acceleration
解析条件	浮き上がりの有無	浮き上がり範囲の割合	加速度応答倍率
Case1	浮き上がり無し	0%	2.417
Case2	No uplift	1～2%	2.417
Case3	浮き上がる	1～2%	1.612
Case4	Uplift	10%	2.417

表 4.1.1 解析結果のまとめ
Summary of analysis result

		Angular acceleration	Absolute maximum response acceleration of the tank bulging motion	Base shear
		角加速度	バルジング絶対応答加速度	ベースシアー
	Target values (1a), (1b) and (2)	Rad/s²	m/s²	N
Hayashi らの	目標値(1a) : Rigid Stiffener :	0.016	2.165	9.642E+07
解析結果	目標値(1b) : Higher Stiffener	0.027	2.163	8.820E+07
Result of research by Hayashi et al.	目標値(2) : Basic Stiffener	0.041	2.426	8.420E+07
	Case1	0.000	4.101	1.707E+08
本研究の	Case2	0.049～0.058	4.009～4.030	(1.518～1.558)+08
解析結果	Case3	0.091～0.097	2.582～2.604	(8.336～8.745)E+07
Result of the study	Case4	0.103	3.833	1.117E+08

REFERENCES

[1] Housner, G. W., 1957, “Dynamic Pressure on Accelerated Fluid Containers,” Bulletin of the Seismological Society of America, Vol. 47, pp. 15-35.

[2] Jacobsen L. S., 1949, “Impulsive Hydrodynamics of Fluid Inside a Cylindrical Tank and of Fluid Surrounding a Cylindrical Pier”, Bulletin of the Seismological Society of America.

[3] Senda K., Nakagawa K., 1954, “On the Vibration of an Elevated Water Tank (I)”, The 4-th Japan National Congress of Applied Mechanics, pp. 247-264.

[4] Baron M. L., Shalak R., 1963, “Free Vibration of Fluid – Filled Cylindrical Shells”, American Society of Civil Engineers, Vol. 128, Part I.

[5] Bauer H. F., 1963, “Theory of Liquid Sloshing in Compartmented Cylindrical Tanks Due to Bending Excitation”, AIAA Journal, Vol. 1, No. 7.

[6] 柴田碧、曽我部潔, 1971, “流体・弾性系の固有値解析に対する一提案”, 日本鋼構造協会第 5 回大会研究発表論文集.

[7] Edwards N. W., 1969, “A Procedure for the Dynamic Analysis of Thin Walled Cylindrical Liquid Storage Tanks Subjected to Lateral Ground Motions”, US Government Research Literatures, Contract No. 4504.

[8] Coale C. W., Nagano M., 1965 ,“Axisymmetric Modes of an Elastic Cylindrical – Hemispherical Tank Partially Filled with a Liquid”, Symposium on Structural Dynamics and Aeroelasticity Boston,MA,U.S.A.

[9] Guyan R. J., Ujihara B. H., Welch P. W.,1968, “ Hydro - elastic Analysis of Axisymmetric Systems by a Finite Element Method”, AFFDL TR-68–150, Proc. 2nd Conf Matrix Methods in Structural Mechanics, Wright Patterson Air Force Base, pp. 1165–1203.

[10] Palmer J. H., Asher G. W.,1965, “Calculation of Axisymmetric Longitudinal Modes for Fluid-Elastic Tank – Ullage Gas Systems and Comparison with Model Test Results”, Symposium on Structural Dynamics and Aeroelasticity Boston, MA, U.S.A.

[11] Veletsos A. S., Yang J. Y., 1976, “Dynamics of Fixed-Base Liquid-Storage Tanks”, U.S.-Japan Seminar for Earthquake Engineering Research with Emphasis on Life Line System, Tokyo, pp.317 – 341.

[12] 岡田綻夫、坂井藤一、迫田治行、多田文三, 1975（第 1 報）, 1976（続報）, “有限要素法による大型液体タンクの地震応答解析 2”, （第 1 報）川崎重工技報、No. 59, pp. 69 – 74, （続報）川崎重工技報、No. 61、pp. 120 – 125

[13] 坂井藤一、迫田治行、小川浩, 1979, “石油タンクの耐震設計法、川崎重工技報、No. 71、pp. 52 – 59.

[14] 浅井修、内藤潔、石田和雄、越智義夫、小林信之: 固定屋根を有する円筒液体タンクの耐震設計（第 1 報）圧力技術、Vol. 17、No. 3、pp. 113 – 120、1979.3

[15] 日本瓦斯協会, 1979, “ガス工作物設置基準調査について－昭和 54 年度　ガス導管、有水式ガスホルダー及び LNG 地上式貯槽に関する調査報告書－”.

[16] 日本ガス協会, 2002, “ LNG 地上式貯槽指針”, p.84.
[17] Tani, S. and Hori, N., 1982. “Dynamic Interaction of Fluid-Tank-Soil System by Ryleigh-Rits Method”, 6th Japan Earthquake Engineering Symposium, JAEE.
[18] Clough, D. P., 1977, “Experimental Evaluation of Seismic Design Methods for Broad Cylindrical Tanks”, Univ. of California, EERC Rep., No. UCB/EERC-77/10.
[19] Isoe, A., 1994, “Investigation on the Uplift and Slip Behavior of Flat-Bottom Cylindrical Shell Tank during Earthquake”, Ph. D. thesis, University of Tokyo (in Japanese).
[20] Maekawa, A., et al., 2006, “Nonlinear Vibration Response of a Cylindrical Water Storage Tank Caused by Coupling Effect between Beam-Type Vibration and Oval-Type Vibrations Part 1- Vibration Experiment”, Proceedings of ASME PVP Conference, PVP2006-ICPVT-11-93261.
[21] Maekawa, A., et al., 2006, “Nonlinear Vibration Response of a Cylindrical Water Storage Tank Caused by Coupling Effect between Beam-Type Vibration and Oval-Type Vibrations Part 2- Simulation” ,Proceedings of ASME PVP Conference, PVP2006-ICPVT-11-93263.
[22] Maekawa A., Fujita K., Suzuki M., 2007, “Seismic Response Reduction Caused by Coupling between Beam-Type and Oval-Type Vibrations of a Cylindrical Water Storage Tank under Large Excitation”, Proceedings of ASME PVP Conference, PVP2007-26465.
[23] Wozniak, R. S. and Mitchell, W. W., 1978, “Basis of Seismic Design Provisions for Welded Steel Oil Storage Tanks”, API Refining Dept. 43rd Midyear Meeting, Toronto.
[24] 小林信之、石田和雄、他, 1984, “アンカーの無い円筒タンクのロッキングに対する耐震解析法”, 機械学会論文集, 50巻, 451, 453号.
[25] Taniguchi, T., 2004, “Rocking Behavior of Unanchored Flat-Bottom Cylindrical Shell Tanks under Action of Horizontal Base Excitation,” Engineering Structure, 26, pp. 415-426.
[26] Taniguchi, T., 2005, “Rocking Mechanics of Flat-Bottom Cylindrical Shell Model Tanks Subjected to Harmonic Excitation,” Journal of Pressure Vessel Technology, Vol. 127, pp. 373-386.
[27] Taniguchi T., Segawa T., 2009, “Effective mass of Fluid for Rocking Motion of Flat-Bottom Cylindrical Tanks”, Proceedings of ASME PVP Conference, PVP2009-77580.
[28] Taniguchi T., 2010, “Effective mass of Fluid for Rocking-Bulging Interaction of Rigid Rectangular Tank whose Bottom Plate Rectilineary Uplifts, Proceedings of ASME PVP Conference, PVP2010-25374.
[29] Taniguchi T., Segawa T., 2008, “Fluid Pressure on Rectangular Tank Consisting of Rigid Side Walls and Rectilinearly Deforming Bottom Plate due to Uplift Motion”, Proceedings of ASME PVP Conference, PVP2008-61166.
[30] Taniguchi, T. and Shirasaki, T., 2013, “Approximation of Fluid Pressure on the Cylindrical Tanks in Rock With the Crescent-Like Uplift Part in the Bottom Plate by Radially Sliced Tank Model”, Proc. Seismic Engineering, ASME, Paper No. PVP2013-97306.

[31] Taniguchi, T. and Katayama, Y., 2014, “Mass of Fluid Contribution to Rocking Motion of Cylindrical Tanks With Partial Uplift of Bottom Plate”, Proc. Seismic Engineering, ASME, Paper No. PVP2014-28634.

[32] Taniguchi T., Okui D., 2014, “A Case Study of Evaluation of Tank Rock Motion with Simplified Analysis Procedure”, Proceedings of ASME PVP Conference, PVP2014-28635.

[33] 奥井大輔, 2013, “応答スペクトルを用いた平底円筒貯槽の底板浮き上がり現象を特徴付ける物理量の簡易算定方法に関する検討”, 鳥取大学大学院工学研究科博士前期課程　社会基盤工学専攻土木工学コース　修士論文, p.39.

[34] D’Amico M., Taniguchi, T., Nakashima T., 2017, “Simplified Analysis of the Rocking Motion of A Cylindrical Tank Focusing on the Role of Dynamical Forces Involved in Rocking-Bulging”, Proceedings of ASME PVP Conference, PVP2017-65442.

[35] 中島照浩, 2012, “平底円筒貯槽の地震時浮上り挙動の半解析的有限要素法に基づく静的有限変位解析に関する研究”, 鳥取大学大学院工学研究科博士後期課程　社会基盤工学専攻土木工学コース　博士論文, pp.55-128.

CHAPTER 3

DYNAMIC RESPONSE BEHAVIOR DURING EARTHQUAKES

CHAPTER 3
DYNAMIC RESPONSE BEHAVIOR DURING EARTHQUAKES

In this chapter, the fluid-structural coupled 3-dimensional time-history FE analysis was performed for three different structural conditions with three seismic waves and an equivalent static condition (constantly increasing horizontal acceleration up to the maximum value), hereinafter 'constant horizontal acceleration case'. This analysis was conducted for researching dynamic behavior including uplift of a bottom plate during earthquakes. The findings are applied for developing mathematical models used in the proposed seismic design procedure specified in section 3-3, which is used for design of a connection between a bottom plate and a sidewall of tanks.

3-1 TIME-HISTORY FE ANALYSIS MODEL OF TANK

3-1-1 Specifications of the tank and FE analysis model

Figure 3-1 shows dimensions of a LNG tank used in the EE analysis. The analytical conditions were determined based on the maximum design liquid level of the tank. The tank has a T shaped top stiffener ring and four plate type stiffener rings on the sidewall.

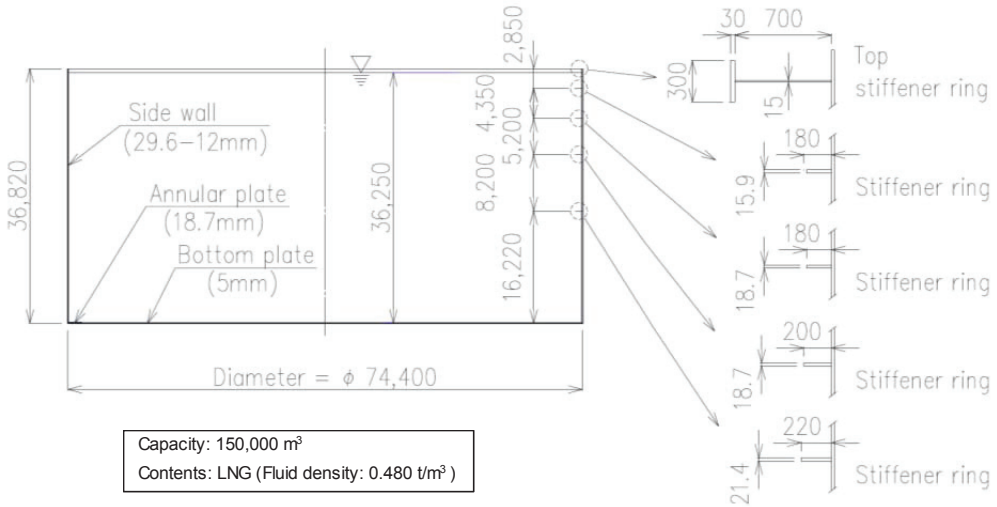

FIGURE 3-1: TANK CONFIGURATION

Figure 3-2 shows the FE analysis model used in the time-history FE analysis. The features of this model are as follows.

(1) Explicit method for structure and fluid physical quantity was applied.

(2) Symmetrical half model with respect to 0 – 180 degrees center line, which is oscillation direction of seismic wave, was established for reducing the calculation duration.

(3) Non-linear and large deformation model was established. In this model, contact element was installed between the bottom plate and the bottom insulation. (Friction coefficient: 0.5. This value is experientially used for tank design)

(4) An arbitrary lagrangian eulerian (ALE) method using Euler elements was adopted for fluid elements.

(5) A penalty-coupling method was adopted for the fluid-structure interface.

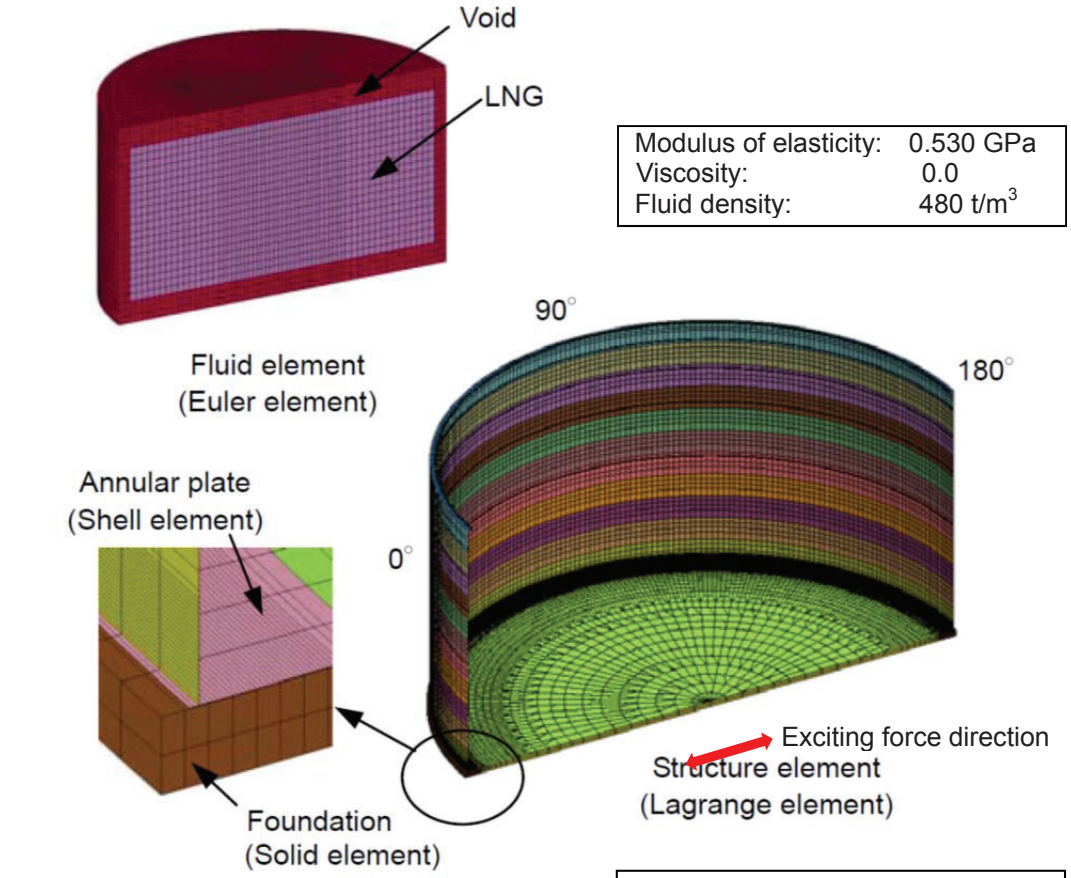

FIGURE 3-2: TIME-HISTORY NUMERICAL MODEL

An explicit method has the possibility of accumulating numerical errors, because physical values (liquid pressure, displacement, stress and so on) of each time step are calculated from the values of previous time step. In this paper, general purpose program LS-DYNA developed by Livermore Software Technology Corporation was used. The applicability and calculation accuracy of this model were verified by comparison with tilt test result and dynamic shaking test results. [1] (Refer to APPENDIX A). In addition, finer mesh elements were rearranged at the annular plate and the bottom of the sidewall for obtaining a more exact result of displacement and stress.

3-1-2 Applied seismic wave

The following three seismic acceleration waves were applied to confirm influences of difference of each of the seismic waves on tank response. The intervals of acceleration data (unit is gravity acceleration 'G') are 0.01 seconds for Artificial Seismic Wave and 0.02 seconds for other two waves and applied to the center of tank foundation. Since the natural period of subject tank is 0.498 seconds, interval of the data is sufficient for response analysis. Each wave has different acceleration level, however the characteristic is similar. Only EL Centro NS includes a component like a pulsive wave around 2 seconds.

(1) Artificial Seismic Wave (Figure 3-3) was generated from the design response acceleration spectrum shown in Figure 3-6.
(2) Taft EW (Figure 3-4 [2])
(3) EL Centro NS (Figure 3-5 [2,3])

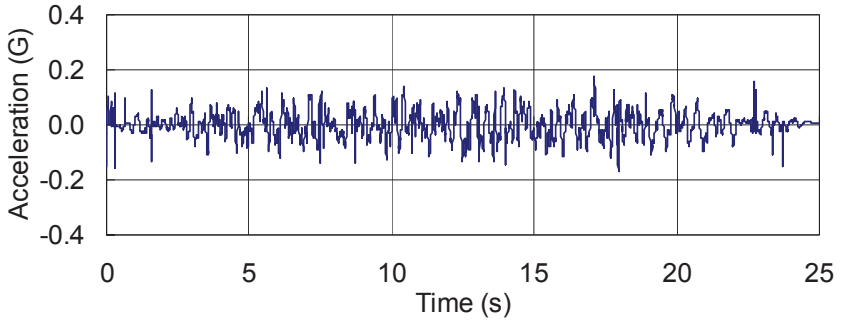

FIGURE 3-3: ARTIFICIAL SEISMIC WAVE

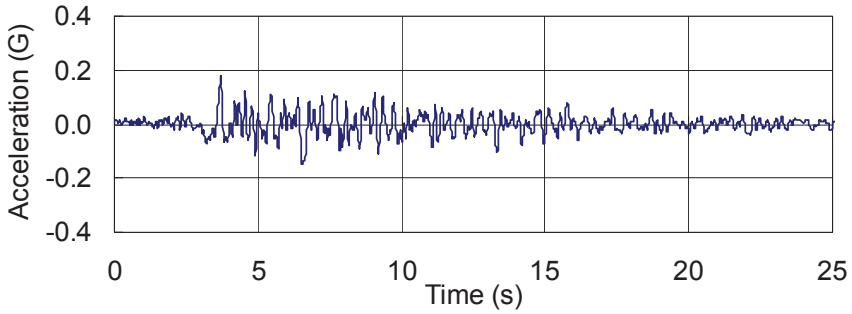

FIGURE 3-4: SEISMIC WAVE OF TAFT EW

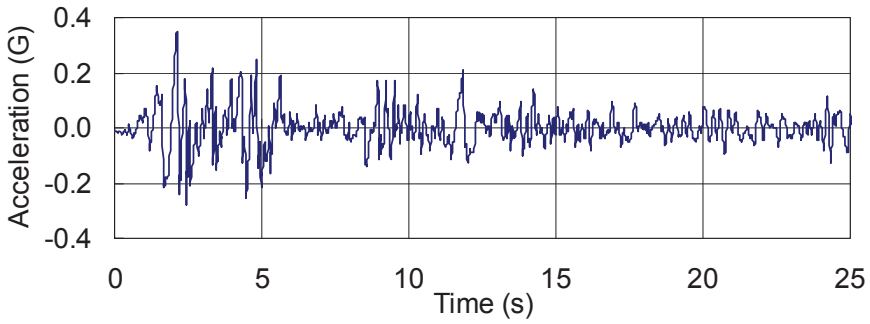

FIGURE 3-5: SEISMIC WAVE OF EL CENTRO NS

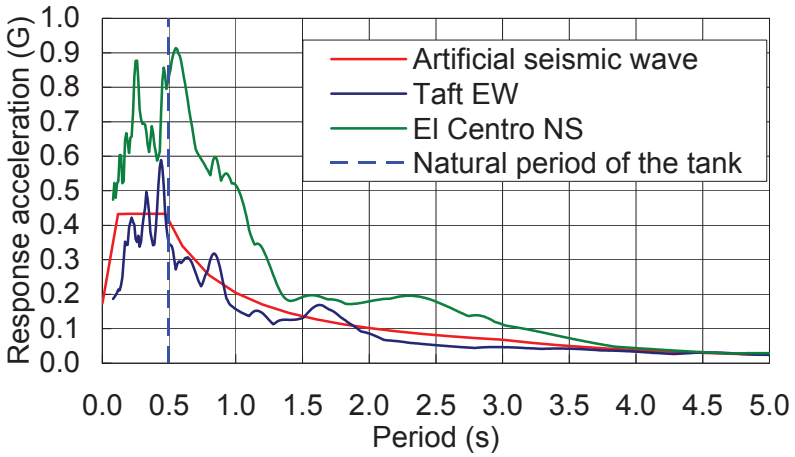

FIGURE 3-6: RESPONSE ACCELERATION SPECTRUM

TABLE 3-1: RESPONSE ACCELERATION OF THE TANK

(G)

	Artificial seismic wave	Taft EW	EL Centro NS
	0.4094	0.3467	0.8343
Ratio	1.00	0.85	2.04

Figure 3-6 shows the response acceleration spectrum of each seismic wave and the natural period of the tank (0.498 s) that was obtained from an eigenvalue analysis under no-uplift conditions. Short period seismic wave component is dominant in each wave. As shown in Table 3-1, the response acceleration of the tank by Artificial Seismic Wave, Taft EW and EL Centro are 0.4094 G, 0.3467 G and 0.8343 G, respectively. It is expected to highlight the influence of different acceleration magnitudes and characteristics of seismic waves on tank response by applying Taft EW and EL Centro NS.

3-1-3 Analysis case

Table 3-2 shows summary of the analysis cases. Case 11 and Case 21 are basic models for no-uplift and uplift conditions, respectively. From the results of these cases, difference of behavior between no-uplift and uplift conditions is confirmed. Case 21R is the model for studying effects of undulating deformation at the top of the sidewall on tank response. All stiffeners of this model are changed to a top ring type with reinforced dimension as shown in Figure 1-13 of Chapter 1. In addition, its modulus elasticity is increased 100 times of steel property. By reducing sidewall deformation with rigid stiffeners, find out the differences of

behavior with that of the basic uplift model. Cases 31 (Taft EW case) and 32 (EL Centro NS case) are the cases applied to verify influences of the magnitude and characteristics of input waves on tank response.

TABLE 3-2: ANALYSIS CASES

	Uplift	Stiffener stiffness	Applied seismic wave
Case 11	No-uplift	Basic stiffener stiffness	Artificial seismic wave
Case 21	Uplift	Basic stiffener stiffness	Artificial seismic wave
Case21R	Uplift	Rigid stiffener stiffness	Artificial seismic wave
Case 31	Uplift	Basic stiffener stiffness	Taft EW
Case 32	Uplift	Basic stiffener stiffness	EL Centro NS
Case 41	Uplift	Basic stiffener stiffness	Constant horizontal acceleration

Additionally, the constant horizontal acceleration case (Case 41) is selected. The magnitude of its acceleration is determined so that base shear becomes equal to that of Case 11. Further, the acceleration is loaded on the tank taking enough time (in this case 5.3 seconds) so as to be the same situation as statically loading. This case is expected to highlight differences of tank response between a static analysis with the maximum dynamic pressure and a historical analysis with oscillating loading of dynamic pressure.

3-2 ANALYSIS RESULTS

3-2-1 Response acceleration

Figure 3-7 shows example results of the response acceleration at the point of 2/3 height of the sidewall whose value corresponds to the maximum acceleration of the tank.

Figure 3-8 shows the distribution of the response acceleration along the height of the sidewall.

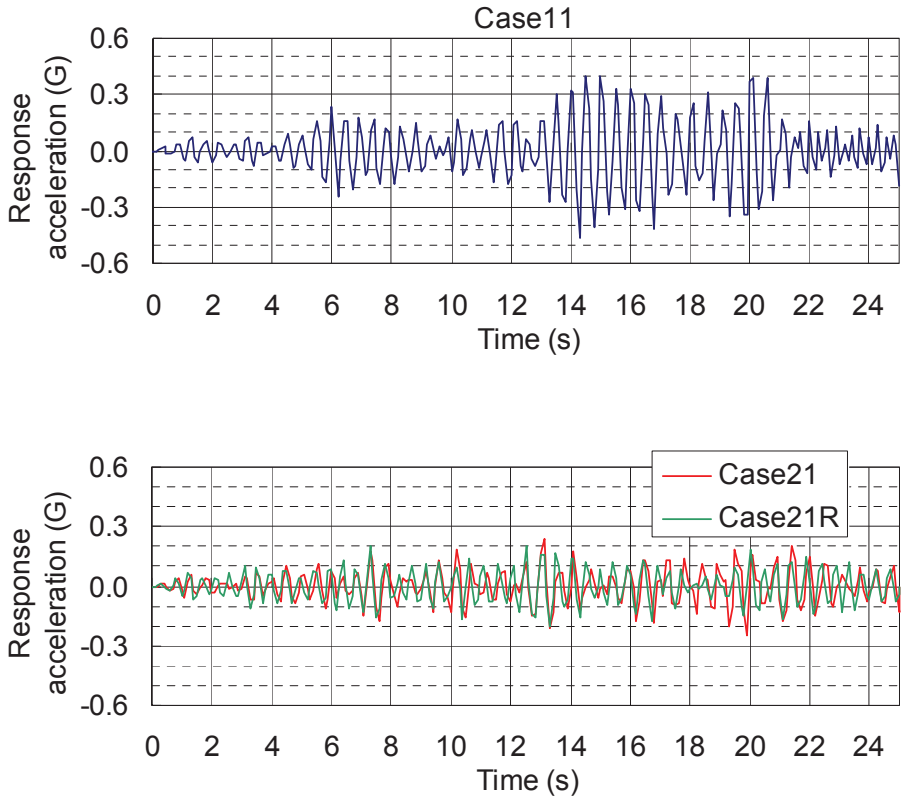

FIGURE 3-7: EXAMPLE OF THE MAXIMUM RESPONSE ACCELERATION AT THE SIDEWALL (at the point of 2/3 height)

According to the distribution of Cases 21 and 21R in Figure 3-8, as the stiffness of stiffeners increase, the acceleration at the upper part of the sidewall becomes smaller, while the acceleration at the lower part grow larger.

Table 3-3 shows the maximum and average (arithmetic mean) of the response acceleration in the sidewall of each case and the ratio of those of average against Case 11 and Case 21. The maximum response acceleration of Case 11 (0.4655) was 13.7% larger than that obtained from the response acceleration spectrum shown in Figure 3-6. While the response acceleration of uplift case (Case 21) was about half of that of Case 11. This implies that at tank response under

uplift conditions clearly differs from that under no-uplift conditions. However, the stiffness of the stiffeners has the relationship with the response acceleration. As their stiffness increase, the average response acceleration becomes larger. The ratio of the average response acceleration of Case 31 and 32 against Case 21 are 0.900 and 2.099, respectively, while the ratio obtained from natural period and the response acceleration spectrum shown in Table 3-1 (no-uplift condition) are 0.85 and 2.04. Variability ratio of response acceleration against difference seismic waves seems to maintain the same proportion when uplift occurs.

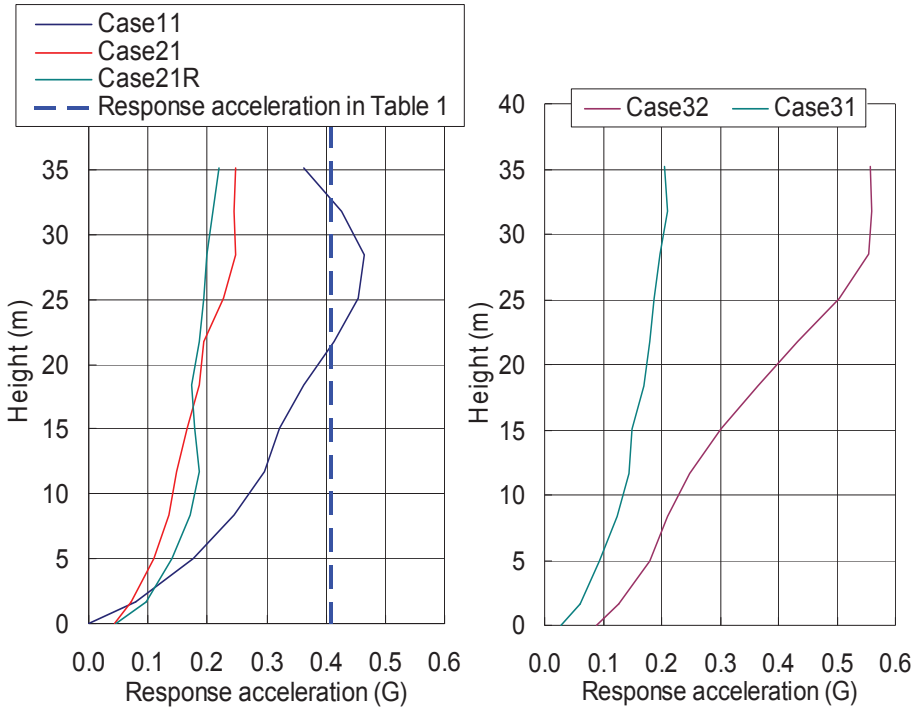

FIGURE 3-8: THE DISTRIBUTION OF THE RESPONSE ACCELERATION AT THE SIDEWALL

TABLE 3-3: THE RESPONSE ACCELERATION

(G)

	Case 11	Case 21	Case 21R	Case 31	Case 32
Max.	0.4655	0.2469	0.2003	0.1975	0.5535
Average	0.2437	0.1246	0.1910	0.1121	0.2615
Ratio of average against Case 11	1.000	0.511	0.784	0.460	1.073
Ratio of average against Case 21	1.956	1.000	1.533	0.900	2.099

3-2-2 Base shear

Figure 3-9 shows the results of the base shear (total shearing force at the bottom plate caused by the seismic force) of Case 11 and Case 21. The magnitude of the base shear under the no-uplift conditions based on Housner's [4] and Veletsos's theory [5] are also plotted on the graphs.

Table 3-4 shows the maximum of the base shear of each case and the ratio of those against Case 11 and Case 21. The magnitude of the base shear of the uplift case (Case 21) is about 40% of that of the no-uplift case (Case 11). However this ratio is smaller than that of the acceleration response, both response result show the same trend. These results indicate when uplift occurs, tank response considerably decreases.

The stiffness of the stiffeners also has the relationship with the base shear. According to the result of Case 21 and Case 21R, as the stiffness of the stiffeners increase (Case 21R), the base shear becomes larger. The ratio of the magnitude of the maximum base shear of Case 31 (Taft EW) and 32 (EL Centro NS) against Case 21 (Artificial wave) is 0.937 and 1.638. While the ratio of that of the response acceleration shown in Table 3-1, which is obtained from a natural period for no-uplift condition and the response acceleration spectrum, are 0.85 and 2.04. It implies that the trend of amplification of tank response with uplift condition is almost the same as that with no-uplift condition.

The graph of Case 11 in Figure 3-9 shows that the maximum base shear of the no-uplift case was larger than that of Housner's theory (170MN) or Veletsos's theory (144MN). This difference seems to be the influence of undulating deformation at the top of the sidewall which appears mainly after 14 seconds (this influence on tank response is discussed in the section 3-2-3). On the other hand, the maximum base shear up to 14 seconds specified in Table 3-4 is rather close to the value of Housner's or Veletsos's theory.

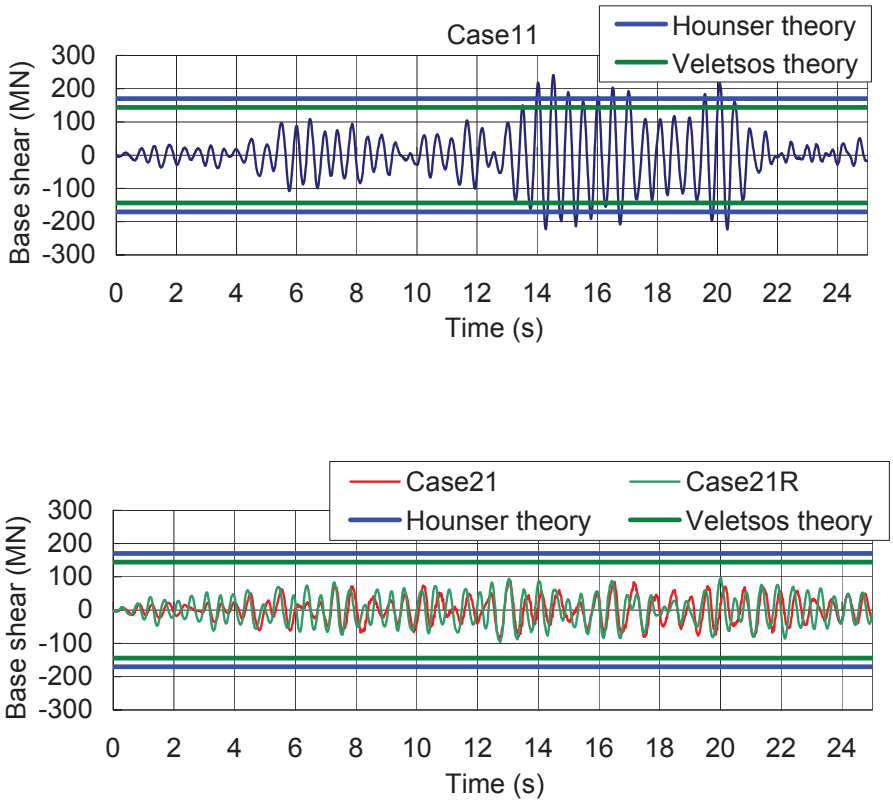

FIGURE 3-9: EXAMPLE OF THE BASE SHEAR

TABLE 3-4: THE MAXIMUM BASE SHEAR

(MN)

	Case 11	Case 11 (up to 14s)	Case 21	Case 21R	Case 31	Case 32	Case 41
	241.6	161.9	87.9	97.3	82.4	144.0	170.9
Ratio against Case 11	1.000	0.670	0.364	0.403	0.341	0.596	0.707
Ratio against Case 21	2.870	1.843	1.000	1.107	0.937	1.638	1.945
Housner (no-uplift)	170	170	170	170	144	346	170
Veletsos (no-uplift)	144	144	144	144	122	292	144

3-2-3 Dynamic pressure

Figure 3-10-1 to 3-10-3 show distribution of the maximum and minimum values of fluid gauge pressure (in MPaG) acting on the sidewall of each case. In each graph, static pressure and theoretical dynamic pressure under no-uplift conditions obtained from the theoretical equations of Housner [4] and Veletsos and Yang [5] are also plotted. The values of Housner's theory are based on the assumption of a rigid sidewall, while those of Veletsos's theory includes an influence of sidewall flexibility.

The dynamic pressure of Case 11 is larger than the theoretical pressures. This tendency corresponds to the base shear of Case 11. An actual tank response under oscillating loading has some difference from that based on theory, since the theoretical model is based on an ideal assumption. In the FE analysis under oscillating loading, undulating deformation at the top of the sidewall appeared which is not treated in the theoretical model. When this mode increases, the dynamic pressure increases.

To highlight this tendency, additional analysis of Case 11', whose model has smaller sized stiffeners, was performed. Figure 3-11 shows the result of the sidewall deformation and the dynamic pressure at the 90 degrees direction as shown in Figure 3-2. According to the theoretical equations proposed by Housner [4] and Veletsos and Yang [5], no dynamic pressure appears at this direction. While in the FE analysis, the undulating deformation and the dynamic pressure appeared. This pressure increased after 14 seconds in proportion to the progress of the undulating deformation. Therefore, this pressure is considered to be induced by the undulation deformation. For confirming this consideration, the dynamic pressures of Case 11*, which is calculated by the values at 0° or 180° minus the values at 90°, are plotted in Figure 3-10-1. These pressures are expected the dynamic pressure without the effect of the undulation deformation. The plotted data shows good agreement with the values of theoretical equation. Therefore, exceed pressure component than theoretical pressure is considered to be caused by the undulating deformation.

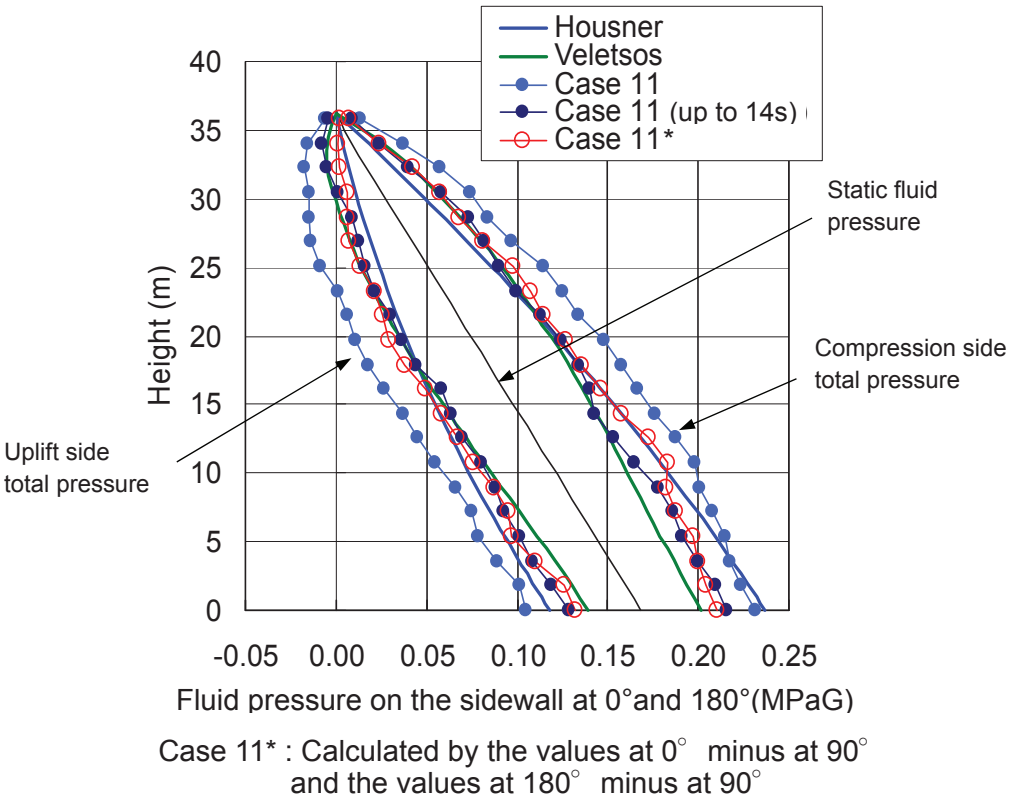

FIGURE 3-10-1: THE DYNAMIC PRESSURE ON THE SIDEWALL FOR CASE 11

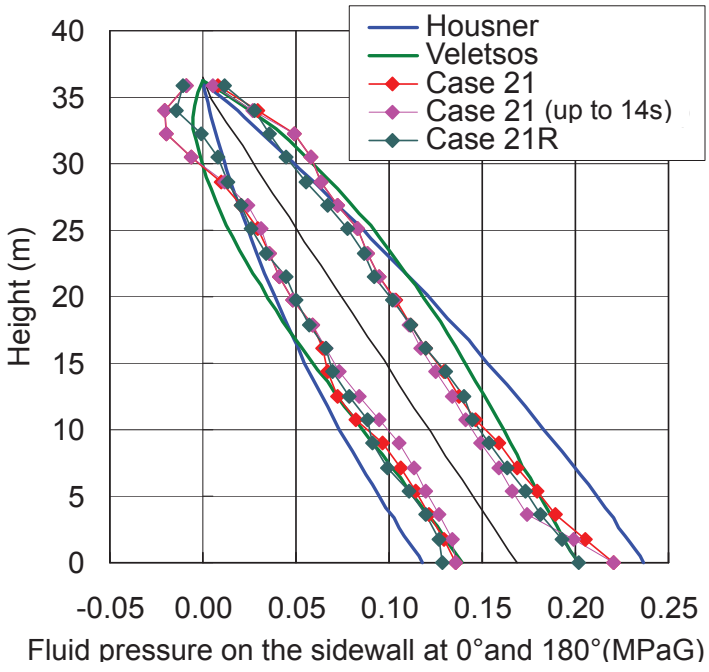

FIGURE 3-10-2: THE DYNAMIC PRESSURE ON THE SIDEWALL FOR CASE 21 AND CASE 21R

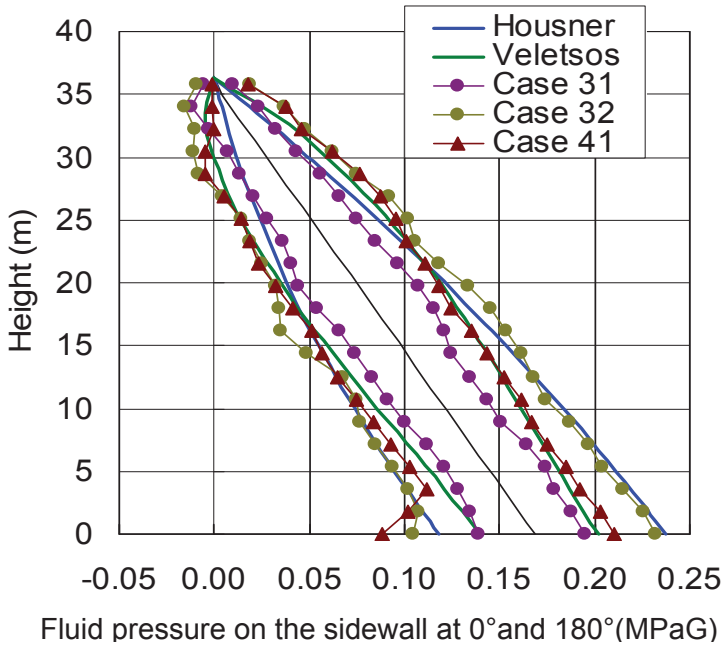

FIGURE 3-10-3: THE DYNAMIC PRESSURE ON THE SIDEWALL FOR CASE 31, CASE 32 AND CASE 41

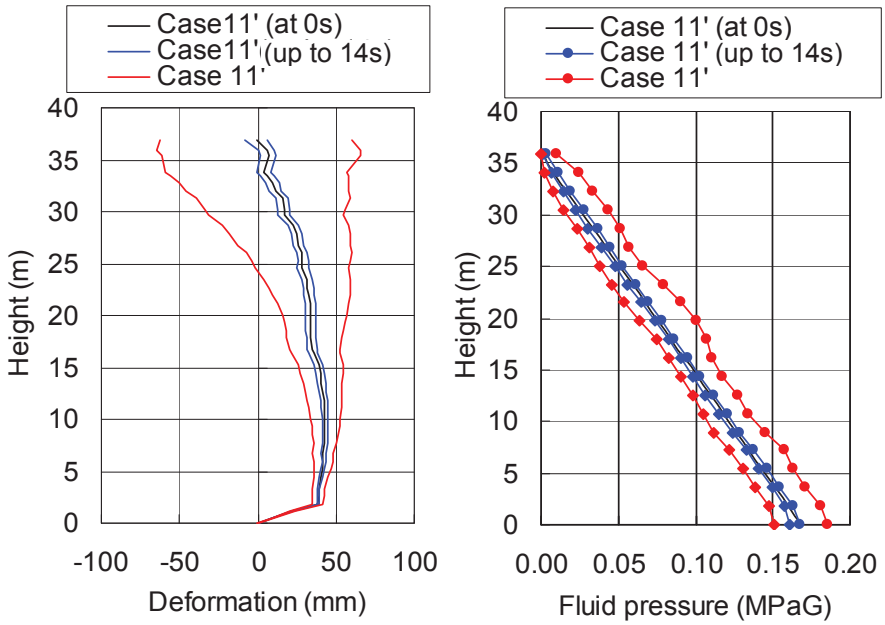

FIGURE 3-11: DEFORMATION AND THE DYNAMIC PRESSURE OF THE SIDEWALL AT 90 °DIRECTION

Figure 3-10-2 shows the result of the dynamic pressure of Case 21 and Case 21 (up to 14s) (before undulation deformation appears). Form the result it is considered that the effect of undulation deformation on dynamic pressure does not appear under uplift conditions, because the values of the dynamic pressure of Case 21 and Case 21(up to 14s) are almost the same value.

The comparison of the result of Case 21 with that of 21R implies the stiffness of stiffeners also seems to have the relationship with dynamic pressure caused by oscillation loading. As the stiffness of the stiffeners varied, the distribution of the dynamic pressure slightly changed. The results of Case 31 and 32 in Figure 3-10-3, shows that the magnitude of dynamic pressure also changed depending on the magnitude of response acceleration.

3-2-4 Uplift height

Figure 3-12 shows the uplift height of the tank bottom plate at 180° for each case.

The pattern of the response acceleration (Figure 3-7) is similar to the pattern of the base shear (Figure 3-9). However, the pattern of the uplift height response (Figure 3-13) does not follow the pattern of the response acceleration.

This phenomenon is assumed to be caused by two factors. The first factor is the magnitude of the acceleration response of the tank. (as the acceleration of the tank becomes larger, then the base shear will become larger also.) The second factor is the undulation deformation at the top of the sidewall. If the out-of-round sidewall deformation is large, then the uplift will be large also. Both factors have different frequency as shown in Figure 3-13. In case both factors become large simultaneously as shown in Figure 3-13, the uplift becomes larger.

Since the frequency of undulation deformation differs from the natural period of the bulging mode of a tank, uplift occurs at unstable intervals. To confirm this assumption, the value obtained by Eq. (3-1) is introduced as an indication pointer, hereinafter called ‘contribution factor’.

Each graph in Figures 3-12 shows when uplift occurs the contribution factor also increases. Consequently, it is confirmed that the magnitude of deformation at the top of sidewall is one of the major factors of uplift height in the same way as the magnitude of tank response such as acceleration and base shear.

$$\text{Contribution factor} = \frac{\text{Base shear}}{\text{Max. Base shear}} \times \frac{\text{Sidewall deformation}}{\text{Max. sidewall deformation}} \qquad (3\text{-}1)$$

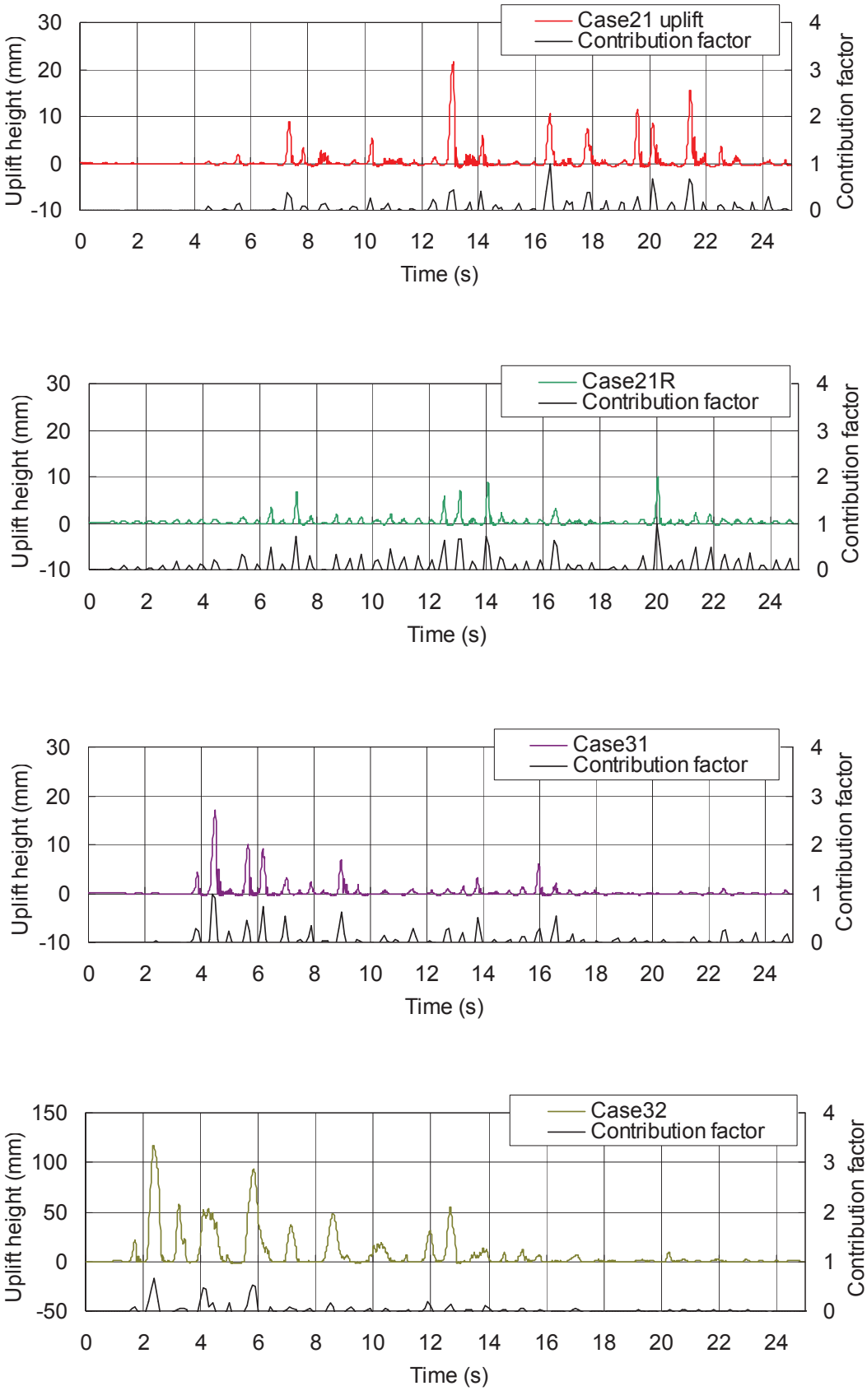

FIGURE 3-12: THE UPLIFT HEIGHT

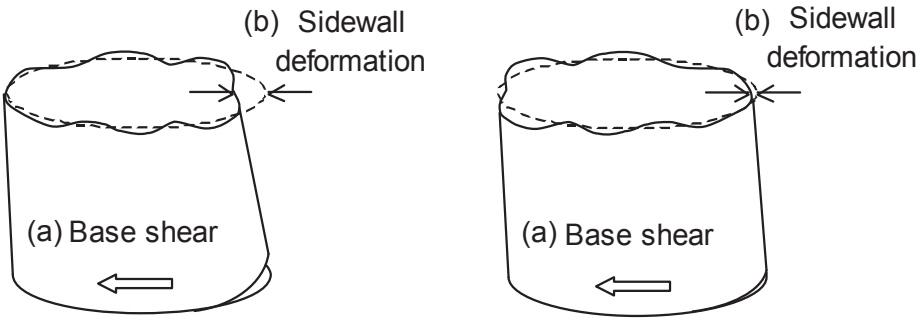

(a) Base shear : large
(b) Sidewall deformation : large
--> Uplift height : large

(a) Base shear : large
(b) Sidewall deformation : small
--> Uplift height : small

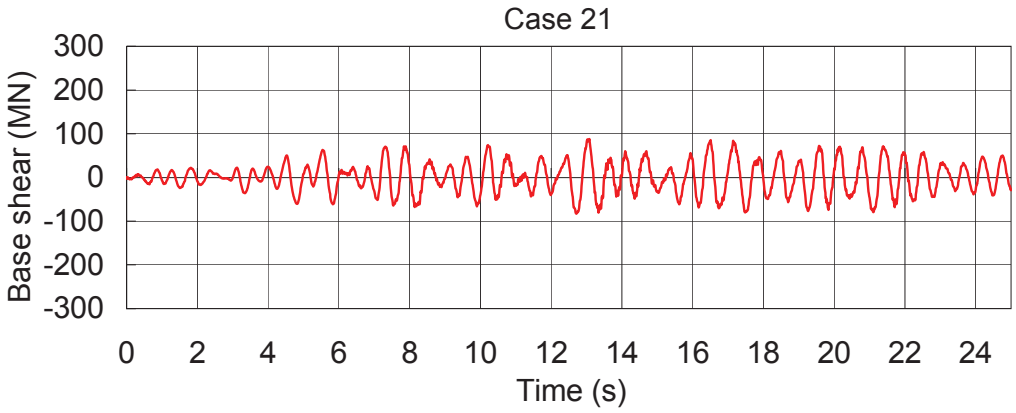

(a) Variation of base shear

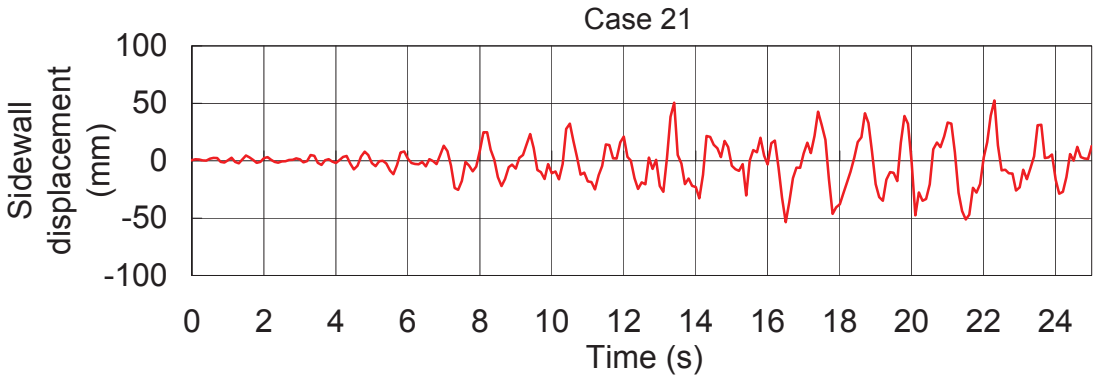

(b) Variation of sidewall displacement

FIGURE 3-13: SITUATION OF THE BASE SHEAR AND THE DEFORMATION

Table 3-5 shows the maximum uplift height of each case and the ratio of those against Case 21. It is important that the uplift result from Case 41, arising from the equivalent static loading of the dynamic pressure, is significantly larger than those of base case (Case 21). This demonstrates that the tank response under oscillating loading conditions is absolutely different from that of static conditions. From this viewpoint static tilt test is not equivalent to earthquake conditions.

The stiffness of the stiffeners also has the relationship with the uplift height. As the stiffness of the stiffeners increased, the uplift height becomes smaller. The ratio of the uplift height of Case 32 compared to Case 21 is in proportion to 2.58 times the ratio of the average response acceleration of Case 32 as described in Table 3-3. It demonstrates that the response acceleration is only one factor for the magnitude of uplift. As above specified, deformation at the top of the sidewall is considered another contributory factor.

TABLE 3-5: THE MAXIMUM UPLIFT HEIGHT

(mm)

	Case 21	Case 21R	Case 31	Case 32	Case 41
	21.6	9.9	16.9	116.8	215.8
Ratio	1.000	0.461	0.784	5.407	9.994

3-2-5 Uplift width and height

Figure 3-14 shows the relationship between uplift width of the bottom plate along the radial direction and uplift height at the bottom of sidewall for Cases 21, 32 and 41. Once small height uplift occurs, about 1m width of the tank bottom plate is instantly lifted. It seems to be an effect of thicker annular plate installed at periphery part of the bottom plate. Its width is 1900 mm, then, initial uplift width corresponds to about 55% of the annular plate width. After that, the uplift width gradually increases corresponding to increase in uplift height. The ratio between the uplift height and the width is within about 1:13 to 1:23 for the subject tank.

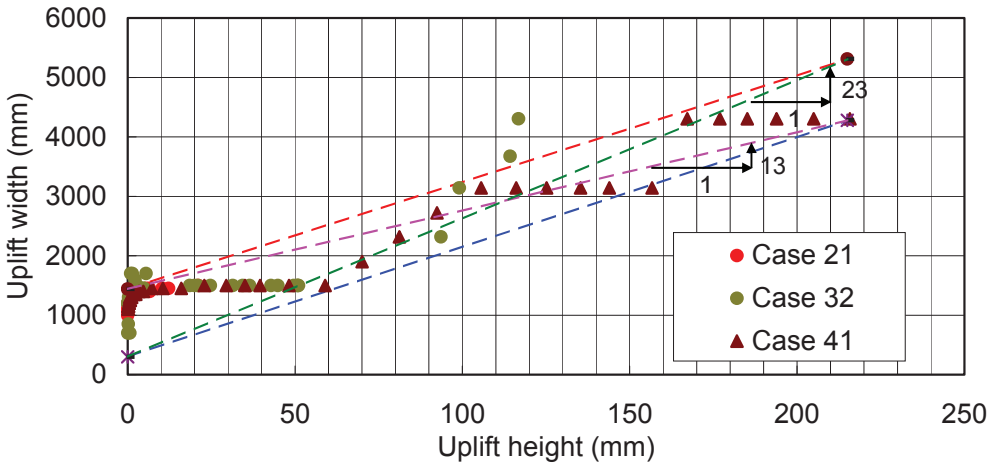

FIGURE 3-14: RELATIONSHIP OF UPLIFT HEIGHT AND UPLIFT WIDTH

The points of Case 32 at the height of 113.8 mm and 116.8 mm have a different trend than other points. These data are response during pulsive like wave period around 2 seconds. The relationship of uplift height and width is expected to change by characteristic of wave.

Figure 3-15 shows a color contour of uplift height and Figure 3-16 shows uplift height and width of the bottom plate at each direction of Case 41. The color of scale is adjusted so as to highlight the uplift area. These Figures indicate that the uplift starts at the area of beyond 50 degrees. The phenomenon of 'instantly uplift of bottom plate' shown in Figure 3-14 is also confirmed in Figure 3-16. According to the trend of lines of 50.3 degrees (before uplift) and 52.5 degrees (after uplift), when uplift occurs, the uplift width becomes more than 1 m instantly. This reason is considered that the effect of the thicker annular plate installed at periphery part of the bottom plate.

Figure 3-17 shows the deformation trend of the bottom of the sidewall at compression side along circumferential direction. Since the nominal in-plane shear stiffness of the sidewall is enough, the bottom of the sidewall seems to be rigid in the vertical direction. However, from a microscopic viewpoint, it deforms slightly in an arch shape up to the neutral axis, while it drops in the area around 0 degree.

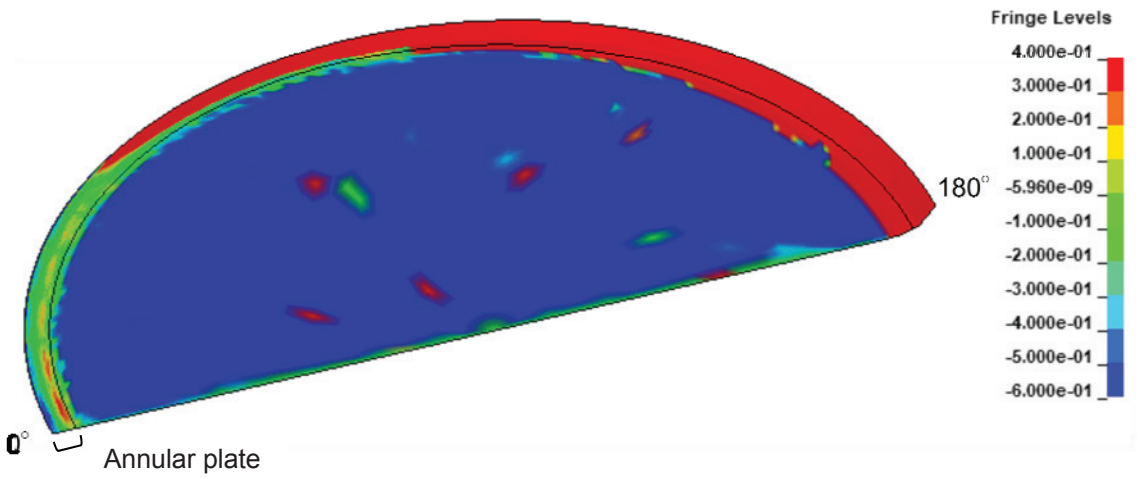

FIGURE 3-15: DISPLACEMENT OF TANK BOTTOM PLATE

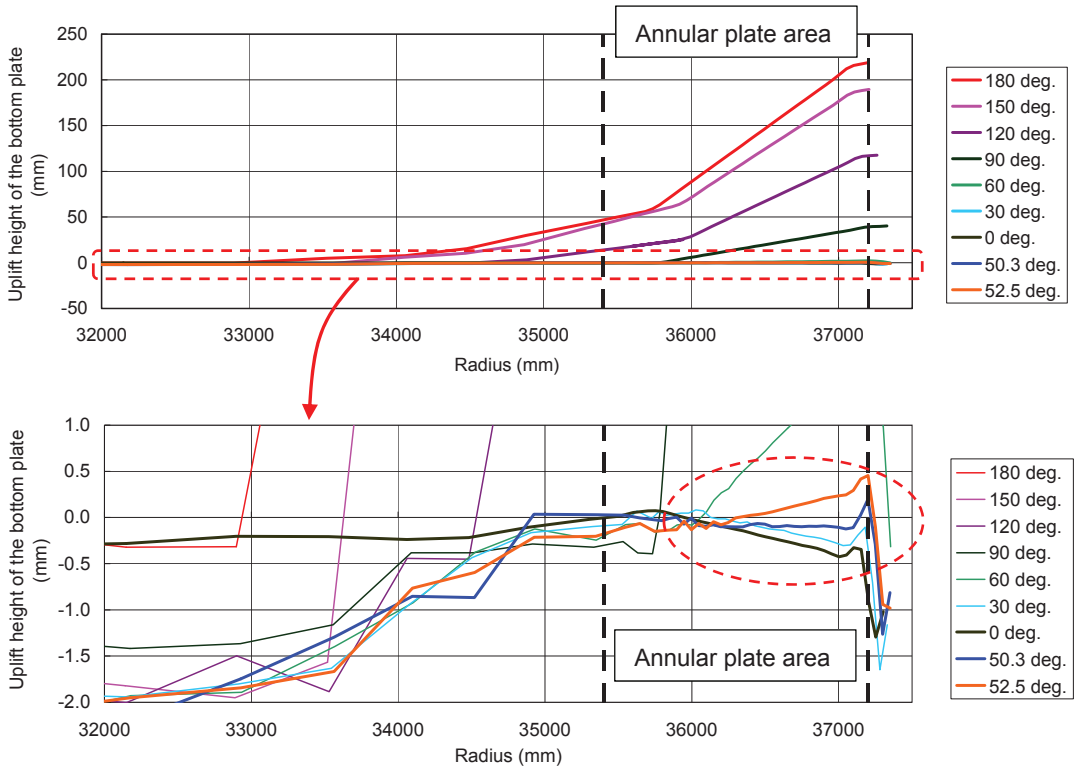

FIGURE 3-16: DISPLACEMENT OF BOTTOM PLATE IN EACH DIRECTION

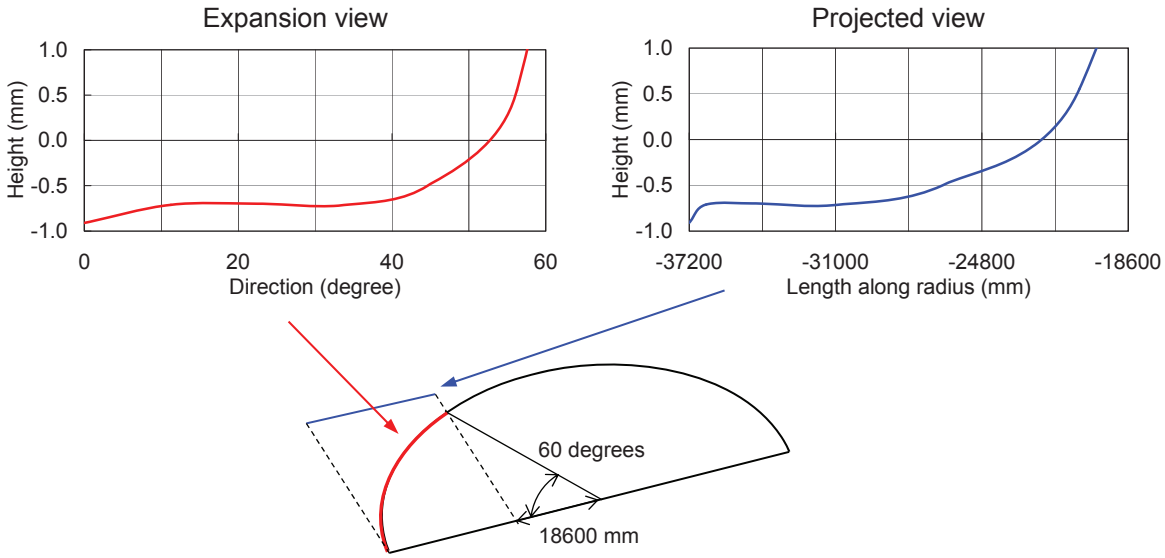

FIGURE 3-17: DISPLACEMENT OF THE BOTTOM OF THE SIDEWALL

3-2-6 Axial force in the sidewall

Figure 3-18-1 to 4 show the axial force distribution in the sidewall for Cases 21, 32①, 32② and 41, respectively. The data of Case 32① is at the moment of occurring small uplift (50.0mm) in Case 32, while the data of Case 32② is at the moment of occurring large uplift (116.8mm). These values are the average of cross sectional force in elements of bottom strake (course) of the sidewall at each direction. The axial force of the sidewall at uplift side (180 degrees) is tensile, while contact side (0 degree) is compressive. The axial force of Case 41, which is constant horizontal acceleration case (equivalent static conditions), is obviously larger than that of Case 21. Around 0 –10 degrees, the axial force decreases locally, which is correspond to the trend of deformation of bottom of the sidewall shown in Figure 3-17.

Table 3-6 shows the relationship of uplift width and an axial force in the sidewall. The pressure load acting on the uplift area is supported by the tank bottom insulation and the sidewall. As the sidewall supports the pressure loads, the axial force in the sidewall may increase. In the Table 3-6, the width of the tank bottom plate, on which pressure loads correspond to the axial force in the sidewall is also specified. This width is calculated by the axial force divided by the liquid pressure. The size of this width against the uplift width means the ratio of pressure load supported by sidewall against the load of act on uplift area. In Table 3-6-1 to 3-6-4, the ratio of that obtained from the reaction force of bottom insulation is also specified. The same trend is shown in both ratio (calculated from the axial force and that obtained from the reaction force).

In the constant horizontal acceleration case (Case 41), the ratio is almost a half. It indicates that the sidewall and the tank bottom insulation evenly support the pressure load. This is the same as the theory used to describe the behavior of the ends of a simply supported beam. While in the seismic event cases, Case 21 and Case 32, the ratio of supported by sidewall becomes larger. It may imply that most of pressure load on the uplifted tank bottom pate is supported by the sidewall during the dynamic uplift process.

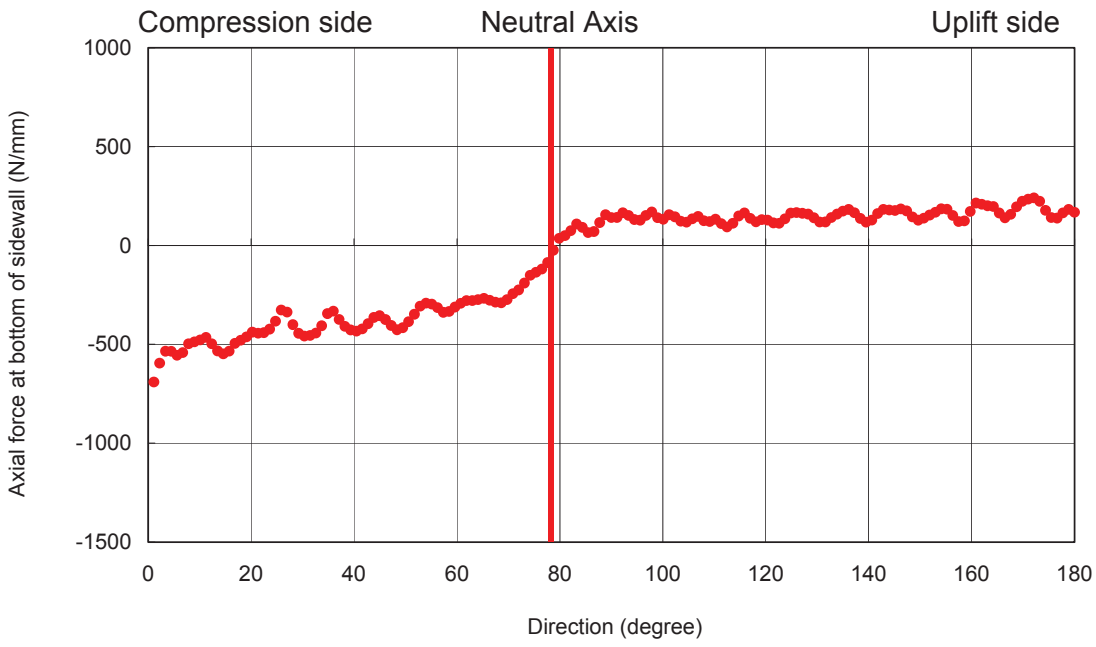

FIGURE 3-18-1: DISTRIBUTION OF AXIAL FORCE ON SIDEWALL (Case 21)

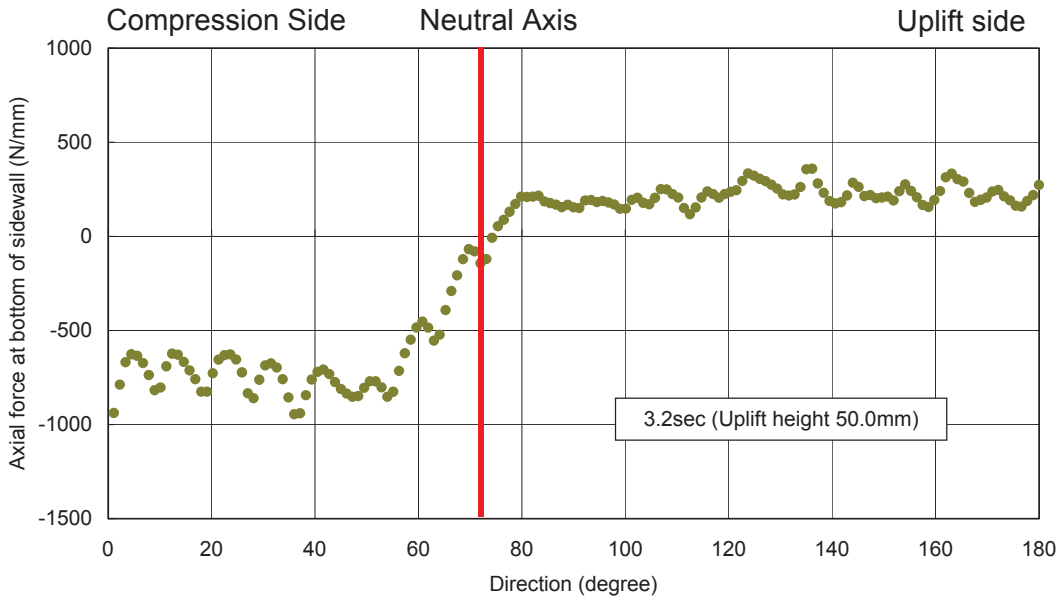

FIGURE 3-18-2: DISTRIBUTION OF AXIAL FORCE ON SIDEWALL (Case 32①)

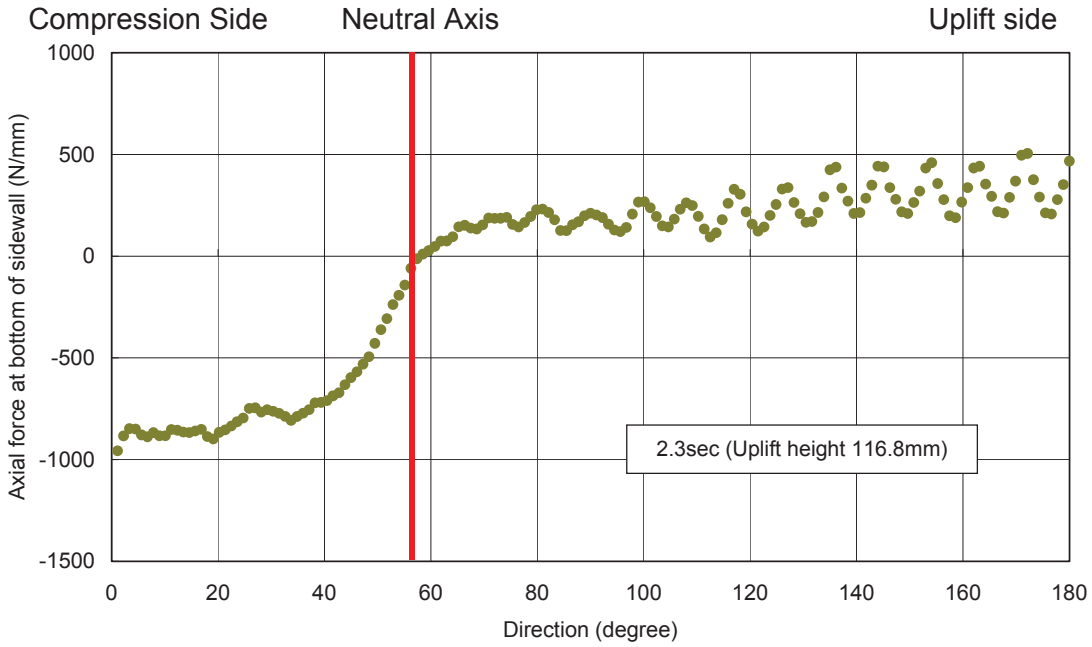

FIGURE 3-18-3: DISTRIBUTION OF AXIAL FORCE ON SIDEWALL (Case 32②)

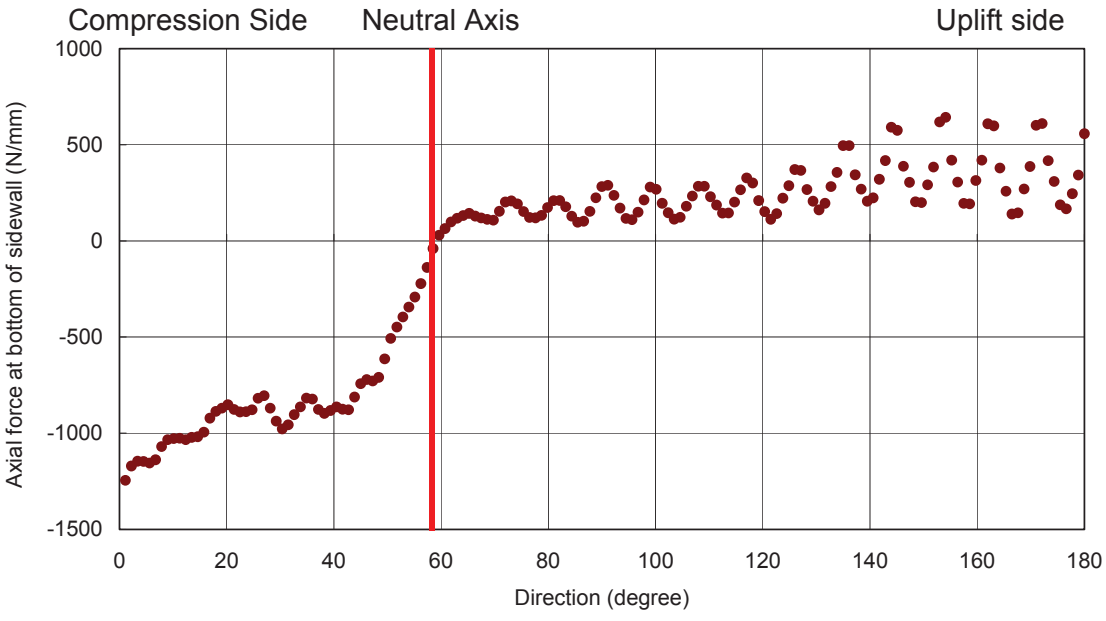

FIGURE 3-18-4: DISTRIBUTION OF AXIAL FORCE ON SIDEWALL (Case 41)

TABLE 3-6-1: THE RATE OF THE UPLIFT WIDTH SUPPORTED BY SIDEWALL

		Case 21	Case 32①	Case 32②	Case 41
		13.1 sec	3.2 sec	2.35 sec	-
Uplift height	(mm)	21.6	50.0	116.8	215.8
Uplift width	(mm)	1450.0	1500.0	4303.4	4303.4
Pressure	(N/mm^2)	0.1559	0.1531	0.1261	0.1506
Axial force	(N/mm)	186.1	230.5	358.9	366.1
Uplift width supported by sidev	(mm)	1193.6	1505.9	2846.6	2431.2
Ratio against width of annular plate		0.82	1.00	0.66	0.56
	Average		0.83		-

TABLE 3-6-2: THE RATE OF THE UPLIFT WIDTH SUPPORTED BY SIDEWALL
(Case 21: 12.9 – 13.15 sec)

		Case 21			
		12.9 sec	13.0 sec	13.1 sec	13.15 sec
Uplift height	(mm)	0.6	12.2	21.6	13.0
Uplift width	(mm)	1250.0	1450.0	1450.0	825.0
Pressure	(N/mm^2)	0.1874	0.1741	0.1559	0.1518
Axial force	(N/mm)	124.0	147.4	186.1	67.3
Uplift width supported by sidewall	(mm)	661.5	846.5	1193.5	443.1
Ratio against width of annular plate	(obtained from axial force)	0.53	0.58	0.82	0.54
Ratio against width of annular plate	(obtained from bottom reaction force)	0.76	0.79	0.73	0.68

TABLE 3-6-3: THE RATE OF THE UPLIFT WIDTH SUPPORTED BY SIDEWALL
(Case 32①: 3.1 – 3.4 sec)

		Case 32①			
		3.1 sec	3.2 sec	3.3 sec	3.4 sec
Uplift height	(mm)	3.8	50.0	42.9	17.7
Uplift width	(mm)	1450.0	1500.0	1500.0	1500.0
Pressure	(N/mm^2)	0.1698	0.1531	0.1686	0.1613
Axial force	(N/mm)	186.1	230.5	256.1	200.2
Uplift width supported by sidewall	(mm)	1096.2	1505.9	1518.7	1241.4
Ratio against width of annular plate	(obtained from axial force)	0.76	1.00	1.01	0.83
Ratio against width of annular plate	(obtained from bottom reaction force)	0.69	0.91	0.87	0.79

TABLE 3-6-4: THE RATE OF THE UPLIFT WIDTH SUPPORTED BY SIDEWALL
(Case 32②: 2.2 – 2.6 sec)

		Case 32②					
		2.2 sec	2.3 sec	2.35 sec	2.4 sec	2.5 sec	2.6 sec
Uplift height	(mm)	35.8	98.5	116.8	113.8	92.9	30.6
Uplift width	(mm)	1500.0	3141.1	4303.4	3672.4	2317.1	1500.0
Pressure	(N/mm^2)	0.1404	0.1307	0.1261	0.1294	0.1554	0.2008
Axial force	(N/mm)	186.7	323.7	358.9	349.8	326.5	288.1
Uplift width supported by sidewall	(mm)	1329.2	2476.3	2846.6	2704.0	2100.2	1434.5
Ratio against width of annular plate	(obtained from axial force)	0.89	0.79	0.66	0.74	0.91	0.96
Ratio against width of annular plate	(obtained from bottom reaction force)	0.89	0.77	0.84	0.90	0.88	0.65

* This is ratio of the portion of uplift width supported by the sidewall compare to total uplift width at the point of the maximum uplift.

Table 3-7 shows the force couple of tensile side and compressive side at the time of rising and descending of the bottom plate. These values are calculated form axial force in the sidewall and the distance from neutral axis to each point. According to the result, the force couple of tensile and compressive side is not even in the dynamic rocking transition. Expect for the data of at 2.3 seconds of Case 32② and Case 41, during rising of the bottom plate, force couple of compressive side becomes larger than that of tensile side. On the other hand, during descending of the bottom plate, force couple of tensile side becomes larger.

TABLE 3-7: FORCE COUPLE OF TENSILE SIDE AND COMPRESSIVE SIDE

			Case 21		Case 32①		Case 32②			Case 41
			13.0 sec	13.1 sec	3.2 sec	3.3 sec	2.2 sec	2.3 sec	2.4 sec	-
Uplift height		(mm)	12.2	21.6	50.0	42.9	35.8	98.5	113.8	215.8
		Situation	rising	rising	rising	descending	rising	rising	descending	rising
Location of neutral axis		(degree)	87.8	79.9	72.0	63.0	95.6	57.4	61.9	58.5
Overturning moment		(N-mm)	1.38E+12	1.44E+12	2.10E+12	1.90E+12	2.09E+12	2.52E+12	1.83E+12	2.47E+12
Force couple	Tensile side	(N-mm)	-4.02E+11	-5.74E+11	-9.68E+11	-1.17E+12	-4.13E+11	-1.54E+12	-1.42E+12	-1.65E+12
	Compressive side	(N-mm)	-8.71E+11	-8.71E+11	-1.13E+12	-7.28E+11	-1.67E+12	-9.85E+11	-4.08E+11	-8.20E+11
Ratio of force couple	Tensile side		0.291	0.397	0.462	0.617	0.198	0.609	0.776	0.668
	Compressive side		0.631	0.603	0.538	0.383	0.802	0.391	0.224	0.332

As shown in Figure 3-18-1 to 4, variation is observed in the axial force distribution along the circumference. It is considered to be the effect of gravitational force loading at the preparation stage before the start of the time-history FE analysis.

In the preparation stage of the analysis, a gravitational force was applied then a stationary state period of 3 seconds was provided before starting the horizontal base excitation. This is to mitigate any vibration due to gravity loading.

Figure 3-19 shows the axial force distribution of at 2.5 sec. and that at the instant of the maximum uplift height. The vibration of each time frame seems to have the same cycle length. Figure 3-20 shows the result of Fast Fourier Transforms (FFT) of the values of the axial force distributions of every 1.125 degree. The ordinate shows the amplitude (Fourier Spectrum) of FFT of the axial force. Then it is confirmed that both distributions have the same cycle wave length. Therefore, it is considered that the remaining vibration effect on the result of the time-history FE analysis. Consequently, the axial force is expected to be the center of vibrated values.

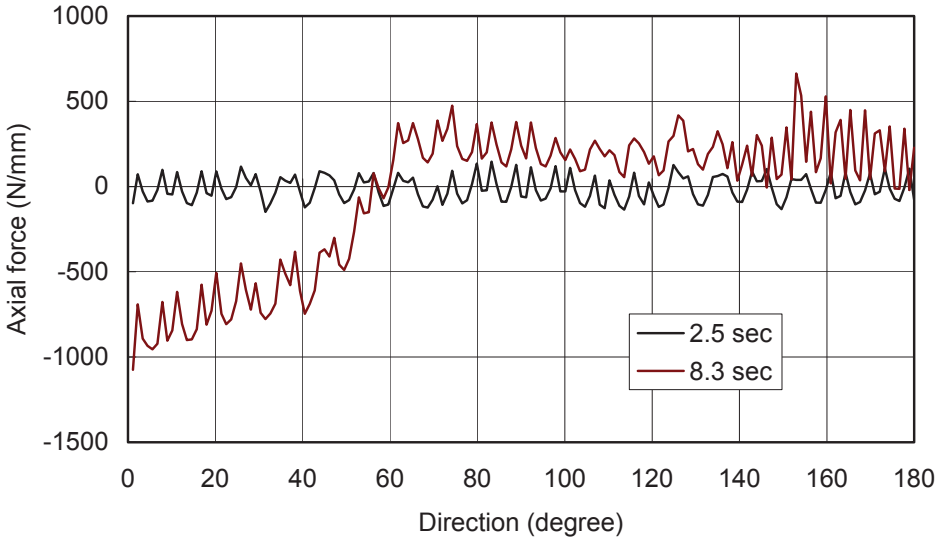

FIGURE 3-19: COMPARISON OF AXIAL FORCE DISTRIBUTION

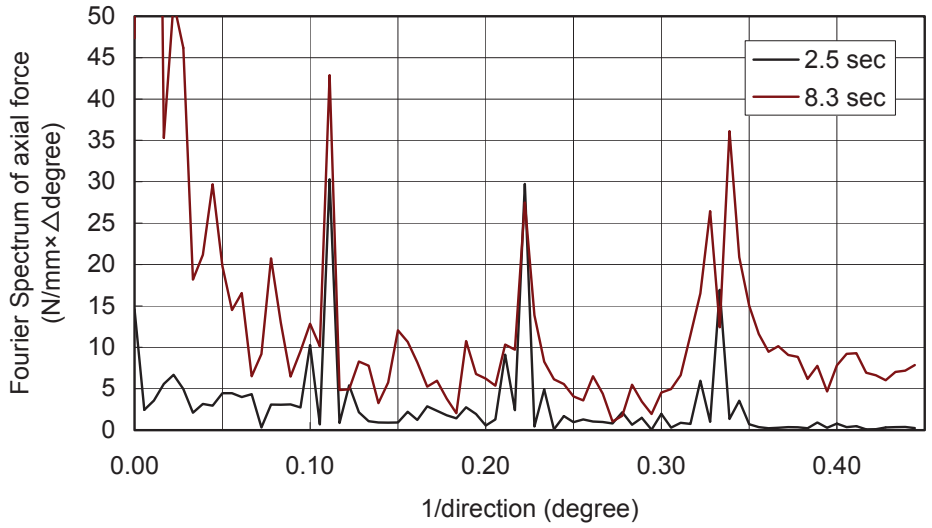

Note: Fourier Spectrum has the unit that multiplied direction step (Δdegree = 1.125 degree) of data to amplitude.

FIGURE 3-20: FFT OF AXIAL FORCE ON SIDEWALL

3-2-7 Sidewall deformation

Figure 3-21 shows the observed typical undulating deformation at the top of the sidewall for each case. According to the results, the extent of the undulating deformation under uplift conditions depends on the stiffness of the stiffeners and the magnitude of response acceleration. As the stiffness of the stiffeners increases, the undulating deformation and the uplift height become smaller. While as the result of Case 32 shows, high response acceleration stimulates the large undulating deformation.

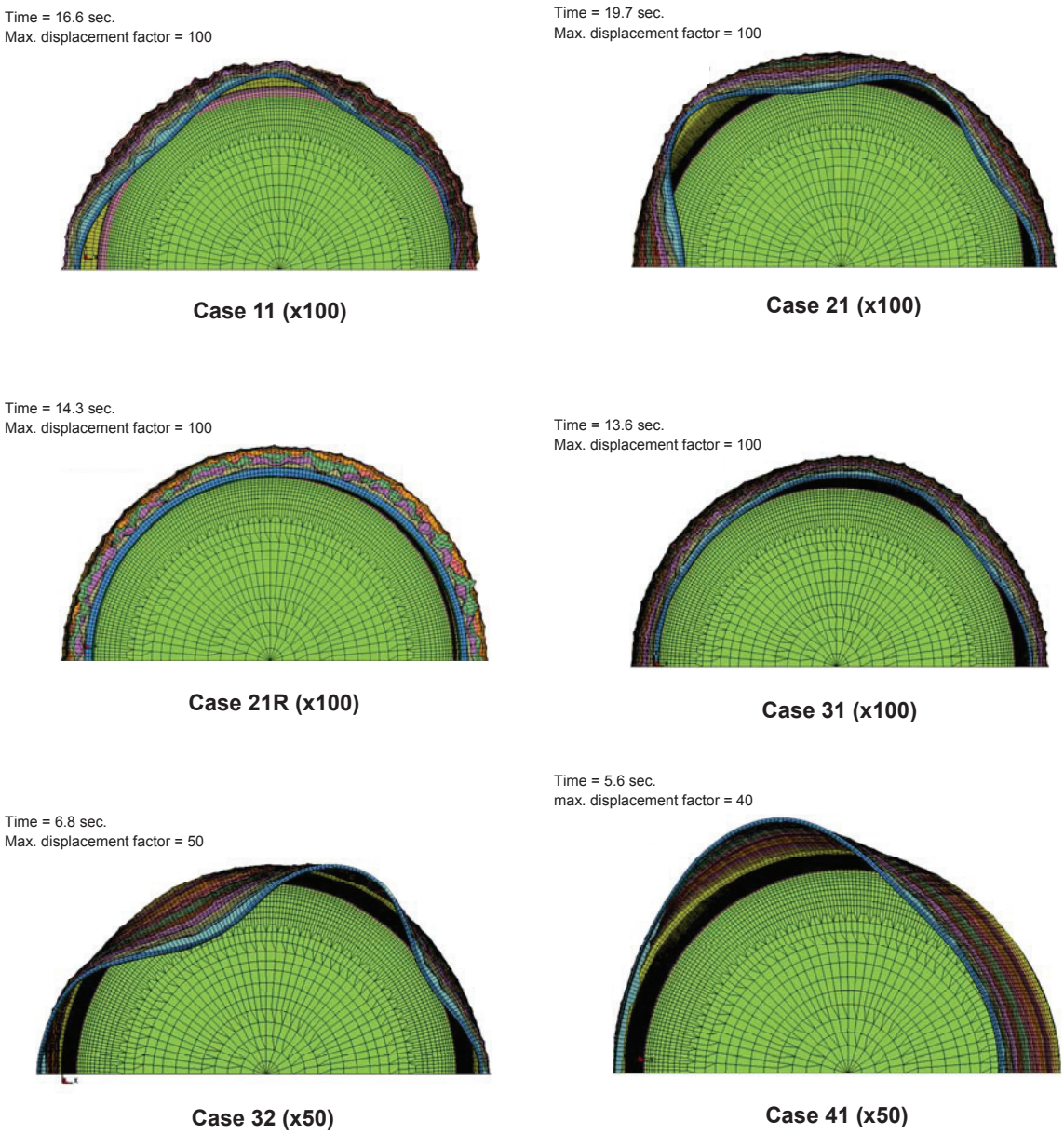

FIGURE 3-21: THE SIDEWALL DEFORMATION

The result of Case 41 shows the top of the sidewall ovally deformed and the magnitude of the deformation was exceedingly larger than the other case. This difference of mode proves that the tank response under oscillating loading fundamentally differs from that under statically loading conditions.

Table 3-8 shows the maximum displacement at the top of the sidewall for each case and the ratio of those against Case 11 and Case 21. As the same as for the uplift height, the displacement of Case 41 was significantly larger than that of basic case (Case 21). Also, the stiffness of the stiffeners has an influence on the displacement. As the stiffness of the stiffeners increased, the displacement became smaller. The ratio of the maximum displacement of Case 32 against Case 21 was about 2.2 times of the ratio of average response acceleration of Case 32 as specified in Table 3-3. It demonstrates that tank response acceleration is only one factor for the magnitude of the displacement at the top of the sidewall. It is considered that sympathetic vibration between the undulating deformation and seismic wave occurs.

TABLE 3-8: THE MAXIMUM DISPLACEMENT AT THE TOP OF THE SIDEWALL

(mm)

	Case 11	Case 21	Case 21R	Case 31	Case 32	Case 41
	43.6	53.6	24.3	36.7	250.9	274.9
Ratio against Case 11	1.000	1.227	0.557	0.840	5.748	6.298
Ratio against Case 21	0.815	1.000	0.454	0.684	4.685	5.133

3-2-8 FFT analysis of base shear and sidewall displacement

To verify the vibration characteristics of tank response, FFT analysis is performed for the base shear and the sidewall displacement of time step $\Delta t = 0.1$ second for sidewall displacement, $\Delta t = 0.01$ second for base shear. Figures 3-22-1 to 5 show the results of FFT analysis of the base shear and the sidewall displacement of each case. The ordinate shows the amplitude (Fourier Spectrum) of FFT of the sidewall displacement and the base shear.

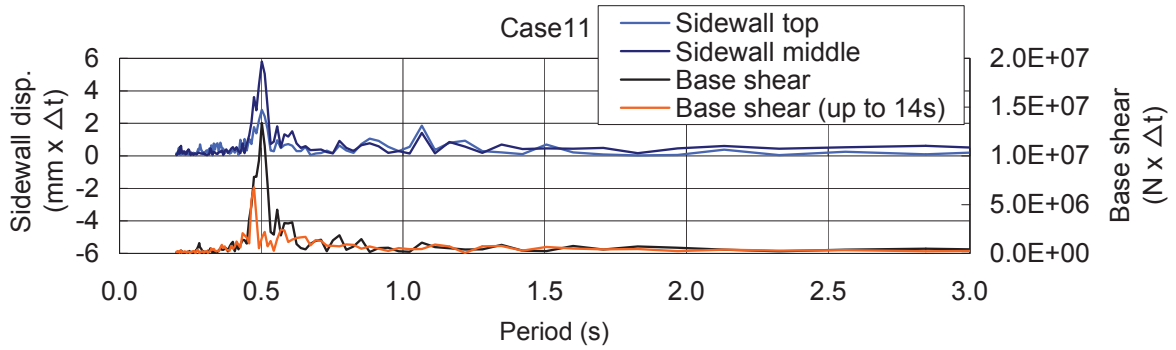

Note: Fourier Spectrum has the unit that multiplied time step of data (Δt) to amplitude.

FIGURE 3-22-1: FFT ANALYSIS OF THE SIDEWALL DISPLACEMENT (CASE 11)

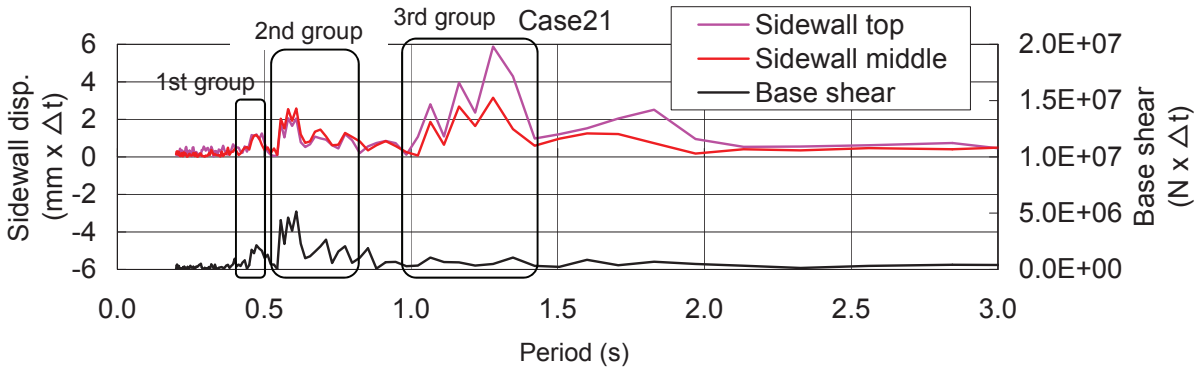

FIGURE 3-22-2: FFT ANALYSIS OF THE SIDEWALL DISPLACEMENT (CASE 21)

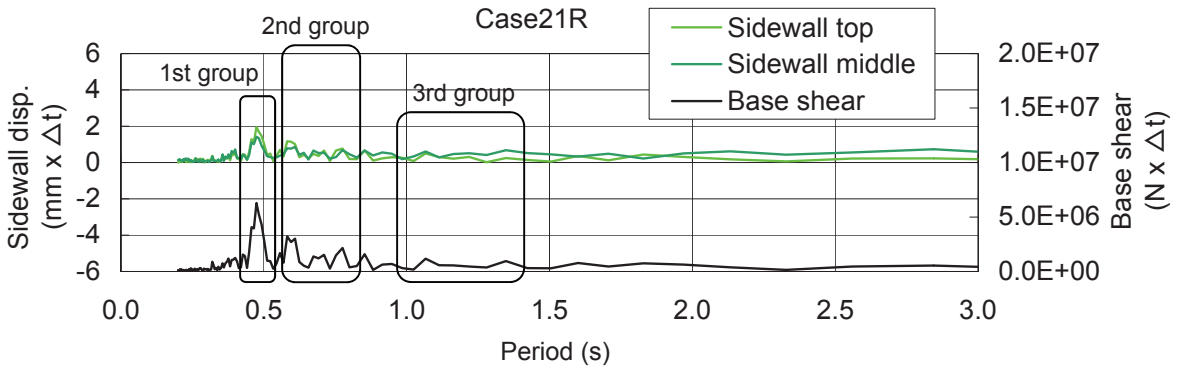

FIGURE 3-22-3: FFT ANALYSIS OF THE SIDEWALL DISPLACEMENT (CASE 21R)

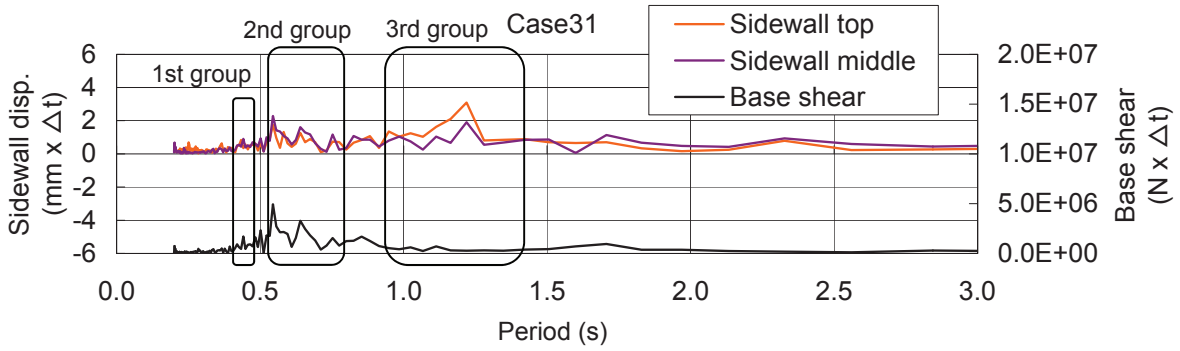

FIGURE 3-22-4: FFT ANALYSIS OF THE SIDEWALL DISPLACEMENT (CASE 31)

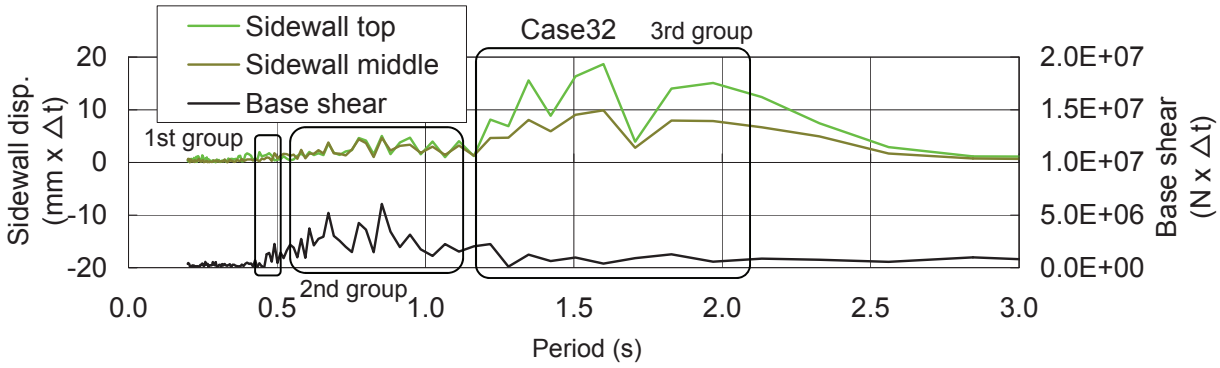

FIGURE 3-22-5: FFT ANALYSIS OF THE SIDEWALL DISPLACEMENT (CASE 32)

TABLE 3-9: REPRESENTATIVE NATURAL PERIOD OF THE SIDEWALL FOR EACH GROUP

		Case 11	Case 21	Case 21R	Case 31	Case 32
Natural period (sec)	1st group	0.502	0.474	0.474	0.441	0.492
	2nd group	-	0.610	0.582	0.545	0.853
	3rd group	-	1.280	-	1.219	1.600
Frequency (Hz)	1st group	1.992	2.109	2.109	2.266	2.031
	2nd group	-	1.641	1.719	1.836	1.172
	3rd group	-	0.781	-	0.820	0.625

Figure 3-22-1 (Case 11) shows a typical vibration characteristic of the tank, known as bulging mode. In many cases, the tank structure is considered as a single spring-mass system and in that case a unique natural period appears. The frequency and the natural period were 1.992 Hz and 0.502 seconds, respectively. These were the same as the results of the eigenvalue analysis (0.498 seconds). In this figure, the FFT results for the data of the base shear up to 14 seconds are also plotted. Since during this period the undulating deformation at the top of the sidewall does not appeared, the natural period without the effect of that deformation can be confirmed. This natural period is slightly shorter than that obtained from the eigenvalue analysis. However, it is almost the same as eigenvalue analysis. (Its amplitude is smaller than that of full period result. This trend depends on the magnitude of base shear.) From this consideration and the fact of no other significant natural period observed, the undulating deformation does not effect on vibration characteristics of the tank under no-uplift conditions.

The results of the uplift cases show the different vibration characteristics. Instead of decreasing amplitude, of 1st natural period, 2nd and 3rd natural period groups become larger. These natural period groups are longer than that of the bulging mode. According to the result of Case 21 and 21R, with an increase of stiffener stiffness, the amplitude of the 2nd and 3rd natural period groups becomes smaller. Therefore, it is estimated that these natural periods have the relationship with the uplift behavior and the undulating deformation, respectively. Particularly, it is believed that result of the 3rd natural period group is due to not by bulging response but the undulating deformation. Because that appears only in FFT result of sidewall displacement, and when undulation deformation is small (Case 21R), this group disappears. The band of 3rd natural period group of Case 32 is longer than that of other cases. It is presumed that uplift behavior affects natural period of undulation deformation, because Case 32 has considerably higher uplift than other cases.

3-2-9 Angular acceleration at the bottom of the sidewall and uplift induced dynamic pressure

As described in Ref. [6], angular acceleration at the bottom of the sidewall dominates the magnitude of the dynamic pressure induced by uplifting. This pressure acts adversely to the

dynamic pressure due to bulging mode, and has an offset effect on the total dynamic pressure. To confirm the relationship between stiffener stiffness and level of the dynamic pressure induced by uplifting, angular acceleration is investigated. Figure 3-23 shows the results of the angular acceleration at the bottom of the sidewall for Case 21 and 21R.

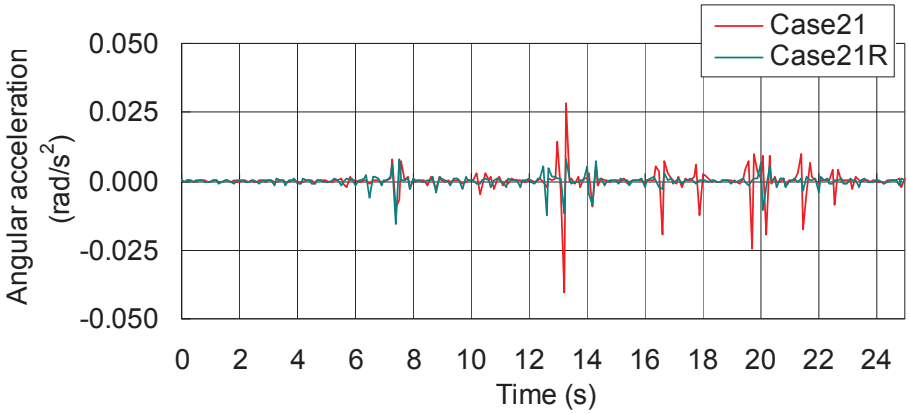

FIGURE 3-23: EXAMPLE OF THE ANGULAR ACCELERATION AT THE BOTTOM OF THE SIDEWALL

Table 3-10 shows the maximum angular acceleration at the bottom of the sidewall for each case and the ratio of those against Case 21. As the stiffness of the stiffeners increased, the angular acceleration became smaller. According to Table 3-5, the ratio of the maximum uplift height of Case 32 against Case 21 is 5.407. On the contrary the ratio of the maximum angular acceleration of Case 32 against Case 21 is 1.930 shown in Table 3-9. When the oscillation period of the tank is the same, increasing of ratio of angular acceleration is proportional to that of uplift height. This discrepancy is considered due to the difference of transition speed of the uplift between Case 21 and Case 32. As above discussed in the section 3-2-4, the uplift has the relationship with undulating deformation. The natural period of the undulating deformation of Case 32 (3rd group in Figure 3-22-5) is longer than that of Case 21(3rd group in Figure 3-22-2). Therefore, the transition speed of both cases is expected to different.

TABLE 3-10: THE MAXIMUM ANGULAR ACCELERATION

(rad/s^2)

		Case 21	Case 21R	Case 31	Case 32
	Max.	0.029	0.008	0.020	0.055
	Min.	-0.041	-0.016	-0.030	-0.072
Ratio	Max.	1.000	0.284	0.694	1.930
	Min.	1.000	0.391	0.749	1.774

It has been known that the uplift induces dynamic pressure, refer previous study [6] based on an assumption of an inviscid, incompressible, irrotational fluid, by applying the velocity potential theory and using a rectangular tank model with a unit width.

Figure 3-24 shows the rectangular tank model and boundary conditions used in deriving the mathematical solutions.

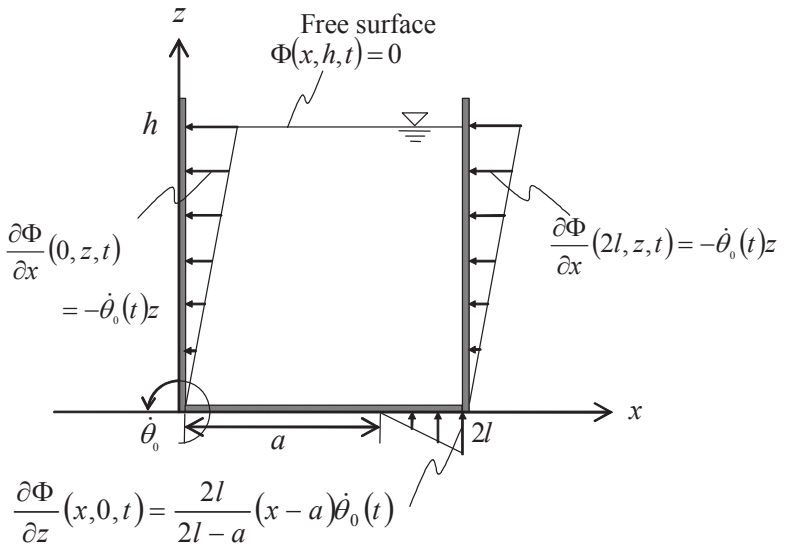

FIGURE 3-24: MECHANICAL MODEL OF RECTANGULAR RIGID TANK WITH UNIT WIDTH DURING UPLIFTING MOTION [6]

The theoretical equation for dynamic pressure is given as follows from the continuous conditions $\nabla^2\varphi=0$ and boundary conditions.

$$
\begin{aligned}
p(x,z,t) = -\rho\ddot{\theta}_0(t)\Bigg[&\left(l-\frac{a}{2}\right)(z-h) \\
&+\frac{4l}{\pi^2}\sum_{n=1}^{\infty}\Bigg(\left\{(-1)^n-\cos\frac{n\pi a}{2l}\right\}\frac{2l}{n^3\pi}\times \\
&\qquad\frac{2l}{2l-a}\left(\tanh\frac{n\pi z}{2l}-\tanh\frac{n\pi h}{2l}\right)\cosh\frac{n\pi z}{2l} \\
&\qquad+\left\{1-(-1)^n\right\}\frac{1}{n^2}\Bigg[z-\frac{2l}{n\pi}\sinh\frac{n\pi z}{2l} \\
&\qquad\qquad+\left(\frac{2l}{n\pi}\tanh\frac{n\pi h}{2l}-\frac{h}{\cosh\frac{n\pi h}{2l}}\right)\cosh\frac{n\pi z}{2l}\Bigg]\Bigg)\cos\frac{n\pi x}{2l}\Bigg]
\end{aligned}
\tag{3-2}
$$

Where,

p: Dynamic pressure

ρ: Fluid density

$\ddot{\theta}_0$: Angular acceleration of the sidewall

$2l$: Tank length (= diameter)

a: Start point of uplift

h: Tank height

The uplift induced dynamic pressure is able to be obtained from Eq. (3-2) by using angular acceleration calculated by the FE analysis. This is considered as one of factors causing the difference between fluid pressure of the no-uplift case and the uplift case.

Figure 3-25 shows the pressure distribution of Case 21 (uplift case) minus Case 11 (no-uplift case) as calculated by the FE analysis, and the uplift induced dynamic pressure calculated by the theoretical equation with the same conditions of Case 21. The both pressure (red line and blue or green line) implies uplift induced pressure. However the difference exists between the values of the FE analysis and that of theoretical equation, the direction of both of that pressure is opposite to bulging pressure (i.e. Bulging pressure at uplift side is negative, while induced dynamic pressure is positive. Bulging pressure at compression side is positive, while induced dynamic pressure is negative.). This means that bulging pressure is reduced by the effect of rocking-translation interaction [7- 9].

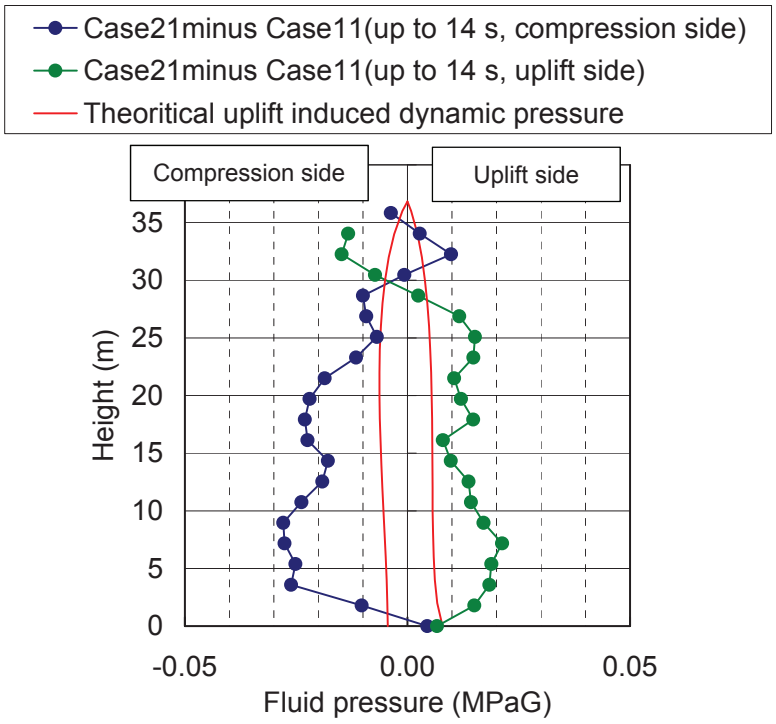

FIGURE 3-25: UPLIFT INDUCED DYNAMIC PRESSURE

3-3 CONCEPT OF INTRODUCING DYNAMIC EFFECT TO A STATIC ANALYSIS

According to the results obtained so far, tank responses such as acceleration, base shear and dynamic pressure significantly decrease compared to the no-uplift conditions, when uplift occurs. The reduction in these responses is led by a rather small uplift. Eventually, these will reach a certain balanced state. Figure 3-26 shows the relationship between the uplift height and the base shear that represents the tank response. If the uplift is larger than 50mm, the tank response becomes small less than half of that under no-uplift conditions. Up to 20 mm of the uplift height, the tank response decreases drastically rather than that after 20 mm. It is considered the relationship with the features of uplift shown in Figure 3-14. When small height uplift occurs, about 1m width of the tank bottom plate is instantly lifted. This behavior is considered to introduce the significant decrease within 20 mm of uplift height.

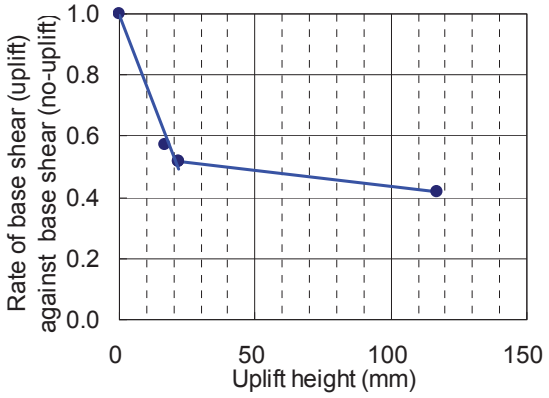

FIGURE 3-26: RELATIONSHIP BETWEEN UPLIFT HEIGHT AND RESPONSE OF THE BASE SHEAR

It is expected that two major elements exist to reduce the tank response such as acceleration and base shear, during dynamic vibration.

The first element is that due to change of natural period. As Figure 3-22 shows, 2nd natural period groups, which is arose by uplift of the bottom plate, appears. The 2nd natural period is longer than that of 1st natural period. According to the response spectrum feature in Figure 3-6, when a natural period is longer, magnitude of response acceleration becomes small. (The 3rd natural period is due to undulating deformation and thought to be correlation with the tank excitation response)

Generally, it is sufficiently suitable to regard 1st natural period as a sole representative value of the tank natural period, from a seismic design viewpoint. Because tank structure closes to single mass structure, moreover amplification of response acceleration by 1st natural period is larger than that form 2nd. In case the mode of 2nd natural period has a considerable effective mass, estimation of seismic force from only 1st natural period becomes too conservative. In this

case, taking into account of 2nd natural period is thought to be practical. The detail investigation for establishing of a procedure to provide a natural period of tanks with uplift condition is required for applying this concept.

If it is possible to establish the relationship between the uplift height and the ratio of reduction as shown in Figure 3-26, then it will be possible to establish a response acceleration spectrum for the uplift conditions similar to that shown in Figure 3-27. If the natural period of the tank for the uplift conditions can also be determined, tank response can be determined through the same process as used in the current seismic design procedures. To establish the response acceleration spectrum for general use in dynamic uplift conditions, further investigation based on the FE analysis for a range of tank dimension may be required.

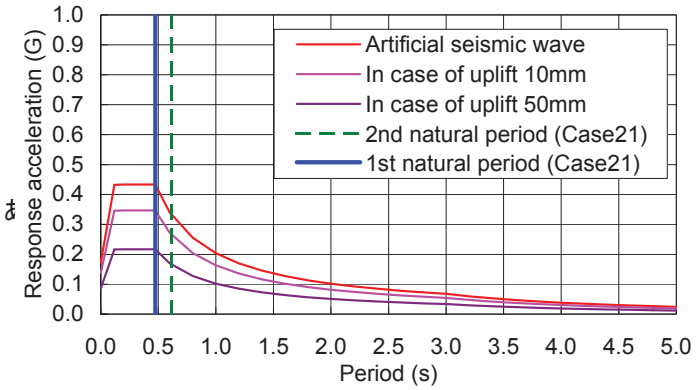

FIGURE 3-27: NATURAL PERIOD, FREQUENCY AND RESPONSE ACCELERATION UNDER UPLIFT CONDITIONS

This study also focuses on a second element for establishing of seismic design procedure for the tank bottom plate corner connection. That element is the effect of uplift induced dynamic pressure during rocking motion.

As specified in Chapter 1, present seismic design standard does not take into account this element. The dynamic pressure quoted in the standard is based on the achievement of research for no-uplift condition. Research of effect of this element on response behavior of tanks and introducing in the procedure is required for rational design. Difference of the response dynamic pressure between uplift and no-uplift conditions is expected to arise from the uplift induced dynamic pressure which is due to bulging-rocking interaction. The effect of uplift induced pressure is taken into account for seismic design by the proposed procedure as shown in Figure 3-28. The procedure consists of the outcomes of previous studies and the proposed model presented in this paper.

The dynamic pressure due to bulging mode is calculated from conventional theories [4], [5]. However, the dynamic pressure induced by rocking motion is also obtained from two theories on the open literature. From one theory comes the calculation of angular acceleration of the tank

bottom plate by using the assumed uplift [10], [11]. From another theory comes the calculation of the dynamic pressure induced by uplift of the tank bottom plate during rocking motion by using the angular acceleration [6]. Once the two dynamic pressures are obtained, the tank overturning moment is calculated.

The assessment of the bottom corner connection is performed by determining the stress level in the tank bottom plate and the bottom of the sidewall. For achieving this, the Structural Mathematical Model (b) of bottom plate and sidewall is developed, which is specified in Chapter 4. To apply this model, the axial force at the bottom of the sidewall is required. Then the Force Coupling Mathematical Model (a) for calculating the axial force from the tank overturning moment is also developed as specified in Chapter 5. In the previous studies regarding modeling of axial force in a sidewall, its distribution is assumed from experimental or analytical result. For establish the rational design procedure, the model (a) is developed according to theoretical discussion based on research of dynamic behavior by the FE analysis. An assumed uplift width, which is used for the calculation of angular acceleration, is obtained from the model (b). In other words, this design procedure is conducted through an iterative process.

In the later chapters, development of the Structural Mathematical Model (b) of the tank bottom plate and sidewall, the Force Coupling Mathematical Model (a) for axial force and design procedure are specified.

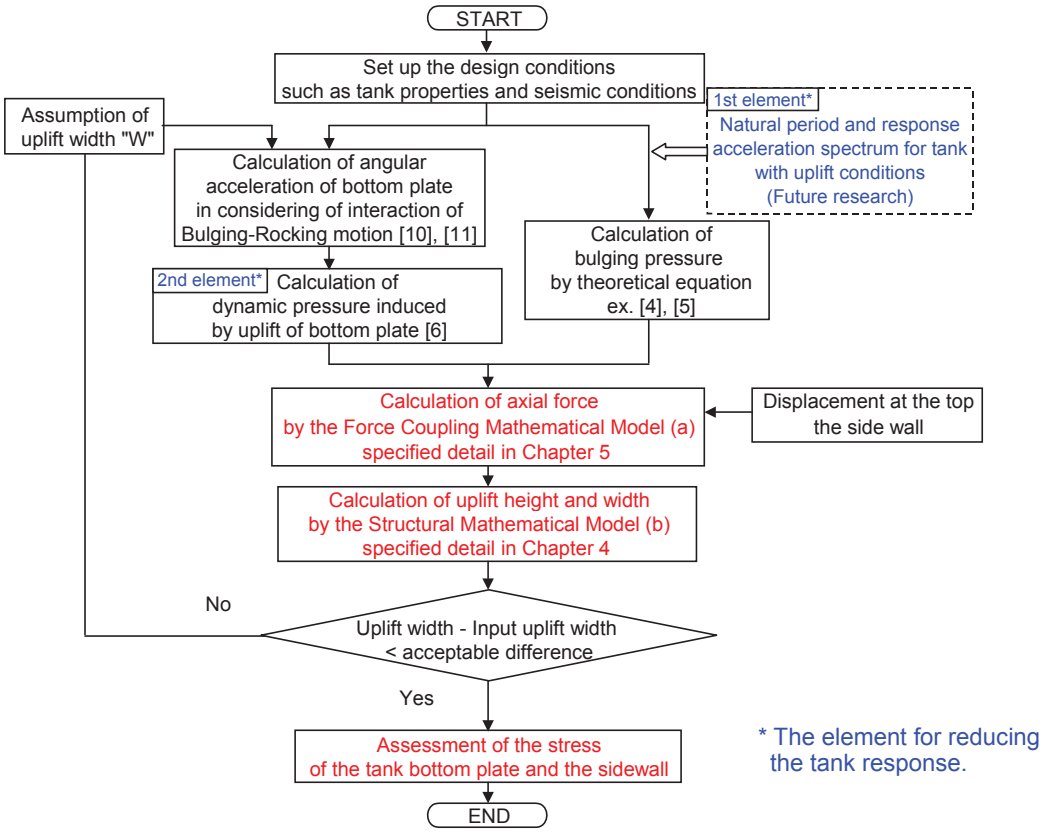

FIGURE 3-28: FLOWCHART FOR OBTAINING THE DYNAMIC PRESSURE UNDER UPLIFT CONDITIONS AND ASSESSMENT OF BOTTOM CORNER

3-4 FINDINGS

In this chapter, fluid-structure coupled 3-dimensional time-history FE analysis was performed for investigating dynamical behavior of tanks including uplift of a tank bottom plate. Several cases, which are no-uplift case, rigid stiffener stiffness case and 3 different seismic wave cases (artificial seismic wave, Taft EW and EL Centro NS), were calculated and effects of structural conditions on the tank response are mainly verified.

Findings from this research are summarized below.

- The response acceleration and the base shear of the uplift case become about half and 40% of the no-uplift cases, respectively. This tendency is also observed for the result of the fluid pressure. These results provide that the tank response under uplift conditions is absolutely different from that under no-uplift conditions.
- The stiffness of the stiffeners has the relationship with the tank response under uplift conditions. As the stiffness of the stiffeners increases, the average response acceleration and the base shear grow larger. Meanwhile the uplift height and the sidewall displacement become smaller. In addition, the stiffness of stiffeners affects the distribution of the response acceleration and the fluid pressure on the sidewall.
- When the uplift occurs, about a 1 m (correspond to about 55% of annular plate width) of bottom plate is lifted. The thicker annular plate installed at the periphery of the tank bottom plate may cause it. It implies the necessity to take into account this phenomenon for developing the mathematical model in Chapter 5.
- Since the nominal in-plane shear stiffness of the sidewall is enough, the bottom of the sidewall seems to be rigid in the vertical direction. However, from a microscopic viewpoint, it deforms slightly in an arch shape up to the neutral axis, while it drops in the area around 0 degree (compression side).
- Liquid pressure, which acts on the uplifted tank bottom plate, is supported by the sidewall and tank bottom insulation evenly under the static loading conditions. While during the dynamic uplift process, the amount of the load supported by the sidewall becomes larger. This point should be considered when develop the mathematical model in Chapter 5.
- The force couple of tensile and compressive side is not even in the dynamic rocking transition. During rising of the bottom plate, force couple of compressive side becomes larger than that of tensile side. On the other hand, during descending of the bottom plate, force couple of tensile side becomes larger
- The undulating deformation at the top of the sidewall is observed under the oscillating loading conditions. While under constant horizontal acceleration case, which equivalent static loading, oval shape deformation appears at the top of the sidewall and the uplift height

becomes significantly larger. From these results, it is confirmed that the tank response due to oscillating loading is fundamentally different from that of static conditions.

- The Contribution Factor, which consists of the magnitude of the base shear and the sidewall displacement, is introduced for investigating of the appearance of the uplift. Then it is confirmed that the undulating deformation at the top of the sidewall is one of the major factors of enhance the uplift in the same way as oscillation force.
- The angular acceleration at the bottom of the sidewall, which is an indication pointer of the magnitude of the dynamic pressure induced by uplifting, also has the relationship with the stiffness of the stiffeners. As the stiffness of the stiffeners increases, the uplift decreases, then consequently the angular acceleration becomes smaller.
- The natural periods of the tank are obtained from FFT analysis for the base shear and the sidewall displacement. The natural period under the uplift conditions shows different vibration characteristics than that of the no-uplift conditions, because unlike no-uplift conditions dominated by only 1^{st} natural period, 1^{st}, 2^{nd} and 3^{rd} natural period groups appear. Here, 1^{st} group is the natural period of the bulging mode, while 2^{nd} and 3^{rd} groups are caused by the uplift and the undulating deformation. In addition, these vibration characteristics are affected by features of the seismic waves and the stiffness of the stiffeners.

REFERENCES

[1] Hayashi, S. and Taniguchi, T., et al., 2011, “A Study of Fluid-Structure Coupled Analysis for Large LNG Storage Tanks in Consideration of Uplift”, Proceedings of ASME PVP Conference, PVP2011-57925.

[2] Strong Motion Earthquake Accelerograms, Digitized and Plotted Data, 1971, Report of CALTEC Vol. II, Part A, EERL71-50.

[3] Trifunac, M. D. and J. N. Brune, “Complexity of Energy Release during the Imperial Valley”, 1970, California, Earthquake of 1940, BSSA, Vol. 60.

[4] Housner, G. W., 1957, “Dynamic Pressure on Accelerated Fluid Containers”, Bulletin of the Seismological Society of America, Vol. 47, pp. 15-35.

[5] Veletsos, A. S. and Yang, J. Y., 1976, “Dynamics of Fixed-Base Liquid-Storage Tanks”, U.S.-Japan Seminar for Earthquake Engineering Research with Emphasis on Life Line System, Tokyo, pp. 317-341.

[6] Taniguchi, T. and Segawa, T., 2008, “Fluid Pressure on Rectangular Tank Consisting of Rigid Side Walls and Rectilinearly Deforming Bottom Plate due to Uplift Motion”, Proceedings of ASME PVP Conference, PVP2008-61166.

[7] Taniguchi, T., 2005, “Rocking Mechanics of Flat-Bottom Cylindrical Shell Model Tanks Subjected to Harmonic Excitation”, Journal of Pressure Vessel Technology, Vol. 127, pp. 373-386.

[8] Taniguchi, T. and Segawa, T., 2009, “Effective mass of Fluid for Rocking Motion of Flat-Bottom Cylindrical Tanks”, Proceedings of ASME PVP Conference, PVP2009-77580.

[9] Taniguchi, T., 2010, “Effective mass of Fluid for Rocking-Bulging Interaction of Rigid Rectangular Tank whose Bottom Plate Rectilineary Uplifts”, Proceedings of ASME PVP Conference, PVP2010-25374.

[10] Taniguchi, T., Okui, D., 2014, “A Case Study of Evaluation of Tank Rock Motion with Simplified Analysis Procedure”, Proceedings of ASME PVP Conference, PVP2014-28635.

[11] Taniguchi, T., D’Amico M., Nakashima T., 2017, “Simplified Analysis of the Rocking Motion of A Cylindrical Tank Focusing on the Role of Dynamical Forces Involved in Rocking-Bulging”, Proceedings of ASME PVP Conference, PVP2017-65442.

CHAPTER 4

MODELING OF UPLIFT BEHAVIOR AT BOTTOM PLATE

CHAPTER 4
MODELING OF UPLIFT BEHAVIOR AT BOTTOM PLATE

In this chapter, the integrated mathematical model (referred to as the Structural Mathematical Model) of the sidewall, the bottom plate and the bottom insulation is developed for calculating uplift height and width, deformation and stress of a bottom plate corner connection. This model takes into account of an effect of subsidence of a tank bottom plate and bulging deformation of a sidewall due to liquid pressure on uplift behavior of a bottom plate.

4-1 MODELING OF THE BOTTOM PLATE

4-1-1 Modeling of the bottom plate

The response behavior of a bottom plate during an earthquake differs from place to place. At a periphery part, a bottom plate repeats uplift and landing. At a supported part, a bottom plate is supported by bottom insulation and slightly sinks in bottom insulation. Therefore, the bottom plate model for the uplift part and the supported part are established respectively by applying different mathematical models. Then each model is combined using interface conditions. In the study, a cantilever beam model an elastic bearing beam are adopted for each part.

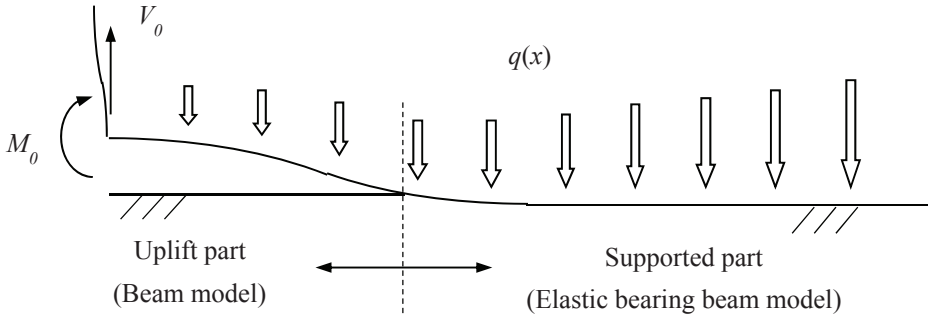

Cross section of periphery part of the tank bottom plate

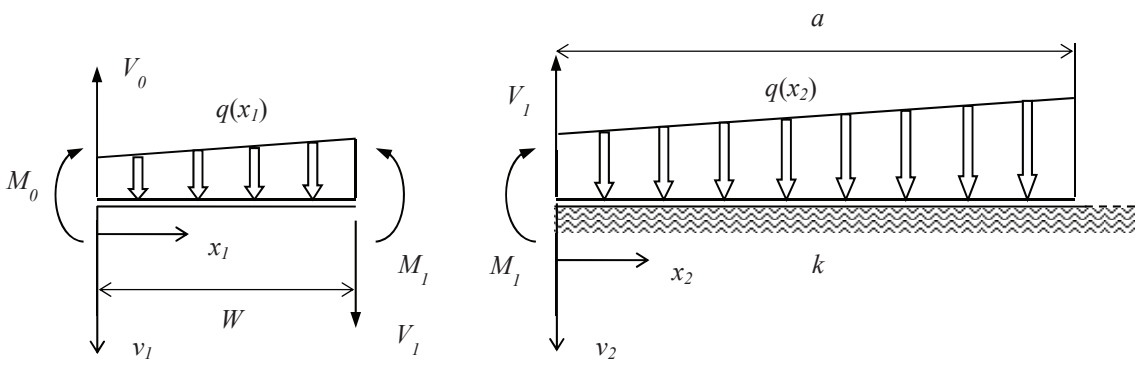

FIGURE4-1: MODEL OF THE BOTTOM PLATE

Where, v_1: Displacement of the bottom plate at uplift part

v_2: Displacement of the bottom plate at supported part

M_0: Moment of the bottom plate at the sidewall side

V_0: Force of the bottom plate at the sidewall side

$q(x_1)$, $q(x_2)$: Liquid pressure on the bottom plate along x_1, x_2 axis

M_1: Moment at interface of beams

V_1: Force at interface of beams

W: Uplift width of the bottom plate

a: Length of bottom plate on elastic foundation

k: Reaction coefficient of tank bottom

Consider the coordinate system, which has x axis along the radius direction and v axis along the sidewall direction. In the beam model for the uplift part, the origin of the coordinate system is placed at the bottom of the sidewall and each axis is expressed as x_1 and v_1. In the elastic bearing beam model for the supported part, the origin of the coordinate system is placed at the starting point of uplift and each axis is expressed as x_2 and v_2.

4-1-2 Modeling of the uplift part

The fundamental equation of the beam is generally expressed as;

$$EI \times \frac{d^4 v_1}{dx_1^4} = q(x_1) \tag{4-1}$$

Where,

v_1: Displacement of the bottom plate at uplift part

$q(x_1)$: Liquid pressure on the bottom plate along x_1 axis

E: Modulus of elasticity of steel

I: Momentum of inertia for rectangular cross section beam

$$I = \frac{w_b \times t_b^3}{12}$$

w_b: Unit width of bottom plate

t_b: Thickness of bottom plate (annular plate)

Distribution of q consists of static and dynamic liquid pressure on the bottom plate during earthquake. In past studies, the dynamic pressures are theoretically derived. Housner [1] (see Eq. (4-2)) derived these equations, which is based on the assumption of a rigid sidewall. Figure 4-2 shows that typical distribution, which is calculated with following conditions.

$$P_d = -\rho u'_0 h \frac{\sqrt{3}}{2} \times \frac{\sinh\left\{\sqrt{3} \times \left(\frac{r\cos\phi}{h}\right)\right\}}{\cosh\left\{\sqrt{3} \times \left(\frac{R\cos\phi}{h}\right)\right\}} \quad (4\text{-}2)$$

Where,

P_d: Dynamic pressure on the bottom plate (MPaG)

ρ: Fluid density (= 480kg/m^3)

u'_0: Horizontal acceleration (= 0.45)

h: Liquid height (= 36,250 mm)

R: Tank radius (=37,200 mm)

r: Distance from the tank center (37,200mm)

ϕ: Angle from acceleration direction (= 0)

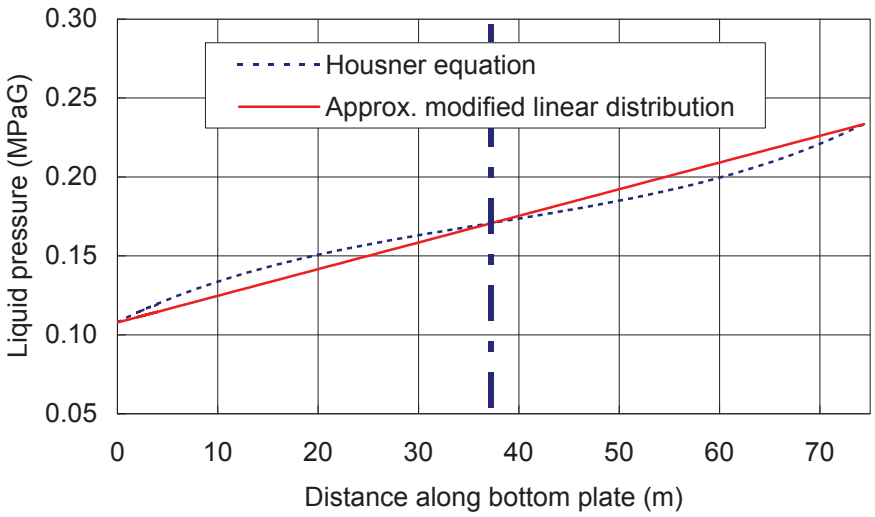

FIGURE 4-2: LIQUID PRESSURE CONSISTS OF STATIC AND DYNAMIC PRESSURE AT THE BOTTOM PLATE

To simplify the problem, distribution of dynamic pressure is approximated as linear distribution as follows and shown in Figure 4-2.

$$P = p_\alpha \times x_1 + p_\gamma$$
$$p_\alpha = \frac{P_d}{R} \quad , \quad p_\gamma = P_0 - P_d \quad (4\text{-}3)$$

Where,

P: Liquid pressure (MPaG)

P_0: Static pressure (MPaG)

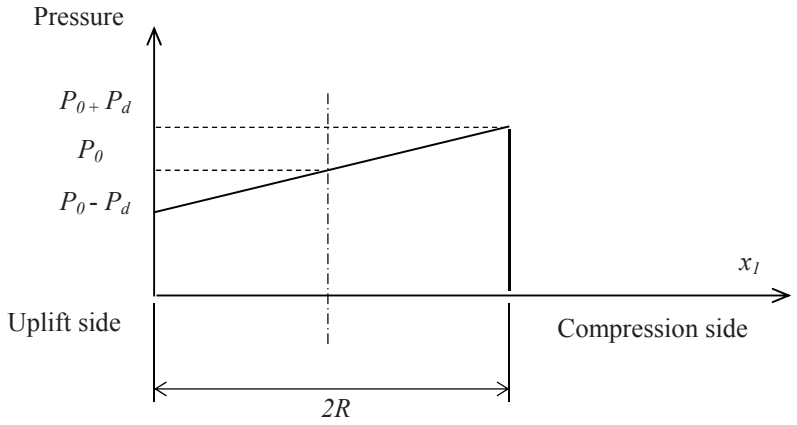

FIGURE 4-3: MODELING OF PRESSURE ON THE BOTTOM PLATE FOR UPLIFT PART

Substituting Eq. (4-3) for Eq. (4-1), the fundamental equation of beam with distribution load becomes;

$$EI \times \frac{d^4 v_1}{dx_1^4} = p_\alpha \times x_1 + p_\gamma \tag{4-4}$$

The derived functions of Eq. (4-4) are derived as;

$$\frac{d^3 v_1}{dx_1^3} = \frac{1}{EI} \times \left(\frac{p_\alpha}{2} \times x_1^2 + p_\gamma \times x_1 + C_{11} \right) \tag{4-5}$$

$$\frac{d^2 v_1}{dx_1^2} = \frac{1}{EI} \times \left(\frac{p_\alpha}{6} \times x_1^3 + \frac{p_\gamma}{2} \times x_1^2 + C_{11} \times x_1 + C_{12} \right) \tag{4-6}$$

$$\frac{dv_1}{dx_1} = \frac{1}{EI} \times \left(\frac{p_\alpha}{24} \times x_1^4 + \frac{p_\gamma}{6} \times x_1^3 + \frac{C_{11}}{2} \times x_1^2 + C_{12} \times x_1 + C_{13} \right) \tag{4-7}$$

$$v_1 = \frac{1}{EI} \times \left(\frac{p_\alpha}{120} \times x_1^5 + \frac{p_\gamma}{24} \times x_1^4 + \frac{C_{11}}{6} \times x_1^3 + \frac{C_{12}}{2} \times x_1^2 + C_{13} \times x_1 + C_{14} \right) \tag{4-8}$$

4-1-3 Modeling of the supported part

The fundamental equation of the elastic bearing beam is generally expressed as;

$$EI \times \frac{d^4 v_2}{dx_2^4} = q(x_2) - k \times v_2 \tag{4-9}$$

Rewriting as $\beta = \sqrt[4]{k/(4EI)}$, Eq. (4-9) becomes;

$$\frac{d^4 v_2}{dx_2^4} + 4\beta^4 \times v_2 = \frac{q(x_2)}{EI} \tag{4-10}$$

The solution v_2 of Eq. (4-10) is given as a total of the general solution $v_{2g,}$ which is obtained by substituting 0 for the right side of Eq. (4-10) and the particular solution v_{2s}.

$$v_2 = v_{2g} + v_{2s} \tag{4-11}$$

The general solution v_{2g} and that derived functions are derived as follows.

$$\begin{aligned} v_{2g} &= e^{\beta x_2}\left(C_{21}\cos\beta x_2 + C_{22}\sin\beta x_2\right) \\ &\quad + e^{-\beta x_2}\left(C_{23}\cos\beta x_2 + C_{24}\sin\beta x_2\right) \end{aligned} \tag{4-12}$$

$$\begin{aligned} \frac{dv_{2g}}{dx_2} &= \beta e^{\beta x_2}\left[C_{21}\left(\cos\beta x_2 - \sin\beta x_2\right) + C_{22}\left(\cos\beta x_2 + \sin\beta x_2\right)\right] \\ &\quad - \beta e^{-\beta x_2}\left[C_{23}\left(\cos\beta x_2 + \sin\beta x_2\right) - C_{24}\left(\cos\beta x_2 - \sin\beta x_2\right)\right] \end{aligned} \tag{4-13}$$

$$\begin{aligned} \frac{d^2 v_{2g}}{dx_2^2} &= 2\beta^2 e^{\beta x_2}\left[-C_{21}\sin\beta x_2 + C_{22}\cos\beta x_2\right] \\ &\quad - 2\beta^2 e^{-\beta x_2}\left[-C_{23}\sin\beta x_2 + C_{24}\cos\beta x_2\right] \end{aligned} \tag{4-14}$$

$$\begin{aligned} \frac{d^3 v_{2g}}{dx_2^3} &= 2\beta^3 e^{\beta x_2}\left[-C_{21}\left(\cos\beta x_2 + \sin\beta x_2\right) + C_{22}\left(\cos\beta x_2 - \sin\beta x_2\right)\right] \\ &+ 2\beta^3 e^{-\beta x_2}\left[C_{23}\left(\cos\beta x_2 - \sin\beta x_2\right) + C_{24}\left(\cos\beta x_2 + \sin\beta x_2\right)\right] \end{aligned} \tag{4-15}$$

The particular solution v_{2s}, one of which is the solution of the bearing beam equation with limited range distribution load, is derived by using the technique described on Ref. [2] (Refer to APPENDIX B)

$$
\begin{aligned}
v_{2s} = \frac{\beta}{2k} \times \Bigg[\Bigg[& \frac{\{p_\alpha(2R - x_2) + p_\alpha(x_2 + W) + p_\gamma\}}{2\beta} \\
& \underline{\times e^{-\beta(2R-x_2)} \times \{-2\cos\beta(2R - x_2)\}} + \frac{\{p_\alpha(x_2 + W) + p_\gamma\}}{\beta} \\
& + \frac{p_\alpha \times \{e^{-\beta(2R-x_2)} \times (\sin\beta(2R - x_2) - \cos\beta(2R - x_2)) + 1\}}{2\beta^2} \Bigg] \\
& + \Bigg[\frac{\{p_\alpha x_2 + p_\alpha(x_2 + W) + p_\gamma\} \times e^{-\beta x_2} \times (-2\cos\beta x_2)}{2\beta} \\
& + \frac{\{p_\alpha(x_2 + W) + p_\gamma\}}{\beta} + \frac{p_\alpha \times \{e^{-\beta x_2} \times (\sin\beta x_2 - \cos\beta x_2) + 1\}}{2\beta^2} \Bigg] \Bigg]
\end{aligned}
\tag{4-16}
$$

$$
\begin{aligned}
\frac{dv_{2s}}{dx_2} = -\frac{\beta^2}{k} \times \Bigg[\Bigg[& \frac{\{p_\alpha(2R - x_2) + p_\alpha(x_2 + W) + p_\gamma\} \times e^{-\beta(2R-x_2)}}{2\beta} \\
& \underline{\times \{-\sin\beta(2R - x_2) - \cos\beta(2R - x_2)\}} \\
& + \frac{\{p_\alpha(x_2 + W) + p_\gamma\}}{2\beta} - \frac{p_\alpha \times \{e^{-\beta(2R-x_2)} \times \cos\beta(2R - x_2) - 1\}}{2\beta^2} \Bigg] \\
& + \Bigg[\frac{\{p_\alpha x_2 + p_\alpha(x_2 + W) + p_\gamma\} \times e^{-\beta x_2} \times (-\sin\beta x_2 - \cos\beta x_2)}{2\beta} \\
& + \frac{\{p_\alpha(x_2 + W) + p_\gamma\}}{2\beta} - \frac{p_\alpha \times \{e^{-\beta x_2} \times \cos\beta x_2 - 1\}}{2\beta^2} \Bigg] \Bigg]
\end{aligned}
\tag{4-17}
$$

$$
\begin{aligned}
\frac{d^2 v_{2s}}{dx_2^2} = \frac{1}{4\beta EI} \times \Bigg[\Bigg[& \frac{\{p_\alpha(2R - x_2) + p_\alpha(x_2 + W) + p_\gamma\}}{2\beta} \\
& \underline{\times e^{-\beta(2R-x_2)} \times \{-2\sin\beta(2R - x_2)\}} \\
& - \frac{p_\alpha \times \{e^{-\beta(2R-x_2)} \times (\cos\beta(2R - x_2) + \sin\beta(2R - x_2)) - 1\}}{2\beta^2} \Bigg] \\
& + \Bigg[\frac{\{p_\alpha x_2 + p_\alpha(x_2 + W) + p_\gamma\} \times e^{-\beta x_2} \times (-2\sin\beta x_2)}{2\beta} \\
& - \frac{p_\alpha \times \{e^{-\beta x_2} \times (\cos\beta x_2 + \sin\beta x_2) - 1\}}{2\beta^2} \Bigg] \Bigg]
\end{aligned}
\tag{4-18}
$$

$$\frac{d^3v_{2s}}{dx_2^3}=\frac{1}{2EI}\times\left[\left[\frac{\left\{p_\alpha(2R-x_2)+p_\alpha(x_2+W)+p_\gamma\right\}}{2\beta}\right.\right.$$
$$\times e^{-\beta(2R-x_2)}\times\left\{-\cos\beta(2R-x_2)+\sin\beta(2R-x_2)\right\}$$
$$\left.+\frac{\left\{p_\alpha(x_2+W)+p_\gamma\right\}}{2\beta}+\frac{p_\alpha\times e^{-\beta(2R-x_2)}\times\sin\beta(2R-x_2)}{2\beta^2}\right]$$
$$+\left[\frac{\left\{p_\alpha x_2+p_\alpha(x_2+W)+p_\gamma\right\}\times e^{-\beta x_2}\times(-\cos\beta x_2+\sin\beta x_2)}{2\beta}\right.$$
$$\left.\left.+\frac{\left\{p_\alpha(x_2+W)+p_\gamma\right\}}{2\beta}+\frac{p_\alpha\times e^{-\beta x_2}\times\sin\beta x_2}{2\beta^2}\right]\right] \tag{4-19}$$

The equations of the elastic bearing beam are obtained by combining Eqs. (4-12) - (4-15) and Eqs. (4-16) - (4-19).

$$v_2=e^{\beta x_2}(C_{21}\cos\beta x_2+C_{22}\sin\beta x_2)$$
$$+e^{-\beta x_2}(C_{23}\cos\beta x_2+C_{24}\sin\beta x_2)+v_{2s} \tag{4-20}$$

$$\frac{dv_{2g}}{dx_2}=\beta e^{\beta x_2}\left[C_{21}(\cos\beta x_2-\sin\beta x_2)+C_{22}(\cos\beta x_2+\sin\beta x_2)\right]$$
$$-\beta e^{-\beta x_2}\left[C_{23}(\cos\beta x_2+\sin\beta x_2)-C_{24}(\cos\beta x_2-\sin\beta x_2)\right]+\frac{dv_{2s}}{dx_2} \tag{4-21}$$

$$\frac{d^2v_{2g}}{dx_2^2}=2\beta^2e^{\beta x_2}\left[-C_{21}\sin\beta x_2+C_{22}\cos\beta x_2\right]$$
$$-2\beta^2e^{-\beta x_2}\left[-C_{23}\sin\beta x_2+C_{24}\cos\beta x_2\right]+\frac{d^2v_{2s}}{dx_2^2} \tag{4-22}$$

$$\frac{d^3v_{2g}}{dx_2^3}=2\beta^3e^{\beta x_2}\left[-C_{21}(\cos\beta x_2+\sin\beta x_2)+C_{22}(\cos\beta x_2-\sin\beta x_2)\right]$$
$$+2\beta^3e^{-\beta x_2}\left[C_{23}(\cos\beta x_2-\sin\beta x_2)+C_{24}(\cos\beta x_2+\sin\beta x_2)\right]+\frac{d^3v_{2s}}{dx_2^3} \tag{4-23}$$

4-1-4 Connection of the uplift and the supported part

The boundary conditions and interface conditions between the uplift model and the supported model are as follows.

$$-EI\left[\frac{d^2v_1}{dx_1^2}\right]_{x_1=0} = M_0 \tag{4-24a}$$

$$-EI\left[\frac{d^3v_1}{dx_1^3}\right]_{x_1=0} = V_0 \tag{4-24b}$$

$$\left[v_2\right]_{x_2=\infty} = \left[\frac{dv_2}{dx_2}\right]_{x_2=\infty} = 0 \tag{4-24c}$$

$$\left[v_1\right]_{x_1=W} = \left[v_2\right]_{x_2=0} = 0 \tag{4-24d}$$

$$\left[\frac{dv_1}{dx_1}\right]_{x_1=W} = \left[\frac{dv_2}{dx_2}\right]_{x_2=0} \tag{4-24e}$$

$$\left[\frac{d^2v_1}{dx_1^2}\right]_{x_1=W} = \left[\frac{d^2v_2}{dx_2^2}\right]_{x_2=0} \tag{4-24f}$$

$$\left[\frac{d^3v_1}{dx_1^3}\right]_{x_1=W} = \left[\frac{d^3v_2}{dx_2^3}\right]_{x_2=0} \tag{4-24g}$$

Employing the boundary conditions given by Eqs. (4-24a) and (4-24b), constants of integration C_{11} and C_{12} are obtained as;

$$C_{11} = -V_0 \quad (4\text{-}25) \quad , \qquad C_{12} = -M_0 \tag{4-26}$$

Considering the situation to satisfy the condition given by Eq. (4-24c), C_{21} and C_{22} become;

$$C_{21} = 0 \quad (4\text{-}27) \quad , \qquad C_{22} = 0 \tag{4-28}$$

Employing the conditions given by Eqs. (4-24d), (4-24e), (4-24f) and (4-24g), constants of integration C_{14}, C_{23}, C_{13} and C_{24} are respectively obtained as;

$$C_{14} = -\frac{p_\alpha}{120}\times W^5 - \frac{p_\gamma}{24}\times W^4 - \frac{C_{11}}{6}\times W^3 - \frac{C_{12}}{2}\times W^2 - C_{13}\times W \tag{4-29}$$

$$C_{23} = -\frac{\beta}{2k}\times\left[\left[\frac{\left(2p_\alpha R + p_\alpha + p_\gamma\right)\times e^{-2\beta R}\times\left(-2\cos 2\beta R\right)}{2\beta} + \frac{\left\{p_\alpha W + p_\gamma\right\}}{\beta} + \frac{p_\alpha\times\left\{e^{-2\beta R}\times\left(\sin 2\beta R - \cos 2\beta R\right)+1\right\}}{2\beta^2}\right]\right. \tag{4-30}$$

$$C_{13} = -\frac{p_\alpha}{24}\times W^4 - \frac{p_\gamma}{6}\times W^3 + \frac{V_0}{2}\times W^2 + M_0 \times W$$
$$-\frac{\beta^2 EI}{k}\times\left[\frac{\left(2p_\alpha R + p_\alpha W + p_\gamma\right)\times e^{-2\beta R}\times\left(-\sin 2\beta R - \cos 2\beta R\right)}{2\beta}\right. \tag{4-31}$$
$$\left.+\frac{\left(p_\alpha W + p_\gamma\right)}{2\beta} - \frac{p_\alpha\times\left(e^{-2\beta R}\times\cos 2\beta R - 1\right)}{2\beta^2}\right] + \beta EI\times\left(-C_{23} + C_{24}\right)$$

$$C_{24} = -\frac{1}{2\beta^2 EI}\times\left[\frac{p_\alpha}{6}W^3 + \frac{p_\gamma}{2}W^2 - V_0 W - M_0\right]$$
$$+\frac{1}{8\beta^2 EI}\times\left[\frac{\left(2p_\alpha R + p_\alpha W + p_\gamma\right)\times e^{-2\beta R}\times\left(-\sin 2\beta R\right)}{2\beta}\right. \tag{4-32}$$
$$\left.-\frac{p_\alpha\times\left\{e^{-2\beta R}\times\left(\cos 2\beta R + \sin 2\beta R\right) - 1\right\}}{2\beta^2}\right]$$

$$C_{24} = \frac{1}{2\beta^2 EI}\times\left[\frac{p_\alpha}{2}W^2 + p_\gamma W - V_0\right]$$
$$-\frac{1}{4\beta^3 EI}\times\left[\frac{\left(2p_\alpha R + p_\alpha W + p_\gamma\right)\times e^{-2\beta R}\times\left(-\cos 2\beta R + \sin 2\beta R\right)}{2\beta}\right. \tag{4-33}$$
$$\left.+\frac{p_\alpha W + p_\gamma}{2\beta} + \frac{p_\alpha\times e^{-2\beta R}\times\sin 2\beta R}{2\beta^2}\right] - C_{23}$$

Arranging the Eqs. (4-30), (4-32) and (4-33), cubic equation of W is obtained as;

$$\frac{p_\alpha\beta}{6}W^3 + \left[\frac{p_\alpha}{2} + \frac{\beta p_\gamma}{2}\right]\times W^2 + \left(p_\gamma - \beta V_0\right)\times W - \beta M_0 - V_0 = 0 \tag{4-34}$$

Employing the solution formula for cubic equation, and selecting the significant solutions, uplift width W is given as following formula.

$$W = Y - \left(\frac{1}{\beta} + \frac{p_\gamma}{p_\alpha}\right)$$

$$Y = \sqrt[3]{-q + \sqrt{q^2 + p^2}} + \sqrt[3]{-q - \sqrt{q^2 + p^2}} \qquad \left(q^2 + p^2 > 0\right)$$
$$Y = 2\times\sqrt{-p}\times\cos\left(\frac{u}{3}\right) \qquad \left(q^2 + p^2 > 0\right)$$
$$\cos(u) = \frac{q}{p\sqrt{-p}}\ , \qquad 0 < u < \pi \tag{4-35}$$
$$p = -\frac{1}{\beta^2} - \frac{{p_\gamma}^2}{{p_\alpha}^2} - \frac{2}{p_\alpha}V_0\ ,\quad q = \frac{1}{\beta^3} + \frac{{p_\gamma}^3}{{p_\alpha}^3} + \frac{3p_\gamma}{{p_\alpha}^3}V_0 - \frac{3}{p_\alpha}M_0$$

4-1-5 Trial calculation of the bottom plate model

When the uplift width W is obtained from Eq. (4-35), the displacement and cross sectional force of the bottom plate are calculated by Eqs. (4-8), (4-20) and the integral constants C_{11} –C_{24}.

The trial calculation of the bottom plate is performed with following values. Here, M_0 is the value, when the angle at $x_1 = 0$ becomes 0. And k (nominal reaction of the foundation per unit length) corresponds to the elasticity of the bottom insulation, which consists of Fromglass (insulation material made from expanded glass) and concrete.

R:	37,200 mm	ρ:	480 kg/m^3
h:	36,250 mm	k:	25.5 N/mm^2
M_0:	-1.4×10^5 N-mm	E:	204,000 MPa
V_0:	200 N/mm	I:	666.7 mm^4
P_0:	0.1706 MPaG	w_b:	1.0 mm
P_d:	0.0628 MPaG	t_b:	20.0 mm

FE analysis program: MSC NASTRAN

Figure 4-4 shows a non-linear beam static FE analysis model, which consists of beam and spring support elements and to be performed for comparison with the calculation results. For this numerical calculation, general purpose program NX Nastran provided by Numerical Simulation Tech Corporation is used. The results of the non-linear beam static FE analysis include simplified linear distribution load case and Housner's distribution load case. Figure 4-5 compares the calculation results and the numerical one.

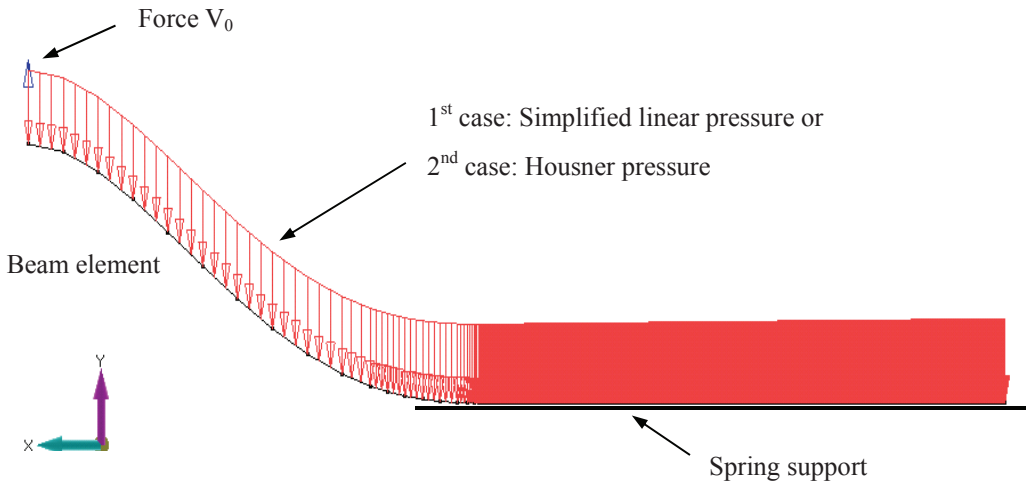

FE analysis program: NX NASTRAN

FIGURE 4-4: FE ANALYSIS MODEL OF THE BOTTOM PLATE

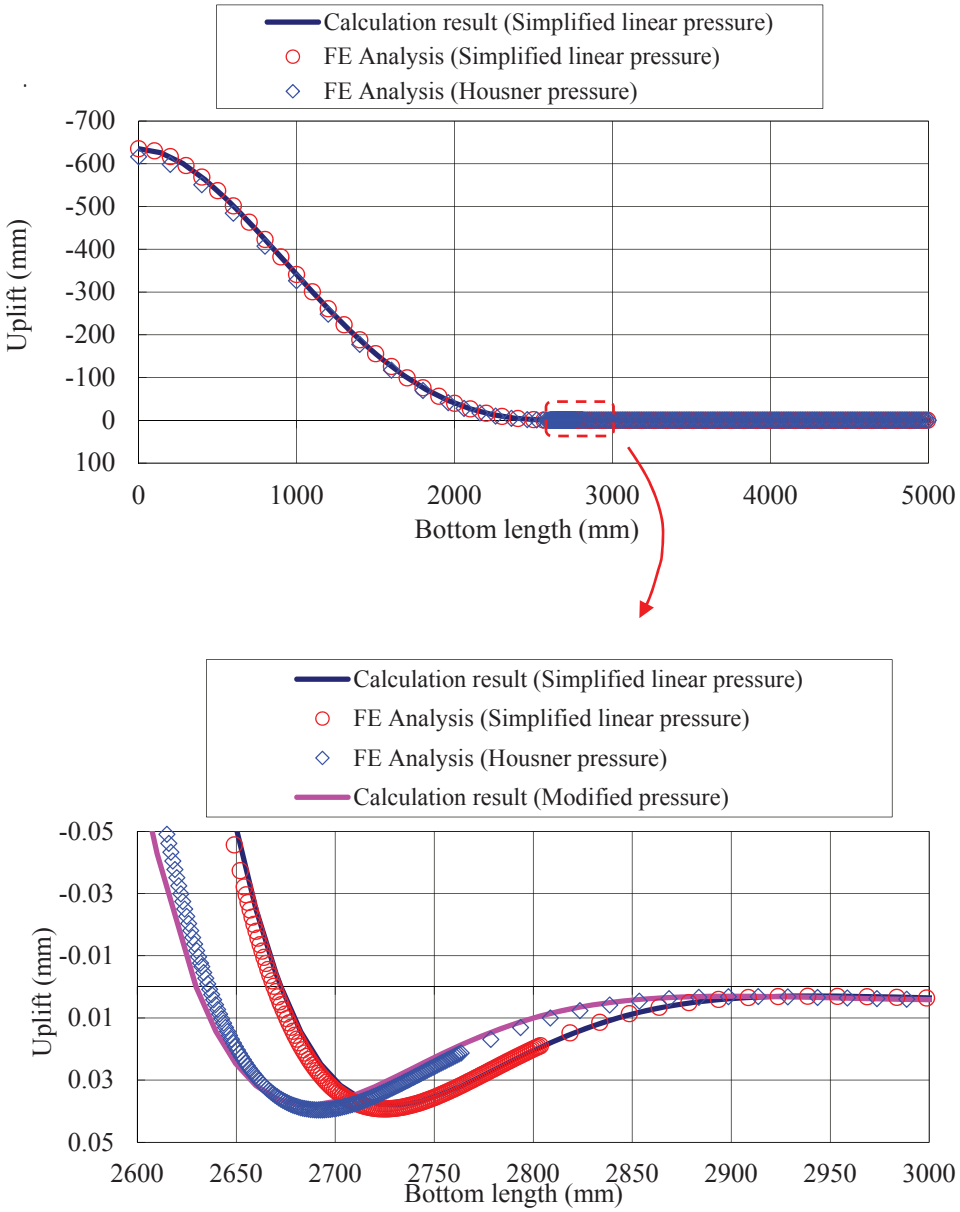

FIGURE 4-5: DISPLACEMENT OF THE BOTTOM PLATE

From Figure 4-5, the results of the mathematical model, which apply the simplified linear pressure distribution, are the same as the results of the non-linear beam static FE analysis with linear pressure. The uplift height of the mathematical model and the non-linear beam static FE analysis with Housner's distribution are 635mm and 616mm, the uplift width are 2,673mm and 2,637mm, respectively. These values are sufficiently close and it demonstrates the simplified linear distribution pressure model is acceptable for a estimation of the bottom plate displacement.

In enlarged view graph shows that the bottom plate at uplift starting point sinks deeper in the bottom insulation than other part. The difference between the mathematical model with linear pressure and the non-linear beam static FE analysis with Hounser pressure is caused by only difference of pressure distribution. In the graph, calculation result of the mathematical model with modified liner pressure distribution as shown in Figure 4-6 to correspond with Hounser pressure, are also plotted. This modified distribution is made so as to close the average values within 3m from 0 m or 74.4m to Housner's value. The calculation result with modified liner pressure distribution shows rather corresponding to the result of the non-linear beam static FE analysis with Housner's pressure than the result with liner pressure distribution. Even so, the liner pressure distribution model shows sufficiently good agreement and acceptable accuracy, therefore, liner pressure distribution model is selected for this study.

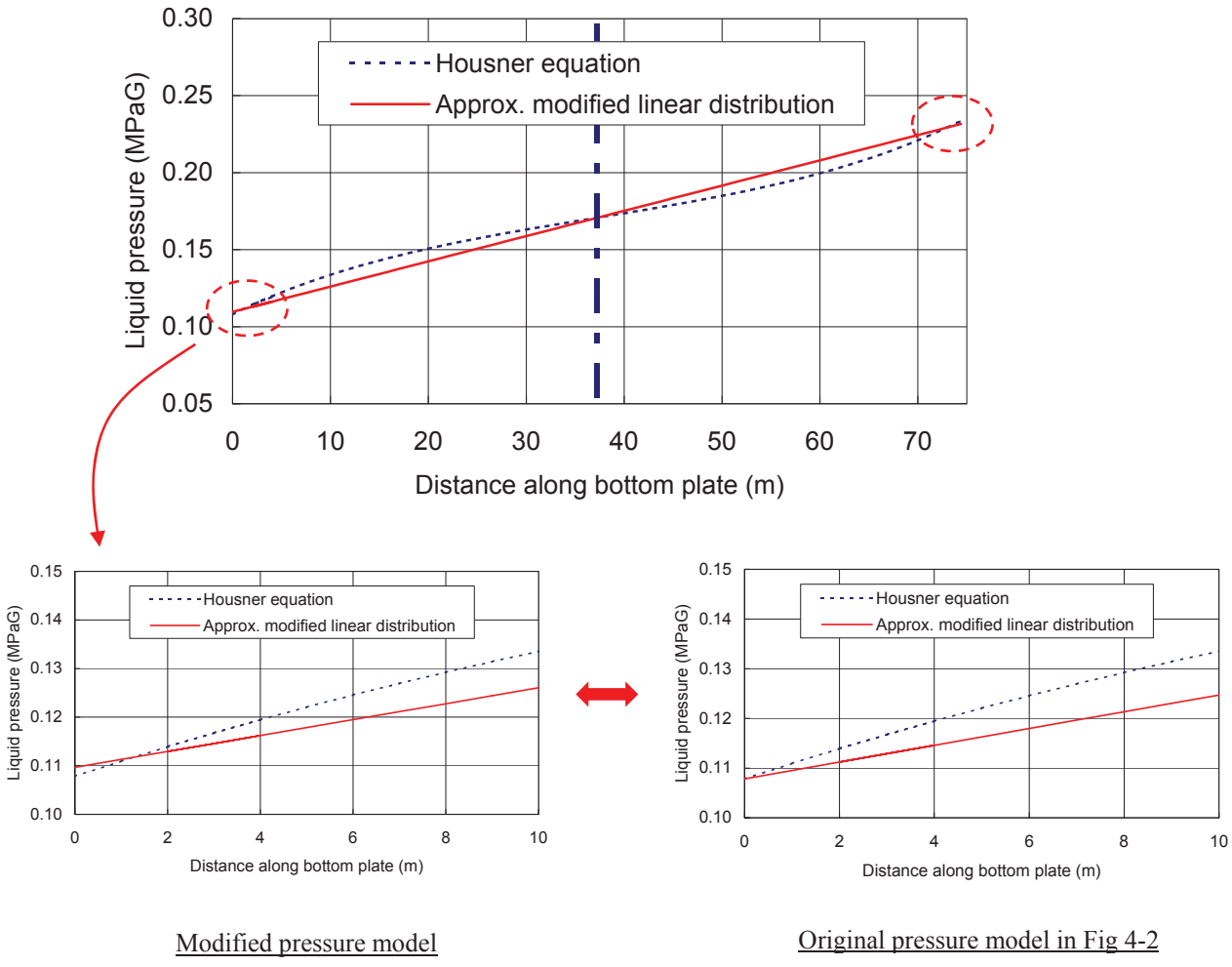

Modified pressure model

Original pressure model in Fig 4-2

FIGURE 4-6: MODIFIED PRESSURE MODEL

4-2 MODELING OF THE SIDEWALL

4-2-1 Modeling of the sidewall

A sidewall bulges and deforms by static and dynamic pressure, and this deformation is expected to affect a bottom plate displacement. To consider an effect of sidewall bulging deformation on uplift of a bottom plate, the sidewall mathematical model with inner pressure is established by applying a cylindrical shell theory, and combined with the bottom plate model.

Consider the cylindrical coordinate system, which has x_3 axis along the tank height direction and R axis along radius direction and the bulging displacement of the sidewall is expressed as v_3.

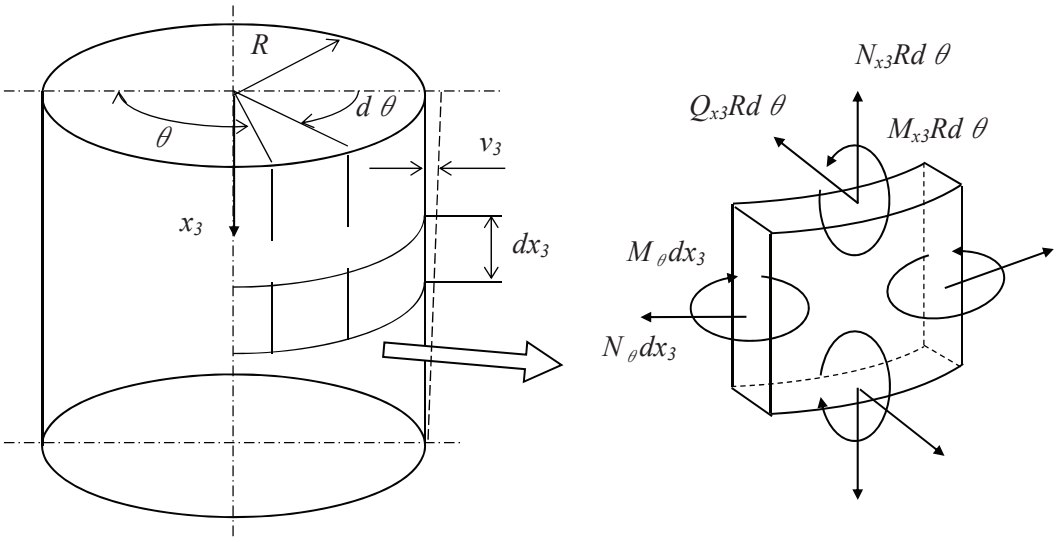

FIGURE 4-7: MODEL OF THE SIDEWALL

Where,

M_{x3}, M_θ:	Moment at the sidewall
N_{x3}, N_θ:	Membrane force at the sidewall
Q_{x3}, Q_θ:	Shear force at the sidewall

Cut out the shell element of $Rd\theta\, dx$ and consider the force balance conditions as;

$$\frac{dNx_3}{dx_3} = 0 \quad , \quad N_\theta = R \times \frac{dQ_{x_3}}{dx_3} \quad , \quad Q_{x_3} = \frac{dM_{x_3}}{dx_3} \tag{4-36}$$

The relationship with bulging displacement v_3 and strain of circumferential direction of the sidewall ε is;

$$v_3 = \varepsilon \times R \tag{4-37}$$

Employing the sidewall thickness t_s and modulus of elasticity of sidewall E_s and Hook's low, circumferential cross sectional force N_θ becomes;

$$N_\theta = \sigma \times t_s = E_s \times \varepsilon \times t_s = \frac{E_s t_s v_3}{R} \tag{4-38}$$

Substituting the relationship $N_\theta = R \times P_T$ for Eq. (4-38), bulging displacement v_3 is expressed as;

$$v_3 = \frac{P_T \times R^2}{E_s t_s} \tag{4-39}$$

Here, liquid pressure P_T consists of static and dynamic pressure. Approximating each heightwise pressure distribution as linear, bulging displacement of the sidewall caused by inner pressure is expressed as;

$$v_3 = \frac{\left[\rho(h - x_3) + P_{ds1} + P_{ds2}\left(1 - \frac{x_3}{h}\right)\right] \times R^2}{E_s t_s} \tag{4-40}$$

Where,

ρ:	Fluid density
h:	Liquid height
P_{ds1}, P_{ds2}:	Dynamic pressure on the sidewall
R:	Tank radius
E_s:	Modulus of elasticity of the sidewall
t_s:	Thickness of bottom of the sidewall

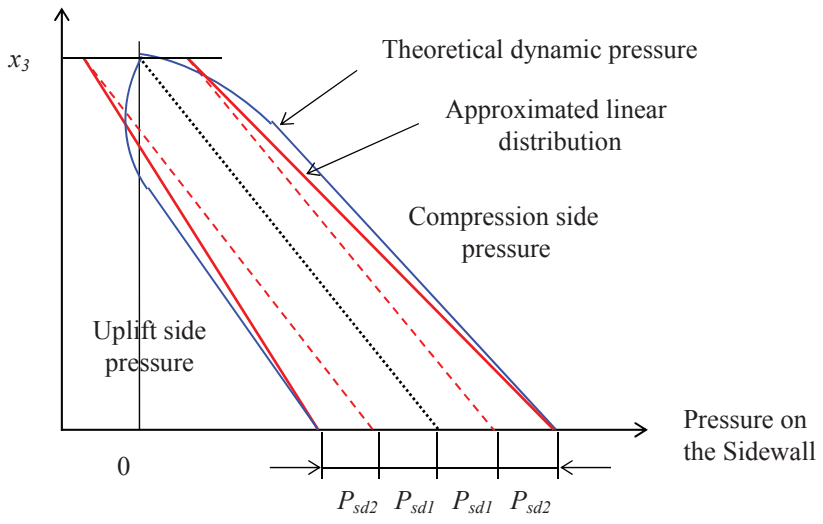

FIGURE 4-8: MODELING OF PRESSURE ON THE SIDEWALL

Bending moment at boundary of the shell element M_{x3} is expressed with deformed radius R_1, as follows.

$$M_{x_3} = \frac{D}{R_1} = -D\frac{d^2 v_3}{dx_3^2} \quad , \quad D = \frac{E_s t_s^3}{\left[12\left(1-\nu^2\right)\right]} \tag{4-41}$$

Therefore, Q_{x3}, N_θ becomes;

$$Q_{x_3} = -D\frac{d^3 v_3}{dx_3^3} \quad , \quad N_\theta = -D\frac{d^4 v_3}{dx_3^4} \tag{4-42}$$

Employing Eq. (4-38), Eq. (4-42) becomes;

$$\frac{d^4 v_3}{dx_3^4} + \frac{E_s t_s v_3}{DR^2} = 0 \tag{4-43}$$

Rewriting as $K = \sqrt[4]{3\left(1-\nu^2\right)/\left(R^2 t_s^2\right)}$, Eq. (4-43) becomes;

$$\frac{d^4 v_3}{dx_3^4} + 4K^2 \times v_3 = 0 \quad , \quad K = \sqrt[4]{\frac{3\left(1-\nu^2\right)}{R^2 t_s^2}} \tag{4-44}$$

The solution of this equation is the bulging displacement of the sidewall considering the boundary conditions and to be derived as follows.

$$\begin{aligned} v_3 = {} & C_{31} \times e^{-Kx_3} \cos Kx_3 + C_{32} \times e^{-Kx_3} \sin Kx_3 \\ & + C_{33} \times e^{Kx_3} \cos Kx_3 + C_{34} \times e^{Kx_3} \sin Kx_3 \end{aligned} \tag{4-45}$$

The bulging displacement is expressed by addition of Eqs. (4-40) and (4-45).

$$\begin{aligned} v_3 = {} & \frac{\left[\rho\left(h-x_3\right) + P_{ds1} + P_{ds2}\left(1-\frac{x_3}{h}\right)\right] \times R^2}{E_s t_s} \\ & + C_{31} \times e^{-Kx_3} \cos Kx_3 + C_{32} \times e^{-Kx_3} \sin Kx_3 \\ & + C_{33} \times e^{Kx_3} \cos Kx_3 + C_{34} \times e^{Kx_3} \sin Kx_3 \end{aligned} \tag{4-46}$$

The derived functions of Eq. (4-46) are derived as follows.

$$\frac{dv_3}{dx_3} = \frac{\left(-\rho - \frac{P_{ds2}}{h}\right) \times R^2}{E_s t_s} + Ke^{-Kx_3}\left[(C_{31} - C_{32})\cos Kx_3 + (C_{31} + C_{32})\sin Kx_3\right] \tag{4-47}$$

$$\frac{d^2 v_3}{dx_3^2} = 2K^2 e^{-Kx_3}\left(C_{31}\sin Kx_3 - C_{32}\cos Kx_3\right) \tag{4-48}$$

The boundary condition at the top of sidewall and interface conditions between the sidewall and the bottom plate are;

$$\left[v_3\right]_{x_3=h} = \frac{\left[\rho(h-h) + P_{ds1} + P_{ds2}\left(1 - \frac{h}{h}\right)\right] \times R^2}{E_s t_s} = \frac{P_{ds1} \times R^2}{E_s t_s} \tag{4-49a}$$

$$\left[v_3\right]_{x_3=0} = 0 \tag{4-49b}$$

$$-\left[\frac{dv_3}{dx_3}\right]_{x_3=0} = \left[\frac{dv_1}{dx_1}\right]_{x_1=0} \tag{4-49c}$$

$$D\left[\frac{d^2 v_3}{dx_3^2}\right]_{x_3=0} = -EI\left[\frac{d^2 v_1}{dx_1^2}\right]_{x_1=0} \tag{4-49d}$$

Employing the boundary conditions given by Eq. (4-49a), constants of integration C_{33} and C_{34} are obtained.

$$C_{33} = C_{34} = 0 \tag{4-50}$$

Employing the boundary conditions given by Eqs. (4-49b), (4-49c) and (4-49d), constants of integration C_{31}, C_{32} and M_0 are respectively obtained as;

$$C_{31} = (\rho h + P_{ds1} + P_{ds2}) \times \frac{R^2}{E_s t_s} \tag{4-51}$$

$$C_{32} = C_{31} + \frac{C_{13}}{KEI} - \left(\rho + \frac{P_{ds2}}{h}\right) \times \frac{R^2}{KE_s t_s} \tag{4-52}$$

$$\begin{aligned} M_0 &= 2DK^2 \times C_{32} \\ &= 2DK^2 \times \left[(\rho h + P_{ds1} + P_{ds2}) \times \frac{R^2}{E_s t_s} - \left(\rho + \frac{P_{ds2}}{h}\right)\frac{R^2}{KE_s t_s}\right] + \frac{2DK}{EI} C_{13} \end{aligned} \tag{4-53}$$

Substituting C_{13} of Eq. (4-31) for Eq. (4-53), quartic equation of the uplift width W is obtained as;

$$
\begin{aligned}
&-\frac{p_\alpha DK}{4EI}\times W^4+\left[\frac{p_\alpha}{6}-\frac{p_\alpha DK}{\beta EI}-\frac{2DK\lambda}{3EI}\right]\times W^3\\
&+\left[\frac{p_\alpha}{2\beta}+\frac{p_\gamma}{2}-\frac{p_\alpha DK}{2\beta^2 EI}-\frac{2p_\gamma DK}{\beta EI}+\frac{DKV_0}{EI}\right]\times W^2\\
&+\left[-V_0+\frac{p_\gamma}{\beta}-\frac{p_\gamma DK}{\beta^2 EI}+\frac{2DKV_0}{\beta EI}\right.\\
&\qquad\left.-\frac{p_\alpha DK\beta\times e^{-2\beta R}\times\sin 2\beta R}{k}+\frac{p_\alpha DK\times e^{-2\beta R}\times\sin 2\beta R}{4\beta^3 EI}\right]\times W\\
&-\frac{V_0}{\beta}+\frac{DKV_0}{\beta^2 EI}-2DK^2\left[\frac{(\rho h+P_{ds1}+P_{ds2})R^2}{E_s t_s}-\frac{\left(\rho+\frac{P_{ds2}}{h}\right)R^2}{KE_s t_s}\right.\\
&-\frac{DK\beta}{k}\times\left[(2p_\alpha R+p_\gamma)\times e^{-2\beta R}\times\sin 2\beta R+\frac{p_\alpha\left\{e^{-2\beta R}\times(\sin 2\beta R+\cos 2\beta R)-1\right\}}{2\beta}\right]\\
&+\frac{DK}{8\beta^3 EI}\times\left[(2p_\alpha R+p_\gamma)\times e^{-2\beta R}\times 2\sin 2\beta R\right.\\
&\qquad\left.\left.+\frac{p_\alpha\left\{e^{-2\beta R}\times(\sin 2\beta R+\cos 2\beta R)-1\right\}}{\beta}\right]=0
\end{aligned}
\tag{4-54}
$$

4-2-2 Introducing the equivalent stiffness

In this study, a beam theory is applied for the bottom plate to simplify the problem. In the actual structure, the bottom plate is a circle plate and its periphery part is connected to the sidewall. Therefore, some stiffness difference exists between the proposed model and actual structure. To compensate for this difference, this study tries to introduce the bottom plate model.

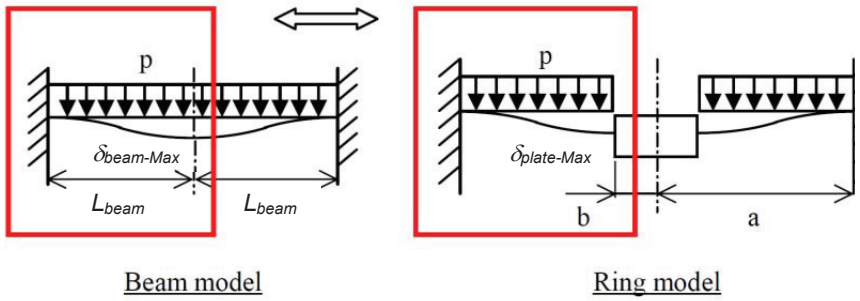

FIGURE 4-9: BEAM AND PLATE MODEL

Where,

p:	Uniformed distribution load
L_{beam}:	Half length of beam
a:	Radius of ring
b:	Radius of inner edge guide
$\delta_{beam\text{-}Max}$:	Maximum displacement of beam
$\delta_{plate\text{-}Max}$:	Maximum displacement of plate

A maximum displacement of the ring plate with uniformed distribution load, periphery fixed and inner edge guided conditions is expressed by Eq. (4-55) [3]. On the other hand, the maximum displacement of the beam with uniformed load and both edges fixed conditions is expressed by Eq. (4-56).

$$\delta_{plate-Max} = \frac{pa^4}{D}\left(\frac{C_2 L_{beam14}}{C_5} - L_{beam11}\right)$$

$$D = \frac{E_{plate} \times t_{br}^3}{\left[12\left(1-\nu^2\right)\right]}$$

$$C_2 = \frac{1}{4}\left[1-\left(\frac{b}{a}\right)^2\left(1+2\ln\frac{a}{b}\right)\right] \quad , \quad C_5 = \frac{1}{2}\left[1-\left(\frac{b}{a}\right)^2\right] \tag{4-55}$$

$$L_{beam11} = \frac{1}{64}\left[1+4\left(\frac{b}{a}\right)^2 - 5\left(\frac{b}{a}\right)^4 - 4\left(\frac{b}{a}\right)^2\left\{2+\left(\frac{b}{a}\right)^2\right\}\ln\frac{a}{b}\right]$$

$$L_{beam14} = \frac{1}{16}\left[1-\left(\frac{b}{a}\right)^4 - 4\left(\frac{b}{a}\right)^2 \ln\frac{a}{b}\right]$$

$$\delta_{beam-Max} = \frac{p\left(2L_{beam}\right)^4}{384E_{beam}I} \quad , \quad I = \frac{W_{beam} \times t_{br}^3}{12} \tag{4-56}$$

Where,

$\delta_{beam\text{-}Max}$:	Maximum displacement of beam
$\delta_{plate\text{-}Max}$:	Maximum displacement of plate
E_{beam}:	Modulus of elasticity of beam
E_{plate}:	Modulus of elasticity of ring
ν:	Poisson's ratio
W_{beam}:	Width of beam
t_{br}:	Thickness of beam and ring

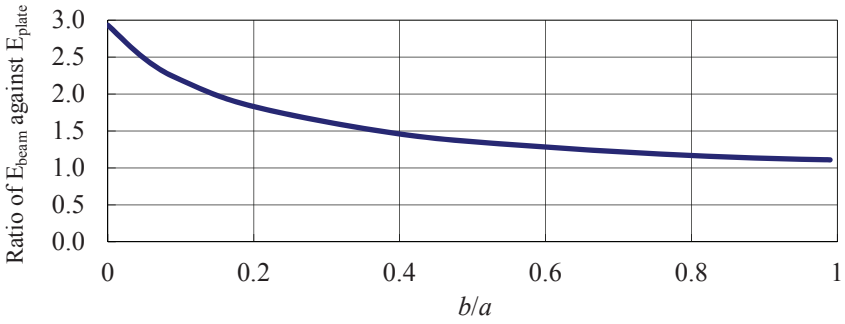

FIGURE 4-10: RELATION OF E_{beam} and E_{plate}

To equate the maximum displacements of both models, relation of modulus elasticity of the beam and the ring plate should be as Figure 4-10. As later calculation shows, *b/a* becomes 0.93 with the assumed conditions, then E_{beam} corresponds to about 1.12 times of E_{plate}.

$$E_{beam} = 1.12 \times E_{plate} \tag{4-57}$$

Employing this rate, the relation of the modulus of elasticity of the bottom plate E and that of sidewall E_s becomes;

$$E = 1.12 \times E_s \tag{4-58}$$

4-2-3 Trial calculation of the bottom plate and the sidewall model

When the uplift width W is obtained from Eq. (4-54), the displacement and cross sectional force of the bottom plate and the sidewall are calculated by Eqs. (4-8), (4-20), (4-46) and coefficients C_{11} –C_{34}.

R: 37,200 mm
h: 36,250 mm
ρ: 480 kg/m^3
V_0: 230 N/mm
(Same condition as FE analysis)
P_0: 0.1831 MPaG
= 0.1686MPaG + 0.0145 MPaG
(Static pressure + Vertical earthquake pressure)
k: 25.5 N/m^2
E: = 1.12E_s = 213,920 MPa
E_s: 191,000 MPa
t_b: 18.7 mm
t_{sa}: 20.8 mm (Average thickness of top and bottom sidewall)
P_d: 0.0380 MPaG
P_{ds1}: 0.0209 MPaG (55% of P_d)
P_{ds2}: 0.0171 MPaG (45% of P_d)

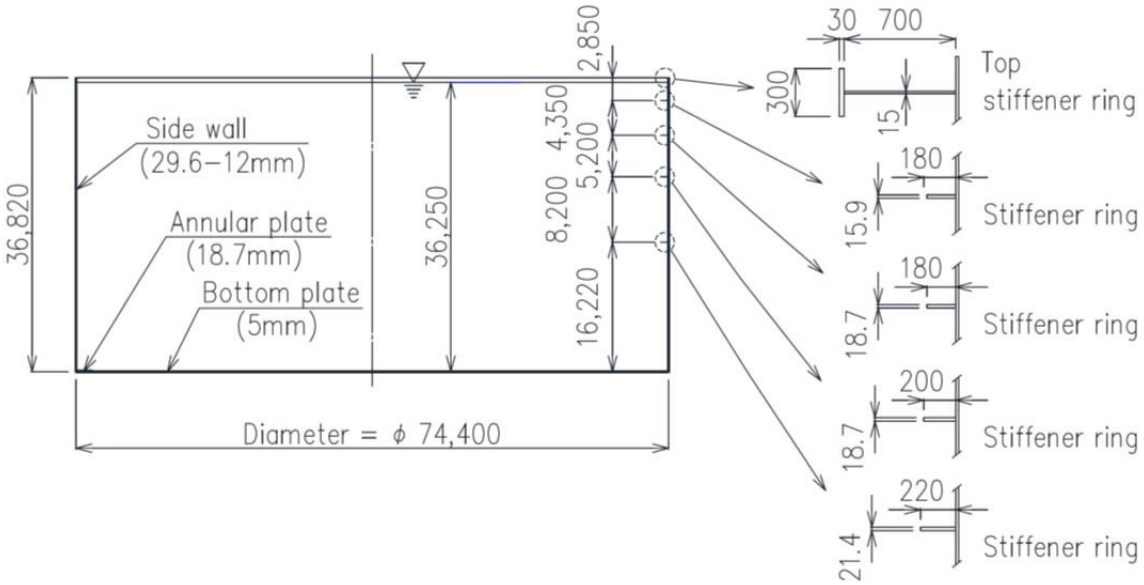

FIGURE 4-11: TANK CONFIGURATION

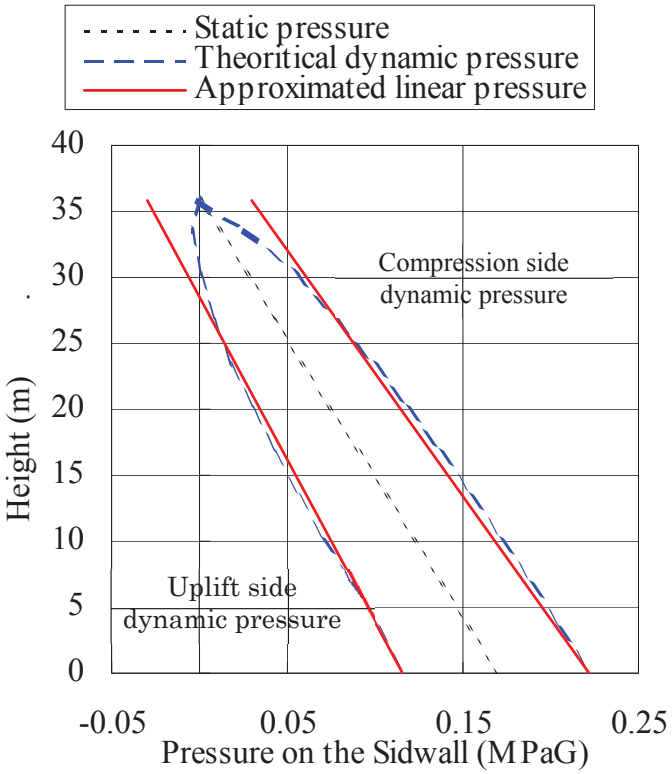

FIGURE 4-12: APPLIED PRESSURE ON THE SIDEWALL

The displacement of the bottom plate and the sidewall are calculated with the values in Figure 4-11 and the approximated uplift side dynamic pressure shown in Figure 4-12. The values of P_{ds1} and P_{ds2} are decided as the total force due to approximated linear dynamic pressure

became equal to that of theoretical dynamic pressure. Average thickness of the tank is applied for representative sidewall thickness t_s. To verify the calculation result, the non-linear 3D static FE analysis of the tank shown in Figure 4-13 was also performed with the same conditions and each result is compared. For this numerical calculation, general purpose program Abaqus developed by Dassault Systèmes is used. Figure 4-12 shows the approximated dynamic pressure distribution applied for the calculation and the theoretical dynamic pressure used for the non-linear 3D static FE analysis.

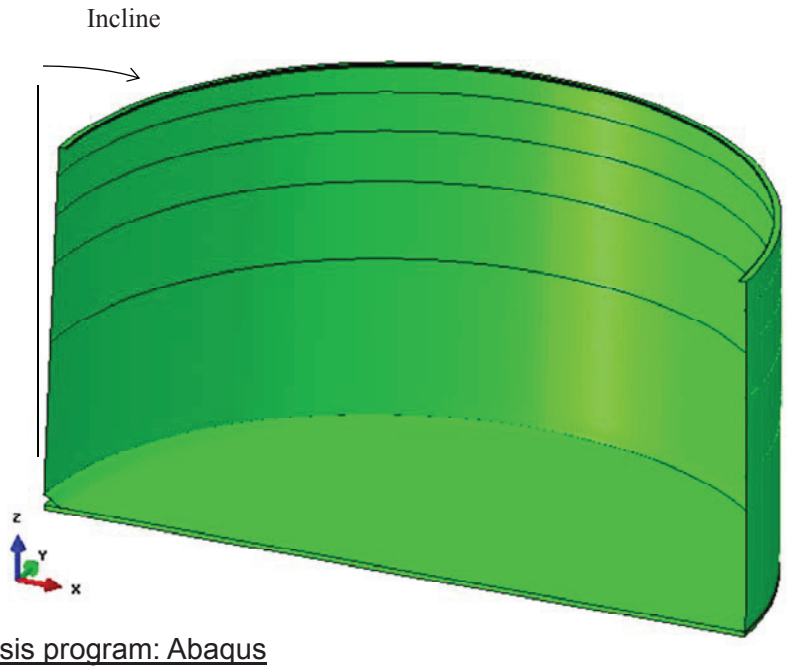

FE analysis program: Abaqus

FIGURE 4-13: DISPLACEMENT OF THE FE ANALYSIS

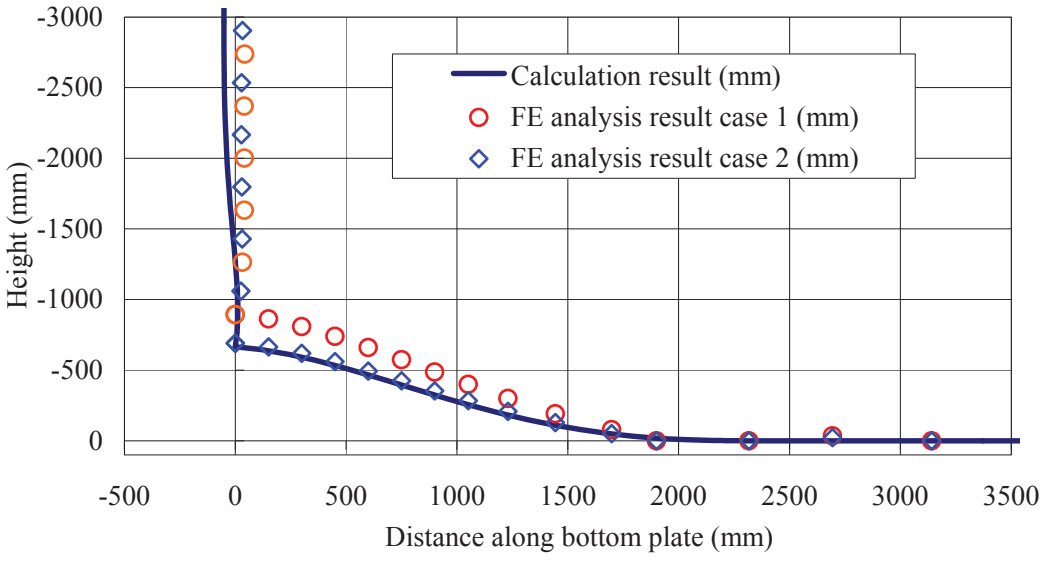

FIGURE 4-14: CALCULATION RESULT

Figure 4-14 shows the displacement calculated by the mathematical model and the non-linear 3D static FE analysis. The non-linear 3D static FE analysis was performed with 2 cases, which had different stiffness of stiffeners. The uplift height and width of the mathematical model are 662mm and 2,341mm, and those of the non-linear 3D static FE analysis are 691 – 894mm and 1,900mm, respectively. The results of the model and the non-linear 3D static FE analysis show the same trend, however differences of uplift height exist. As shown in Figure 4-13, the sidewall of uplift side leaned toward the tank center about 1.3 – 1.7 degree and the top of the sidewall deformed as oval shape. This deformation mode has an influence on the uplift height and considered as one of major cause of the difference between the proposed model and the non-linear 3D static FE analysis. As introduced the result of previous study in Figure 2-3, this phenomenon (deformation mode of sidewall and uplift height) is directly in proportion as increasing of compressive stress at sidewall. Therefore, this phenomenon has to be investigated in detail and will be researched at other opportunities. In Chapter 5, relation between oval shape deformation at top of the sidewall and uplift height of bottom plate is modeled mathematically.

4-3 CASE STUDY

4-3-1 Case study of the uplift

To understand the influence of the thickness of the bottom plate and sidewall thickness and elasticity of the bottom insulation on uplift behavior, the calculation by the mathematical model is performed with varied conditions.

Figures 4-15-1 to 3 show the obtained displacement for varied conditions.

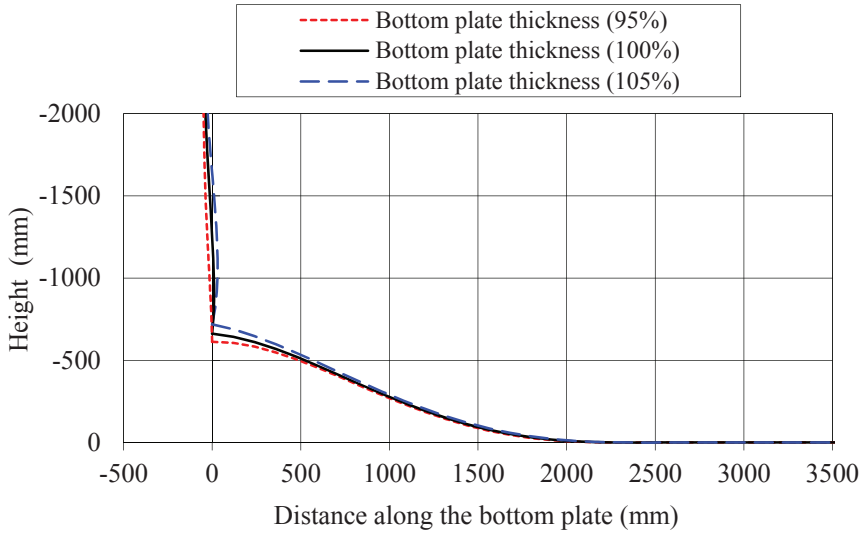

FIGURE 4-15-1: DISPLACEMENT OF THE BOTTOM AND THE SIDEWALL (DIFFERENCE OF BOTTOM PLATE THICKNESS)

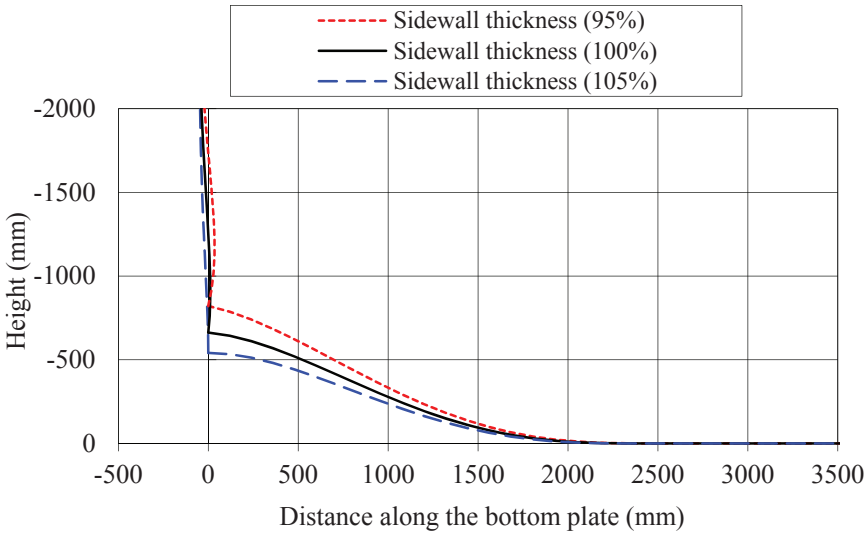

FIGURE 4-15-2: DISPLACEMENT OF THE BOTTOM AND THE SIDEWALL (DIFFERENCE OF SIDEWALL THICKNESS)

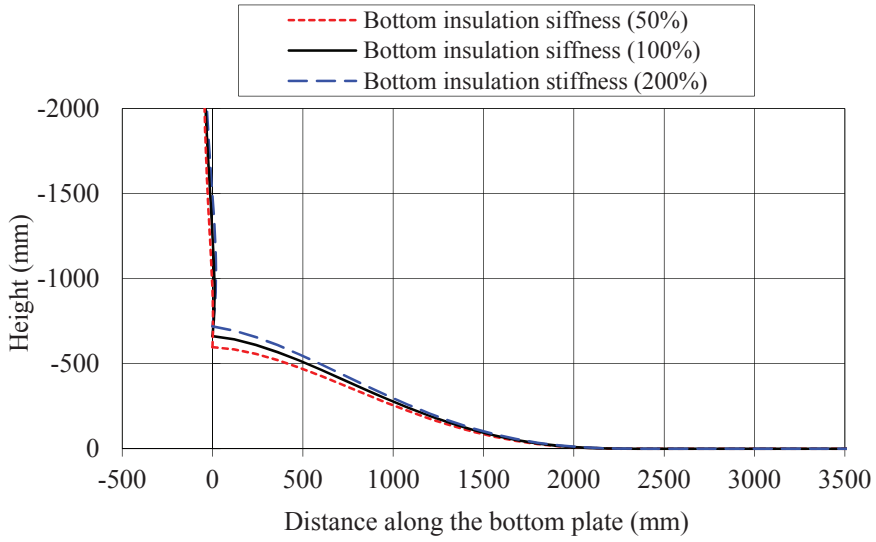

FIGURE 4-15-3: DISPLACEMENT OF THE BOTTOM AND THE SIDEWALL (DIFFERENCE OF INSULATION STIFFNESS)

As Figures 4-15-1 to 3 show, the uplift height and width are different due to thickness of the bottom plate and sidewall, and elasticity of the bottom insulation. Table 4-1 summarizes those tendencies. The difference of the uplift width is relatively small. On the contrary, the uplift varied by conditions. Particularly, it is found that the thickness of sidewall affects the uplift height significantly.

TABLE 4-1: SUMMARY OF PARAMETER STUDY

Bottom plate thickness (%)	Uplift height	Uplift width	Sidewall thickness (%)	Uplift height	Uplift width	Insulation stiffness (%)	Uplift height	Uplift width
95	92%	98%	95	***124%***	***102%***	50	90%	99%
100	100%	100%	100	100%	100%	100	100%	100%
105	109%	102%	105	***82%***	***98%***	200	109%	101%

4-3-2 Influence of the uplift on dynamic pressure

The extent of the influence due to various conditions on the uplift-induced dynamic pressure is estimated by employing Eq. (4-59), which is established in the previous study [4] based on an assumption of an inviscid, incompressible, irrotational fluid, by applying the velocity potential theory and using a rectangular tank model with a unit width.

$$p(x,z,t) = -\rho\ddot{\theta}_0(t)\left[\left(l-\frac{a}{2}\right)(z-h)\right.$$

$$+\frac{4l}{\pi^2}\sum_{n=1}^{\infty}\left(\left\{(-1)^n-\cos\frac{n\pi a}{2l}\right\}\frac{2l}{n^3\pi}\times\frac{2l}{2l-a}\left(\tanh\frac{n\pi z}{2l}-\tanh\frac{n\pi h}{2l}\right)\cosh\frac{n\pi z}{2l}\right.$$

$$+\left\{1-(-1)^n\right\}\frac{1}{n^2}\left[z-\frac{2l}{n\pi}\sinh\frac{n\pi z}{2l}\right.$$

$$\left.\left.\left.+\left(\frac{2l}{n\pi}\tanh\frac{n\pi h}{2l}-\frac{h}{\cosh\frac{n\pi h}{2l}}\right)\cosh\frac{n\pi z}{2l}\right]\right)\cos\frac{n\pi x}{2l}\right] \tag{4-59}$$

Where,

p: Dynamic pressure

ρ: Fluid density

$\ddot{\theta}_0$: Angular acceleration of the sidewall

$2l$: Tank length (= diameter)

a: Start point of uplift

h: Tank height

In the previous study [5], the value of $\ddot{\theta}_0$ for the same dimension tank as this study is estimated as 0.05 – 0.15 rad/s^2 from the time historical FE analysis in Chapter 3.

As Table 4-1 shows, 5% thickness variation of the sidewall causes about 24% difference of the uplift height. Angular acceleration $\ddot{\theta}_0$ is in proportion to the uplift height, since it is considered that the uplift period is depends on bulging period and has no relationship with uplift height. Therefore, when uplift height increases, angular acceleration proportionally increases.

Then, in this parameter study, 0.15 rad/s^2 is used for the angular acceleration of the 100% sidewall thickness case, 0.19 rad/s^2 (1.24 times of 0.15 rad/s^2) is used for the 95% sidewall thickness case. Also uplift width ratio listed in Table 4-1 is applied.

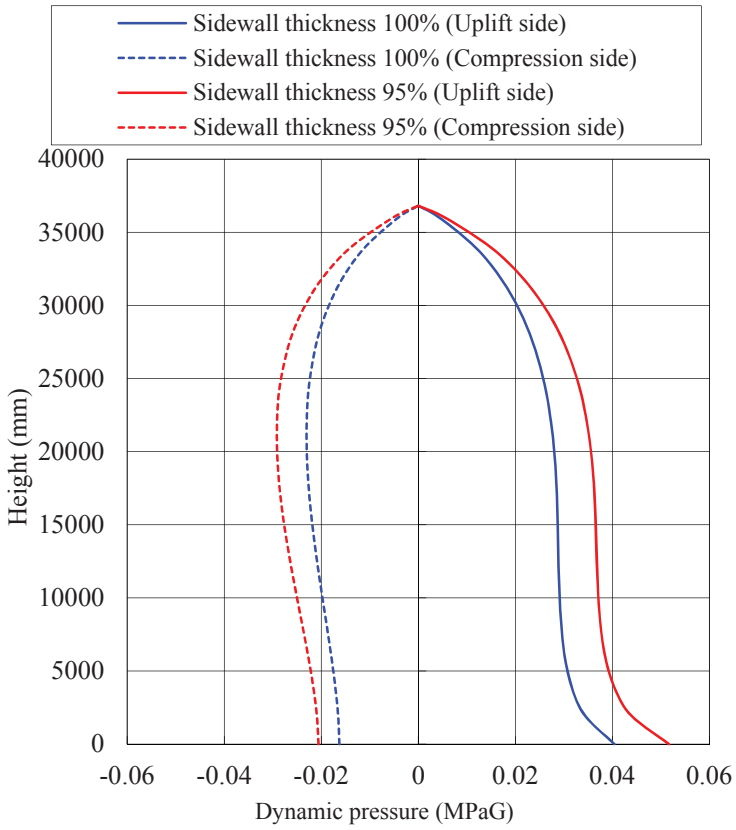

FIGURE 4-16: DYNAMIC PRESSURE CAUSED BY UPLIFT

Figure 4-16 shows the calculation results of uplift-induced dynamic pressure of uplift and compression side, respectively. It indicates that 5% sidewall thickness variation causes about maximum 27% difference on the uplift-dynamic pressure.

Since the magnitude of the uplift-induced dynamic pressure is estimated as about 20% of overall dynamic pressure [5], the afore mentioned pressure difference is equivalent to about 6% of overall dynamic pressure.

4-4 FINDINGS

In this chapter, the mathematical model (referred to as the Structural Mathematical Model) for the tank bottom plate was established, which included the uplift behavior and the influence of the sidewall deformation. In addition, this proposed mathematical model was verified by comparing with the result of the non-linear beam static FE analysis and the non-linear 3D static FE analysis, which was performed with the same conditions as the mathematical model. Besides parameter study by the mathematical model was performed to investigate the influence of thickness of the bottom plate and the sidewall and the elasticity of the bottom insulation on the uplift behavior.

Findings from this research are summarized below.

- The thickness of the bottom plate and the sidewall and the elasticity of the bottom insulation affect the uplift height. Beside the uplift width receives small influence by these variations.
- In case of thinner bottom plate, the uplift height becomes small. On the contrary, thinner sidewall, the uplift height becomes larger.
- In case of high elasticity of the bottom insulation, the uplift becomes larger.
- The variation of the sidewall thickness has the most impact to the uplift height. In the parameter study, 5% thickness variation causes about 24% uplift height difference.
- The magnitude of uplift-induced dynamic pressure is affected by the conditions of the bottom plate and the sidewall thickness and the elasticity of the bottom insulation.
- In the parameter study, 5% thickness variation of the sidewall causes about 6% difference of the overall dynamic pressure.

REFERENCES

[1] Housner, G. W., 1957, “Dynamic Pressure on Accelerated Fluid Containers”, Bulletin of the Seismological Society of America, Vol. 47, pp. 15-35.

[2] Stephen P. T., 1956. “Strength of Materials Part II Advanced Theory and Problems”, D. Van Nostrand Company, Inc.

[3] Warren C. Young, 1989, “ROARK’S Formulas for stress & Strain 6th edition”, McGraw-Hill Book Company.

[4] Taniguchi, T. and Segawa, T., 2008, “Fluid Pressure on Rectangular Tank Consisting of Rigid Side Walls and Rectilinearly Deforming Bottom Plate Due to Uplift Motion”, PVP2008-61166.

[5] Hayashi. S., Taniguchi, T., etc., 2011, “A Study of Fluid-Structure Coupled Analysis for Large LNG Storage Tanks in Consideration of Uplift”, PVP2011-57925.

CHAPTER 5

MODELING OF AXIAL FORCE DISTRIBUTION AT BOTTOM OF SIDEWALL WHEN UPLIFT OF BOTTOM PLATE OCCURS

CHAPTER 5

MODELING OF AXIAL FORCE DISTRIBUTION AT BOTTOM OF SIDEWALL WHEN UPLIFT OF BOTTOM PLATE OCCURS

In this chapter, the mathematical model (referred to as the Force Coupling Mathematical Model) is established for obtaining axial force distribution at a bottom of a sidewall of a cylindrical tank due to the tank's response to an earthquake.

The model demonstrates that a crescent shaped area of the bottom plate of the tank is expected to lift away from the tank bottom insulation due to a change in the axial forces. This change is caused by the overturning moment generated by the bulging and the rocking motion of the tank and its contents as the result of an earthquake. The overturning moment generates the axial forces which act on the bottom of the tank sidewall. Around the perimeter of the tank, these axial forces vary from being compressive to being tensile.

Chord = Neutral axis for equilibrium of overturning moment and force couple
Minor Segment = relatively small area under net compressive forces
Major Segment = relatively large area under net tensile forces
Annular plate = thicker and width plate under the sidewall

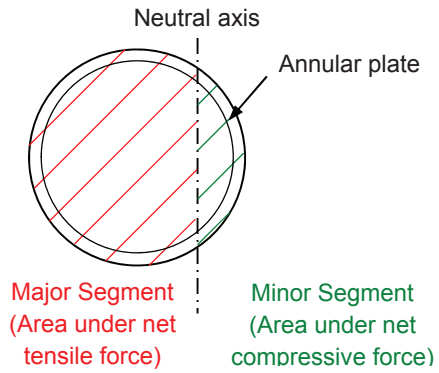

FIGURE 5-1: DEFINITION OF SEGMENT

5-1 MODELING OF THE EXTENT OF THE UPLIFT AREA DUE TO SUBSIDENCE OF THE TANK'S BOTTOM PLATE

5-1-1 Modeling of the extent of the uplift area

The extent of the uplift area of the bottom plate is affected by:

- Subsidence of the tank bottom due to the overturning moment,
- Width of the annular plate of the tank bottom part which is located underneath the tank's sidewall,

- Effects of oval shape deformation at the top of the sidewall on uplift height.

This chapter develops the mathematical model (the Force Coupling Mathematical Model) of a tank experiencing an earthquake. The model includes the effect of subsidence of the tank's bottom plate and the corresponding uplift of the opposite end of the bottom plate.

The parameters derived from the model are:

- the location of the neutral axis due to the overturning moment arising from an earthquake,
- the extent of the uplift of the bottom plate,
- the distribution of the axial forces at the bottom of the sidewall.

The results of these calculations can then be used to the design of a connection between a bottom plate and a sidewall of tanks.

The model is based on the following assumptions.

- The overturning moment is the force couple formed by the reaction force due to subsidence of the tank bottom versus the resistance force against uplift caused by the weight of liquid in the tank on the uplift area in major segment of the bottom plate. (Refer to Figure 5-2 and 5-3)
- The sidewall does not have any in-plane shear deformation in the vertical direction. In other words, the sidewall deforms rigidly when uplift occurs.
- The point where the tank bottom plate subsidence is zero is the location of the neutral axis of the tank. (Refer to Figure 5-2)
- The vertical axial force in the sidewall in the major segment becomes tensile. (Refer to Figure 5-2)
- Meanwhile, the vertical axial force in the minor segment becomes compressive. (Refer to Figure 5-2)
- The tensile axial force is caused by the weight of the liquid acting down on the uplift area in major segment as it tries to move upward away from the tank's bottom insulation. (Refer to Figure 5-3)
- The liquid pressure during earthquake consists of static pressure and dynamic pressure due to bulging and rocking mode. (Refer to Figure 5-3)
- The region of uplift consists of two, adjacent crescent shaped portions. One portion has a constant width. The other portion is wider at the point of maximum tensile force, tapering to zero as the crescent approaches the neutral axis. The constant width area (annular shaped area) is formed by the effect of a thicker annular plate which is installed at the connection with the side wall. (Refer to Figure 5-3)
- In the minor segment, the reaction force from the tank bottom plate is introduced to the sidewall as a compressive force. This force acts through the constant effective width of bottom plate which is located underneath the tank's sidewall. (Refer to Figure 5-3)

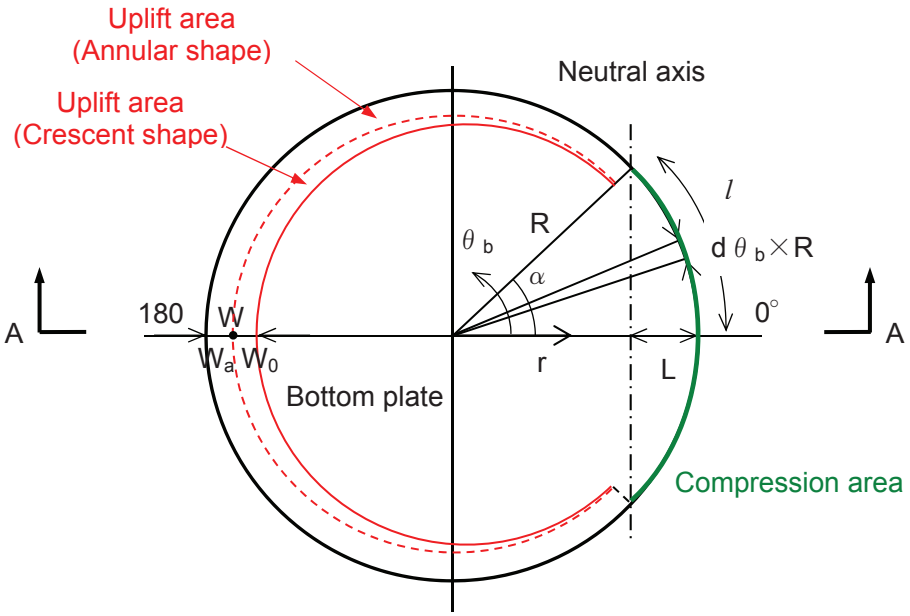

(a) Area of uplift and compression

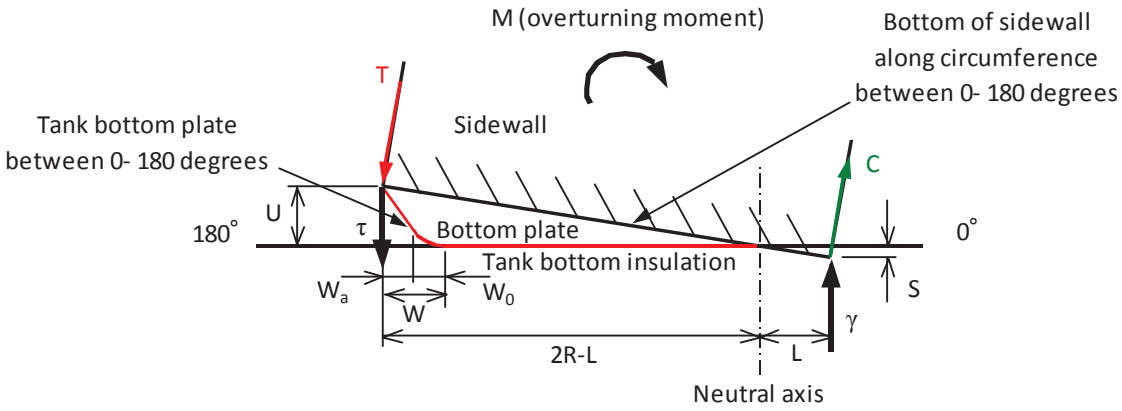

(b) Section A - A

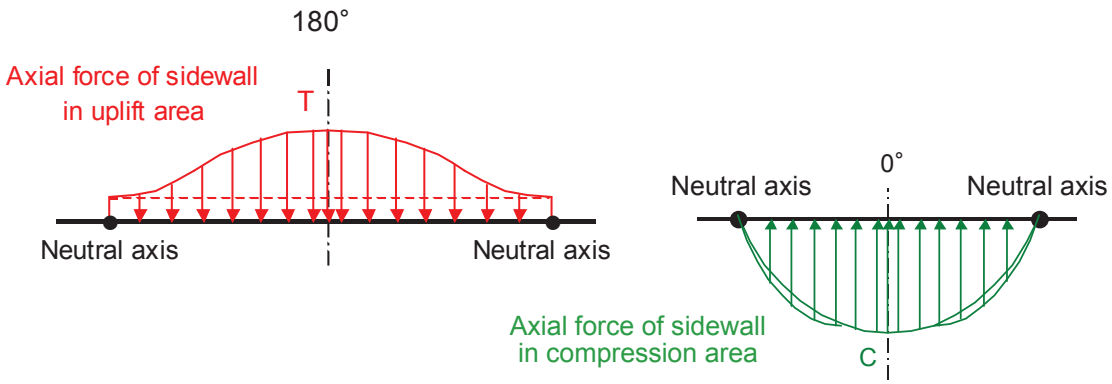

(c) Distribution of axial force along the bottom of the sidewall
in potential uplift and compression area

FIGURE 5-2: MODEL OF THE TANK BOTTOM

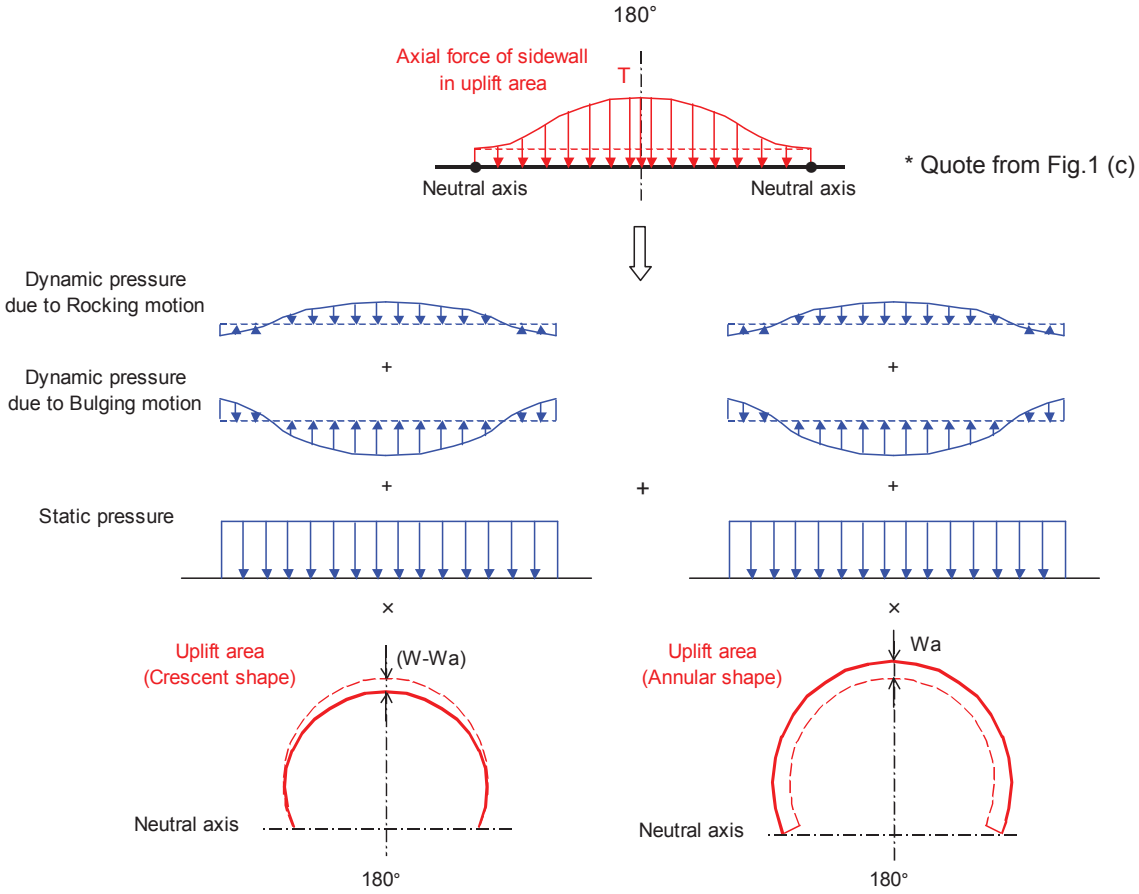

(a) Composition of Tensile axial force

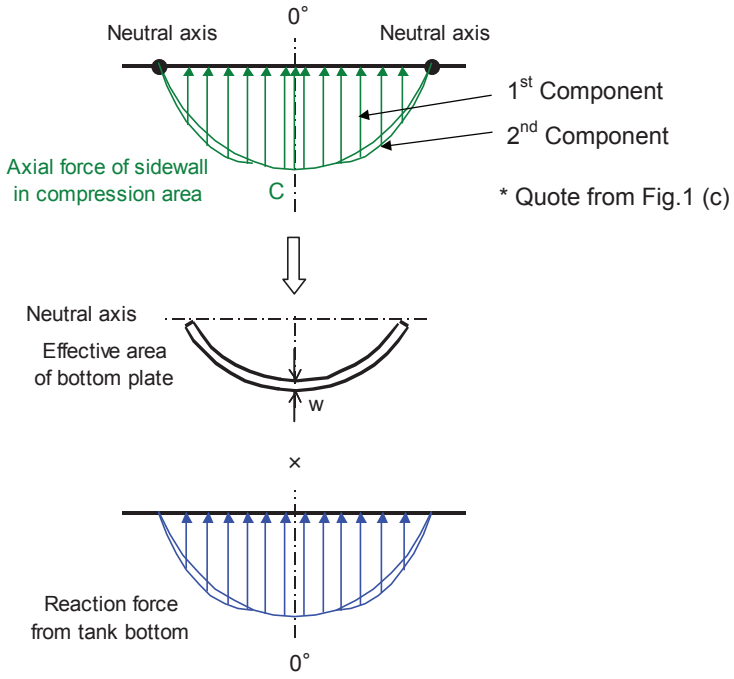

(b) Composition of Compressive axial force

FIGURE 5-3: MODEL OF AXIAL FORCE

For obtaining actual location of a neutral axis and realistic distribution of tensile axial force and compressive axial force, a formula of axial force is established based on the result of the FE analysis, and theoretical consideration. Each symbol in Figure 5-2 and 5-3 is as follows,

R: Tank radius

α: Angle indicating location of neutral axis

l: Circular length of subsidence $\quad l = \alpha \times R$ (5-1)

L: Length from neutral axis to sidewall $\quad L = R \times (1 - \cos(\alpha))$ (5-2)

W: Uplift width of bottom plate $\quad W = W_0 + W_a$ (5-3)

W_0: Fundamental uplift width

W_a: Width of bottom plate effected by annular plate

M: Over turning moment

γ: Force couple of compressive side

τ: Force couple of tensile side

S: Subsidence depth at 0 degree $\quad S = -\dfrac{L}{(2R - L)} \times U$ (5-4)

U: Uplift height at 180 degree

C: Compressive axial force per unit width

C is assumed that it consists of 1st component C_1 based on cosine curve and 2nd component C_2 based on sine curve for approximating the trend of the axial force in the result of the FE analysis as show in Figure 5-4.

$$C = \underbrace{C_1 \times \cos\left(\theta_b \times \frac{\pi}{2\alpha}\right)}_{1^{st}\text{ component}} + \underbrace{C_2 \times \sin\left[\left(\frac{4\theta_b}{\alpha} - 1\right) \times \left(\frac{\pi}{3}\right)\right]}_{2^{nd}\text{ component}} \quad (5\text{-}5)$$

$$C_1 = k \times d_r \times S \times w \quad (5\text{-}6)$$

$$C_2 = k \times (1 - d_r) \times S \times w \quad (5\text{-}7)$$

Where, C_2 is applied only for when $\theta_b = \dfrac{\alpha}{4} \sim \alpha$.

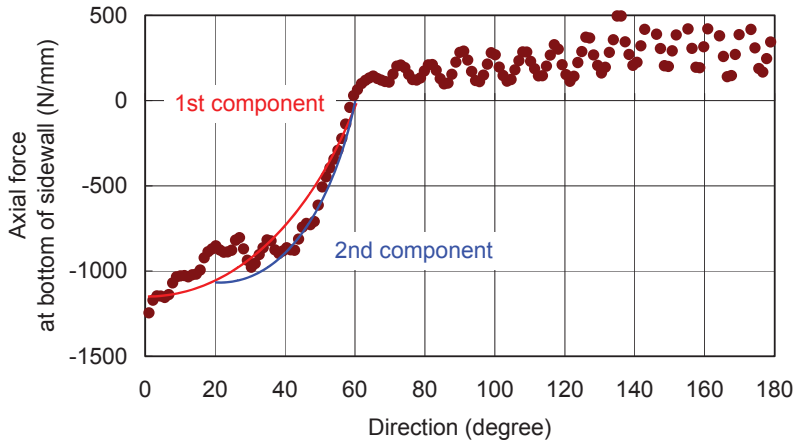

FIGURE 5-4: EXAMPLE OF AXIAL FORCE AT BOTTOM OF SIDEWALL (CASE 41)

k: Reaction coefficient of tank bottom

d_r: Coefficient for a supplemental bulge shape of subsidence of bottom plate

w: Effective width of bottom plate (The reaction force of the insulation is introduced into the tank's sidewall through width w bottom plate. This effective width is taken as being equal to 16 x the thickness of the bottom plate and thickness of the sidewall)

T: Tensile axial force per unit width at 180 degrees

It is assumed that T at 180 degrees consists of components of T_1, T_2, T_{d1} and T_{d2}. T_1 is the component due to static liquid pressure and T_{d1} is that due to dynamic liquid pressure, which act on the crescent shaped area. While T_2 is the component due to static liquid pressure and T_{d2} is that due to dynamic liquid pressure, which acts on the annular shaped area.

$$T = T_1 + T_2 + T_{d1} + T_{d2} \tag{5-8}$$

$T_1 + T_2$: Component due to static pressure

$$T_1 + T_2 = \rho \times g \times h \times w_{ef} \times W \tag{5-9}$$

$$T_1 = \rho \times g \times h \times w_{ef} \times (W - W_a) \tag{5-10}$$

$$T_2 = \rho \times g \times h \times w_{ef} \times W_a \tag{5-11}$$

ρ: Fluid density

g: Gravity acceleration

h: Liquid height

w_{ef}: Coefficient expressing of increase in axial force at the bottom of sidewall

Note: In a static situation w_{ef} is 0.5. In a dynamic situation, w_{ef} determines a portion of the force, which acts on the tank's sidewall. This value is found by the FE analysis. The remainder of the force acts on the tank's bottom insulation. Refer Chapter 3 for further explanation.

$T_{d1} + T_{d2}$: Component of dynamic pressure

$$T_{d1} + T_{d2} = \left[P_{db}(\theta_b = 180) + P_{dr}(\theta_b = 180)\right] \times w_{ef} \times W \tag{5-12}$$

$$T_{d1} = \left[P_{db}(\theta_b = 180) + P_{dr}(\theta_b = 180)\right] \times w_{ef} \times (W - W_a) \tag{5-13}$$

$$T_{d2} = \left[P_{db}(\theta_b = 180) + P_{dr}(\theta_b = 180)\right] \times w_{ef} \times W_a \tag{5-14}$$

$P_{db}(\theta_b = 180)$: Dynamic pressure at 180 degrees due to bulging mode

Housner's theory [1] as below is applied to calculate the distribution of the axial force.

$$P_{db} = \rho u'_o \, h \frac{\sqrt{3}}{2} \times \frac{\sinh\left\{\sqrt{3} \times \left(\frac{r \times \cos\theta_b}{h}\right)\right\}}{\cosh\left\{\sqrt{3} \times \left(\frac{R \times \cos\theta_b}{h}\right)\right\}} \tag{5-15}$$

u'_0: Horizontal acceleration

According to Eq. (5-15), pressure act on the bottom plate has a certain distribution along radius direction. For simplifying the model, average of dynamic pressure at $r = R$ and $r = R\text{-}W$ of uplift side (θ_b= 180) is considered. It becomes,

$$P_{db}(\theta = 180) = \rho u'_o \, h \frac{\sqrt{3}}{2} \times \frac{\left[\sinh\left\{\sqrt{3} \times \left(\frac{R}{h}\right)\right\} + \sinh\left\{\sqrt{3} \times \left(\frac{R-W}{h}\right)\right\}\right]}{2 \times \cosh\left\{\sqrt{3} \times \left(\frac{R}{h}\right)\right\}} \tag{5-16}$$

$P_{dr}(\theta_b = 180)$: Dynamic pressure at 180 degrees due to rocking mode

Taniguchi and Segawa's theory [2] is applied, as shown below, to calculate the dynamic pressure on the bottom plate and the sidewall.

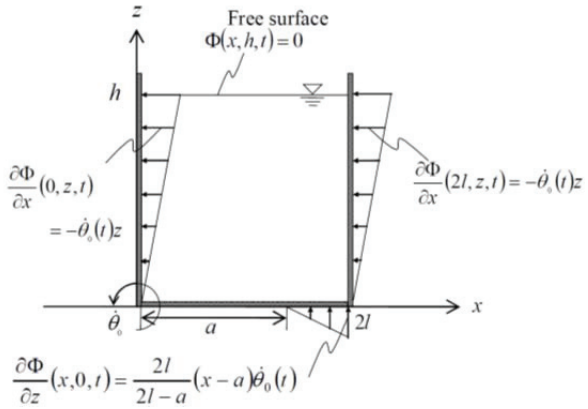

FIGURE 5-5: MODEL OF THE RECTANGULAR TANK [2]

$$P_{dr}(x,0,t) = -\rho \times \ddot{\theta}_0\ (t) \times \left[-h\left(l - \frac{a}{2} \right) \right.$$
$$+ \frac{4l}{\pi^2} \sum_{n=1}^{\infty} \left(\left\{ (-1)^n - \cos\frac{n\pi a}{2l} \right\} \frac{2l}{n^3\pi} \frac{2l}{2l-a} \left(-\tanh\frac{n\pi h}{2l} \right) \right. \tag{5-17}$$
$$\left. + \left\{ 1 - (-1)^n \right\} \frac{1}{n^2} \left(\frac{2l}{n\pi} \tanh\frac{n\pi h}{2l} - \frac{h}{\cosh\frac{n\pi h}{2l}} \right) \cos\frac{n\pi x}{2l} \right.$$

According to Eq. (5-17), pressure act on the bottom plate also has a certain distribution along radius direction. For simplifying the model, average of dynamic pressure at $x = 2l$ and $x = a$ of uplift side is considered. Then the equation becomes as shown below (using the co-ordinate conversions of $2l = 2R$, and $a = 2l\text{-}W$).

$$P_{dr}(\theta_b = 180) = -\rho \times \theta''_o \times \left[-\frac{h \times W}{2} + \frac{4R}{\pi^2} \right.$$
$$+ \frac{4l}{\pi^2} \sum_{n=1}^{\infty} \left(\left\{ (-1)^n - \cos\left(n\pi \left(1 - \frac{W}{2R} \right) \right) \right\} \frac{2R}{n^3\pi} \frac{2R}{W} \left(-\tanh\frac{n\pi h}{2R} \right) \right. \tag{5-18}$$
$$\left. + \left\{ 1 - (-1)^n \right\} \frac{1}{n^2} \left(\frac{2R}{n\pi} \tanh\frac{n\pi h}{2R} - \frac{h}{\cosh\frac{n\pi h}{2R}} \right) \times \frac{1}{2} \times \left\{ 1 + \cos\left(\frac{n\pi a}{1 - \frac{W}{2R}} \right) \right\} \right.$$

5-1-2 Modeling of force couple and axial force at compression area

The force couple at compression area γ, which consists from reaction force of the tank bottom insulation, is assumed to be expressed by the formula consisting of two components, by using Eqs. (5-5), (5-6) and (5-7).

① $k \times d_r \times S \times \cos\left(\theta_b \times \frac{\pi}{2\alpha} \right) \times w$ and ② $k \times (1 - d_r) \times S \times \sin\left[\left(\frac{4\theta_b}{\alpha} - 1 \right) \times \left(\frac{\pi}{3} \right) \right] \times w$ are the components of reaction force from tank bottom, ③ $R(\cos\alpha - \cos\theta_b)$ is the length from natural axis of the tank and ④ $d\theta_b \times R$ is infinitesimal distance, respectively. Then the equation of force couple at the compression area γ becomes;

$$\gamma = 2\times\int_0^{\alpha} k\times d_r \times S\times\cos\left(\theta_b\times\frac{\pi}{2\alpha}\right)\times w\times R(\cos\alpha-\cos\theta_b)d\theta_b\times R$$
$$+2\times\int_{\alpha/4}^{\alpha} k\times(1-d_r)\times S\times\sin\left[\left(\frac{4\theta_b}{\alpha}-1\right)\times\left(\frac{\pi}{3}\right)\right]\times w\times R(\cos\alpha-\cos\theta_b)d\theta_b\times R \quad (5\text{-}19)$$

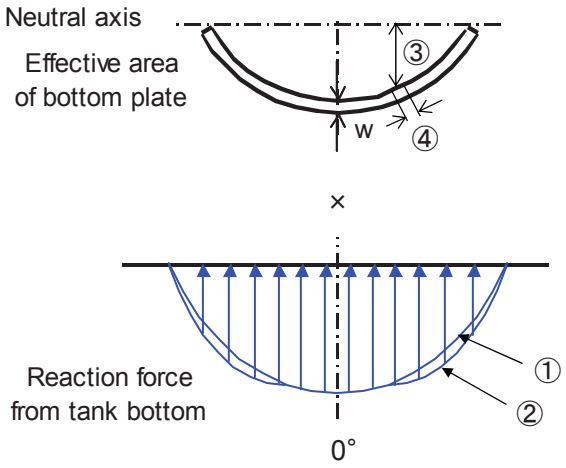

FIGURE 5-6: FORCE COUPLE OF COMPRESSIVE SIDE

The equation is transformed by applying C_1 and C_2, as follows.

$$\gamma = \gamma_1 + \gamma_2 \quad (5\text{-}20)$$

$$\gamma_1 = 2\times C_1\times\int_0^{\alpha}\cos\left(\theta_b\times\frac{\pi}{2\alpha}\right)\times R(\cos\alpha-\cos\theta_b)d\theta_b\times R \quad (5\text{-}21)$$

Where,

$$C_1 = k\times d_r\times S\times w \quad (5\text{-}6)$$

$$\gamma_2 = 2\times C_2\times\int_{\alpha/4}^{\alpha}\sin\left[\left(\frac{4\theta_b}{\alpha}-1\right)\times\left(\frac{\pi}{3}\right)\right]\times R(\cos\alpha-\cos\theta_b)d\theta_b\times R \quad (5\text{-}22)$$

Where,

$$C_2 = k\times(1-d_r)\times S\times w \quad (5\text{-}7)$$

γ is obtained by solving the Eqs. (5-21) and (5-22) as follows.

$$\gamma = \gamma_1 + \gamma_2 = 2\times C_1\times C_{mp1}(\alpha)+2\times C_2\times C_{mp2}(\alpha) \quad (5\text{-}23)$$

Where,

$$C_{mp1}(\alpha)=\frac{\left\{\left(\alpha\pi^2-2\alpha^2\pi\right)\sin\left(\frac{\pi+2\alpha}{2}\right)+\left(\alpha\pi^2+2\alpha^2\pi\right)\sin\left(\frac{\pi-2\alpha}{2}\right)+\left(8\alpha^3\cos(\alpha)-2\alpha\cos(\alpha)\pi^2\right)\right\}\times R^2}{\pi^3-4\alpha^2\pi} \tag{5-24}$$

$$C_{mp2}(\alpha)=\left[\frac{\left(24\alpha\pi^2-18\alpha^2\pi\right)\cos(\pi+\alpha)+\left(24\alpha\pi^2+18\alpha^2\pi\right)\cos(\pi-\alpha)-\left(27\alpha^3\cos(\alpha)-48\alpha\cos(\alpha)\pi^2\right)}{64\pi^3-36\alpha^2\pi}+\frac{\left(48\alpha\cos(\alpha)-48\alpha\cos\left(\frac{\alpha}{4}\right)\right)\pi^2-27\alpha^3\cos(\alpha)}{64\pi^3-36\alpha^2\pi}\right]\times R^2 \tag{5-25}$$

While, the total of the compressive force C_f is expressed by following formula.

$$C_f=2\times C_1\times\int_0^{\alpha}\cos\left(\theta_b\times\frac{\pi}{2\alpha}\right)\times Rd\theta_b+2\times C_2\times\int_{\alpha/4}^{\alpha}\sin\left[\left(\frac{4\theta_b}{\alpha}-1\right)\times\left(\frac{\pi}{3}\right)\right]\times Rd\theta_b \tag{5-26}$$

Then C_f is obtained by solving the Eq. (5-26) as follows.

$$C_f=\frac{4C_1\alpha R}{\pi}\sin\left(\frac{\pi}{2}\right)+\frac{3C_2\alpha R}{2\pi}\left(1-\cos(\pi)\right) \tag{5-27}$$

5-1-3 Modeling of force couple and axial force at tensile area

The force couple of the tensile area τ, consists of two components of τ_1 and τ_2. These are functions of cosine curve pressure distribution, rectangular shape pressure distribution, the size of the crescent shaped uplift area and the size of the annular shaped uplift area.

① $\rho\times g\times h\times w_{ef}\times(W-W_a)\times\sin\left\{\frac{(\theta_b-\alpha)\pi}{2(\pi-\alpha)}\right\}$ and ② $\left(P_{db}(\theta_b)+P_{dr}(\theta_b)\right)\times w_{ef}\times(W-W_a)\times\sin\left\{\frac{(\theta_b-\alpha)\pi}{2(\pi-\alpha)}\right\}$ are the components of static pressure and dynamic pressure which act on crescent uplift area, while ③ $\rho\times g\times h\times w_{ef}\times W_a$ and ④ $\left(P_{db}(\theta_b)+P_{dr}(\theta_b)\right)\times w_{ef}\times W_a$ are the components of those which act on the annular shaped uplift area. Then, ⑤ $R(\cos\alpha-\cos\theta_b)$ is the length from the natural axis of the tank and ⑥ $d\theta_b\times R$ is an infinitesimal distance, respectively. Then the equation of force couple at compression area τ becomes;

$$\tau_1 = 2\times\int_{\alpha}^{\pi}\left[\rho\times g\times h\times w_{ef}\times(W-W_a)\times\sin\left\{\frac{(\theta_b-\alpha)\pi}{2(\pi-\alpha)}\right\}\times R(\cos\alpha-\cos\theta_b)\times R\right]d\theta_b$$
$$+2\times\int_{\alpha}^{\pi}\left[(P_{db}(\theta_b)+P_{dr}(\theta_b))\times w_{ef}\times(W-W_a)\times\sin\left\{\frac{(\theta_b-\alpha)\pi}{2(\pi-\alpha)}\right\}\times R(\cos\alpha-\cos\theta_b)\times R\right]d\theta_b \quad (5\text{-}28)$$

$$\tau_2 = 2\times\int_{\alpha}^{\pi}\left[\rho\times g\times h\times w_{ef}\times W_a\times R(\cos\alpha-\cos\theta_b)\times R\right]d\theta_b$$
$$+2\times\int_{\alpha}^{\pi}\left[(P_{db}(\theta_b)+P_{dr}(\theta_b))\times w_{ef}\times W_a\times R(\cos\alpha-\cos\theta_b)\times R\right]d\theta_b \quad (5\text{-}29)$$

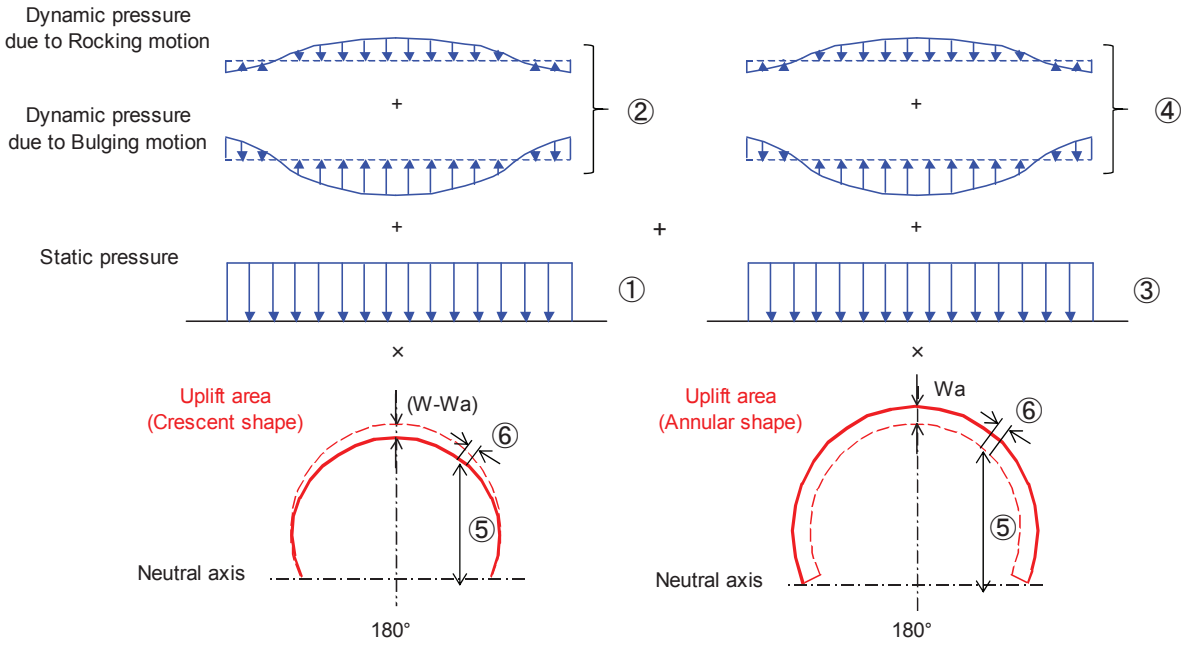

FIGURE 5-7: FORCE COUPLE OF TENSILE SIDE

$P_{db}(\theta_b)$ and $P_{dr}(\theta_b)$ around the circumference of the tank are obtained from the theoretical equations of the bulging mode (Eq. (5-15)) and rocking mode (Eq. (5-17)). However, the equation is complicated to integrate into the model, practically. Therefore, a cosine curve is applied to the distribution of $P_{db}(\theta_b)$ and $P_{dr}(\theta_b)$ along the tank's sidewall.

Figure 5-8 shows the comparison of the pressure value (total of static and dynamic pressure) between theories (Housner's theory [1] for the bulging mode and Taniguchi and Segawa's theory [2] for the rocking mode) and cosine curve model of the dynamic pressure arising from the bulging mode and the rocking mode being applied to the subject tank.

The difference in the values obtained from the two different methods is typically about 4 - 5% on average. Refer Figure 5-8 for further details. The trends are considered to be the same to any proportion's tanks, even if degree of difference slightly varies due to tank dimensions. The pressure load on the uplift area of the tank's bottom plate contributes to the resistance force against overturning moment. The difference of the values in uplift area directly decreases

accuracy. Therefore, supplementing these differences to achieve the result of the model to the current theories is essential.

For improving the accuracy of the model, an additional function Eq. (5-30) is introduced to the model.

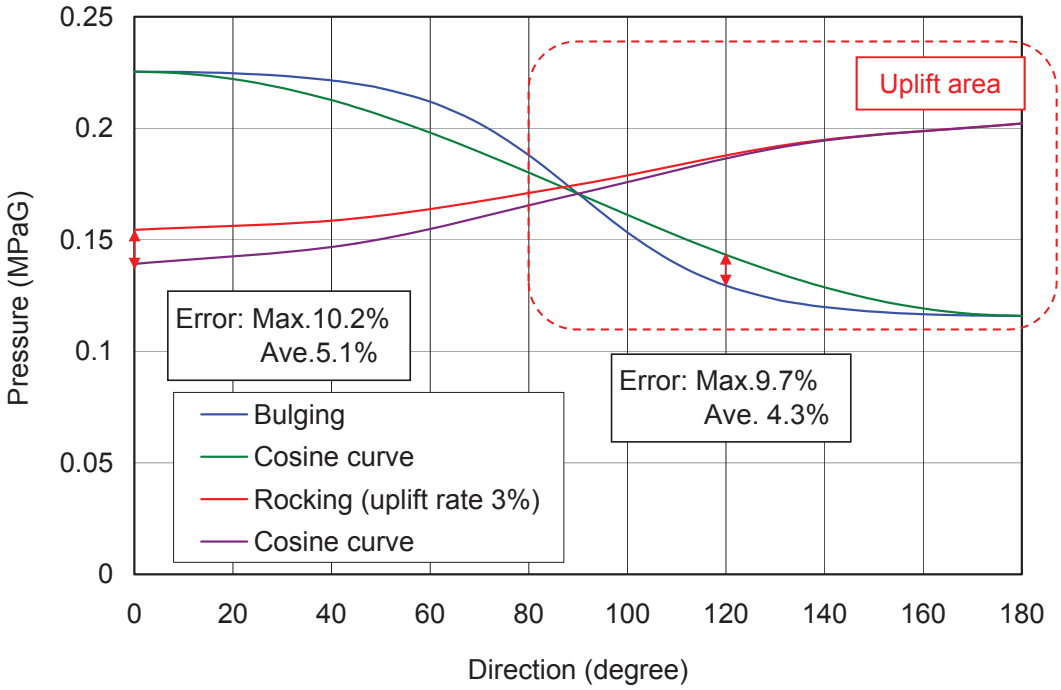

FIGURE 5-8: PRESSURE DIFFERENCE BETWEEN THEORY AND THE MODEL

$$P_{apd(Cosine)} = \frac{P_{d(Theory)}(\theta_b = 180)}{a_{pd}} \times \sin(2\theta_b) = \frac{1}{a_{pd}} \times u'_o \, h \frac{\sqrt{3}}{2} \times \frac{\sinh\left\{\sqrt{3} \times \left(\frac{-R}{h}\right)\right\}}{\cosh\left\{\sqrt{3} \times \left(\frac{-R}{h}\right)\right\}} \times \sin(2\theta_b) \tag{5-30}$$

In this equation, a_{pd} is decided from following relationship.

$$P_{d(Theory)}(\theta_b = 135) = P_{d(Cosine)}(\theta_b = 135) + P_{apd(Cosine)}(\theta_b = 135) \tag{5-31}$$

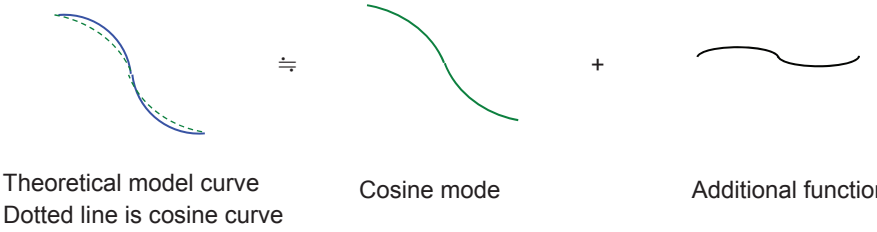

FIGURE 5-9: SCHEMATIC VIEW OF SUPPLEMENT BY ADDITIONAL FUNCTION

Where,

$$P_{d(Theory)}(\theta_b = 135) = \rho u'_o \, h \frac{\sqrt{3}}{2} \times \frac{\sinh\left\{\sqrt{3} \times \left(\frac{R}{h} \times \cos\left(\frac{3}{4}\pi\right)\right)\right\}}{\cosh\left\{\sqrt{3} \times \left(\frac{R}{h} \times \cos\left(\frac{3}{4}\pi\right)\right)\right\}} \tag{5-32}$$

$$P_{d(Cosine)}(\theta_b = 135) = P_{d(Theory)}(\theta = 180) \times \cos\left(\frac{3}{4}\pi\right) \tag{5-33}$$

$$P_{apd(Cosine)}(\theta_b = 135) = \frac{P_{d(Theory)}(\theta = 180)}{a_{pd}} \times \sin\left(2 \times \frac{3}{4}\pi\right) \tag{5-34}$$

a_{pd} : Coefficient for optimization of the model

When Eq. (5-31) is solved, the value of a_{pd} is obtained as 5.18.

Figure 5-10 shows the comparison of total of static and theoretical pressure and those from the modified model. It is in good agreement around the uplift area, especially the area which is greater than 90 degrees. Though some amount of difference still remains at the area less than 90 degrees, it may be a minor effect on the model since most of the area less than 90 degrees is in the area of compression.

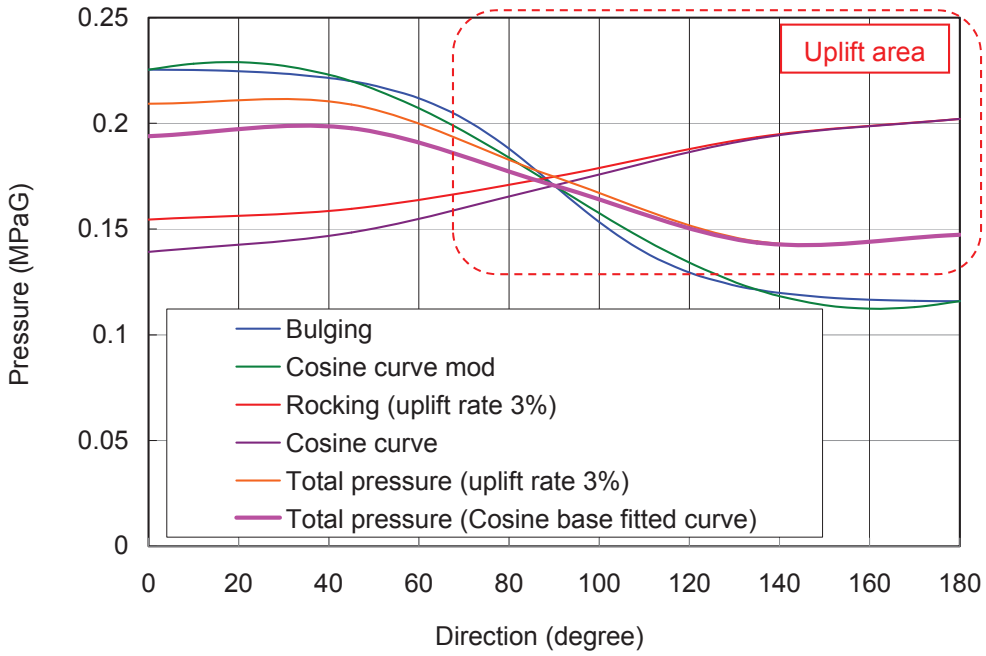

FIGURE 5-10: MODIFIED DYNAMIC PRESSRE MODEL

When modified model in Figure 5-10is applied, τ_1 becomes as follows.

$$\begin{aligned}\tau_1 = {} & 2\times T_1 \times \int_\alpha^\pi \left[\sin\left\{ \frac{(\theta_b-\alpha)\pi}{2(\pi-\alpha)} \right\} \times R(\cos\alpha - \cos\theta_b)\times R \right] d\theta_b \\ & + 2\times T_{d1} \times \int_\alpha^\pi \left[\cos(\pi-\theta_b)\times \sin\left\{ \frac{(\theta_b-\alpha)\pi}{2(\pi-\alpha)} \right\} \times R(\cos\alpha - \cos\theta_b)\times R \right] d\theta_b \\ & + 2\times T_{da1} \times \int_\alpha^\pi \left[\sin(2\pi-2\theta_b)\times \sin\left\{ \frac{(\theta_b-\alpha)\pi}{2(\pi-\alpha)} \right\} \times R(\cos\alpha - \cos\theta_b)\times R \right] d\theta_b \end{aligned} \quad (5\text{-}35)$$

Where,

$$T_1 = \rho \times g \times h \times w_{ef} \times (W - W_a) \quad (5\text{-}10)$$

$$T_{d1} = \left[P_{db}(\theta_b = 180) + P_{dr}(\theta_b = 180) \right] \times w_{ef} \times (W - W_a) \quad (5\text{-}13)$$

$$T_{da1} = \frac{P_{db}(\theta_b = 180)}{a_{pdb}} \times w_{ef} \times (W - W_a) \quad (5\text{-}36)$$

While, τ_2 is specified as follows.

$$\begin{aligned}\tau_2 = {} & 2\times T_2 \times \int_\alpha^\pi \left[R(\cos\alpha - \cos\theta_b)\times R \right] d\theta_b \\ & + 2\times T_{d2} \times \int_\alpha^\pi \left[\cos(\pi-\theta_b)\times R(\cos\alpha - \cos\theta_b)\times R \right] d\theta_b \\ & + 2\times T_{da2} \times \int_\alpha^\pi \left[\sin(2\pi-2\theta_b)\times R(\cos\alpha - \cos\theta_b)\times R \right] d\theta_b \end{aligned} \quad (5\text{-}37)$$

Where,

$$T_2 = \rho \times g \times h \times w_{ef} \times W_a \quad (5\text{-}11)$$

$$T_{d2} = \left[P_{db}(\theta_b = 180) + P_{dr}(\theta_b = 180) \right] \times w_{ef} \times W_a \quad (5\text{-}14)$$

$$T_{da2} = \frac{P_{db}(\theta_b = 180)}{a_{pdb}} \times w_{ef} \times W_a \quad (5\text{-}38)$$

In addition, unit tensile reaction *T* of each direction is expressed by following formula.

$$
\begin{aligned}
T = {} & T_1 \times \sin\left(\frac{(\theta_b - \alpha)\pi}{2(\pi - \alpha)}\right) + T_{d1} \times \cos(\pi - \theta_b) \times \sin\left\{\frac{(\theta_b - \alpha)\pi}{2(\pi - \alpha)}\right\} \\
& - T_{da1} \times \sin(2\pi - 2\theta_b) \times \sin\left\{\frac{(\theta_b - \alpha)\pi}{2(\pi - \alpha)}\right\} \\
& + T_2 + T_{d2} \times \cos(\pi - \theta_b) + T_{da2} \times \sin(2\pi - 2\theta_b)
\end{aligned}
\tag{5-39}
$$

τ_1 and τ_2 are obtained by solving the Eqs. (5-35) and (5-37).

$$
\begin{aligned}
\tau = \tau_1 + \tau_2 = {} & 2T_1 \times T_{ns1}(\alpha) + 2T_{d1} \times T_{nsbr1}(\alpha) + 2T_{da1} \times T_{nsba1}(\alpha) \\
& + 2T_2 \times T_{ns2}(\alpha) + 2T_{d2} \times T_{nsbr2}(\alpha) + 2T_{da2} \times T_{nsba2}(\alpha)
\end{aligned}
\tag{5-40}
$$

Where,

$$
T_{ns1}(\alpha) = \frac{8\cos(\alpha)\pi^3 - 24\alpha\cos(\alpha)\pi^2 + 24\alpha^2\cos(\alpha)\pi - 8\alpha^3\cos(\alpha)}{(3\pi^3 - 8\alpha\pi^2 + 4\alpha^2\pi)} R^2
\tag{5-41}
$$

$$
\begin{aligned}
T_{nsbr1}(\alpha) = {} & [-[\{30\pi^5\cos(\alpha) - 94\alpha\pi^4\cos(\alpha) + 96\alpha^2\pi^3\cos(\alpha) - 32\alpha^3\pi^2\cos(\alpha)\} \times \cos(\pi - \alpha) \\
& + (-3\pi^5 + 11\alpha\pi^4 - 12\alpha^2\pi^3 + 4\alpha^3\pi^2) \times \cos(\pi - 2\alpha) \\
& - (45\pi^5 - 261\alpha\pi^4 + 580\alpha^2\pi^3 - 620\alpha^3\pi^2 + 320\alpha^4\pi - 64\alpha^5)]] \\
& \times \frac{R^2}{(45\pi^5 - 261\alpha\pi^4 + 364\alpha^2\pi^3 - 256\alpha^3\pi^2 + 64\alpha^4\pi)}
\end{aligned}
\tag{5-42}
$$

$$
\begin{aligned}
T_{nsba1}(\alpha) = {} & \Bigg[-[-(900\pi^6 - 5400\alpha\pi^5 + 13364\alpha^2\pi^4 - 17456\alpha^3\pi^3 + 12688\alpha^4\pi^2 - 4864\alpha^5\pi + 768\alpha^6) \\
& + \{(-840 \times \cos(\alpha) - 420)\pi^6 + (5648\alpha \times \cos(\alpha) + 2936\alpha)\pi^5 + (-15368\alpha^2 \times \cos(\alpha) - 8340\alpha^2)\pi^4 \\
& + (21760\alpha^3 \times \cos(\alpha) + 12368\alpha^3)\pi^3 + (16960\alpha^4 \times \cos(\alpha) - 10128\alpha^4)\pi^2 \\
& + (6912\alpha^5 \times \cos(\alpha) + 4352\alpha^5)\pi - 1152\alpha^6 \times \cos(\alpha) - 768\alpha^6\}] \\
& \times \frac{1}{(1575\pi^6 - 10800\alpha\pi^5 + 29912\alpha^2\pi^4 - 42944\alpha^3\pi^3 + 33776\alpha^4\pi^2 - 13824\alpha^5\pi + 2304\alpha^6)} \\
& - \{(525\pi^6 - 2725\alpha\pi^5 + 5604\alpha^2\pi^4 - 5708\alpha^3\pi^3 + 2880\alpha^4\pi^2 - 576\alpha^5\pi) \times \sin(2\pi - \alpha) \\
& + (-210 \times \cos(\alpha) \times \pi^6 + 1202\alpha \times \cos(\alpha) \times \pi^5 - 2640\alpha^2 \times \cos(\alpha) \times \pi^4 + 2800\alpha^3 \times \cos(\alpha) \times \pi^3 \\
& - 1440\alpha^2 \times \cos(\alpha) \times \pi^2 + 288\alpha^5 \times \cos(\alpha) \times \pi) \times \sin(2\pi - 2\alpha) \\
& + (45\pi^6 - 261\alpha\pi^5 + 5804\alpha^2\pi^4 - 620\alpha^3\pi^3 + 320\alpha^4\pi^2 - 64\alpha^5\pi) \times \sin(2\pi - 3\alpha)\} \\
& \times \frac{1}{(1575\pi^6 - 10800\alpha\pi^5 + 29912\alpha^2\pi^4 - 42944\alpha^3\pi^3 + 33776\alpha^4\pi^2 - 13824\alpha^5\pi + 2304\alpha^6)}\Bigg] \times R^2
\end{aligned}
\tag{5-43}
$$

$$T_{ns2}(\alpha) = (-\sin(\pi) + \cos(\alpha)\pi + \sin(\alpha) - \alpha\cos(\alpha))R^2 \tag{5-44}$$

$$T_{nsbr2}(\alpha) = \frac{[4\cos(\alpha)\times\sin(\pi-\alpha) - \sin(\pi-2\alpha) - 2\alpha + 2\pi]}{4}\times R^2 \tag{5-45}$$

$$T_{da2}(\alpha) = \frac{4 + 3\cos(\alpha) + 3\cos(2\pi-\alpha) - 3\cos(\alpha)\times\cos(2\pi-2\alpha) + \cos(2\pi-\alpha)}{6}\times R^2 \tag{5-46}$$

While, the total of tensile force T_f is expressed by following formula.

$$\begin{aligned} T_f = {} & 2\times T_1 \times \int_\alpha^\pi \left[\sin\left(\frac{(\theta_b-\alpha)\pi}{2(\pi-\alpha)} \right) \times R \right] d\theta_b + 2\times T_{d1} \times \int_\alpha^\pi \left[\cos(\pi-\theta_b)\times\sin\left\{ \frac{(\theta_b-\alpha)\pi}{2(\pi-\alpha)} \right\} \times R \right] d\theta_b \\ & 2\times T_{da1} \times \int_\alpha^\pi \left[\sin(2\pi-2\theta_b)\times\sin\left\{ \frac{(\theta_b-\alpha)\pi}{2(\pi-\alpha)} \right\} \times R \right] d\theta_b \\ & + 2\times T_2 \times \int_\alpha^\pi R\,d\theta_b + 2\times T_{d2} \times \int_\alpha^\pi [\cos(\pi-\theta_b)\times R]\,d\theta_b + 2\times T_{da2} \times \int_\alpha^\pi [\sin(2\pi-2\theta_b)\times R]\,d\theta_b \end{aligned} \tag{5-47}$$

Then T_f is obtained by solving Eq. (5-47).

$$\begin{aligned} T_f = {} & 4T_1 \times \frac{(\pi-\alpha)}{\pi}\times R - 4T_{d1} \times \frac{(\pi^2-\alpha\pi)\times\cos(\pi-\alpha)}{3\pi^2-8\alpha\pi+4\alpha^2}\times R \\ & - 2T_{da1} \times \frac{(2\pi^2-2\alpha\pi)\times\sin(2\pi-2\alpha) - (8\pi^2-16\alpha\pi+8\alpha^2)}{15\pi^2-32\alpha\pi+16\alpha^2}\times R \\ & + 2T_2 \times (\pi-\alpha)\times R + 2T_{d2}\times\sin(\pi-\alpha)\times R - T_{da2}\times\{\cos(2\pi-2\alpha)-1\}\times R \end{aligned} \tag{5-48}$$

5-1-4 Formula of angle indicating the location of neutral axis

To obtain the formula for the angle indicating the location of neutral axis α (or l or L) and parameter of subsidence S and uplift U, the equations of overturning moment M, force couple at the compression area γ and the tensile area τ given below are applied. (Detail of each symbol is explained in Figure 5-1)

$$M = \gamma + \tau \tag{5-49}$$

$$\gamma = \tau \tag{5-50}$$

$$l = \alpha \times R \tag{5-1}$$

$$L = R \times (1 - \cos(\alpha)) \tag{5-2}$$

$$S = -\frac{L}{(2R-L)}\times U \tag{5-4}$$

$$\gamma = \gamma_1 + \gamma_2 = 2 \times C_1 \times C_{mp1}(\alpha) + 2 \times C_2 \times C_{mp2}(\alpha) \quad (5\text{-}23)$$

$$C = C_1 \times \cos\left(\theta_b \times \frac{\pi}{2\alpha}\right) + C_2 \times \sin\left[\left(\frac{4\theta_b}{\alpha} - 1\right) \times \left(\frac{\pi}{3}\right)\right] \quad (5\text{-}5)$$

$$C_1 = k \times dr \times S \times w \quad (5\text{-}6)$$

$$C_2 = k \times (1 - dr) \times S \times w \quad (5\text{-}7)$$

$$\begin{aligned}\tau = \tau_1 + \tau_2 = {} & 2T_1 \times T_{ns1}(\alpha) + 2T_{d1} \times T_{nsbr1}(\alpha) + 2T_{da1} \times T_{nsba1}(\alpha) \\ & + 2T_2 \times T_{ns2}(\alpha) + 2T_{d2} \times T_{nsbr2}(\alpha) + 2T_{da2} \times T_{nsba2}(\alpha)\end{aligned} \quad (5\text{-}40)$$

$$\begin{aligned}T = {} & T_1 \times \sin\left(\frac{(\theta_b - \alpha)\pi}{2(\pi - \alpha)}\right) + T_{d1} \times \cos(\pi - \theta_b) \times \sin\left\{\frac{(\theta_b - \alpha)\pi}{2(\pi - \alpha)}\right\} \\ & - T_{da1} \times \sin(2\pi - 2\theta_b) \times \sin\left\{\frac{(\theta_b - \alpha)\pi}{2(\pi - \alpha)}\right\} \\ & + T_2 + T_{d2} \times \cos(\pi - \theta_b) + T_{da2} \times \sin(2\pi - 2\theta_b)\end{aligned} \quad (5\text{-}51)$$

$$T_1 + T_2 = \rho \times g \times h \times w_{ef} \times W \quad (5\text{-}9)$$

$$T_1 = \rho \times g \times h \times w_{ef} \times (W - W_a) \quad (5\text{-}10)$$

$$T_2 = \rho \times g \times h \times w_{ef} \times W_a \quad (5\text{-}11)$$

$$T_{d1} + T_{da1} + T_{d2} + T_{da2} = \left[P_{db}(\theta_b = 180) + \frac{P_{db}(\theta_b = 180)}{a_{pdb}} + P_{dr}(\theta_b = 180)\right] \times w_{ef} \times W \quad (5\text{-}52)$$

$$T_{d1} + T_{da1} = \left[P_{db}(\theta_b = 180) + \frac{P_{db}(\theta_b = 180)}{a_{pdb}} + P_{dr}(\theta_b = 180)\right] \times w_{ef} \times (W - W_a) \quad (5\text{-}53)$$

$$T_{d2} + T_{da2} = \left[P_{db}(\theta_b = 180) + \frac{P_{db}(\theta_b = 180)}{a_{pdb}} + P_{dr}(\theta_b = 180)\right] \times w_{ef} \times W_a \quad (5\text{-}54)$$

$$T_f + C_f = 0 \quad (5\text{-}55)$$

From Eqs. (5-3), (5-10), (5-11), (5-40), (5-49) and (5-50), the equation to calculate α is;

$$\begin{aligned}&\rho gh\times w_{ef}\times\left(W_0+W_a-W_a\right)\\&\quad-\frac{1}{T_{ns1}(\alpha)}\times\left[\frac{M}{4}-\left(P_{db}\left(\theta_b=180\right)+P_{dr}\left(\theta_b=180\right)\right)\times w_{ef}\times\left(W_0+W_a-W_a\right)\times T_{nsbr1}(\alpha)\right.\\&\quad\left.-\rho gh\times w_{ef}\times W_a\times T_{ns2}(\alpha)-\left(P_{db}\left(\theta_b=180\right)+P_{dr}\left(\theta_b=180\right)\right)\times w_{ef}\times W_a\times T_{nsbr2}(\alpha)\right]=0\end{aligned}\tag{a}$$

From Eqs. (5-6), (5-7), (5-23), (5-49) and (5-50) the equation to calculate S is;

$$S=\frac{M}{4\times k\times w\times\left[dr\times\left(C_{m1}(\alpha)-C_{m2}(\alpha)\right)+C_{m2}(\alpha)\right]}\tag{b}$$

From Eqs. (5-2), (5-4) and (b) the equation for calculate U is obtained as;

$$U=-\frac{2R-\left\{R\times\left(1-\cos(\alpha)\right)\right\}}{R\times\left(1-\cos(\alpha)\right)}\times\frac{M}{4\times k\times w\times\left[dr\times\left(C_{m1}(\alpha)-C_{m2}(\alpha)\right)+C_{m2}(\alpha)\right]}\tag{c}$$

Using Eqs. (a) to (c), the key parameters forming the model can be found by the following steps below.

Step1: Calculate the parameter of angle indicating the location of neutral axis α by Eq. (a).
Step2: Calculate the parameter of subsidence S and uplift U by Eqs. (b) and (c), respectively.
Step3: Calculate the compressive axial force per unit width at 180 degrees C and the tensile axial force per unit width at 180 degrees T by Eqs. (5-5) and (5-51), respectively.

5-2 MODELING OF RELATIONSHIP BETWEEN OUT OF ROUND DEFORMATION OF SIDEWALL AND UPLIFT HEIGHT

5-2-1 Modeling of deformation of sidewall and uplift height

According to the results of the FE analysis in Chapter 3, magnitude of the deformation at the top of the sidewall is one of the major factors which enhance the uplift height of the bottom plate.

The uplift width, which affects the axial force in sidewall, has a relationship with the uplift height as shown in Figure 3-14. While as specified in the section 3-2-4, deformation at the top of the sidewall is one of the important factors to decide the uplift height. Therefore, considering the effect of the deformation at the top of the sidewall is essential for improving the mathematical model.

A supplementary model can be established using geometrical relationships as shown in Figure 5-11. In this supplementary model, it is assumed that the bottom of the sidewall remains in a circular shape while the top of the sidewall at 180 degrees deforms inward towards the tank center, during an earthquake.

The top of the sidewall forms an oval shape with minor axis $2R\text{-}\delta$ running between 0 and 180 degrees. The vertical lines, which are an extension of the sidewall at 0 and 180 degrees, meet a point above the tank and form an angle designated as ξ as shown below.

This extension of the tank's sidewalls, together with the tank bottom plate, form a sector defined by the inclined angle ξ. Using the standard geometrical relationships given below, uplift height v can be calculated.

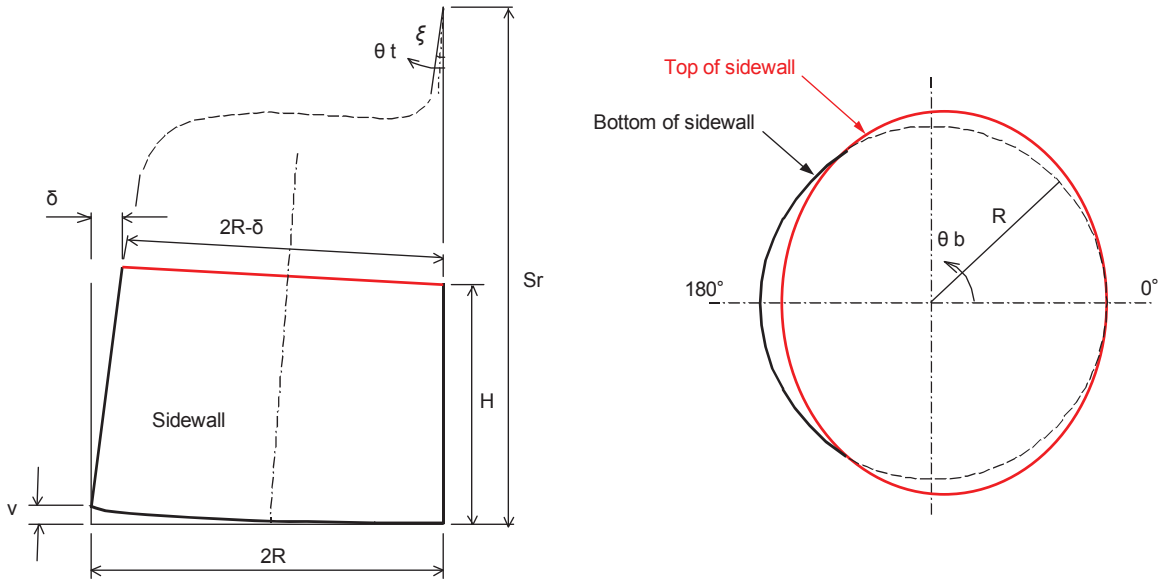

FIGURE 5-11: MODEL OF UPLIFT OF THE BOTTOM PLATE AND INCLINE DEFORMATION OF SIDEWALL

Each symbol in Figure 5-11 show is as follows.

R: Tank radius
H: Tank height
δ: Horizontal displacement (difference in diameter from complete round) of the top of the side wall
S_r: Distance from the meet point of extensions of the sidewall at 0 and 180 degrees to the bottom plate
θ_t: Angle from the sidewall at 0 degree to each point of bottom plate
θ_b: Angle from 0 degree to each point of the sidewall
ξ: Angle at the point of intersection of a line drawn as an extension to the sidewall at 180 degrees and a line drawn as an extension of the sidewall at 0 degree
$v(\pi)$: Uplift height of bottom plate due to horizontal displacement of the top of the sidewall at 180 degrees

When the top of the sidewall deforms as an oval shape, the geometrical relationships between each of the values in Figure 5-11 are:

$$\xi \times S_r = 2 \times R \tag{5-56}$$

$$2 \times (S_r - H) \times \tan\left(\frac{\xi}{2}\right) = 2R - \delta \tag{5-57}$$

$$v(\pi) = S_r \times (1 - \cos\xi) \tag{5-58}$$

$$\xi \fallingdotseq \frac{\delta}{H} \tag{5-59}$$

To obtain the uplift height v at each point along θ_b, the geometrical relationship given in Eq. (5-60) is used:

$$S_r \times \tan\theta_t = R \times (1 - \cos\theta_b) \tag{5-60}$$

Angle of each point of bottom plate θ_t is expressed as function of θ_b as follows.

$$\theta_t = \tan^{-1}\left\{\frac{R}{S_r} \times (1 - \cos\theta_b)\right\} \tag{5-61}$$

Each point of $v(\theta_b)$ is expressed from Eqs. (5-58) and (5-61).

$$v(\theta_b) = S_r \times \left[1 - \cos\left[\tan^{-1}\left\{ \frac{R}{S_r} \times (1 - \cos\theta_b) \right\} \right] \right] \tag{5-62}$$

The exact value of r is derived from Eqs. (5-56) and (5-57). However, to simplify the problem, Eq. (5-59) is applied instead of Eq. (5-57) to obtain r as;

$$S_r = \frac{2RH}{\delta} \tag{5-63}$$

From the Eqs. (5-62) and (5-63), the equation to calculate $v(\theta_b)$ is obtained as;

$$v(\theta_b) = \frac{2RH}{\delta} \times \left[1 - \cos\left[\tan^{-1}\left\{ \frac{\delta}{2H} \times (1 - \cos\theta_b) \right\} \right] \right] \tag{5-64}$$

5-2-2 Comparison of the calculation result with the FE analysis

Figures 5-12 and blue line of 5-13 show the results of the FE analysis of the uplift case (Case 21) specified in Chapter 3. The blue line is obtained by original deformation (green line) minus horizontal rigid deformation. These results show an undulating deformation occurring at the top of the sidewall.

As specified in Chapter 3, this undulating deformation at the top of the sidewall appeared mainly after 14 seconds. It has the relationship with uplift height of the bottom plate. As opposed to an anchored tank, an unanchored tank will have a similar undulating deformation but this configuration does not affect dynamic pressure, as discussed in Chapter 3.

The seismic wave is comprised of a number of different frequencies. One or more of frequencies may match the natural period of the undulating deformation mode of the tank.

The deformation at the top of the sidewall may consist of component of an oval shape and a local undulation. In Figure 5-13, assumed oval shape (red line, expected deformation is 11 mm in radius) also is plotted. The pink line, which is obtained by blue line minus red line, is considered undulation component. If the deformation at the top of the sidewall can be converts to oval shape by removing undulation component, Eq. (5-64) is expected to function effectively.

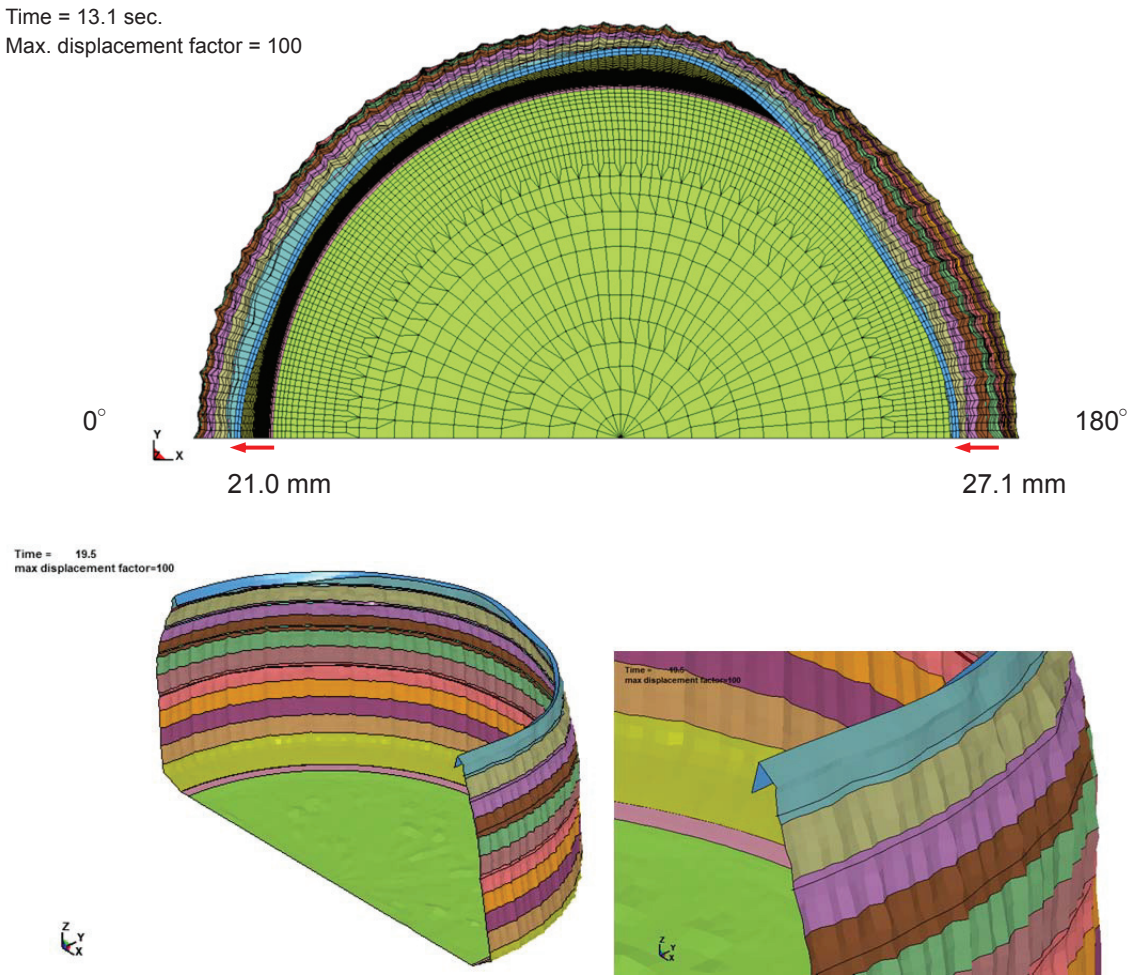

FIGURE 5-12: DISPLACEMENT OF SIDEWALL OBTAINED BY THE FE ANALYSIS CASE 21

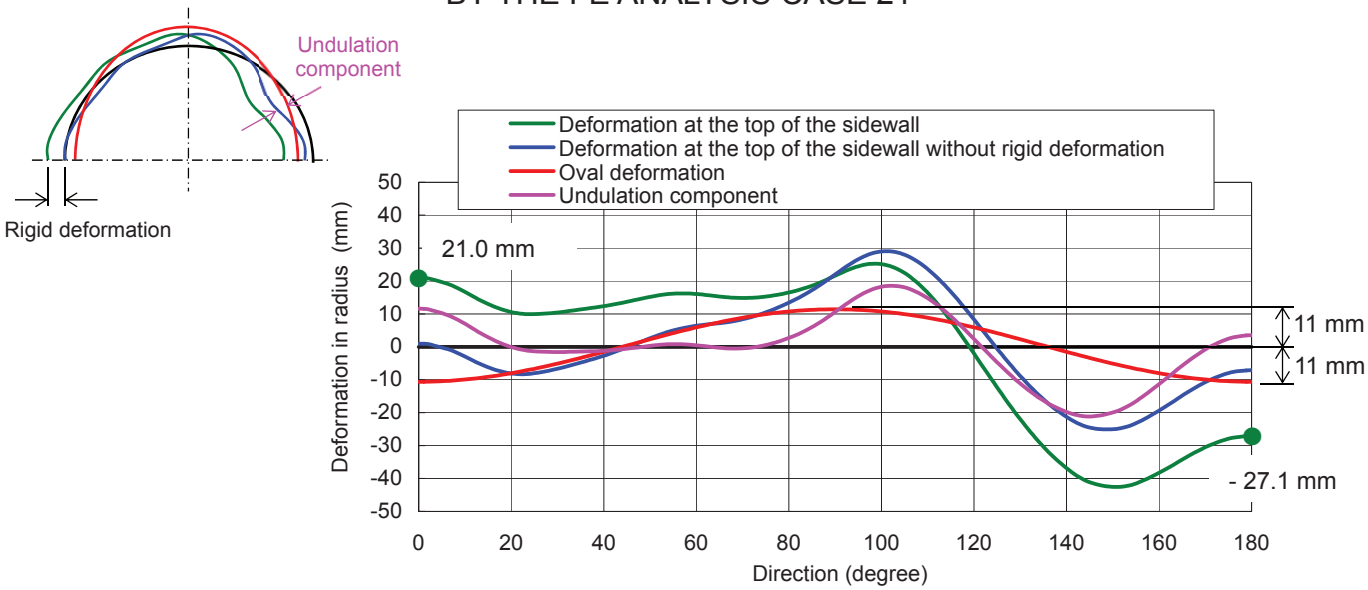

FIGURE 5-13: DISPLACEMENT TREND AT THE TOP OF THE SIDE WALL ALONG THE CIRCUMFERENCE

Table 5-1 shows the result of the trial calculation for the uplift height of the bottom plate by the proposed supplementary model. This calculation is performed by following steps.

From (a) - The displacement of the uplift side
Subtract (b) - The displacement of the compression side, then
To obtain (c) - The oval displacement at the top of the sidewall
Then calculate (d) - The uplift height calculated using Eq.(5-64) and the value from (c)
Then compare this with (e) the uplift height by the FE analysis from Chapter 3.

TABLE 5-1: CALCULATION RESULT OF UPLIFT
DUE TO INCLINE DISPLACEMENT OF SIDEWALL

(mm)

	Case 21	Case 21R	Case 41
(a) The displacement of the uplift side	27.1	24.3	274.9
(b) The displacement of the compression side	21.0	19.5	56.4
(c) The oval displacement at the top of the sidewall	6.1	4.8	218.5
(d) The uplift height calculated using Eq. (5-64) and the value from (c)	6.1	4.8	220.7
(e) The uplift height by the FE analysis from Chapter 3	21.6	9.9	215.8

Note

- Case 21 is a normal tank (uplift conditions) with normal stiffener during earthquake.
- Case 21R is a normal tank during an earthquake but with rigid stiffeners attached around the sidewall to decrease undulation of the sidewall.
- Case 41 is a tank which is subject to a constant horizontal acceleration (constantly increasing horizontal acceleration up to the maximum value) only and it deforms in an oval shape.

The calculation result with the condition of constant horizontal acceleration Case 41, which has oval shape deformation at the top of the sidewall, is in relatively good agreement with the result of the FE analysis. However, other cases are more than 2 times larger than the result of the FE analysis. This different is thought to be caused by the effect of the undulating deformation mode (the maximum displacement seems to be a trend within local area.). The calculation result also implies that the deformation at top of a sidewall has a close relationship with the uplift height and it is affected by a configuration of deformation sensitively. Consequently, converting the undulation deformation to oval deformation by using some kind of average method is necessary to use the supplementary model, as represented by Eq. (5-64), does work effectively. For example, applying moving average to the values of displacement of each direction is one option to evaluate amplitude of the oval deformation.

Investigation of the mechanism of undulating deformation at top of a sidewall and developing the model for introducing the effect of the deformation is necessary in future work for improving the accuracy of the model.

5-2-3 Reflect the effect of sidewall deformation to the formula of angle indicating the location of neutral axis

As specified in Figure 3-14 of Chapter 3, the uplift height has a linear relationship with the uplift width. This relationship is expressed as 'uplift width = $d_u \times$ uplift height', by using the coefficient d_u (this coefficient expresses the ratio of uplift width against uplift height and differs depending on tank dimensions, then preparing the values through FE analysis for each tank proportion is necessary). Then, the uplift width due to uplift caused by sidewall deformation at 180 degree, which is calculated by Eq (5-64), becomes;

$$d_u \times v(\pi) \tag{5-65}$$

Consequently, the effect of uplift due to sidewall deformation on uplift width is integrated in Eq. (a) as follows.

$$\begin{aligned} &\rho g h \times w_{ef} \times (W - W_a) \\ &\quad - \frac{1}{T_{ns1}(\alpha)} \times \left[\frac{M}{4} - \left(P_{db}(\theta_b = 180) + P_{dr}(\theta_b = 180)\right) \times w_{ef} \times (W - W_a) \times T_{nsbr1}(\alpha) \right. \\ &\quad \left. - \rho g h \times w_{ef} \times W_a \times T_{ns2}(\alpha) - \left(P_{db}(\theta_b = 180) + P_{dr}(\theta_b = 180)\right) \times w_{ef} \times W_a \times T_{nsbr2}(\alpha) \right] = 0 \end{aligned} \tag{a-1}$$

Where, total uplift width W is specified as;

$$W = W_0 + d_u \times v(\pi) + W_a \tag{a-2}$$

5-3 CALCULATION OF UPLIFT AREA AND AXIAL FORCE OF SIDE WALL

5-3-1 Conditions of calculation by proposed model

A trial calculation is performed by the mathematical model (the Force Coupling Mathematical Model) under the same conditions as the FE analysis case to verify effectiveness of a proposed model. Figure 5-14 and following values show the dimensions of the subject LNG tank and the parameter values used in the FE analysis for Case 21, 32 and Case 41.

The assumed value of the angular acceleration of Case 41 (constant horizontal acceleration case) is calculated from, (a) estimated 3rd natural period from other cases and (b) the uplift height by the FE analysis of Case 41. As discussed in Chapter 3, the 3rd natural period is considered for the undulating deformation, which has a relationship with uplift height. Therefore, (a) is used for a natural period of the uplift.

The values of parameters W_a, w_{ef}, d_u may be depend on tank characteristics such as proportion and dimension of each part. Therefore, at this moment these values have to be set up based on the result of the FE analysis.

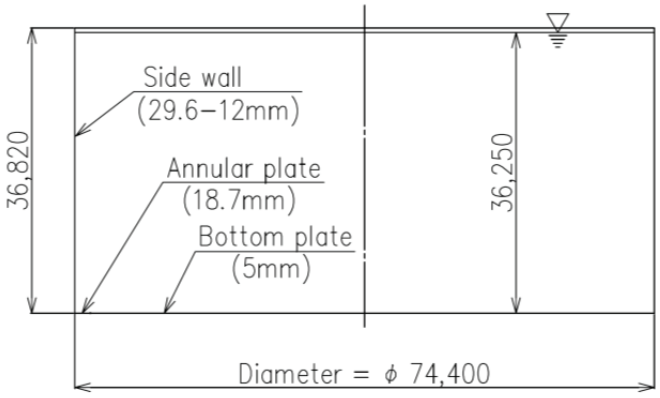

FIGURE 5-14: TANK CONFIGURATION

R: Tank radius	37,200 mm	
H: Tank height	36,250 mm	
t_s: Thickness of bottom of the sidewall	29.6mm	
k: Reaction coefficient of tank bottom	25.5 N/mm^2	
E: Modulus of elasticity of steel	191,000 MPa	
M: Over turning moment	Case 21:	1.44 E+12 N-mm
	Case 32(①):	2.05 E+12 N-mm
	Case 32(②):	2.19 E+12 N-mm
	Case 41:	2.47 E+12 N-mm

(From the FE analysis results of Case 21, 32 and Case 41. Case 32① is the value at the moment of occurring small uplift (50.0mm) in Case 32, while Case 32② is the value at the moment of occurring large uplift (116.8mm).)

W_a: Width of the bottom plate affected by annular plate — 1045 mm (55% of annular plate width)

w_{ef}: Coefficient expressing of increase in axial force at the bottom of sidewall

Case 21 :	85%
Case 32(①):	85%
Case 32(②):	65%
Case 41 :	50%

(These values are set up based on the FE analysis result shown in Table 3-6.)

d_u: Coefficient expressing a ratio of uplift with against uplift height — 16.5

(This value is set up based on the FE analysis result shown in Figure 5-15.)

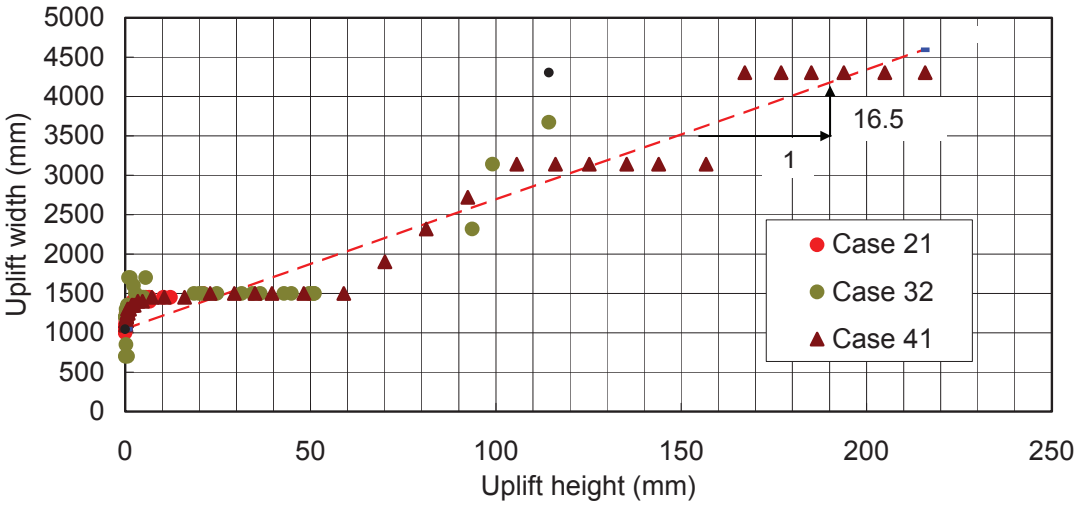

FIGURE 5-15: RELATION OF UPLIFT HEIGHT AND UPLIFT WIDTH

w: Effective width of bottom plate — 349.6 mm

(Assumed as thickness of sidewall and 16 times of thickness of annular plate)

$v(\pi)$: Uplift height of bottom plate due to horizontal displacement of the top of the sidewall at 180 degrees

Case 21:	21.6 mm
Case 32(①):	50.0 mm
Case 32(②):	116.8 mm
Case 41:	215.8 mm

(These values are set up based on FE analysis result shown in Table 3-5.)

ρ: Fluid density — 480 kg/m^3

h: Liquid height — 35,820 mm

g: Gravity acceleration — 9.8 m/s^2

u'_0: Horizontal acceleration

Case 21:	0.2469
Case 32(①):	0.1970
Case 32(②):	0.5535
Case 41:	0.4049

(The value for Case 41 is obtained from natural period and response acceleration spectrum of Artificial seismic wave as shown in Table 3-1. Other values are the maximum response acceleration in the FE analysis. The values of Case 21 and Case 32(②) are specified in Table 3-3)

$\ddot{\theta}_0$: Angular acceleration

Case 21: 0.041 rad/s^2

Case 32(①): 0.072 rad/s^2

Case 32(②): 0.064 rad/s^2

Case 41: 0.030 rad/s^2

(These values are set up based on the FE analysis result. Part of value is shown in Table 3-10. The value for Case 41 is calculated from uplift height of the FE analysis of Case 41 and estimated 3rd natural period from each dynamic uplift case.

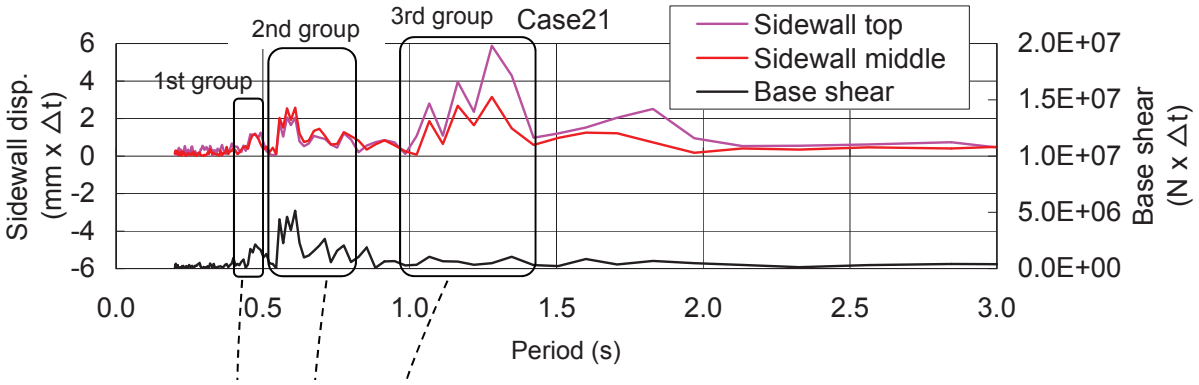

FIGURE 5-16: EXAMPLE OF NATURAL PERIOD OF CASE 21

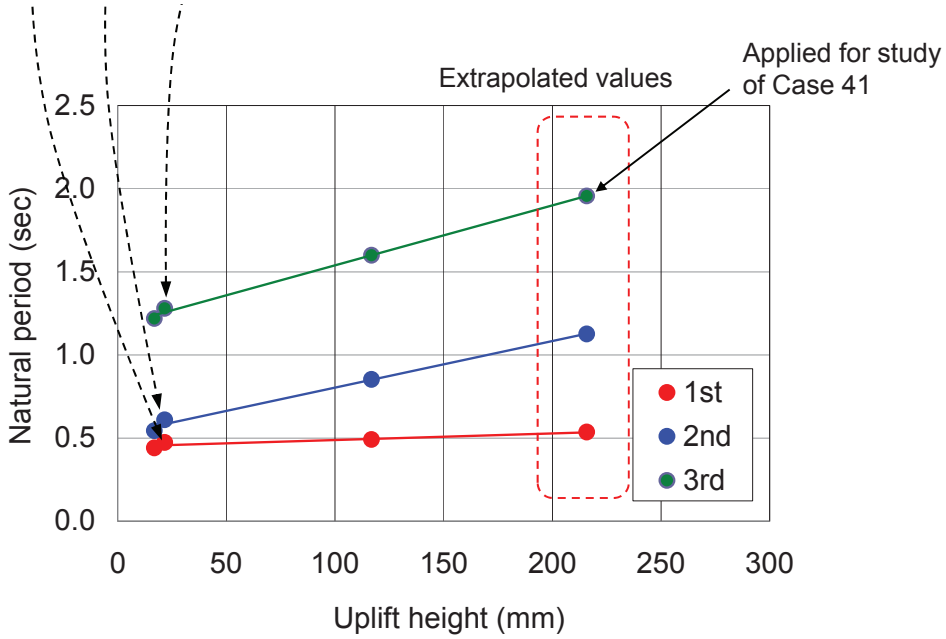

FIGURE 5-17: RELATIONSHIP BETWEEN UPLIFT HEIGHT AND NATURAL PERIOD

TABLE 5-2: RELATION BETWEEN UPLIFT HEIGHT AND NATURAL PERIOD

		Case 21	Case 31	Case 32	Case 41	
Uplift height (mm)		21.6	16.9	116.8	215.8	
Natural period (sec)	1st	0.474	0.441	0.492	0.54	Extrapolated
	2nd	0.610	0.545	0.853	1.13	Extrapolated
	3rd	1.280	1.219	1.600	1.96	Extrapolated (Applied for study)

5-3-2 Result of calculation

Figures 5-18-1 to 5-18-4 and Table 5-3 show the results of the distribution of the axial force on the end of the sidewall of each model by the proposed calculations. Trial calculation cases are selected so as to include various situations. Case 21 is for artificial seismic wave, Case 32 is for EL Centro seismic wave, while Case 41 is for constant horizontal acceleration case. The uplift heights of selected cases are from 16.9 to 215.8 mm. Accordingly, the differences between the results obtained from the mathematical model and the FE analysis are:

- 0 to +25 % in uplift width
- - 7 to +22% in location of neutral axis
- - 22 to -1 % in the maximum tensile axial force of sidewall
- - 8 to +9 % in the minimum compressive axial force of sidewall.

Even though, several values are different more than 20%, trend of calculation result is similar to that of the FE analysis. In the dynamic FE analysis, each value varies with time. In addition, this transient situation (duration) is slightly different by each physical quantities and location that generated. Therefore, local or within short period unstable behavior occurs. This trend is shown in the FE analysis result. For applying the proposed mathematical model, which is established based on the conditions without this kind of unstable, to tank design, suitable allowance for comprising these unstable behavior in actual phenomenon. From this viewpoint, the calculation results are considered within an acceptable level.

TABLE 5-3: CALCULATION RESULTS

		Case 21		Case 32(①)		Case 32(②)		Case 41	
		Model	FE analysis	Model	FE analysis	Model	FE analysis	Model	FE analysis
Uplift width	(mm)	1450.0	1450.0	1870.0	1500.0	4303.4	4303.4	4605.7	4303.4
	Ratio	1.00		1.25		1.00		1.07	
Location of neutral axis	(degree)	74.3	79.9	69.3	72.0	71.3	58.5	66.3	58.5
	Ratio	0.93		0.96		1.22		1.13	
Tensile force at 180 degree *1	(N/mm)	184.6	186.1	253.8	256.1	331.1	336.8	284.0	366.1
	Ratio	0.99		0.99		0.98		0.78	
Compressive force at 0 degree *2	(N/mm)	-481.3	-520.8	-858.3	-796.2	-956.6	-874.5	-1132.0	-1042.4
	Ratio	0.92		1.08		1.09		1.09	

*1 : Average of values at 160 -180 degree
*2 : Average of values at 0 - 20 degree

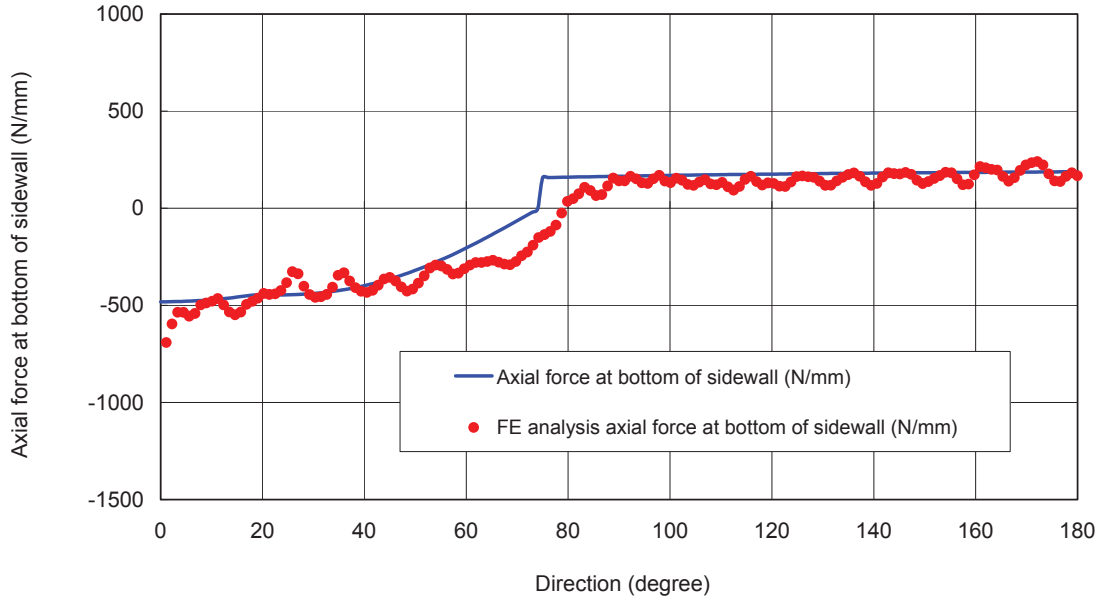

FIGURE 5-18-1: RESULT OF TRIAL CALCULATION (Case 21)

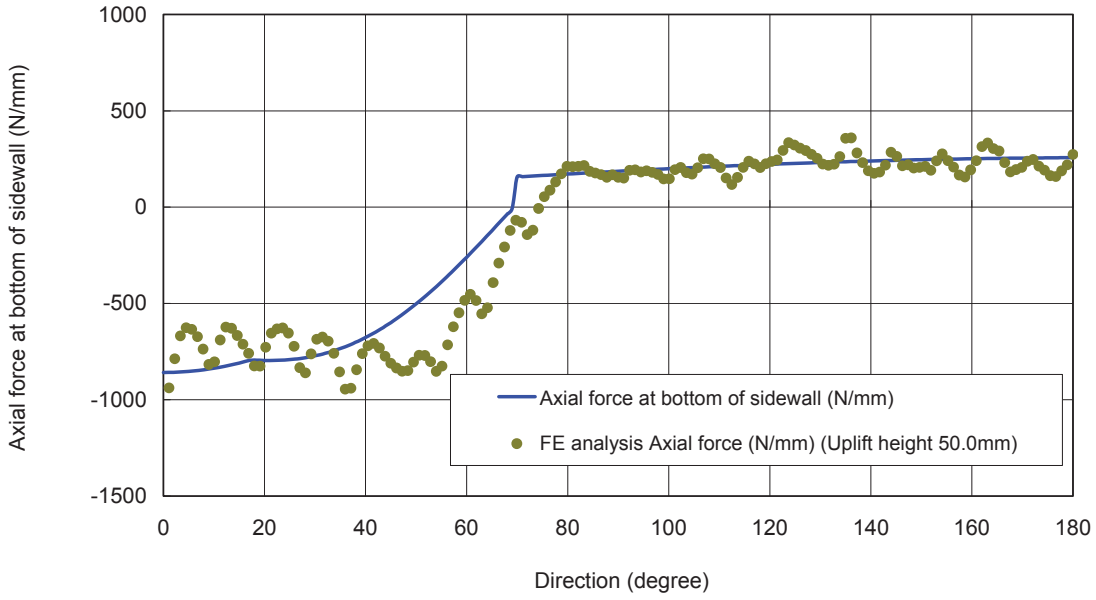

FIGURE 5-18-2: RESULT OF TRIAL CALCULATION (Case 32①)

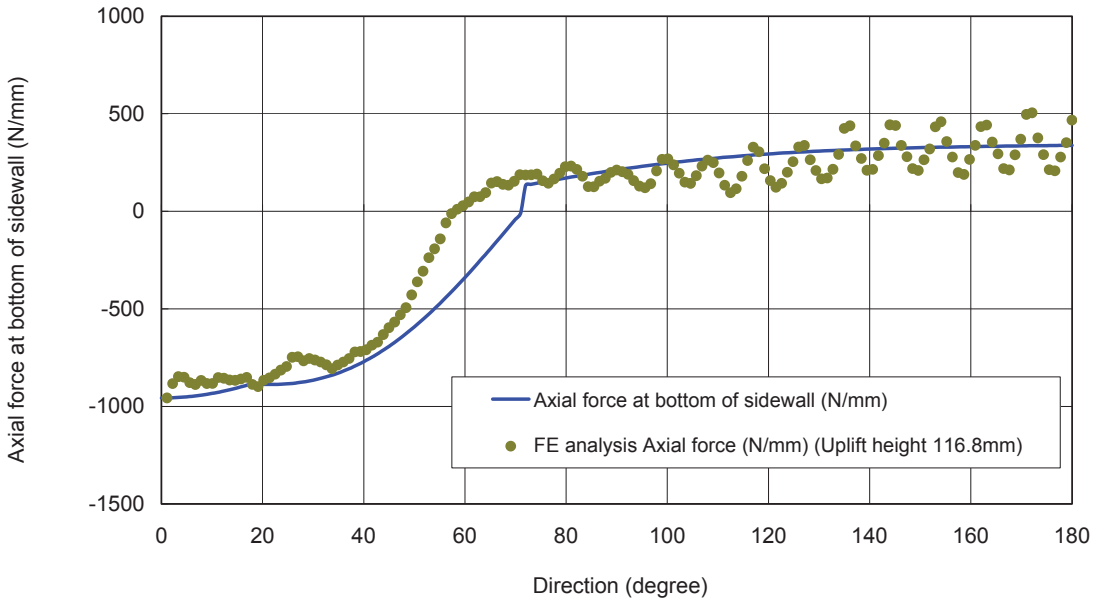

FIGURE 5-18-3: RESULT OF TRIAL CALCULATION (Case 32②)

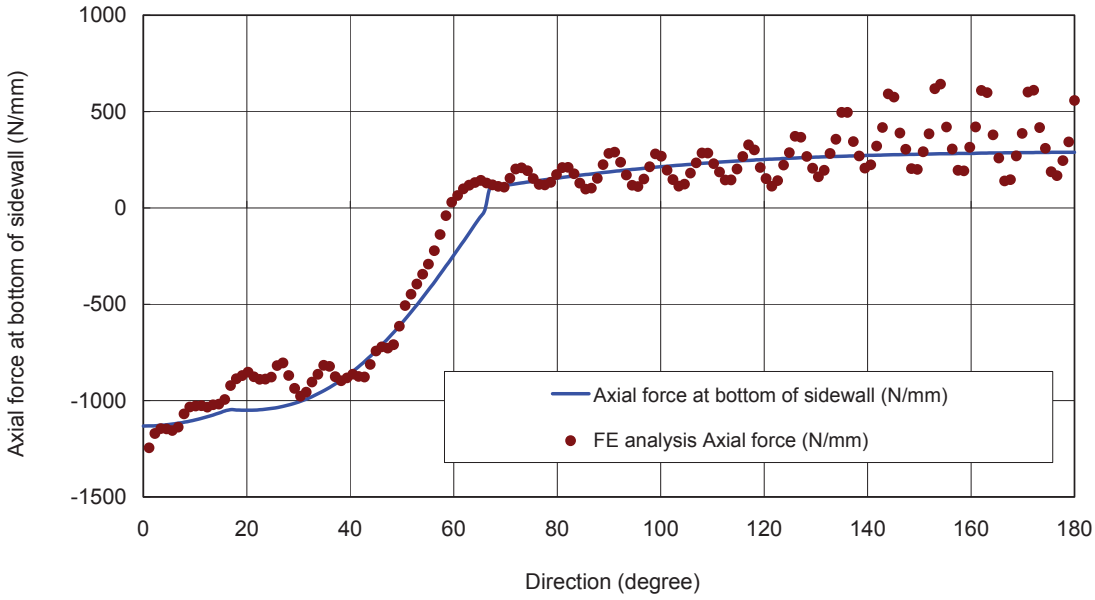

FIGURE 5-18-4: RESULT OF TRIAL CALCULATION (Case 41)

5-4 FINDINGS

In this chapter, the mathematical model (referred to as the Force Coupling Mathematical Model) was proposed to estimate distribution of an axial force on a bottom of a sidewall. This model takes into account physical phenomenon of a force couple formed by a reaction force of a tank bottom due to subsidence, a resistance force against uplift due to liquid weight in uplift area and an effect of deformation at top of a sidewall. Then, comparison of a trial calculation with the same conditions by the FE analysis was performed to verify the applicability of the model.

The findings are summarized below.

- The differences of the result between the proposed mathematical model and between the FE analysis are 25% in uplift width, 11% in location of neutral axis, 22% in the maximum tensile axial force and 24% in the minimum compressive axial force, respectively. While, trend of the calculation result is similar to that of the FE analysis.
- One of the reason of these discrepancies are local or within short period unstable behavior of physical quantities during transient duration in dynamic analysis.
- For applying the proposed mathematical model to tank design, suitable allowance for comprising these difference is required.
- It is considered that the deformation at top of a sidewall has a close relationship with the uplift height and it is affected by a configuration of deformation sensitively.
- Further investigation and development of the model is required for the undulating deformation at the top of the sidewall for improving of calculation accuracy.
- A cosine curve is assumed to be the pressure distribution profile on the surface of the uplift area due to the bulging and rocking modes. This profile is used instead of a theoretical value to simplify the model. It had better to integrate the theoretical formula into the mathematical model for improving the calculation accuracy.

REFERENCES

[1] Housner, G. W., 1957, “Dynamic Pressure on Accelerated Fluid Containers”, Bulletin of the Seismological Society of America, Vol. 47, pp. 15-35.

[2] Taniguchi, T. and Segawa, T., 2008, “Fluid Pressure on Rectangular Tank Consisting of Rigid Side Walls and Rectilinearly Deforming Bottom Plate due to Uplift Motion”, Proceedings of ASME PVP Conference, PVP2008-61166.

CHAPTER 6

PROPOSAL OF DESIGN PROCEDURE FOR TANK BOTTOM PLATE

CHAPTER 6
PROPOSAL OF DESIGN PROCEDURE FOR TANK BOTTOM PLATE

In this chapter, the seismic design procedure (the Simplified Seismic Design Procedure) for a bottom plate corner connection is established from outcomes of previous studies of bulging and rocking motions and the proposed mathematical models (the Structural Mathematical Model and the Forced Coupling Mathematical Model). These mathematical models, together with some additional calculations, form the design procedure. Then trial calculations by the proposed procedure are conducted for a specific standardized tank.

Suggested topics to be studied in the future are also summarized.

6-1 DESIGN PROCEDURE FOR TANK BOTTOM PLATE

Figure 6-1 shows the proposed Simplified Seismic Design Procedure for a bottom plate corner connection and a sidewall.

The Simplified Seismic Design Procedure uses previous studies to calculate some of the variables needed. These include:

- Dynamic pressure due to a bulging mode with no-uplift condition is calculated from the theory of Housner [3] or Veletsos and Yang [4] (Step 5).
- Angular acceleration of a tank bottom plate, which is used for obtaining of uplift induced pressure, is calculated by the mathematical model of Okui [1] or D'Amico et al. [2] (Step 3). In this step, an assumed uplift width is applied.
- Dynamic pressure induced by an uplift of a bottom plate is calculated from the theory of Taniguch and Segawa [5] by using the angular acceleration of a bottom plate (Step 4).

An extent of uplift, a location of neutral axis, an axial force and sidewall stress are calculated from the Force Coupling Mathematical Model developed in this study (Step 7). This is accomplished by using a tank overturning moment (Step 6) obtained from the dynamic pressure derived in Step 4 and Step 5.

Then, values of uplift height and a width of a tank bottom plate are calculated by the Structural Mathematical Model (Step 8).

The value of W' , uplift width assumed, derived from the above steps are then re-introduced to the mathematical model of Okui or D'Amico to converge the results for the uplift induced pressure. Then this value is re-introduced to the subsequent steps of the model to further converge the results.

This iterative process is described below:

- The calculated uplift width of a tank bottom plate *W'* is re-introduced as the assumed width used in Step 3.
- Steps 2 to 9 are repeated until an error becomes less than an acceptable level. Finally, the assessment of integrity of the corner connection of a tank bottom plate is demonstrated by the value of the calculated stress (Step 10).

Following is the description of each step.

Step 1: Set up the design conditions

Select appropriate design conditions of a tank such as dimensions, a natural period, a response spectrum and the horizontal acceleration at ground level

Step 2: Assume an uplift width

Assign an assumed uplift width W (assumed one is described as W'), which consists of W_0, $d_u \times v(\pi)$ and W_a, since this value is essential for Step3. W is corrected by adjusting W_0 through repeated calculation process of the proposed design procedure.

Step 3: Calculate the angular acceleration of the tank bottom plate during uplift

Calculate angular acceleration and the response acceleration of the tank. The response acceleration* of the tank becomes an input to Step 5.

Step 4: Calculate the dynamic pressure induced by the uplift of the tank bottom plate

Calculate the dynamic pressure induced by the uplift of the tank bottom plate by the angular acceleration.

Step 5: Calculate the bulging dynamic pressure

Calculate the dynamic pressure due to the bulging mode by applying the response acceleration* due to the uplift to the tank bottom plate, derived from Step3.

Step 6: Calculate the tank overturning moment

Calculate the tank overturning moment from the dynamic pressure induced by the bulging response and the uplift of the tank bottom plate

Step 7: Calculate the extent of the uplift and the axial force at the bottom of the sidewall

Calculate the extent of the uplift and the axial force at the bottom of the sidewall by the tank overturning moment and the effect of the maximum displacement of the top

of the sidewall. The displacement is inwards towards the center of the tank. This displacement occurs when the tank temporarily becomes an oval shape during an earthquake. The displacement is the difference between the length of the tank's circular diameter and the length of the tank's minor axis.

Step 8: Calculate the uplift height and the width

Calculate uplift height 'v' and the width 'W' of the tank bottom plate due to the axial force acting on the bottom of the sidewall as well as the total of the static and dynamic pressures acting on the sidewall and the tank bottom plate

Step 9: Decide if a further iteration of the calculations is required

Compare the value of W used as an input to the design procedure (W') with the newly calculated value of W. If the difference is large, change the value of Input W' by adjusting W_0 within positive, then, repeat Steps 3 to 9 several times until the difference becomes less than the acceptable level.

Step10: Assess the stress of the tank bottom plate and the sidewall

Combine the stress derived from the above procedure and from other factors affecting the tank such as self-weight. Then re-calculate up to decide the minimum required dimensions for the tank bottom plate and the sidewall, in accordance with an appropriate safety factor.

* In future plan, this value will be obtained from a natural period and response acceleration spectrum of tanks with uplift conditions as specified in 3-3 of Chapter 3.

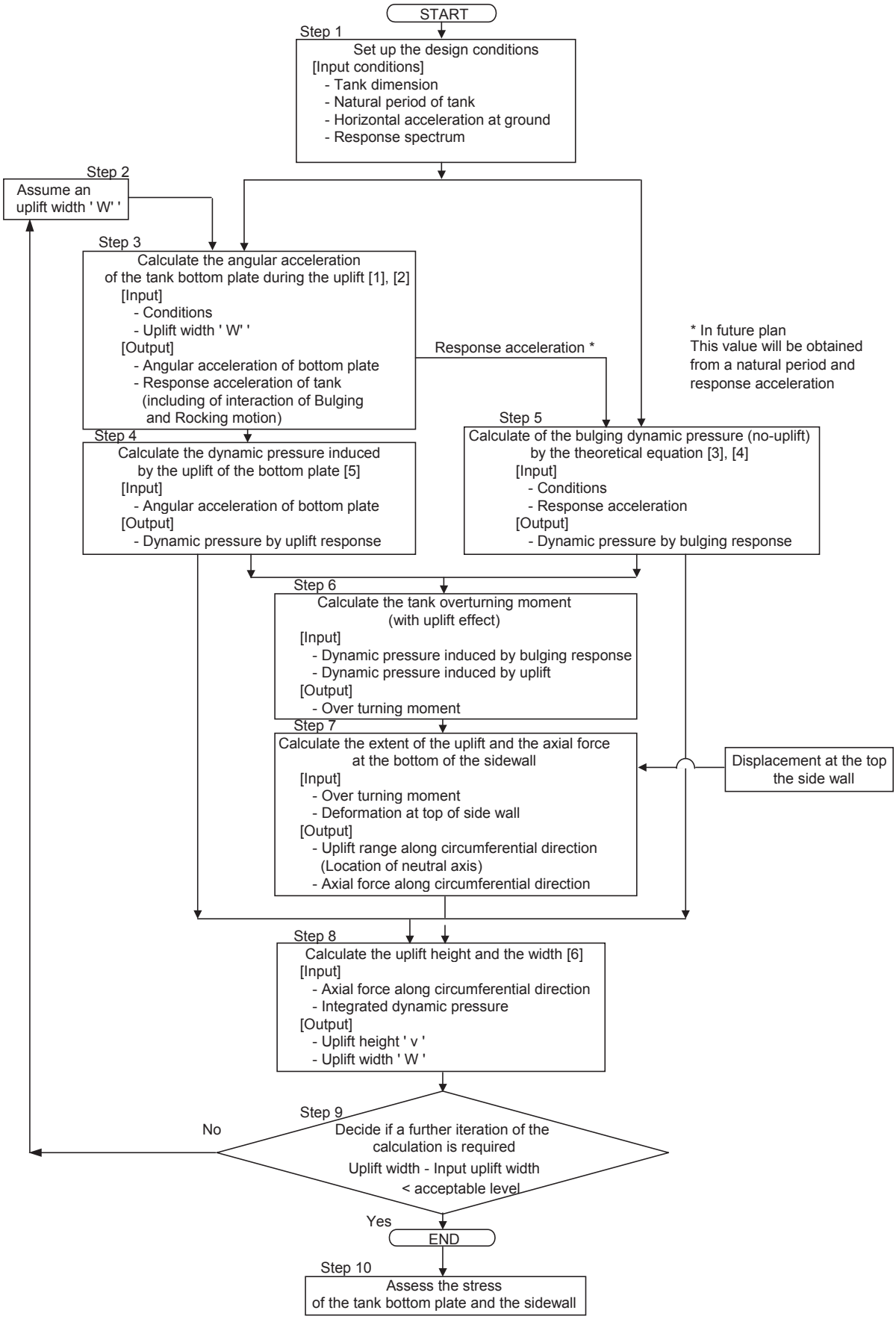

FIGURE 6-1: VERIFICATION PROCEDURE OF TANK BOTTOM PLATE

6-2 CALCULATION METHOD FOR ANGULAR ACCELERATION AND REDUCTION RATIO IN RESPONSE ACCELERATION

In this design procedure, the theory of Okui's model [1] is applied for obtaining two values. The first is an angular acceleration of the sidewall, which is essential factor for estimating the dynamic pressure due to the rocking motion. The second is a reduction ratio in translational response acceleration against the translational response acceleration under no-uplift condition, which is used for calculating of the dynamic pressure due to the bulging motion.

Figure 6-2 compares the uplift width against the tank diameter and the reduction ratio in response acceleration, and the angular acceleration at each response acceleration reduction case for Okui's model. These relationships are based on the subject tank conditions.

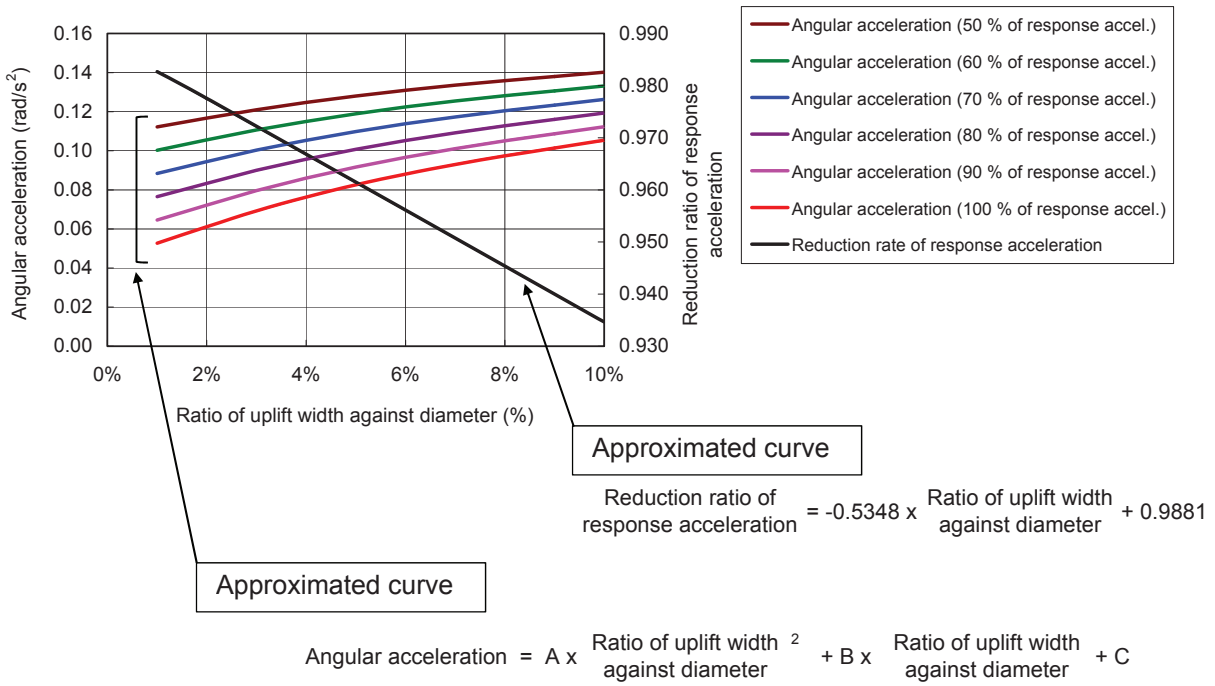

Ratio against response accel. with no uplift condition	A	B	C
50%	-1.6667	0.4896	0.1076
60%	-1.9682	0.5769	0.0949
70%	-2.2697	0.6643	0.0822
80%	-2.5712	0.7517	0.0694
90%	-2.8727	0.8391	0.0567
100%	-3.1742	0.9264	0.0440

FIGURE 6-2: RELATIONSHIP BETWEEN RATE OF UPLIFT WIDTH AND ANGULAR ACCELERATION FOR A SPECIFIC TANK USING OKUI'S MODEL

Okui's model demonstrates that there is a reduction in the response acceleration as above described and in the maximum base shear between the 'no-uplift' case and the 'uplift' case. The maximum angular acceleration of the model shows acceptable agreement. However, the FE analysis provides larger reduction than this model. (Refer to APPENDIX C).

In this paper, the angular acceleration obtained by Okui's model is applied. And the reduction factor r_{ef} for response acceleration based on Okui's model is introduced tentatively for a start point. Regarding obtaining of response acceleration of tanks with uplift conditions, another approach than Okui's theory is specified in section 3-3 of Chapter 3. It is a providing method by using a natural period and responses spectrum. However, to establish the natural period estimation procedure and the response acceleration spectrum for general use in dynamic uplift conditions, further investigation is required.

6-3 SAMPLE CALCULATION OF DEFORMATION AND STRESS OF THE BOTTOM CORNER CONNECTION

6-3-1 Sample calculation of subject tank

In this section, sample calculation is performed along proposed procedure for the subject tank as specified below conditions.

D:	Tank diameter	74,400 mm
H:	Tank height	36,820 mm
h:	Liquid height	36,250 mm
t_s:	Thickness at bottom of sidewall	29.6 mm
t_{sa}:	Average thickness of top and bottom sidewall	20.8 mm
E:	Modulus of elasticity of steel	191,000 MPa
ρ:	Fluid density	480 kg/m^3

The value of W_0 is fundamental uplift width and takes only positive value. The value of W_a is width of the bottom plate effected by the annular plate. This value is decided to 0.55 for the calculation, according to the discussion in the section 3-2-5 of Chapter 3, based on the result of the FE analysis.

The value of w_{ef} is a coefficient expressing of increase in axial force at the bottom of the sidewall, which is induced by liquid pressure act on the uplift part of the bottom plate (hear in after 'coefficient for contribution of width'). This value is decided to 0.85 for the calculation, by referring the result of the FE analysis in Table 3-6 in Chapter 3.

The value of w is effective width of the bottom plate under the sidewall. This value is assumed as thickness at the bottom of the sidewall and 16 times of thickness of the annular plate (this ratio is experimentally applied for estimating a range of plate effected a bending moment).

The value of d_u is a coefficient expressing a ratio of uplift width against uplift height. This value is decided to 16.5 for the calculation, by referring the result of the FE analysis in Table 5-14 in Chapter 3.

The value of d_r is a coefficient for a supplemental bulge shape of subsidence of the bottom plate. This value is decided to 0.85, according to Figure 5-3 in Chapter 5.

The value of δ is horizontal displacement (difference in diameter from complete round) at the top of the sidewall. It is decided to 22 mm which is converted from the result of the FE analysis to expected oval deformation (11 mm in radius) as shown in Figure 5-12 of Chapter 5.

The value of r_{ef} is a reduction factor for response acceleration under uplift condition against that of no-uplift condition. This value is obtained from outcomes of Okui's model [1] shown in Figure 6-2 with a ratio of uplift width against a diameter.

The assumed uplift width W' is addition of W_0, $d_u \times v(\pi)$ and W_a. W' is corrected through repeated calculation process by changing the value of W_0.

Table 6-1 shows the input conditions and the calculation result.

TABLE 6-1: INPUT CONDITIONS AND CALCULATION RESULT

Step 1	R	:	Tank diameter	37,200	mm	
	H	:	Tank height	36,820	mm	
	ts	:	Thickness at bottom of sidewall	29.6	mm	
	tsa	:	Average thickness of top and bottom sidewall	20.8	mm	
			Applied thickness of sidewall	29.6	mm	
	Wb	:	Width of annular plate	1900	mm	
	tb	:	Thickness of annular plate	18.7	mm	
	k	:	Reaction coefficient of tank bottom	25.5	N/mm^2	
	E	:	Modulus of elasticity	191,000	MPa	
	W_0	:	Fundamental uplift width	0.0	mm	W_0 is corrected through repeated re-calculation
	Wa	:	Width effected by annular plate	1045.0	mm	Decide the value to 55% of annular plate width, according to the discussion in 3-2-5 of Chapter 3.
	wef	:	Coefficient for contribution of width	0.85		Decide the value to 0.85, by referring the FE analysis result in Table 3-6 of Chapter 3.
	du	:	Coefficient for ratio of uplift width against uplift width	16.5		Decide the value to 16.5, by referring the FE analysis result in Figure 5-14 of Chapter 5.
	w	:	Effective width of bottom plate	328.8	mm	Assume as thickness of sidewall and 16 times of thickness of annular plate.
	dr	:	Coefficient for subsidence of bottom plate	0.85		Decide the value to 0.85, according to Figure 5-3 in Chapter 5.
	δ	:	Incline displacement of sidewall	22	mm	Apply the value at expected oval deformaion of Case 21.
	ρ	:	Fluid density	480	kg/m^3	
	h	:	Liquid height	36,250	mm	
	g	:	Gravity acceleration	9.8	m/s^2	
	u'_0	:	Horizontal acceleration	0.4049		
	$ref \times u'_0$	:	Horizontal acceleration	0.3786		
	ref	:	Reduction factor for response acceleration	0.935		Decide the value so as to M becomes the same as overturning moment of Case 21.
Step 2	W'	:	Assumed uplift width	1,411.7 1.90	mm %	$W' = W_0 + du \times v(\pi) + W_a$ W_0 is corrected through repeated re-calculation
Step 3	θ''	:	Angular acceleration	0.060	rad/s^2	According to the relation as follows in Figure 6-2 y = -3.1742x2 + 0.9264x + 0.0440
Step 4	$Pdr(\theta=180)$	:	Dynamic presser due to rocking	0.0116	MPa	
Step 5	$Pdb(\theta=180)$	:	Dynamic presser due to bulging	-0.0510	MPa	
Step 6	M	:	Calculated overturning moment	1.45E+12	N-mm	
	Mb	:	Calculated overturning moment of bulging	2.02E+12	N-mm	
	Mr	:	Calculated overturning moment of rocking	-5.69E+11	N-mm	
Step 7	$v(\pi)$	:	Uplift height due to δ	22.2	mm	
	α	:	Angle indicating location of neutral axis	66.8	°	
	T	:	Tensile force at 180 degree	166.1	N/mm	
	C	:	Compressive force at 180 degree	-672.8	N/mm	
Step 8	v	:	Calculated uplift height	55.0	mm	
	W	:	Calculated uplift width	1,741.4	mm	
Step 9		:	Comparison of W and W'	1,741.4	mm ⇔	1,411.7 mm (-329.6 mm) Assumed uplift width ' W' '

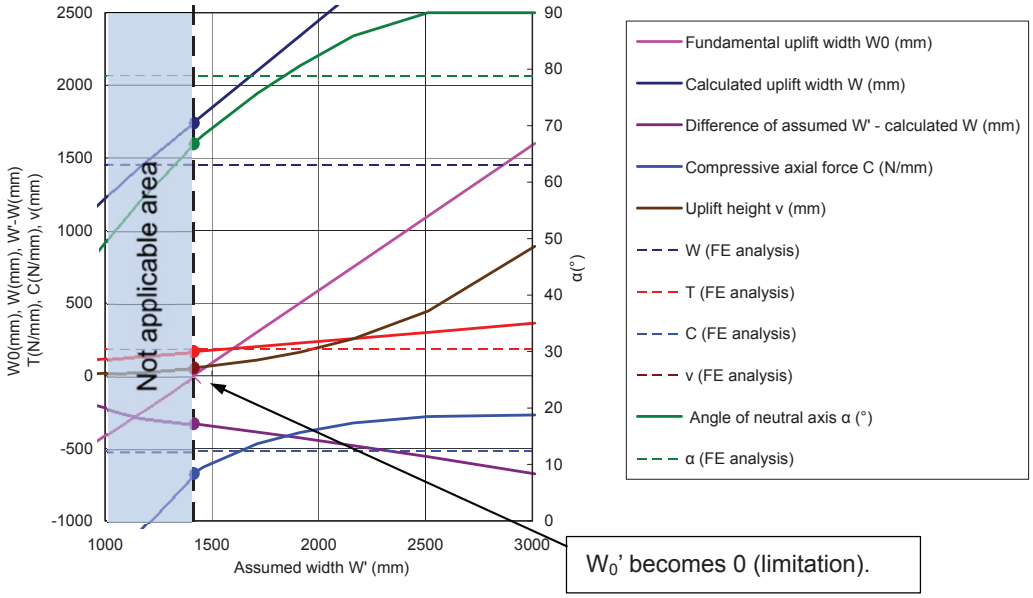

FIGURE 6-3: PROCESS UNTIL CONVERGENCE

According to the results in Table 6-1, the Simplified Seismic Design Procedure is thought to work effectively. However, the uplift width W obtained by the procedure is 23.4 % difference from assumed uplift width W'. This result is outcome in the repeated calculation process.

Figure 6-3 shows this process until convergence. The assumed uplift width W' is corrected through the process by changing W_0 within positive value. In this case, W_0 becomes 0 then the process is finished.

After that the values of axial force at the bottom of the sidewall, uplift height, deformation of the bottom plate and the sidewall, and stress in the tank bottom plate and the sidewall are obtained.

Figure 6-4 shows the calculated distribution of the axial force at bottom of the sidewall. Figure 6-5 shows the displacement of the tank bottom plate and the sidewall and the stress distribution along the tank bottom plate. In both figures, the results of the FE analysis of Case 21 are also plotted, which is similar conditions to the trial calculation. The uplift height of the trial calculation and the FE analysis are 61.2 mm and 21.6 mm, respectively. The value of the trial calculation is 2.8 times larger than that of the FE analysis. The other values of the trial calculation such as the sidewall displacement, the stress of the bottom plate and the compressive force and stress of the sidewall are also larger than that of the FE analysis.

It implied that a possibility of more suitable values for parameters of Wa, w_{ef}, d_u and d_r. Therefore, investigation of effectiveness of parameters on calculation result is performed.

Figure 6-6 to 6-9 show an effect of varying of parameter values on calculation result.

From the Figure 6-6, when Wa is decreased, W closes to W', on the contrary, α (the angle indicating the location of the neutral axis), T (the tensile force) and C (the compressive force) deviate from the result of the FE analysis.

Figure 6-7 and 6-8 show variation of d_u and d_r give a small influence on each value.

According to Figure 6-7, as the value of w_{ef} achieves 0.71, W closes to W', and α and C also close to the result of the FE analysis. It is thought that w_{ef} is an influential parameter than other parameter. Where w_{ef} is less than 0.71, each value seems to diverge.

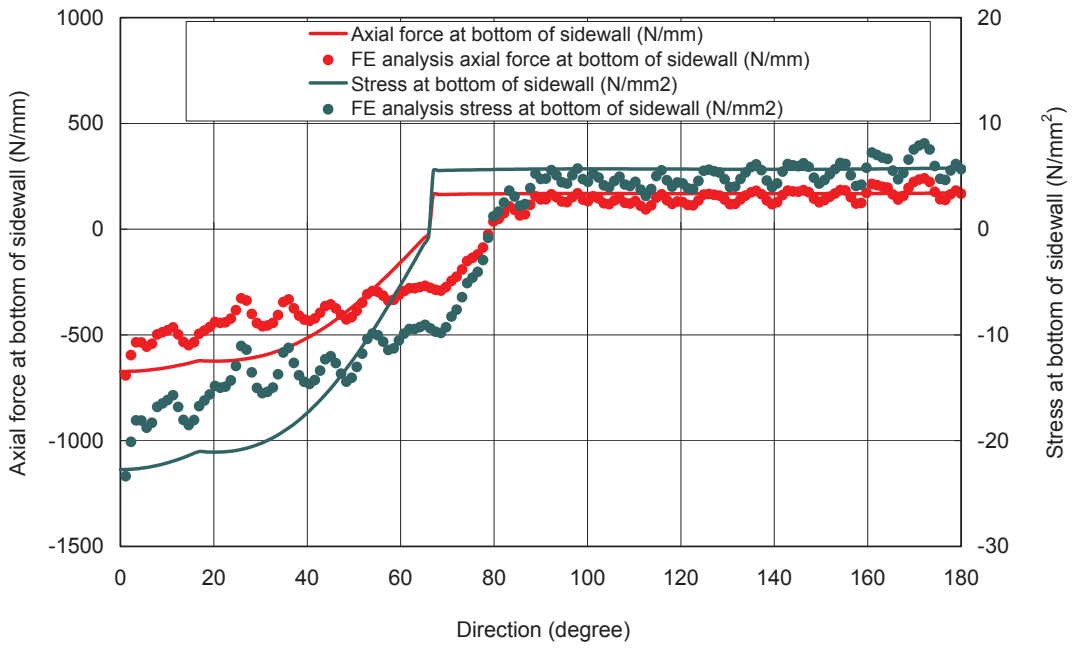

FIGURE 6-4: AXIAL FORCE ALONG BOTTOM OF SIDEWALL

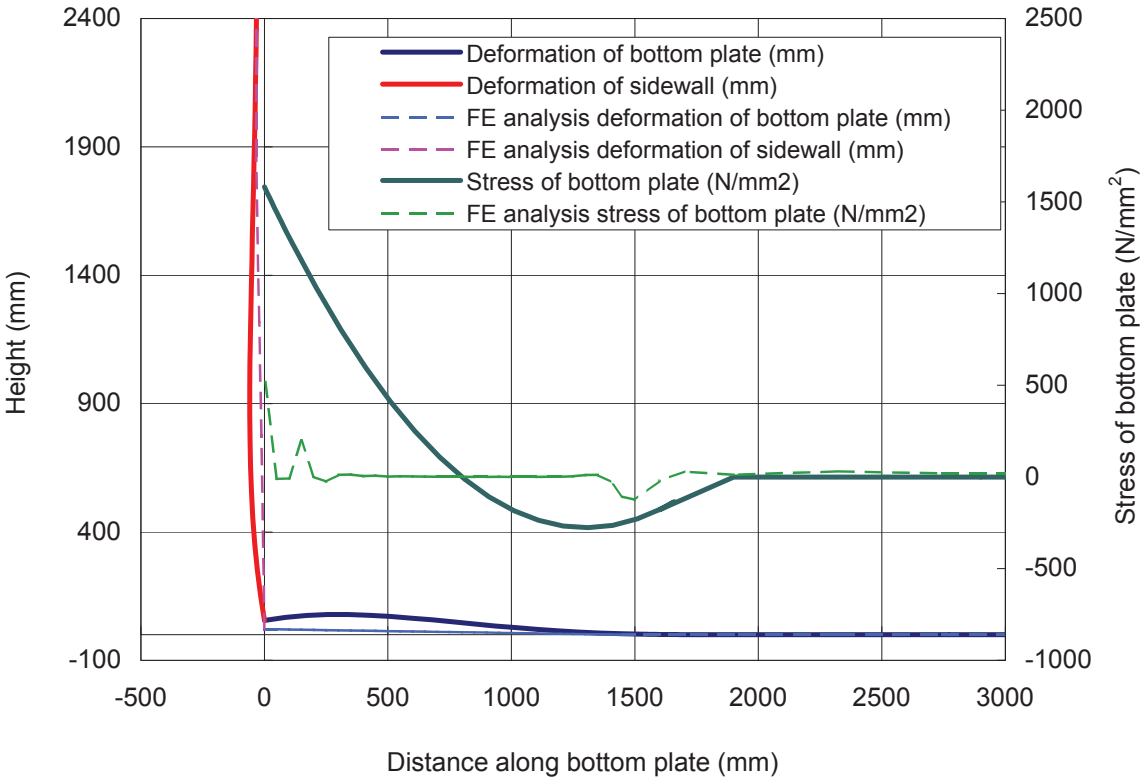

FIGURE 6-5: CHARACTERISTICS OF SIDEWALL AND TANK BOTTOM PLATE

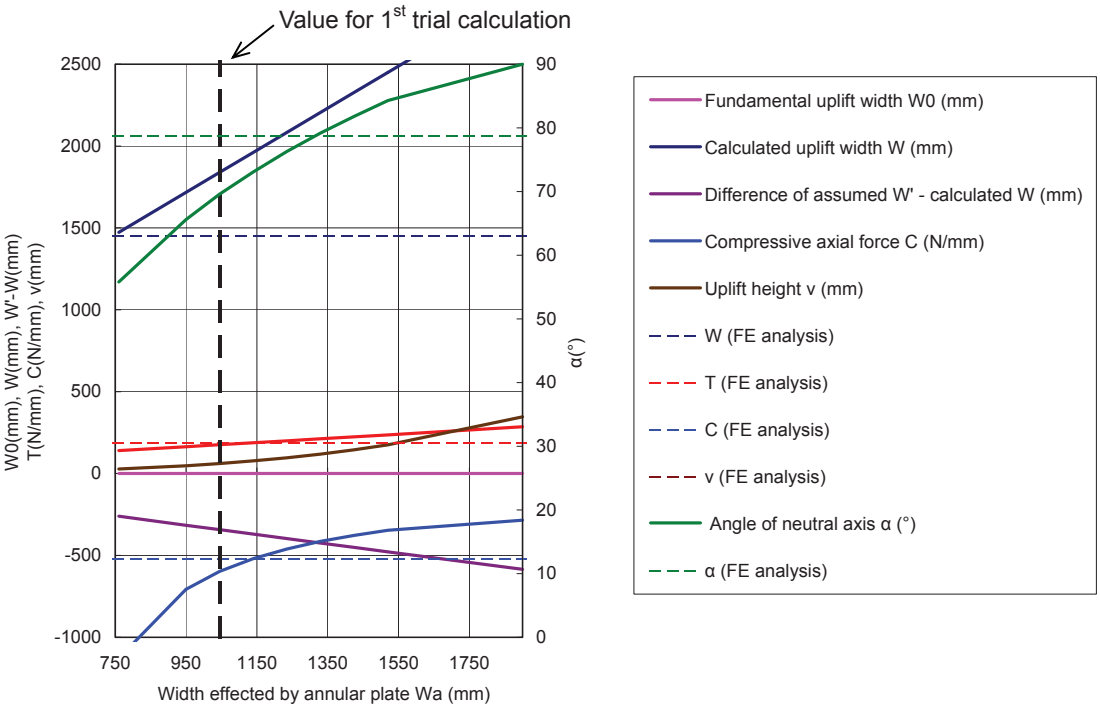

FIGURE 6-6: RELATIONSHIP OF *Wa* (width effected by annular plate) AND EACH VALUES

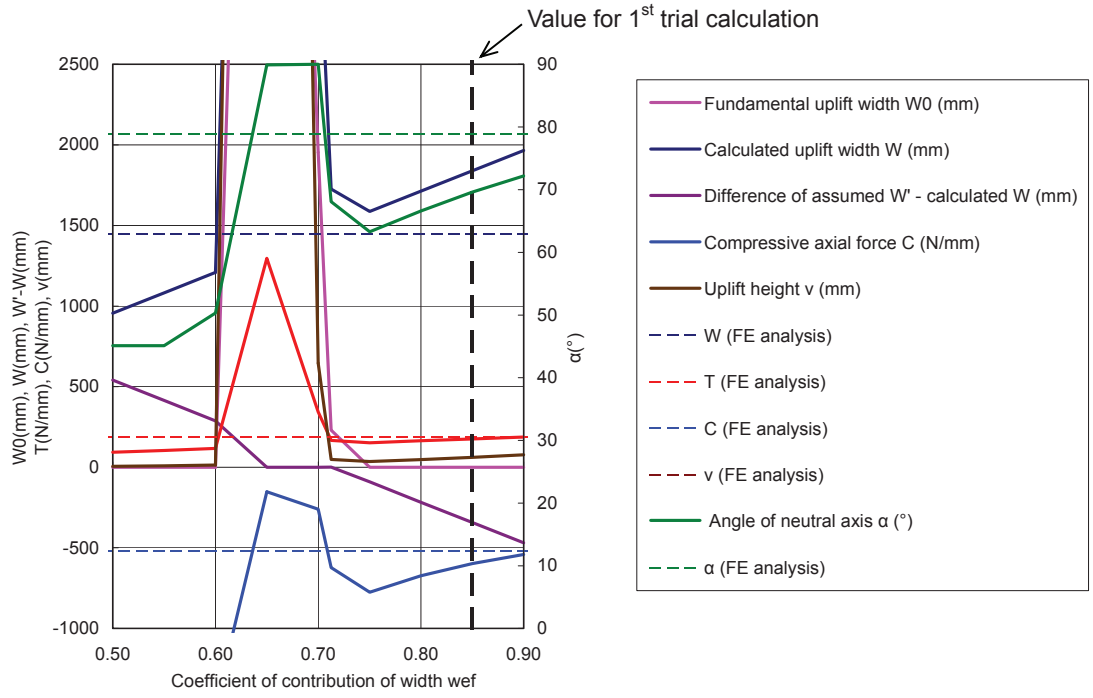

FIGURE 6-7: RELATIONSHIP OF w_{ef} (coefficient of contribution of width) AND EACH VALUES

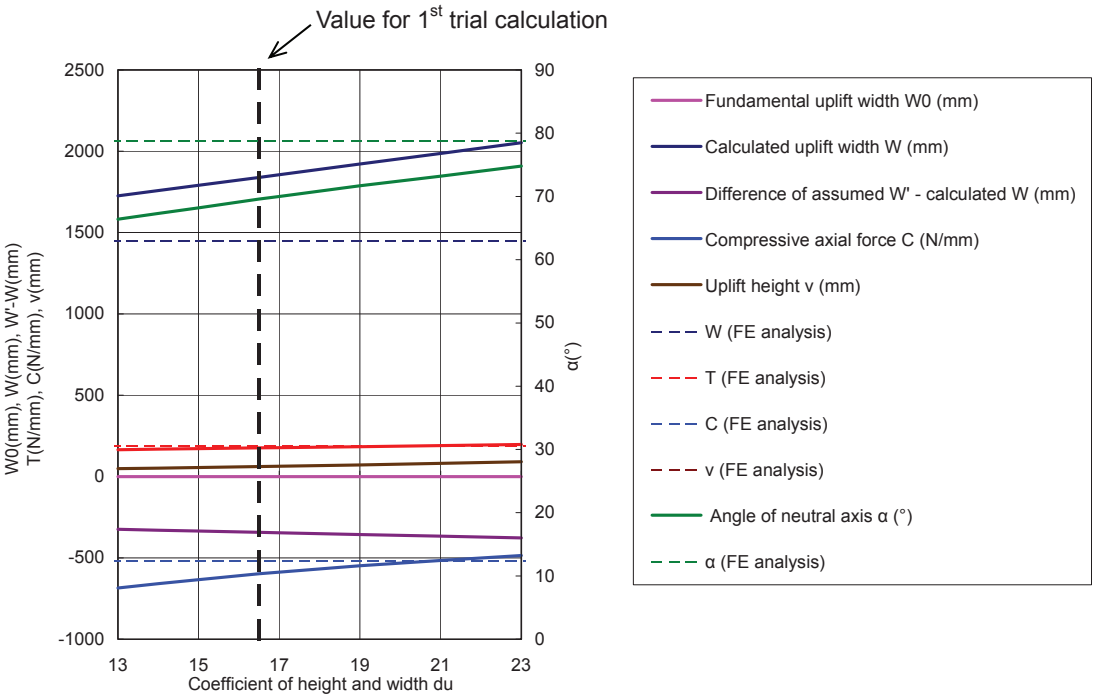

FIGURE 6-8: RELATIONSHIP OF d_u (coefficient of height and width) AND EACH VALUES

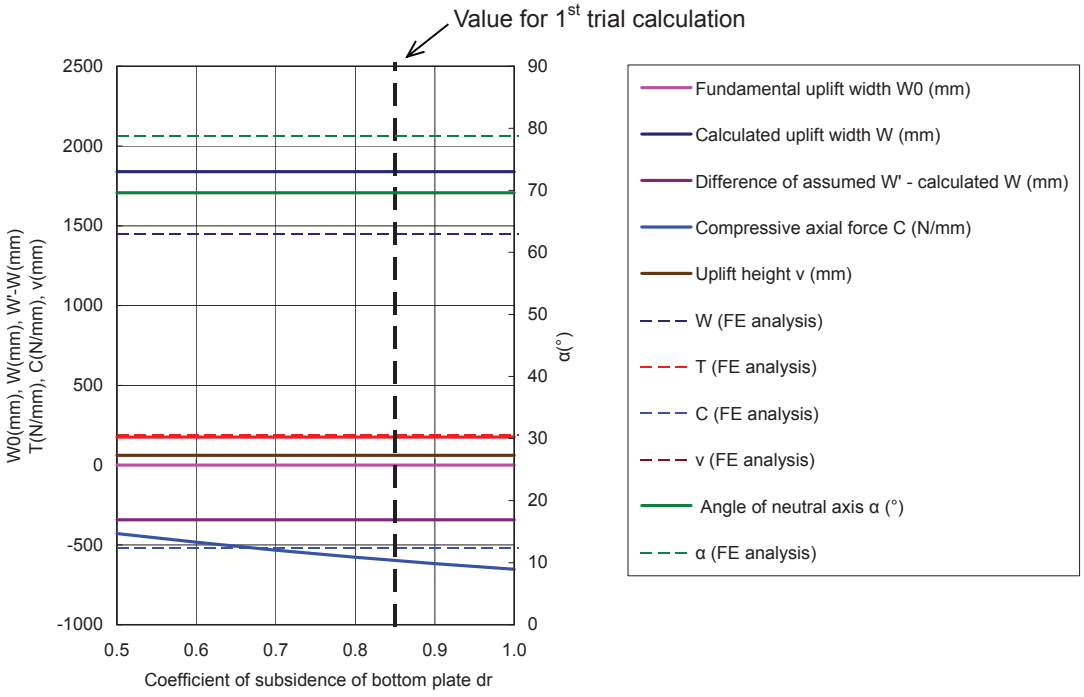

FIGURE 6-9: RELATIONSHIP OF d_r (coefficient of subsidence of bottom plate) AND EACH VALUES

From these finding in parameter study, another trial calculation with revised value of w_{ef} is performed. In this trial calculation, following items area also modified.

(a) The coefficient expressing of increase in axial force at the bottom of sidewall w_{ef}

Change to 0.71 based on the result of parameter study.

(b) The reduction factor for response acceleration under uplift condition against that of no-uplift condition r_{ef}

Change the value of r_{ef} so as the result of calculated overturning moment M to become the same as overturning moment of Case 21. Because the initial value of r_{ef} decided based on Okui's model is not match to the result of the FE analysis as specified in APPENDIX C.

(c) Introducing a parameter f_r , which expresses a ratio of force couple of tensile side against total of force couple.

According to the result of the FE analysis in Table 3-7 in Chapter 3, the force couple of tensile and compressive side is not even in the dynamic rocking transition. In case 21, during rising of the bottom plate, force couple of compressive side becomes larger than that of tensile side. For reflecting this phenomenon on the model, the parameter f_r is introduced in Eqs, (a-1) and (b) in Chapter 5, then modify the equations as follows. The value of f_r is decided 0.35 as an average of the result of the FE analysis in Table 3-7.

$$\begin{aligned}&\rho g h \times w_{ef} \times (W - W_a) \\ &\quad - \frac{1}{T_{ns1}(\alpha)} \times \left[\frac{2 f_r \times M}{4} - \left(P_{db}(\theta_b = 180) + P_{dr}(\theta_b = 180)\right) \times w_{ef} \times (W - W_a) \times T_{nsbr1}(\alpha) \right. \\ &\quad \left. - \rho g h \times w_{ef} \times W_a \times T_{ns2}(\alpha) - \left(P_{db}(\theta_b = 180) + P_{dr}(\theta_b = 180)\right) \times w_{ef} \times W_a \times T_{nsbr2}(\alpha) \right] = 0\end{aligned} \tag{6-1}$$

$$S = \frac{2(1 - f_r) \times M}{4 \times k \times w \times \left[dr \times (C_{m1}(\alpha) - C_{m2}(\alpha)) + C_{m2}(\alpha) \right]} \tag{6-2}$$

Table 6-2 and Figure 6-10 show the input conditions and calculation result with w_{ef} = 0.71 and its process until convergence.

The assumed uplift width W' is corrected through the calculation process by changing W_0 within positive value. In this case, W becomes the same value as W'.

Figure 6-11 shows the calculated distribution of axial force at bottom of the sidewall. Figure 6-12 shows the displacement of the tank bottom plate and the sidewall and the stress distribution along the tank bottom plate. The uplift height of trial calculation and the FE analysis are 30.1 mm and 21.6 mm, respectively. The value of the trial calculation is 1.4 times larger than that of the FE analysis. These results improve than 1st trial calculation. Other values such as sidewall displacement, stress of the bottom plate and compressive force and stress are

also relatively closer to that of the FE analysis than 1st trial calculation. It is thought that the calculated uplift height is sufficiently large (it seems to be beyond accepted level in design standards) so as to be affected by large deformation of the bottom plate. This is one of the reasons of difference of the result between trial calculation and the FE analysis.

This result implies that further investigation and establishing of suitable parameters in future study are essential for improving the procedure. In addition, considering an effect of membrane force in the tank bottom plate due to large deformation, which cannot take into account to the Structural Mathematical Model, is required for understanding the effect of that on the uplift.

TABLE 6-2: INPUT CONDITIONS AND CALCULATION RESULT (In case of w_{ef} = 0.71)

Step 1	R	:	Tank radius	37,200	mm	
	H	:	Tank height	36,820	mm	
	ts	:	Thickness at bottom sidewall	29.6	mm	
	tsa	:	Average thickness of top and bottom sidewall	20.8	mm	
			Applied thickness of sidewall	29.6	mm	
	Wb	:	Width of annular plate	1900	mm	
	tb	:	Thickness of annular plate	18.7	mm	
	k	:	Reaction coefficient of tank bottom	25.5	N/mm^2	
	E	:	Modulus of elasticity	191,000	MPa	
	W_0	:	Fundamental uplift width	60.0	mm	W_0 is corrected through repeated re-calculation
	Wa	:	Width effected by annular plate	1045.0	mm	Decide the value to 55% of annular plate width, according to the discussion in 3-2-5 of Chapter 3.
	wef	:	Coefficient for contribution of width	0.71		Change the value to 0.71.
	du	:	Coefficient for ratio of uplift width against uplift width	16.5		Decide the value to 16.5, by referring the FE analysis result in Figure 5-14 of Chapter 5.
	w	:	Effective width of bottom plate	328.8	mm	Assume as thickness of sidewall and 16 times of thickness of annular plate.
	dr	:	Coefficient for subsidence of bottom plate	0.85		Decide the value to 0.85, according to Figure 5-3 in Chapter 5.
	δ	:	Incline displacement of sidewall	22	mm	Apply the value at expected oval deformaion of Case 21.
	ρ	:	Fluid density	480	kg/m^3	
	h	:	Liquid height	36,250	mm	
	g	:	Gravity acceleration	9.8	m/s^2	
	u'_0	:	Horizontal acceleration	0.4049		
	$ref \times u'_0$	:	Horizontal acceleration	0.3826		
	ref	:	Reduction factor for response acceleration	0.945		Decide the value so as to M becomes the same as overturning moment of Case 21.
Step 2	W'	:	Assumed uplift width	1,471.7 1.98	mm %	$W' = W_0 + du \times v(\pi) + W_a$ W_0 is corrected through repeated re-calculation
Step 3	θ''	:	Angular acceleration	0.061	rad/s^2	According to the relation as follows in Figure 6-2 y = -3.1742x2 + 0.9264x + 0.0440
Step 4	$Pdr(\theta=180)$	:	Dynamic presser due to rocking	0.0119	MPaG	
Step 5	$Pdb(\theta=180)$	:	Dynamic presser due to bulging	-0.0515	MPaG	
Step 6	M	:	Calculated overturning moment	1.47E+12	N-mm	
	Mb	:	Calculated overturning moment of bulging	2.04E+12	N-mm	
	Mr	:	Calculated overturning moment of rocking	-5.76E+11	N-mm	
Step 7	$v(\pi)$	:	Uplift height due to δ	22.2	mm	
	fr	:	Ratio of force couple of tensile side	0.35		Decide the value to 0.35, by referring the FE analysis result in Table 3-7 of Chapter 3.
	α	:	Angle indicating location of neutral axis	76.1	°	
	T	:	Tensile force at 180 degree	140.4	N/mm	
	C	:	Compressive force at 180 degree	-622.0	N/mm	
Step 8	v	:	Calculated uplift height	30.1	mm	
	W	:	Calculated uplift width	1,471.7	mm	
Step 9		:	Comparison of W and W'	1,471.7	mm ⇔	1,471.7 mm (0.0 mm) Assumed uplift width ' W' '

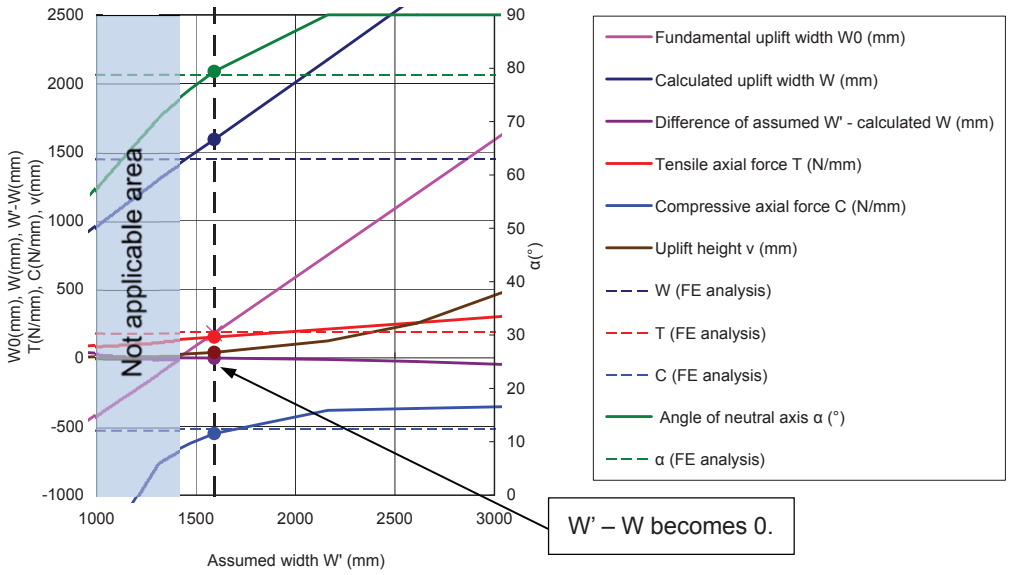

FIGURE 6-10: PROCESS UNTIL CONVERGENCE (In case of w_{ef} = 0.71)

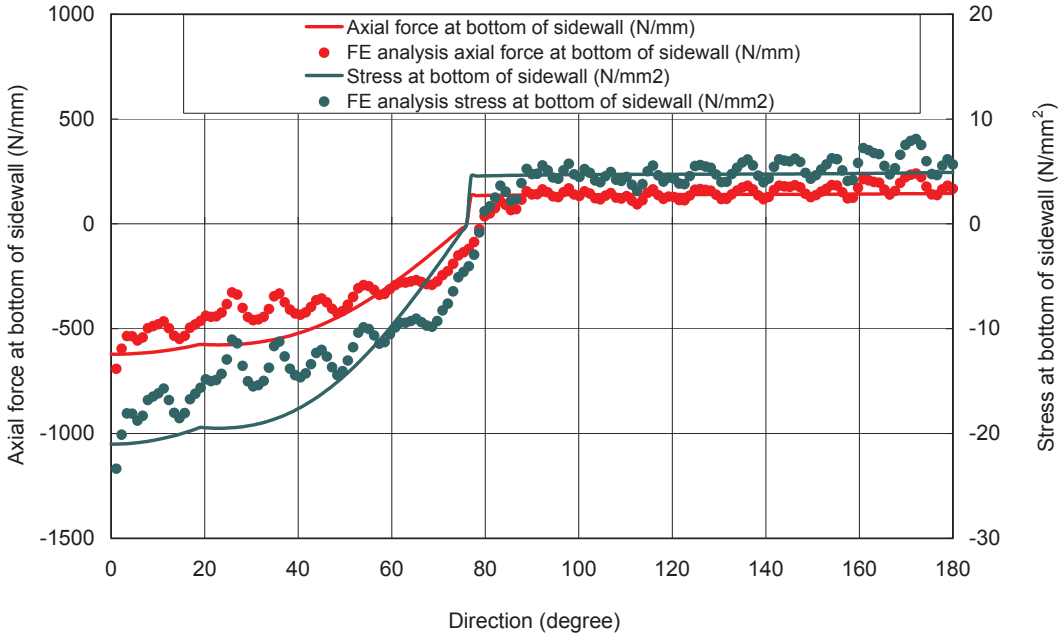

FIGURE 6-11: AXIAL FORCE ALONG BOTTOM OF SIDEWALL (In case of w_{ef} = 0.71)

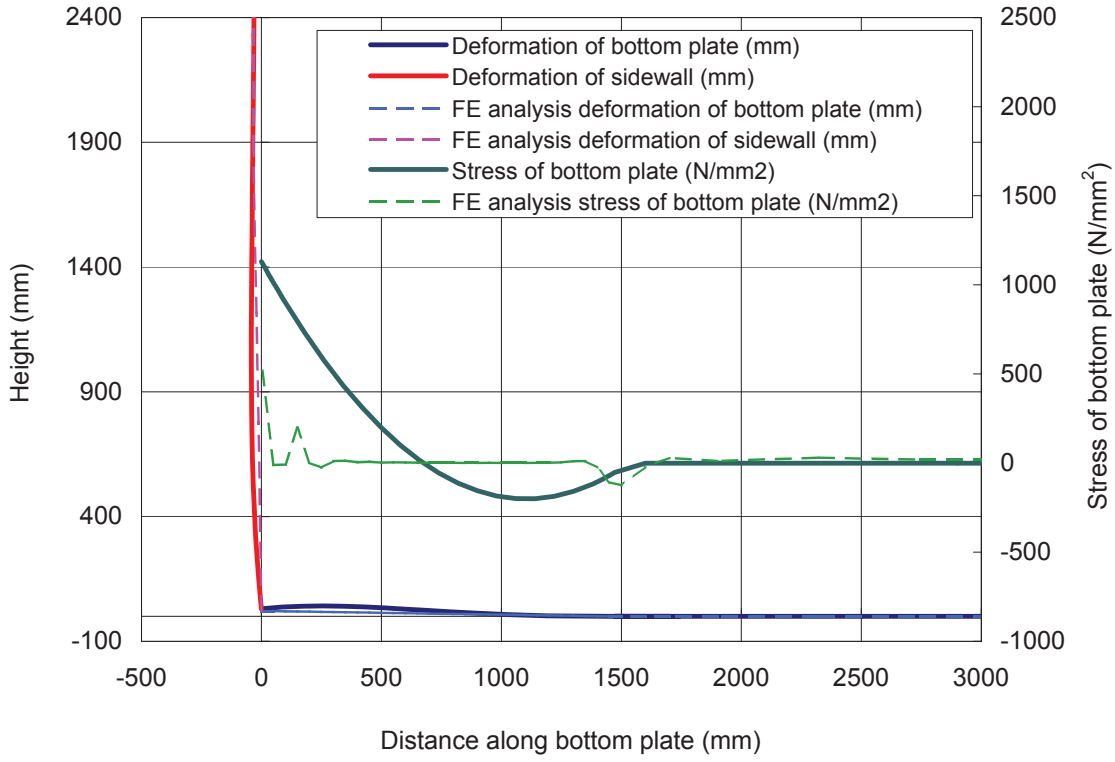

FIGURE 6-12: CHARACTERISTICS OF SIDEWALL AND TANK BOTTOM PLATE (In case of w_{ef} = 0.71)

In the calculation of Table 6-1 and 6-2, thickness at the bottom of the sidewall is applied. While, in Chapter 4, average thickness of top and bottom sidewall is used for trial calculation of the Structural Mathematical Model. It is performed for confirming availability of the model by comparison the result with that of non-linear 3D static FE analysis, and results in good agreement. Table 6-3 and Figure 6-13 and 6-14 show the calculation result with average thickness of top and bottom sidewall. The uplift width *W* does not converge on assumed uplift width *W'* in the repeated calculation process. The uplift height becomes 7.7 times higher than the result of the FE analysis (time-history analysis). Consequently, the thickness at bottom of sidewall leads to better result under dynamic conditions than the average thickness. The Structural Mathematical Model can reflect bulging deformation of a sidewall due to liquid pressure on a bottom plate. For calculation of this deformation, average thickness is thought to be suitable. On the other hand, under dynamic conditions, undulating deformation at the top of sidewall has large effect than bulging deformation on the bottom plate.

TABLE 6-3: INPUT CONDITIONS AND CALCULATION RESULT
(In case of w_{ef} = 0.71, Average thickness of top and bottom sidewall)

Step 1	*R*	:	Tank radius	37,200	mm	
	H	:	Tank height	36,820	mm	
	ts	:	Thickness at bottom sidewall	29.6	mm	
	tsa	:	Average thickness of top and bottom sidewall	20.8	mm	
			Applied thickness of sidewall	20.8	mm	
	Wb	:	Width of annular plate	1900	mm	
	tb	:	Thickness of annular plate	18.7	mm	
	k	:	Reaction coefficient of tank bottom	25.5	N/mm^2	
	E	:	Modulus of elasticity	191,000	MPa	
	W_0	:	Fundamental uplift width	0.0	mm	W_0 is corrected through repeated re-calculation
	Wa	:	Width effected by annular plate	1045.0	mm	Decide the value to 55% of annular plate width, according to the discussion in 3-2-5 of Chapter 3.
	wef	:	Coefficient for contribution of width	0.71		Change the value to 0.71.
	du	:	Coefficient for ratio of uplift width against uplift width	16.5		Decide the value to 16.5, by referring the FE analysis result in Figure 5-14 of Chapter 5.
	w	:	Effective width of bottom plate	320	mm	Assume as thickness of sidewall and 16 times of thickness of annular plate.
	dr	:	Coefficient for subsidence of bottom plate	0.85		Decide the value to 0.85, according to Figure 5-3 in Chapter 5.
	δ	:	Incline displacement of sidewall	22	mm	Apply the value at expected oval deformaion of Case 21.
	ρ	:	Fluid density	480	kg/m^3	
	h	:	Liquid height	36,250	mm	
	g	:	Gravity acceleration	9.8	m/s^2	
	u'_0	:	Horizontal acceleration	0.4049		
	$ref \times u'_0$	:	Horizontal acceleration	0.3826		
	ref	:	Reduction factor for response acceleration	0.945		Decide the value so as to M becomes the same as overturning moment of Case 21.
Step 2	*W'*	:	Assumed uplift width	1,411.7 1.90	mm %	$W' = W_0 + du \times v(\pi) + W_a$ W_0 is corrected through repeated re-calculation
Step 3	*θ''*	:	Angular acceleration	0.060	rad/s^2	According to the relation as follows in Figure 6-2 y = -3.1742x2 + 0.9264x + 0.0440
Step 4	*Pdr(θ=180)*	:	Dynamic presser due to rocking	0.0116	MPaG	
Step 5	*Pdb(θ=180)*	:	Dynamic presser due to bulging	-0.0516	MPaG	
Step 6	*M*	:	Calculated overturning moment	1.48E+12	N-mm	
	Mb	:	Calculated overturning moment of bulging	2.04E+12	N-mm	
	Mr	:	Calculated overturning moment of rocking	-5.69E+11	N-mm	
Step 7	*v(π)*	:	Uplift height due to δ	22.2	mm	
	fr	:	Ratio of force couple of tensile side	0.35		Decide the value to 0.35, by referring the FE analysis result in Table 3-7 of Chapter 3.
	α	:	Angle indicating location of neutral axis	74.3	°	
	T	:	Tensile force at 180 degree	134.5	N/mm	
	C	:	Compressive force at 180 degree	-665.9	N/mm	
Step 8	*v*	:	Calculated uplift height	167.2	mm	
	W	:	Calculated uplift width	1,611.0	mm	
Step 9		:	Comparison of W and W'	1,611.0	mm ⇔	1,411.7 mm (-199.2 mm) Assumed uplift width ' W' '

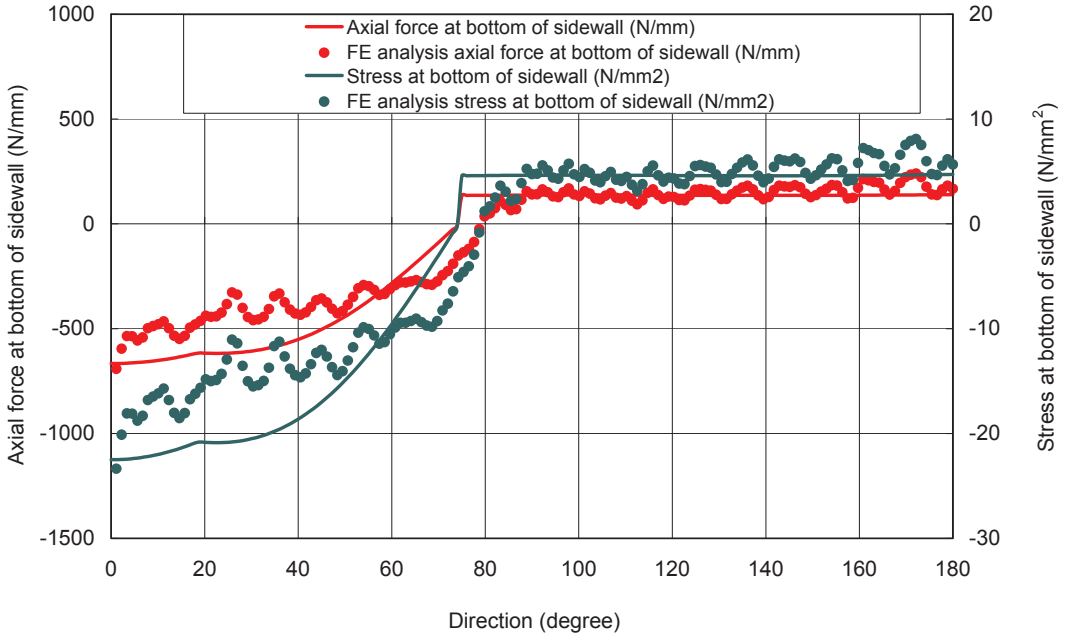

FIGURE 6-13: AXIAL FORCE ALONG BOTTOM OF SIDEWALL
(In case of w_{ef} = 0.71, Average thickness of top and bottom sidewall)

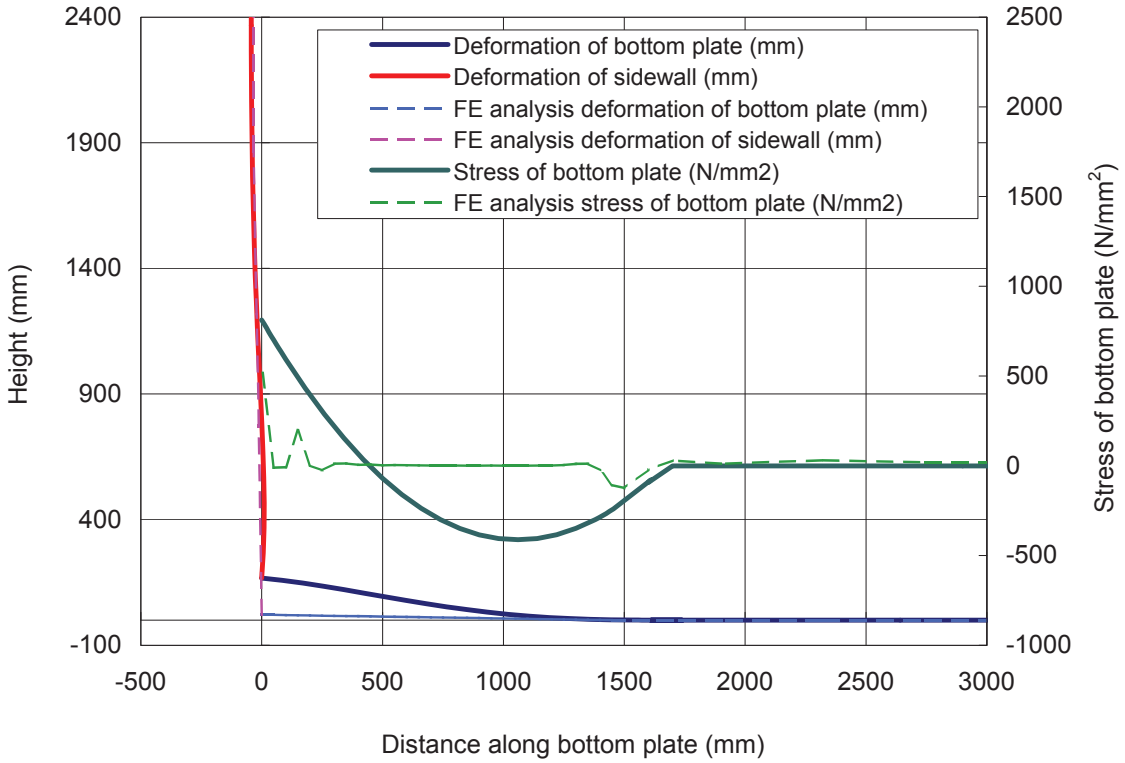

FIGURE 6-14: CHARACTERISTICS OF SIDEWALL AND TANK BOTTOM PLATE
(In case of w_{ef} = 0.71, Average thickness of top and bottom sidewall)

6-3-2 Applicability to other dimensional tanks

For investigating an applicability of the Simplified Seismic Design Procedure for other dimensional tanks, additional several sample calculations are performed. Table 6-4 shows the dimensional conditions of the subject tanks specified in 6-3-1 and 3 additional sample tanks.

The additional sample tanks have different size and proportion, which is expressed by a ratio of a diameter and height. These tanks are actually constructed tanks equipped an anchor and selected from a viewpoint of extensive investigation.

Capacities of additional the sample tanks are from 10,000 to 80,000 m^3 and its proportions are from 0.95 to 2.07. The sample tank 2 (capacity 36,000 m^3) is a relatively small tank for export or import terminal. The sample tank 3 is a tank used to small terminal for domestic transportation.

TABLE 6-4: DIMENSIONAL CONDITIONS OF SAMPLE TANKS

	Capacity	Diameter D	Height H	Ratio of D and H D/H	The max. design liquid height h	Thickness of bottom of sidewall t	Width of annular plate Wb	Thickness of annular plate tb	Horizontal acceleration	Deformation of the sidewall δ
	(m3)	(mm)	(mm)	-	(mm)	(mm)	(mm)	(mm)	(G)	(mm)
Subject tank	157,595	74,400	36,820	2.02	36,250	29.6	1900	18.7	0.4049	22
Sample tank 1	80,079	59,500	28,800	2.07	28,800	28.5	1600	18.0	0.4049	17.2
Sample tank 2	36,191	40,000	28,000	1.43	28,800	21	1600	15.0	0.4049	16.7
Sample tank 3	10,075	23,000	24,250	0.95	24,250	13.4	850	8.1	0.4049	14.5

The parameters of W_a, w_{ef}, d_u and d_r are considered to be difference for each tank and it should be decided from a research by an FE analysis. This research will be conducted in next stage. In this paper, focus on confirming the calculation functions of the Simplified Seismic Design Procedure for other dimensional tanks than the subject tank. For this purpose the parameters for the subject tank are used to calculate tentatively.

Table 6-5 and Figure 6-15 and 16 show the result of the sample tank1, Table 6-6 and Figure 6-17 and 6-18 show that of the sample tank 2, Table 6-7 shows that of the sample tank 3, respectively.

The Simplified Seismic Design Procedure including developed mathematical models is thought to function for the sample tank 1 and 2. However the obtained specific values are for reference, since used parameters are tentative one. The further research and investigation are essential for generalization of the procedure for applying to any size of tanks.

The sample tank 3, the rational result could not be obtained. As shown in Table 6-6, the uplift height is more than 3.5 m. It seems to be divergence the calculation. The size of this tank is considerably smaller and the proportion is different from that of the subject tank, which is base of the present parameters. Therefore, the parameters are considered to be not match to this tank. The other reason is assumption of the Structural Mathematical Model. The model is developed

based on infinitesimal deformation theory. Therefore, in case of large uplift expected condition, calculation accuracy is supposed to decrease.

For reference, change the value of most sensitive parameter w_{ef} to 0.74 for the sample tank 3 and perform a calculation again. The result is obtained without divergence as shown in Table 6-7 and Figure 6-19 and 6-20. It concludes that the parameters should be changed depend on size and proportion of tanks.

The findings and suggested items to be studied in the next step are summarized in next section.

TABLE 6-5: INPUT CONDITIONS AND CALCULATION RESULT (Sample tank 1)

Sample tank 1

Step 1	*R*	:	Tank radius	29,750	mm	
	H	:	Tank height	28,800	mm	
	ts	:	Thickness at of bottom of sidewall	28.5	mm	
	tsa	:	Average thickness of top and bottom sidewall	18.5	mm	
			Applied thickness of sidewall	28.5	mm	
	Wb	:	Width of annular plate	950	mm	
	tb	:	Thickness of annular plate	18.0	mm	
	k	:	Reaction coefficient of tank bottom	25.5	N/mm^2	
	E	:	Modulus of elasticity	191,000	MPa	
	W_0	:	Fundamental uplift width	385.0	mm	W_0 is corrected through repeated re-calculation
	Wa	:	Width effected by annular plate	880.0	mm	Decide the value to 55% of annular plate width, according to the discussion in 3-2-5 of Chapter 3.
	wef	:	Coefficient for contribution of width	0.71		Assume the value as 0.71.
	du	:	Coefficient for ratio of uplift width against uplift width	16.5		Decide the value to 16.5, by referring the FE analysis result in Figure 5-14 of Chapter 5.
	w	:	Effective width of bottom plate	316.5	mm	Assume as thickness of sidewall and 16 times of thickness of annular plate.
	dr	:	Coefficient for subsidence of bottom plate	0.85		Decide the value to 0.85, according to Figure 5-3 in Chapter 5.
	δ	:	Incline displacement of sidewall	17.2	mm	Assume from the value of Case 21 and tank height.
	ρ	:	Fluid density	480	kg/m^3	
	h	:	Liquid height	28,800	mm	
	g	:	Gravity acceleration	9.8	m/s^2	
	u'_0	:	Horizontal acceleration	0.4049		
	$ref \times u'_0$	:	Horizontal acceleration	0.3944		
	ref	:	Reduction factor for response acceleration	0.974		According to the relation as follows in Figure 6-2 y = -0.5348x + 0.9881
Step 2	*W'*	:	Assumed uplift width	1,558.2 2.62	mm %	$W' = W_0 + du \times v(\pi) + W_a$ W_0 is corrected through repeated re-calculation
Step 3	*θ''*	:	Angular acceleration	0.066	rad/s^2	According to the relation as follows in Figure 6-2 y = -3.1742x2 + 0.9264x + 0.0440
Step 4	*Pdr(θ=180)*	:	Dynamic presser due to rocking	0.0104	MPaG	
Step 5	*Pdb(θ=180)*	:	Dynamic presser due to bulging	-0.0417	MPaG	
Step 6	*M*	:	Calculated overturning moment	8.31E+11	N-mm	
	Mb	:	Calculated overturning moment of bulging	1.09E+12	N-mm	
	Mr	:	Calculated overturning moment of rocking	-2.63E+11	N-mm	
Step 7	*v(π)*	:	Uplift height due to δ	17.8	mm	
	fr	:	Ratio of force couple of tensile side	0.50		Assume the value as 0.50. (even condion)
	α	:	Angle of neutral axis	53.0	°	
	T	:	Tensile force at 180 degree	116.1	N/mm	
	C	:	Compressive force at 180 degree	-1146.3	N/mm	
Step 8	*v*	:	Calculated uplift height	25.0	mm	
	W	:	Calculated uplift width	1,558.1	mm	
Step 9		:	Comparison of W and W'	1,558.1	mm ⇔	1,558.2 mm (0.0 mm) Assumed uplift width ' W' '

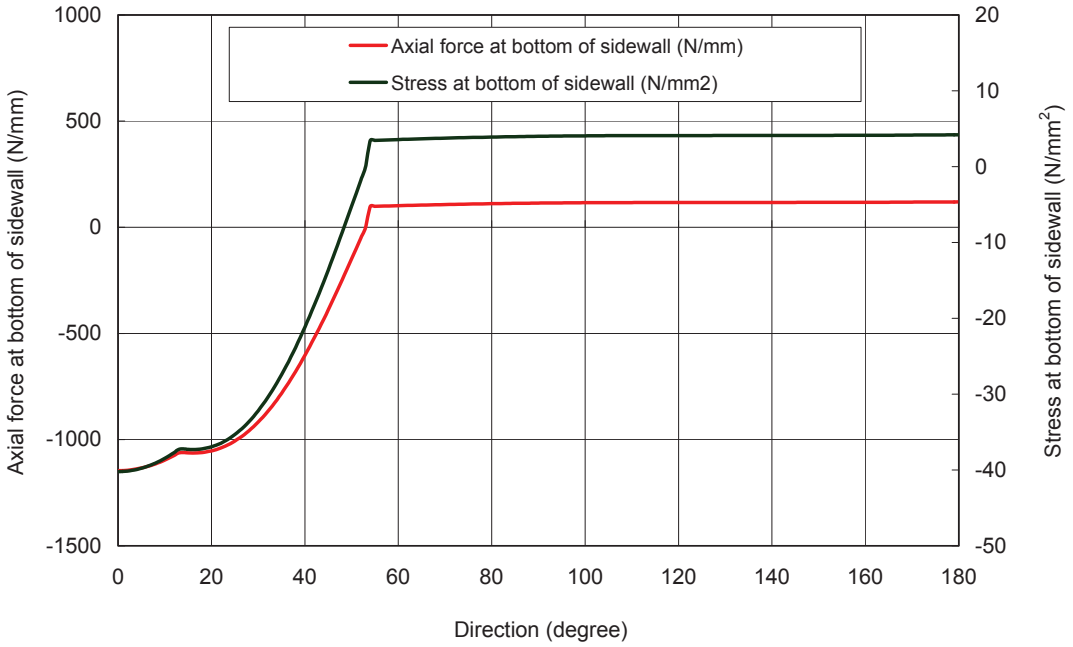

FIGURE 6-15: AXIAL FORCE ALONG BOTTOM OF SIDEWALL (Sample tank 1)

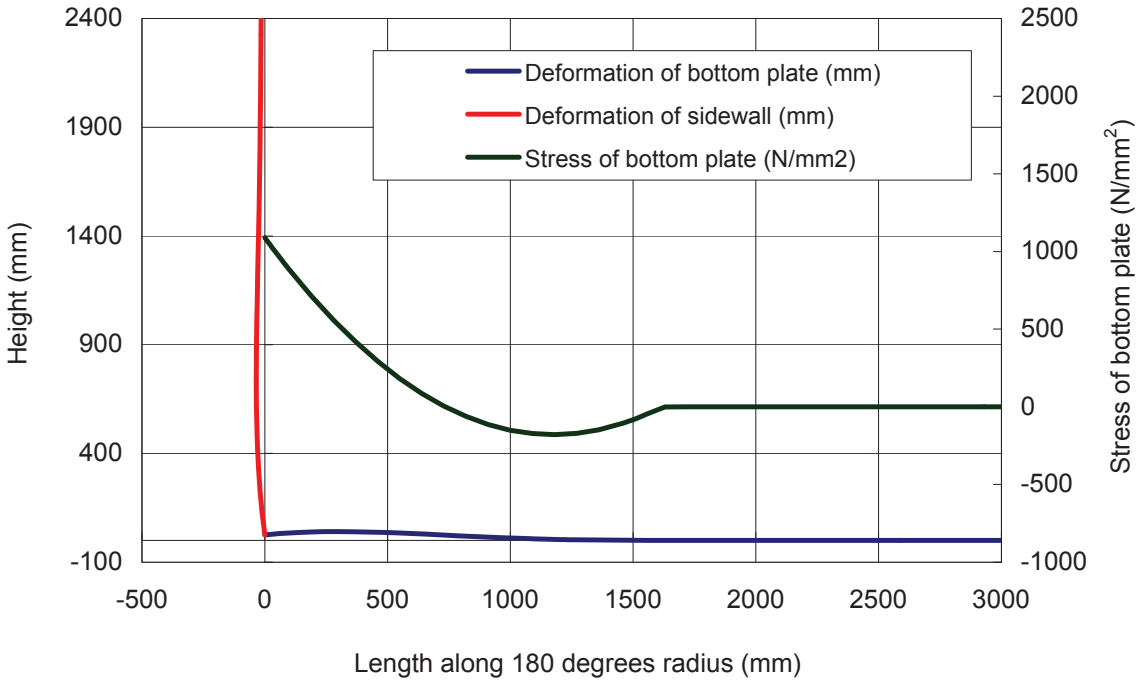

FIGURE 6-16: CHARACTERISTICS OF SIDEWALL AND TANK BOTTOM PLATE (Sample tank 1)

TABLE 6-6: INPUT CONDITIONS AND CALCULATION RESULT (Sample tank 2)

Sample tank 2

Step 1	*R*	:	Tank radius	20,000	mm	
	H	:	Tank height	28,000	mm	
	ts	:	Thickness at bottom of sidewall	21.0	mm	
	tsa	:	Average thickness of top and bottom sidewall	14.5	mm	
			Applied thickness of sidewall	21.0	mm	
	Wb	:	Width of annular plate	1600	mm	
	tb	:	Thickness of annular plate	15.0	mm	
	k	:	Reaction coefficient of tank bottom	25.5	N/mm^2	
	E	:	Modulus of elasticity	191,000	MPa	
	W'_0	:	Fundamental uplift width	495.0	mm	W_0 is corrected through repeated re-calculation
	Wa	:	Width effected by annular plate	880.0	mm	Decide the value to 55% of annular plate width, according to the discussion in 3-2-5 of Chapter 3.
	wef	:	Coefficient for contribution of width	0.71		Assume the value as 0.71.
	du	:	Coefficient for ratio of uplift width against uplift width	16.5		Decide the value to 16.5, by referring the FE analysis result in Figure 5-14 of Chapter 5.
	w	:	Effective width of bottom plate	261.0	mm	Assume as thickness of sidewall and 16 times of thickness of annular plate.
	dr	:	Coefficient for subsidence of bottom plate	0.85		Decide the value to 0.85, according to Figure 5-3 in Chapter 5.
	δ	:	Incline displacement of sidewall	16.7	mm	Assume from the value of Case 21 and tank height.
	ρ	:	Fluid density	480	kg/m^3	
	h	:	Liquid height	28,800	mm	
	g	:	Gravity acceleration	9.8	m/s^2	
	u'_0	:	Horizontal acceleration	0.4049		
	$ref \times u'_0$	:	Horizontal acceleration	0.3916		
	ref	:	Reduction factor for response acceleration	0.967		According to the relation as follows in Figure 6-2 y = -0.5348x + 0.9881
Step 2	*W'*	:	Assumed uplift width	1,571.8 3.93	mm %	$W' = W_0 + du \times v(\pi) + W_a$ W_0 is corrected through repeated re-calculation
Step 3	*θ''*	:	Angular acceleration	0.076	rad/s^2	According to the relation as follows in Figure 6-2 y = -3.1742x2 + 0.9264x + 0.0440
Step 4	*Pdr(θ=180)*	:	Dynamic presser due to rocking	0.0076	MPaG	
Step 5	*Pdb(θ=180)*	:	Dynamic presser due to bulging	-0.0363	MPaG	
Step 6	*M*	:	Calculated overturning moment	3.61E+11	N-mm	
	Mb	:	Calculated overturning moment of bulging	4.98E+11	N-mm	
	Mr	:	Calculated overturning moment of rocking	-1.37E+11	N-mm	
Step 7	*v(π)*	:	Uplift height due to δ	11.9	mm	
	fr	:	Ratio of force couple of tensile side	0.50		Assume the value as 0.50. (even condion)
	α	:	Angle indicating location of neutral axis	57.7	°	
	T	:	Tensile force at 180 degree	121.5	N/mm	
	C	:	Compressive force at 180 degree	-867.3	N/mm	
Step 8	*v*	:	Calculated uplift height	61.8	mm	
	W	:	Calculated uplift width	1,571.8	mm	
Step 9		:	Comparison of W and W'	1,571.8	mm ⇔	1,571.8 mm (0.0 mm) Assumed uplift width ' W' '

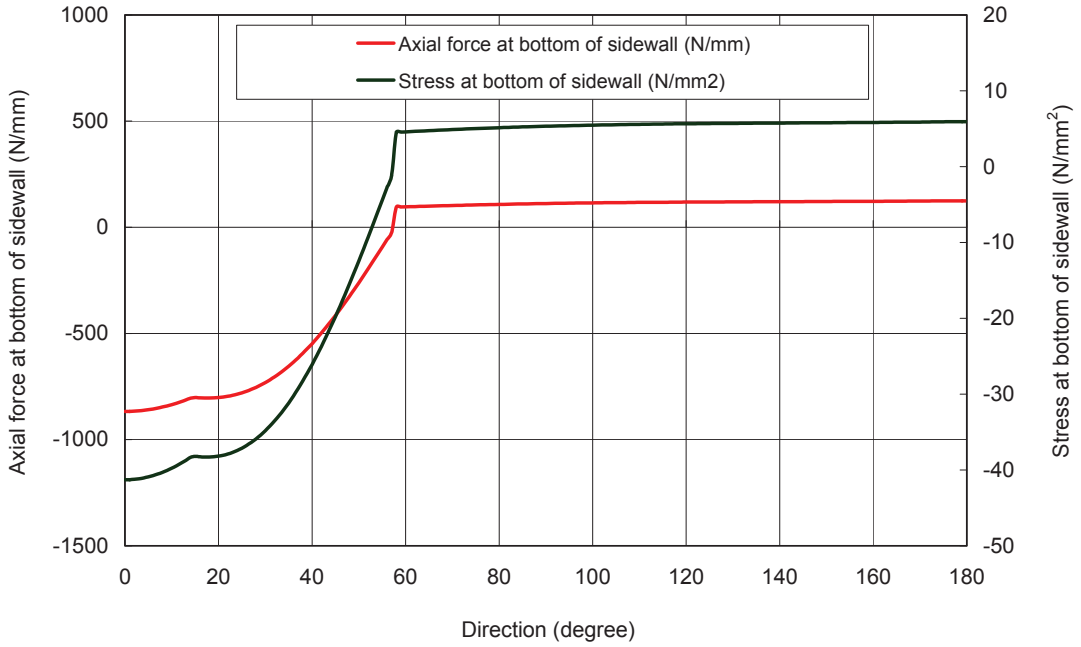

FIGURE 6-17: AXIAL FORCE ALONG BOTTOM OF SIDEWALL (Sample tank 2)

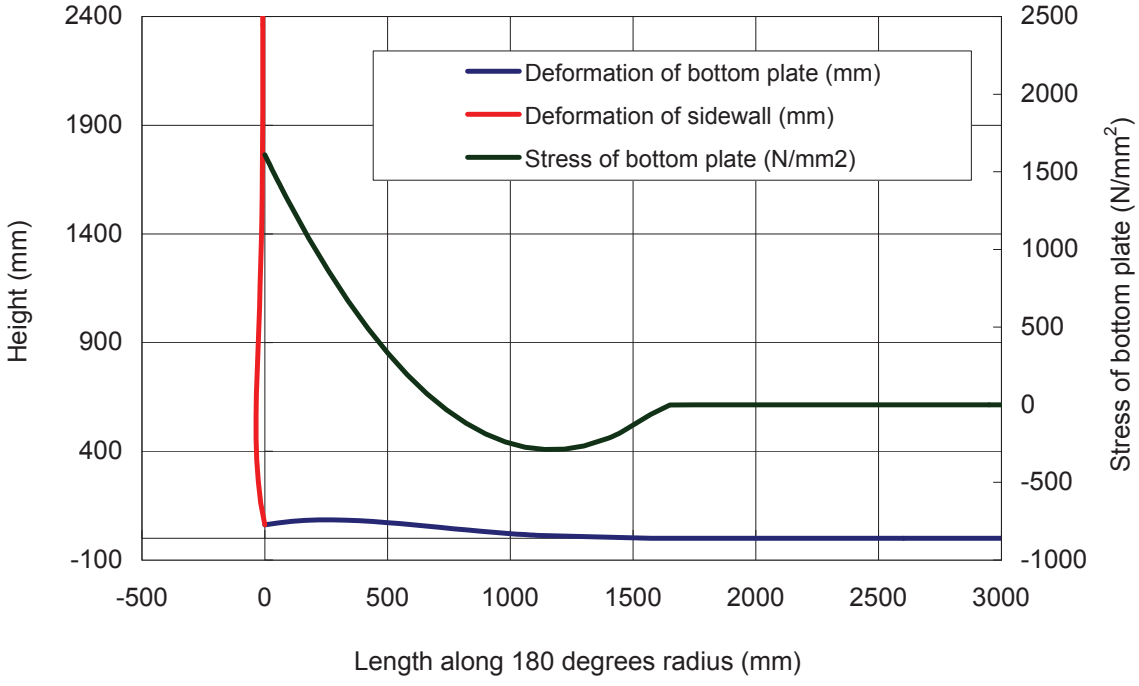

FIGURE 6-18: CHARACTERISTICS OF SIDEWALL AND TANK BOTTOM PLATE (Sample tank 2)

TABLE 6-7: INPUT CONDITIONS AND CALCULATION RESULT (Sample tank 3)

Sample tank 3

Step 1	*R*	:	Tank radius	11,500	mm	
	H	:	Tank height	24,250	mm	
	ts	:	Thickness at bottom sidewall	13.4	mm	
	tsa	:	Average thickness of top and bottom sidewall	9.7	mm	
			Applied thickness of sidewall	13.4	mm	
	Wb	:	Width of annular plate	850	mm	
	tb	:	Thickness of annular plate	8.1	mm	
	k	:	Reaction coefficient of tank bottom	25.5	N/mm^2	
	E	:	Modulus of elasticity	191,000	MPa	
	W_0	:	Fundamental uplift width	2765.0	mm	W_0 is corrected through repeated re-calculation
	Wa	:	Width effected by annular plate	467.5	mm	Decide the value to 55% of annular plate width, according to the discussion in 3-2-5 of Chapter 3.
	wef	:	Coefficient for contribution of width	0.71		Assume the value as 0.71.
	du	:	Coefficient for ratio of uplift width against uplift width	16.5		Decide the value to 16.5, by referring the FE analysis result in Figure 5-14 of Chapter 5.
	w	:	Effective width of bottom plate	143.0	mm	Assume as thickness of sidewall and 16 times of thickness of annular plate.
	dr	:	Coefficient for subsidence of bottom plate	0.85		Decide the value to 0.85, according to Figure 5-3 in Chapter 5.
	δ	:	Incline displacement of sidewall	14.5	mm	Assume from the value of Case 21 and tank height.
	ρ	:	Fluid density	480	kg/m^3	
	h	:	Liquid height	24,250	mm	
	g	:	Gravity acceleration	9.8	m/s^2	
	u'_0	:	Horizontal acceleration	0.4049		
	$ref \times u'_0$	:	Horizontal acceleration	0.3686		
	ref	:	Reduction factor for response acceleration	0.910		According to the relation as follows in Figure 6-2 y = -0.5348x + 0.9881
Step 2	*W'*	:	Assumed uplift width	3,345.9 14.55	mm %	$W' = W_0 + du \times v(\pi) + W_a$ W_0 is corrected through repeated re-calculation
Step 3	*θ''*	:	Angular acceleration	0.112	rad/s^2	According to the relation as follows in Figure 6-2 y = -3.742x2 + 0.9264x + 0.0440
Step 4	*Pdr(θ=180)*	:	Dynamic presser due to rocking	0.0081	MPaG	
Step 5	*Pdb(θ=180)*	:	Dynamic presser due to bulging	-0.0206	MPaG	
Step 6	*M*	:	Calculated overturning moment	7.94E+10	N-mm	
	Mb	:	Calculated overturning moment of bulging	1.30E+11	N-mm	
	Mr	:	Calculated overturning moment of rocking	-5.10E+10	N-mm	
Step 7	*v(π)*	:	Uplift height due to δ	6.9	mm	
	fr	:	Ratio of force couple of tensile side	0.50		Assume the value as 0.50. (even condion)
	α	:	Angle indicating location of neutral axis	90.0	°	
	T	:	Tensile force at 180 degree	240.1	N/mm	
	C	:	Compressive force at 180 degree	-175.8	N/mm	
Step 8	*v*	:	Calculated uplift height	3510.8	mm	
	W	:	Calculated uplift width	3,345.9	mm	
Step 9		:	Comparison of W and W'	3,345.9	mm ⇔	3,345.9 mm (0.0 mm) Assumed uplift width ' W' '

TABLE 6-8: INPUT CONDITIONS AND CALCULATION RESULT (Sample tank 3)
(*wef* = 0.74)

Sample tank 3

Step 1	*R*	:	Tank radius	11,500	mm	
	H	:	Tank height	24,250	mm	
	ts	:	Thickness at bottom sidewall	13.4	mm	
	tsa	:	Average thickness of top and bottom sidewall	9.7	mm	
			Applied thickness of sidewall	13.4	mm	
	Wb	:	Width of annular plate	850	mm	
	tb	:	Thickness of annular plate	8.1	mm	
	k	:	Reaction coefficient of tank bottom	25.5	N/mm^2	
	E	:	Modulus of elasticity	191,000	MPa	
	W_0	:	Fundamental uplift width	572.0	mm	W_0 is corrected through repeated re-calculation
	Wa	:	Width effected by annular plate	467.5	mm	Decide the value to 55% of annular plate width, according to the discussion in 3-2-5 of Chapter 3.
	wef	:	Coefficient for contribution of width	0.74		Assume the value as 0.71.
	du	:	Coefficient for ratio of uplift width against uplift width	16.5		Decide the value to 16.5, by referring the FE analysis result in Figure 5-14 of Chapter 5.
	w	:	Effective width of bottom plate	143.0	mm	Assume as thickness of sidewall and 16 times of thickness of annular plate.
	dr	:	Coefficient for subsidence of bottom plate	0.85		Decide the value to 0.85, according to Figure 5-3 in Chapter 5.
	δ	:	Incline displacement of sidewall	14.5	mm	Assume from the value of Case 21 and tank height.
	ρ	:	Fluid density	480	kg/m^3	
	h	:	Liquid height	24,250	mm	
	g	:	Gravity acceleration	9.8	m/s^2	
	u'_0	:	Horizontal acceleration	0.4049		
	$ref \times u'_0$	:	Horizontal acceleration	0.3892		
	ref	:	Reduction factor for response acceleration	0.961		According to the relation as follows in Figure 6-2 y = -0.5348x + 0.9881
Step 2	*W'*	:	Assumed uplift width	1,152.9 5.01	mm %	$W' = W_0 + du \times v(\pi) + W_a$ W_0 is corrected through repeated re-calculation
Step 3	*θ''*	:	Angular acceleration	0.082	rad/s^2	According to the relation as follows in Figure 6-2 y = -3.742x2 + 0.9264x + 0.0440
Step 4	*Pdr(θ=180)*	:	Dynamic presser due to rocking	0.0039	MPaG	
Step 5	*Pdb(θ=180)*	:	Dynamic presser due to bulging	-0.0245	MPaG	
Step 6	*M*	:	Calculated overturning moment	1.01E+11	N-mm	
	Mb	:	Calculated overturning moment of bulging	1.38E+11	N-mm	
	Mr	:	Calculated overturning moment of rocking	-3.67E+10	N-mm	
Step 7	*v(π)*	:	Uplift height due to δ	6.9	mm	
	fr	:	Ratio of force couple of tensile side	0.50		Assume the value as 0.50. (even condion)
	α	:	Angle indicating location of neutral axis	45.1	°	
	T	:	Tensile force at 180 degree	80.8	N/mm	
	C	:	Compressive force at 180 degree	-1480.5	N/mm	
Step 8	*v*	:	Calculated uplift height	28.4	mm	
	W	:	Calculated uplift width	1,152.8	mm	
Step 9		:	Comparison of W and W'	1,152.8	mm ⇔	1,152.9 mm (0.0 mm) Assumed uplift width ' W' '

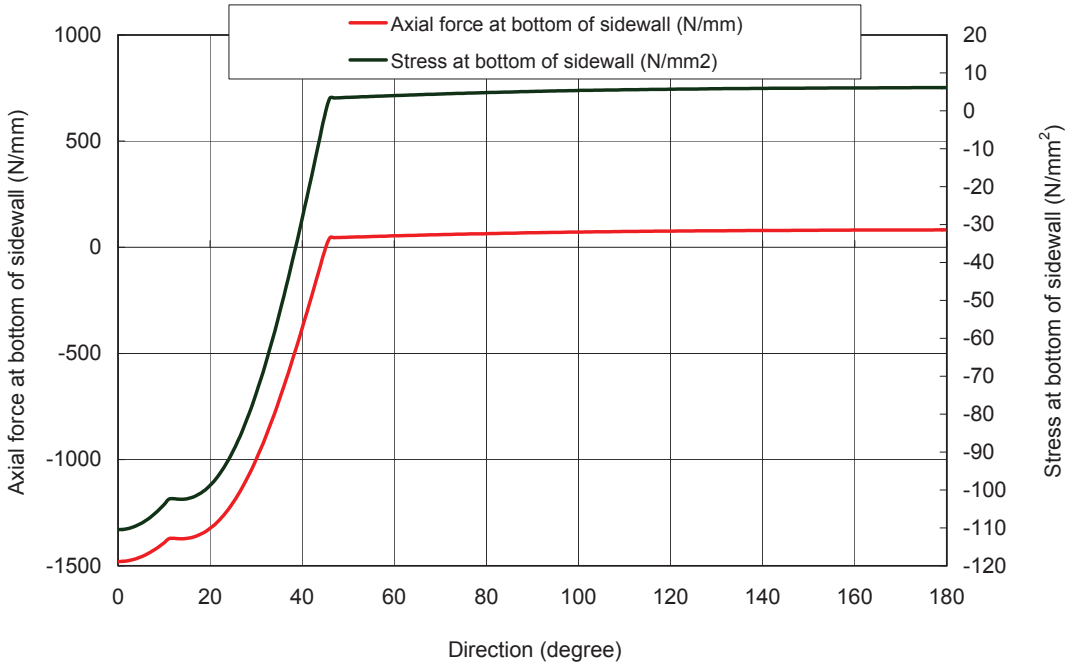

FIGURE 6-19: AXIAL FORCE ALONG BOTTOM OF SIDEWALL (Sample tank 3) (*wef* = 0.74)

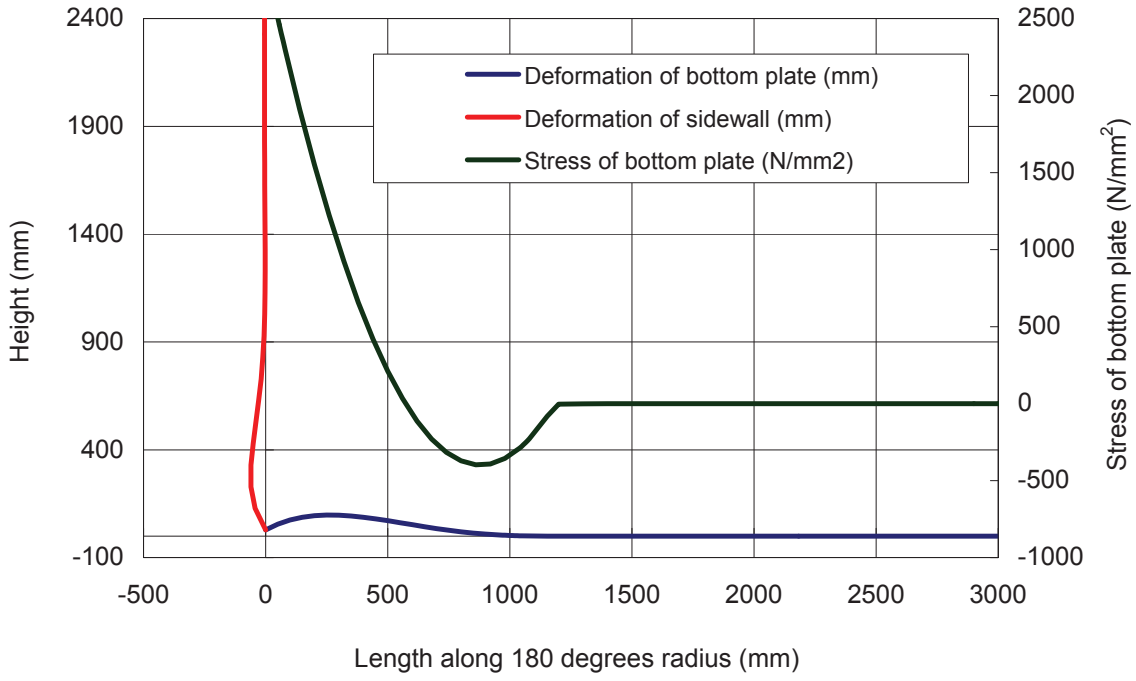

FIGURE 6-20: CHARACTERISTICS OF SIDEWALL AND TANK BOTTOM PLATE (Sample tank 3) (*wef* = 0.74)

6-4 FINDINGS AND SUGGESTED ITEMS TO BE STUDIED IN THE NEXT STEP

This chapter summarized the simplified design procedure (referred to as the Simplified Seismic Design Procedure) for determining a tank bottom plate and sidewall connection, based on the Structural Mathematical Model and the Force Coupling Mathematical Model which are proposed in earlier chapters.

A sample calculation based on the proposed procedure was also presented.

Findings and the items suggested for future study listed as below.

- It is confirmed that the proposed Simplified Seismic Design Procedure is functional for estimating the uplift height and the width of the bottom plate with the consideration of bulging and rocking motion and specific features of response behavior.
- Setting up or adjusting several parameters, which depend on tank characteristics such as size, proportion, thickness of each part and so on, is required for using the Simplified Seismic Design Procedure effectively. Therefore, further research is essential for improving the parameters so as to apply to any size tanks. Especially, w_{ef}, which indicates the increase in reaction force at the bottom of the sidewall during dynamic oscillation loading is one of the most important factor for the model.
- Regarding Step 3, further investigation of the reduction in the response acceleration during uplift is required for improving the procedure.
  (The concept of a providing method of the reduced response acceleration by using a natural period and responses spectrum is discussed in 3-3 of Chapter 3.)
- Regarding Step 7, integrating of the theoretical formula of dynamic pressure due to bulging and rocking motion into the Force Coupling Mathematical Model is recommended for improving the procedure. At present, a cosine curve is used to approximate the dynamic pressure distribution for simplifying the mathematical model.
- Regarding Step 7, further development of the specific estimation method for calculating the maximum displacement at the top of sidewall during an earthquake is required.
- Regarding Step 8, improving the Structural Mathematical Model to asymmetric model is indicated.
- Regarding Step 6 to 8, further integration of the Structural Mathematical Model and the Forced Coupling Mathematical Model is recommended.
- Considering an effect of membrane force in the tank bottom plate due to large deformation is required for understanding the effect of that on the uplift behavior.

REFERENCES

[1] 奥井大輔, 2013.2.8, "応答スペクトルを用いた平底円筒貯槽の底板浮き上がり現象を特徴付ける物理量の簡易算定方法に関する検討", 鳥取大学大学院工学研究科博士前期過程　社会基盤工学専攻土木工学コース　修士論文

[2] D'Amico M., Taniguchi, T., Nakashima T., 2017, "Simplified Analysis of the Rocking Motion of A Cylindrical Tank Focusing on the Role of Dynamical Forces Involved in Rocking-Bulging Interaction", Proceedings of ASME PVP Conference, PVP2017-65442.

[3] Housner, G. W., 1957, "Dynamic Pressure on Accelerated Fluid Containers", Bulletin of the Seismological Society of America, Vol. 47, pp. 15-35.

[4] Veletsos, A. S. and Yang, J. Y., 1976, "Dynamics of Fixed-Base Liquid-Storage Tanks," U.S.-Japan Seminar for Earthquake Engineering Research with Emphasis on Life Line System, Tokyo, pp. 317-341.

[5] Taniguchi, T. and Segawa, T., 2008, "Fluid Pressure on Rectangular Tank Consisting of Rigid Side Walls and Rectilinearly Deforming Bottom Plate due to Uplift Motion", Proceedings of ASME PVP Conference, PVP2008-61166.

[6] Hayashi, S. and Taniguchi, T., 2012, "A Study of Formularization of Uplift Behavior at the Bottom Plate of Large LNG Storage Tanks during Earthquake", Proceedings of ASME PVP Conference, PVP2012-78784.

CHAPTER 7

CONCLUSION

CHAPTER 7
CONCLUSION

In this study, fluid-structure coupled 3-dimensional time-history FE analysis (the FE analysis) was performed for study of dynamic response including uplift of a bottom plate. And the mathematical models of the bottom plate and the sidewall for design of a bottom plate corner connection were presented. Then, the comprehensive design procedure of a bottom plate corner connection based on the proposed mathematical models was established with the consideration of dynamic response including uplift of a bottom plate.

In the Chapter 3, fluid-structure coupled 3-dimensional time-history FE analysis was performed for investigating dynamical behavior of tanks including uplift of a tank bottom plate. Several cases, which are no-uplift case, rigid stiffener stiffness case and 3 different seismic wave cases (artificial seismic wave, Taft EW and EL Centro NS), were calculated and effects of structural conditions on the tank response are mainly verified.

Findings from this research are summarized below.

- The response acceleration and the base shear of the uplift case become about half and 40% of the no-uplift cases, respectively. This tendency is also observed for the result of the fluid pressure. These results provide that the tank response under uplift conditions is absolutely different from that under no-uplift conditions.
- The stiffness of the stiffeners has the relationship with the tank response under uplift conditions. As the stiffness of the stiffeners increases, the average response acceleration and the base shear grow larger. Meanwhile the uplift height and the sidewall displacement become smaller. In addition, the stiffness of stiffeners affects the distribution of the response acceleration and the fluid pressure on the sidewall.
- When the uplift occurs, about a 1 m (correspond to about 55% of annular plate width) of bottom plate is lifted. The thicker annular plate installed at the periphery of the tank bottom plate may cause it. It implies the necessity to take into account this phenomenon for developing the mathematical model in Chapter 5.
- Since the nominal in-plane shear stiffness of the sidewall is enough, the bottom of the sidewall seems to be rigid in the vertical direction. However, from a microscopic viewpoint, it deforms slightly in an arch shape up to the neutral axis, while it drops in the area around 0 degree (compression side).
- Liquid pressure, which acts on the uplifted tank bottom plate, is supported by the sidewall and tank bottom insulation evenly under the static loading conditions. While during the

dynamic uplift process, the amount of the load supported by the sidewall becomes larger. This point should be considered when develop the mathematical model in Chapter 5.

- The force couple of tensile and compressive side is not even in the dynamic rocking transition. During rising of the bottom plate, force couple of compressive side becomes larger than that of tensile side. On the other hand, during descending of the bottom plate, force couple of tensile side becomes larger
- The undulating deformation at the top of the sidewall was observed under the oscillating loading conditions. While under constant acceleration conditions, which emulated static loading, oval shape deformation appears at the top of the sidewall and the uplift height becomes significantly larger. From these results, it is confirmed that the tank response due to oscillating loading is fundamentally different from that of static conditions.
- The Contribution Factor, which consists of the magnitude of the base shear and the sidewall displacement, is introduced for investigating of the appearance of the uplift. Then it is confirmed that the undulating deformation at the top of the sidewall is one of the major factors of generation the uplift in the same way as oscillation force.
- The angular acceleration at the bottom of the sidewall, which is an indication pointer of the magnitude of the dynamic pressure induced by uplifting, also has a relationship with the stiffness of the stiffeners. As the stiffness of the stiffeners increases, the uplift decreases, then consequently the angular acceleration becomes smaller
- The natural periods of the tank are obtained from FFT analysis for the base shear and the sidewall displacement. The natural period under the uplift conditions shows different vibration characteristics than that of the no-uplift conditions, because unlike no-uplift conditions dominated by only 1^{st} natural period, 1^{st}, 2^{nd} and 3^{rd} natural period groups appear. Here, 1^{st} group is the natural period of the bulging mode, while 2^{nd} and 3^{rd} groups are caused by the uplift and the undulating deformation. In addition, these vibration characteristics are affected by features of the seismic waves and the stiffness of the stiffeners.

In the Chapter 4, the mathematical model (referred to as the Structural Mathematical Model) for the tank bottom plate was established, which included the uplift behavior and the influence of the sidewall deformation. In addition, this proposed mathematical model was verified by comparing with the result of non-linear beam static FE analysis and non-linear 3D static FE analysis, which was performed with the same conditions as the mathematical model. Besides parameter study by the mathematical model was performed to investigate the influence of thickness of the bottom plate and the sidewall and the elasticity of the bottom insulation on the uplift behavior.

The findings are summarized below.

- The thickness of the bottom plate and the sidewall and the elasticity of the bottom insulation

affect the uplift height. Beside the uplift width receives small influence by these variations.

- In case of thinner bottom plate, the uplift height becomes small. On the contrary, thinner sidewall, the uplift height becomes larger.
- In case of high elasticity of the bottom insulation, the uplift becomes larger.
- The variation of the sidewall thickness has the most impact to the uplift height. In the parameter study, 5% thickness variation causes about 24% uplift height difference.
- The magnitude of uplift-induced dynamic pressure is affected by the conditions of the bottom plate and the sidewall thickness and the elasticity of the bottom insulation.
- In the parameter study, 5% thickness variation of the sidewall causes about 6% difference of the overall dynamic pressure.

In the Chapter 5, the mathematical model (referred to as the Force Coupling Mathematical Model) was proposed to estimate distribution of an axial force on a bottom of a sidewall. This Model takes into account the physical phenomenon of a force couple formed by a reaction force of a tank bottom due to subsidence, resistance force against uplift due to liquid weight in uplift area and an effect of deformation at top of a sidewall. Then, a trial calculation with the same conditions as used by the FE analysis was performed to verify the applicability of the model.

The findings are summarized below.

- The differences of the result between the proposed mathematical model and between the FE analysis are 25% in uplift width, 11% in location of neutral axis, 22% in the maximum tensile axial force and 24% in the minimum compressive axial force, respectively. While, trend of the calculation result is similar to that of the FE analysis.
- One of the reason of this different is local or within short period unstable behavior of physical quantities during transient duration in dynamic analysis.
- For applying the proposed mathematical model to tank design, suitable allowance for comprising these difference is required.
- It is considered that the deformation at top of a sidewall has a close relationship with the uplift height and it is affected by a configuration of deformation sensitively.
- Further investigation and development of the model is required for the undulating deformation at the top of the sidewall for improving of calculation accuracy.
- A cosine curve is assumed to be the pressure distribution profile on the surface of the uplift area due to the bulging and rocking modes. This profile is used instead of a theoretical value to simplify the model. It had better to integrate the theoretical formula into the mathematical model for improving the calculation accuracy.

In the Chapter 6, it summarized the simplified design procedure (referred to as the Simplified Seismic Design Procedure) for determining a tank bottom plate and sidewall

connection, based on the Structural Mathematical Model and the Force Coupling Mathematical Model which are proposed in earlier chapters.

A sample calculation based on the proposed procedure was also presented.

Findings and the items suggested for future study listed as below.

- It is confirmed that the proposed Simplified Seismic Design Procedure is functional for estimating the uplift height and the width of the bottom plate with the consideration of bulging and rocking motion and specific features of response behavior.
- Setting up or adjusting several parameters, which depend on tank characteristics such as size, proportion, thickness of each part and so on, is required for using the Simplified Seismic Design Procedure effectively. Therefore, further research is essential for improving the parameters so as to apply to any size tanks. Especially, wef, which indicates the increase in reaction force at the bottom of the sidewall during dynamic oscillation loading is one of the most important factor for the model.
- Regarding Step 3, further investigation of the reduction in the response acceleration during uplift is required for improving the procedure.
- (The concept of a providing method of the reduced response acceleration by using a natural period and responses spectrum is discussed in 3-3 of Chapter 3.)
- Regarding Step 7, integrating of the theoretical formula of dynamic pressure due to bulging and rocking motion into the Force Coupling Mathematical Model is recommended for improving the procedure. At present, a cosine curve is used to approximate the dynamic pressure distribution for simplifying the mathematical model.
- Regarding Step 7, further development of the specific estimation method for calculating the maximum displacement at the top of sidewall during an earthquake is required.
- Regarding Step 8, improving the Structural Mathematical Model to asymmetric model is indicated.
- Regarding Step 6 to 8, further integration of the Structural Mathematical Model and the Forced Coupling Mathematical Model is recommended.
- Considering an effect of membrane force in the tank bottom plate due to large deformation is required for understanding the effect of that on the uplift behavior.

ACKNOWLEDGEMENT

ACKNOWLEDGEMENT

I would like to express my greatest gratitude to Professor Tomoyo Taniguchi Graduate School of Tottori University, who provided significant instruction and support, valuable opportunities for publication and presentation of the main thesis for this paper.

In summarizing this paper, Professor Takao Kagawa and Tsuyoshi Nishimura Graduate School of Tottori University gave insightful comments and suggestions through referee reading from a professional viewpoint. I would like to express my deepest appreciation.

In addition, I am deeply grateful to Mr. Daisuke Okui and Mr. Yuichi Yoshida, who extended every possible cooperation and support from a colleague researcher's viewpoint.

Finally, my heartfelt appreciation goes to Mr. Phil Woodford for his dedicated support and valuable guidance for emending the paper.

PAPERS PUBLISHED BY THE AUTHOR IN PREPARING THIS PAPER

PAPERS PUBLISHED BY THE AUTHOR IN PREPARING THIS PAPER

PAPERS

Subject:	A Study of Formularization of Uplift Behavior at the Bottom Plate of Large LNG Storage Tanks during Earthquake
Author:	Shoichiro Hayashi, Tomoyo Taniguchi
Title of academic journal:	Proc. ASME. 55089 (Volume 9: Rudy Scavuzzo Student Paper Symposium and Competition, pp. 139-148)
Publication date:	July, 15th, 2012

Subject:	A Study of Dynamic Response Behavior during Earthquake for Large LNG Storage Tanks in Consideration of Uplift
Author:	Shoichiro Hayashi, Tomoyo Taniguchi
Title of academic journal:	Proc. ASME. 55744 (Volume 8: Seismic Engineering, V008T08A034, 1-10)
Publication date:	July, 14th, 2013

PRESENTATION

Subject:	A Study of Fluid-Structure Coupled Analysis for Large LNG Storage Tanks in Consideration of Uplift
Author:	Shoichiro Hayashi, Tomoyo Taniguchi, Akira Umeda, Hisayuki Yamada, Takumi Kawasaki, Hitoshi Nagahara
Title of academic journal:	Proc. ASME. 44588 (Volume 8: Seismic Engineering, pp. 303-312)
Publication date:	July, 17th, 2011

Subject:	A Study of Formularization of Uplift Behavior at the Bottom Plate of Large LNG Storage Tanks during Earthquake
Author:	Shoichiro Hayashi, Tomoyo Taniguchi
Title of academic journal:	Proc. ASME. 55089 (Volume 9: Rudy Scavuzzo Student Paper Symposium and Competition, pp. 139-148)
Publication date:	July, 15th, 2012

Subject:	A Study of Dynamic Response Behavior during Earthquake for Large LNG Storage Tanks in Consideration of Uplift
Author:	Shoichiro Hayashi, Tomoyo Taniguchi
Title of academic journal:	Proc. ASME. 55744 (Volume 8: Seismic Engineering, V008T08A034, 1-10)
Publication date:	July, 14th, 2013

APPENDIX

APPENDIX A

APPLIED PROGRAM AND VERIFICATION OF ANALYSIS ACCURACY [1]

(1) Analysis Method

In this paper, LS-DYNA is adopted for the numerical analysis because phenomena to be dealt with contained such elements as fluid-structure coupling, time-history loading of seismic wave, and nonlinear behavior of the annular plate represented by contact between the annular part and the foundation [1].

This program is an excellent explicit FEM software capable of solving complex problems as compared to other implicit analysis programs as shown in Table A-1. However, this method should be used with careful verification of analysis accuracy. Physical values of each time step are calculated from the values of previous time step, and this implies a possibility of accumulation of numerical errors. In addition, proper modeling of the fluid and accurate estimation of fluid pressure on the structure are very important especially in handling the fluid-structure coupled problems because these two factors influence the behavior of the structure significantly.

The penalty-coupling method was adopted for the fluid-structure interface of the numerical model where the coupling force was applied in accordance with the relative displacement between the fluid and structure elements.

In this study pre-analysis was conducted to trace the following previous experiments for the verification of the numerical analysis by comparison between the analytical and experimental results.

(a) Static tilt test by large-scale tank model [2]
(b) Dynamic shaking test by scale tank model [3]

The following methods were available for modeling the fluid:

- Lagrange method using solid elements;
- Arbitrary Lagrangian Eulerian (ALE) method using Euler elements in which the analysis space is divided into meshes and fluid properties are applied to the fluid area nodes; and
- Smoothed Particle Hydrodynamics (SPH) method which uses elements consisting only of nodes and does not require a mesh.

Test analysis was carried out using each method, and the ALE method was chosen for its satisfactory result.

TABLE A-1: SUMMARY OF FUNCTIONS OF NUMERICAL ANALYSIS PROGRAMS FOR FLUID ELEMENT [4]

'○' : Applicable, '—' : Not applicable, ' ' : unconfirmed

	Program name	Solution		Analysis field		coupling function			Fluid analysis function						Buckling analysis (plastic large deformation)	Sloshing analysis	Note
		Explicit	Implicit	Structure	Fluid	Virtual mass	Weak couple (staggered)	Strong couple	Analysis method			Type of fluid		Free surface			
									FEM	FDM (FVM)	SPH	Incompressive	Compressive	ALE	Euler (VOF etc.)		
1	MSC/DYTRAN	—	○	○	○	—	○	—	—	○	—	—	○	○	○	○	○	Applicable for large deformation plastic analysis. Many experiences of fluid-structural analysis exist in KHI.
2	LS-DYNA	—	○	○	○	—	○	—	○	—	△*1	△*2	○	○	○	○	○	Applicable for large deformation plastic analysis. Many experiences of non-linear structural and collision analysis of automobile exist in KHI. Fluid analysis with free surface is unstable.
3	RADIOSS RADIOSS/ALE RADIOSS/CFD	—	○	○	○	—	○	—	—	○	—	—	○	○	○	○	○	Applicable for large deformation plastic analysis.
4	PAM-CRASH PAM-FLOW	—	○	○	○	—	○	—	○	—	○	○	○	○	—	○	(SPH used)	Applicable for large deformation plastic analysis. Applicable for non-linear sloshing analysis by SPH.
5	AUTODYN-2D&3D	—	○	○	○	—	○	—	○	○	○	—	○	○	○	○	○	Suitable for high-speed collision analysis.
6	ABAQUS/Explicit	—	○	○	○	—	○	—	○	—	—		○	○	—	○	—	Applicable for large deformation plastic analysis. Applicable within linear sloshing analysis.
7	MSC/NASTRAN	○	—	○	△*3	○	—	○	○	—	—	△*5	○	—	—	—	—	Mainly used to linear analysis. Applicable for eigenvalue analysis to obtain mode of linear sloshing.
8	MARC	○	○	○	△*3	○	—	○	○	—	—	△*5	○	—	—	◎	—	Applicable for large deformation plastic analysis. High reliability in buckling analysis.
9	ABAQUS/Standard	○	—	○	△*3		—	○	○	—	—	—	○	—	—	◎	—	Applicable for large deformation plastic analysis. High reliability in buckling analysis.
10	FINAS	○	—	○	△*3		—	○	○	—	—	○		—	—	◎	—	Applicable for large deformation plastic analysis. High reliability in buckling analysis.
11	ADINA ADINA-F	○	—	○	○	—	○	○	○	—	—	○	○	○	—	○	○	Applicable for large deformation plastic analysis. Applicable within linear sloshing analysis.
12	ANSYS FLOTRAN	○	—	○	○	—	○	—	○	—	—	○	○	○	○	○	○	Applicable for large deformation plastic analysis.
14	FIDAP	○	△	△*4	○	—	○	—	○	—	—	○	○	○	○	—	○	Applicable within elastic condition in structural analysis.
15	Flow-3D	—	○	—	○	—	—	—	—	○	—	○	○	—	○	—	◎	Empirically proven program in fluid analysis with free surface.
16	STREAM	—	○	—	○	—	—	—	—	○	—	○	○	—	○	—	○	Fluid analysis with free surface is unstable.
17	STAR-CD	—	○	—	○	—	△*6	—	—	○	—	○	○	—	○	—	○	Interface function is equipped for coupling to structural analysis.

Virtual mass method : Method to consider an effect of fluid on structure by introducing virtual mass assumption.
Weak coupling : Solving method by performing independent structure analysis and fluid analysis alternately.
Strong coupling : Solving method by using fluid-structure coupling governing equations.
FEM : Finite element method
FDM : Finite difference method
FVM : Finite volume method
VOF : VOF (Volume of Fluid) method
SPH : Analysis method for incompressive fluid based on particle hydrodynamics.

There are two options for modeling of free surface of fluid (moving boundary).
(a) ALE method : Applying moving elements for expressing free surface.
(b) VOF method, MARS method : Moving substance within Euler element.

Method (a) is impossible to solve non-linear sloshing with wave breaking.
Method (b) have a capability to solve non-linear sloshing.
Method (a) solves impulsive pressure induced by colliding fluid with tank roof more accurately.

*1 : Applicable in next version.
*2 : Coupling to structure is not applicable in present version.
*3 : Fluid element which expresses a relationship of density variation and pressure.
*4 : Applicable only for elastic analysis with solid element.
*5 : in virtual mass method, incompressive potential flow is assumed.
*6 : Interface function is equipped for handover physical quantities to structural analysis.

(2) Verification against Experimental Results

(a) Comparison with Tilt Test Results

A large-scale tilt test had been carried out in 1985 [2] to investigate the uplift behavior of a cylindrical tank as shown in Figure A-1. This test was traced numerically in this study, using the same objects and conditions for the verification of the numerical model shown in Figure A-2 as well as calculation accuracy of the analysis program used.

Outline of the scale model

Diameter:	9,600 mm
Height:	8,000 mm
Contents:	Water
Materials	
Sidewall:	Aluminum, 5 mm
Bottom plate:	Aluminum, 3 mm
Tilt angle:	9°

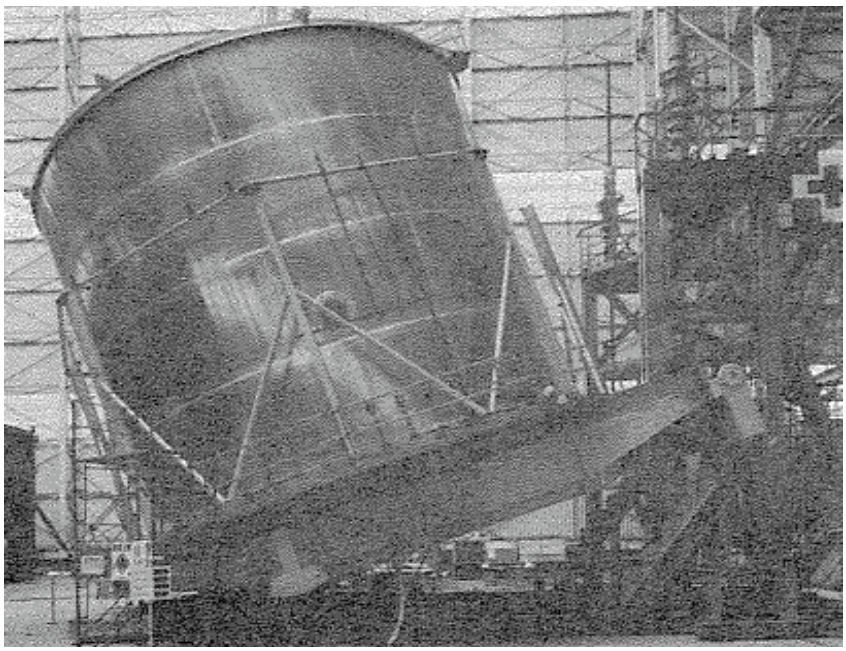

FIGURE A-1: VIEW OF STATIC TILT TEST USING LARGE-SCALE TANK MODEL

Numerical model

Structure elements	
Tank:	Shell element
Foundation:	Solid element
Fluid element:	Euler element

Bottom plate - foundation: Contact element (Coefficient of friction: 0.5)

Properties

Tank

Modulus of elasticity: 70,000 MPa

Poisson's ratio: 0.3

Density: 2,700 kg/m^3

Fluid

Modulus of elasticity: 2,060 MPa

Viscosity: 0

Fluid density: 1,000 kg/m^3

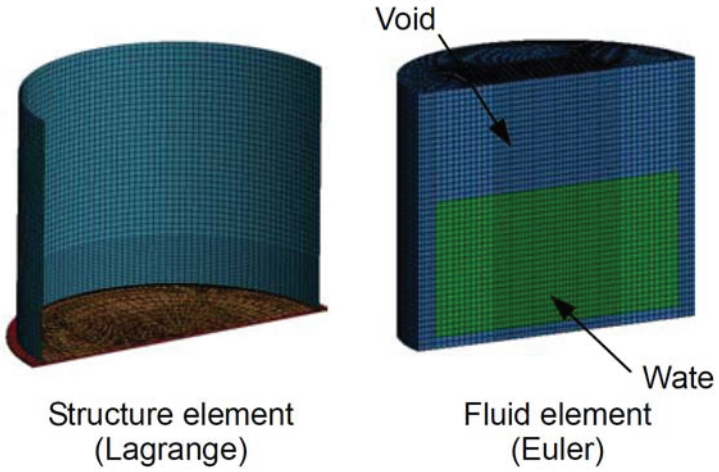

FIGURE A-2: NUMERICAL MODEL FOR VERIFICATION

Table A-2 shows the results of the analysis and the experiment. The analytical fluid pressure values were nearly equal to the tilt test values, and both the height and the width (in the radius direction) of uplift induced by the pressure resulted in similar values between the analysis and the experiment.

TABLE A-2: RESULTS OF FEM ANALYSIS AND TILT TEST

		FEM analysis	Tilt test
Pressure (MPaG)	Uplift side	0.051	0.051
	Compression side	0.038	0.037
Uplift height (mm)		37	41
Width of uplift (mm)		460	500

(a) Comparison with Dynamic Shaking Test Results

The other verification analysis was performed by tracing a horizontal shaking test which was carried out in 1979 [3] to investigate fluid-elastic vibration (so-called bulging) phenomena.

Outline of the scale model

Diameter:	1,000 mm
Height:	1,000 mm
Contents:	Water
Materials	
Sidewall:	Vinyl chloride, 1.5 mm
Bottom plate:	Vinyl chloride, 1.5 mm

Numerical model

Structure and fluid elements:	Same as the tilt test model
Properties	
Tank	
Modulus of elasticity:	3,236 MPa
Poisson's ratio:	0.3
Density:	1,410 kg/m^3
Fluid	
Modulus of elasticity:	2,060 MPa
Viscosity:	0
Fluid density:	1,000 kg/m^3
Acceleration amplitude:	0.1 G, 20 Hz

Figure A-3 compares the verification distributions of total pressure consisting of static and dynamic pressures obtained by the analysis against the measurement results from the experiment.

The analytical results were in good agreement with the experimental data in both pressure distribution along the side wall and pressure values.

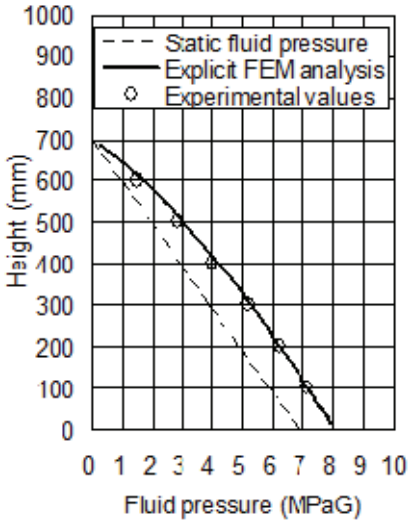

FIGURE A-3: RESULTS OF ANALYSIS AND SHAKING TEST

The above verifications (1) and (2) confirmed that calculation by LS-DYNA using an Euler element for the fluid component and a numerical model coupled by the penalty-based method would ensure sufficient accuracy in dynamic pressure induced by harmonic excitation as well as static pressure.

REFERENCES

[1] Hayashi, S. and Taniguchi, T., et al., 2011, “A Study of Fluid-Structure Coupled Analysis for Large LNG Storage Tanks in Consideration of Uplift”, Proceedings of ASME PVP Conference, PVP2011-57925.

[2] Isoe, A., 1994, “Investigation on the Uplift and Slip Behavior of Flat-Bottom Cylindrical Shell Tank during Earthquake”, Dr. Eng. Thesis, University of Tokyo. (in Japanese)

[3] Sakai, F., Sakoda, H. and Ogawa, H., 1979, “Seismic Design of Oil Storage Tanks Related with the Proposal of American Petroleum Institute”, Kawasaki Heavy Industries Technical Review, No. 71, pp. 52-59. (in Japanese)

[4] 林　尚一郎, 梅田　聡, 山田　久之, 2010, タンクアニュラ部の浮上りを考慮した連成解析技術の確立, 川崎重工業株式会社, 研究開発報告書

APPENDIX B

DERIVATION OF THE BEARING BEAM EQUATION WITH LIMITED RANGE DISTRIBUTION LOAD

In general, the displacement *v* of infinite length elastic bearing beam with concentrated load *P* is given form the general equation and following boundary conditions.

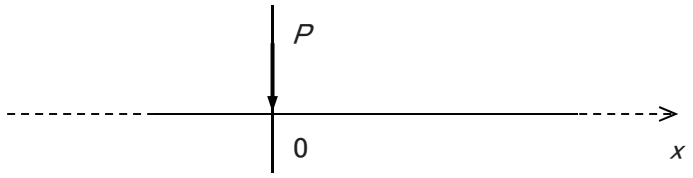

FIGURE B-1: MODELING OF INFINITE LENGTH ELASTIC BEARING BEAM WITH CONCENTRATED LOAD

$$\frac{d^4v}{dx^4} + 4\beta^4 \times v = 0 \tag{B-1}$$

$$\beta = \sqrt[4]{\frac{k}{4EI}} \tag{B-2}$$

$$v_s = 0 \quad (x = \infty) \tag{B-3}$$

$$\frac{dv_s}{dx} = 0 \quad (x = \infty) \tag{B-4}$$

$$\frac{dv_s}{dx} = 0 \quad (x = 0) \tag{B-5}$$

$$EI\frac{d^3v_s}{dx^3} = -\frac{P}{2} \quad (x = 0) \tag{B-6}$$

Where,

P: Concentrated load

v: Displacement of infinite length elastic bearing beam

k: Reaction of the elastic bearing per unit length

E: Modulus of elasticity of beam

I: Momentum of inertia for rectangular cross section beam

The solution and the derived functions are led as;

$$v = \frac{P\beta}{2k} \times e^{-\beta x}\left(\cos \beta x + \sin \beta x\right) \tag{B-7}$$

$$\frac{dv}{dx} = -\frac{P\beta^2}{k} \times e^{-\beta x}\left(\sin \beta x\right) \tag{B-8}$$

$$\frac{d^2v}{dx^2} = \frac{P}{4\beta EI} \times e^{-\beta x}\left(\sin \beta x - \cos \beta x\right) \tag{B-9}$$

$$\frac{d^4v}{dx^4} = \frac{P}{2EI} \times e^{-\beta x}\left(\cos \beta x\right) \tag{B-10}$$

For considering distribution load with the value of p_γ at start point and increasing ratio p_α, replace P to minute section dx as follows.

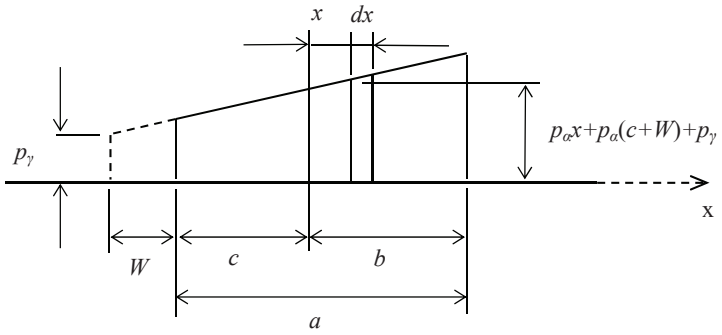

FIGURE B-2: MODELING OF PRESSURE ON THE BOTTOM PLATE FOR SUPPORTED PART

$$P \Rightarrow \left[p_\alpha \times x + p_\alpha\left(c + W\right) + p_\gamma\right] \times dx \tag{B-11}$$

The displacement of the beam with the distribution load within “a” is expressed as;

$$\begin{aligned} v = \int_0^b & \frac{\left[p_\alpha \times x + p_\alpha\left(c + W\right) + p_\gamma\right] \times \beta}{2k} \times e^{-\beta x}\left(\cos \beta x + \sin \beta x\right) dx \\ & + \int_0^c \frac{\left[p_\alpha \times x + p_\alpha\left(c + W\right) + p_\gamma\right] \times \beta}{2k} \times e^{-\beta x}\left(\cos \beta x + \sin \beta x\right) dx \end{aligned} \tag{B-12}$$

The solution of Eq. (B-11) becomes;

$$
\begin{aligned}
v = \frac{\beta}{2k} \times \Bigg[\Bigg[& \frac{\left\{ p_\alpha b + p_\alpha (c+W) + p_\gamma \right\} \times e^{-\beta b} \times (-2\cos \beta b)}{2\beta} \\
& + \frac{\left\{ p_\alpha (c+W) + p_\gamma \right\}}{\beta} + \frac{p_\alpha \times \left\{ e^{-\beta b} \times (\sin \beta b - \cos \beta b) + 1 \right\}}{2\beta^2} \Bigg] \\
& + \Bigg[\frac{\left\{ p_\alpha c + p_\alpha (c+W) + p_\gamma \right\} \times e^{-\beta c} \times (-2\cos \beta c)}{2\beta} \\
& + \frac{\left\{ p_\alpha (c+W) + p_\gamma \right\}}{\beta} + \frac{p_\alpha \times \left\{ e^{-\beta c} \times (\sin \beta c - \cos \beta c) + 1 \right\}}{2\beta^2} \Bigg] \Bigg]
\end{aligned}
\tag{B-13}
$$

Replacing "$a \rightarrow 2R$", "$c \rightarrow x_2$" and "$b \rightarrow 2R\text{-}x_2$", equation of v with distribution load within $2R$ along x_2 axis is obtained. Applying the same method, derived functions are also given.

APPENDIX C

COMPARISON OF CALCULATION RESULT BETWEEN OKUI'S MODEL AND THE FE ANALYSIS

Table C-1 shows a summary of the FE analysis for Case 21 in Chapter 3.

Table C-2 shows the comparison of the calculated values using Okui's model [1] and that of the FE analysis. The results of the calculated angular acceleration are in agreement within an acceptable level. However, for translational response acceleration and base shear, considerable differences are identified. In the FE analysis, response acceleration and base shear of uplift case (Case 21) are about 50-55 % of that of the 'no uplift' case (Case 11).

Okui's model demonstrates that there is a small reduction in the response acceleration and in the maximum base shear between the 'no-uplift' case and the 'uplift' case.

However, the FE analysis provides a larger reduction than the Okui's model.

TABLE C-1: RESPONSE OF THE TANK IN CASE OF NO UPLIFT AND DUPLIT

		Case 11	Case 21				
			7.4 sec	12.5 sec	13.1 sec	19.6 sec	21.5 sec
Response accel. of side wall	(G)	0.4655			0.2469		
Rate compared to the no uplift case	(Case11)	1.000			0.530		
Base shear	(MN)	161.9			87.9		
Rate compared to the no uplift case	(Case11)	1.000			0.543		
Uplift height	(mm)	---	5.6	1.1	21.6	11.4	8.1
Uplift width	(mm)	---	1400	1350	1450	1450	1400
Rate compared to Diameter	(%)		1.88	1.81	1.95	1.95	1.88
Angular acceleration	(rad/s^2)	---	-0.010	-0.003	-0.041	-0.024	-0.018

TABLE C-2: RESPONSE OF THE TANK USING OKUI'S MODEL

		FE analysis (Case21)	Okui' model (Case2)	
Horizontal acceleration of tank	(G)	0.4094	0.4183	
Natural period of tank	(sec)	0.4740	0.4980	
Response acceleration	(G)	0.2469	0.4088	0.4109
	(m/s^2)	2.4213	4.009	4.030
Maximum base shear	(MN)	87.9	151.8	155.8
Maximum Uplift height	(mm)	21.6	16.2	15.8
Uplift width	(mm)	1450	774	1548
	(%)	1.9%	1%	2%
Maximum angular acceleration Max.	(rad/s^2)	0.0286	0.0490	0.0480
Min.	(rad/s^2)	-0.041		

REFERENCES

[1] 奥井大輔, 2013.2.8, "応答スペクトルを用いた平底円筒貯槽の底板浮き上がり現象を特徴付ける物理量の簡易算定方法に関する検討", 鳥取大学大学院工学研究科博士前期課程　社会基盤工学専攻土木工学コース　修士論文, p.39.

NOMENCLATURE

NOMENCLATURE

a: Length of bottom plate on elastic foundation

a_{pd} : Coefficient for optimization of the model

C: Compressive axial force per unit width

C_1: 1st component of C

C_2: 2nd component of C

C_f : Total of the compressive force

D: Tank diameter

d_r: Coefficient for a supplemental bulge shape of subsidence of bottom plate

d_u: Coefficient expressing a ratio of uplift with against uplift height

E: Modulus of elasticity of steel

E_s: Modulus of elasticity of the sidewall

f_r,: Ratio of force couple of tensile side against total of force couple

g: Gravity acceleration

H: Tank height

h: Liquid height

I: Momentum of inertia for rectangular cross section beam

k: Reaction coefficient of tank bottom

L: Length from neutral axis to sidewall

l: Circular length of subsidence

M: Over turning moment

M_0: Moment of the bottom plate at the sidewall side

M_1: Moment at interface of beams

M_{x3}, M_θ: Moment at the sidewall

N_{x3}, N_θ: Membrane force at the sidewall

P_0: Static pressure

P_d: Dynamic pressure on the bottom plate

$P_{db}(\theta_b = 180)$: Dynamic pressure at 180 degrees due to bulging mode

$P_{dr}(\theta_b = 180)$: Dynamic pressure at 180 degrees due to rocking mode

P_{ds1}, P_{ds2}: Dynamic pressure on the sidewall

P_T : Liquid pressure consists of static and dynamic pressure

Q_{x3}, Q_θ: Shear force at the sidewall

$q(x_1)$, $q(x_2)$: Liquid pressure on the bottom plate along x_1, x_2 axis

R: Tank radius

r: Distance from the tank center

r_{ef}: Reduction factor for response acceleration under uplift condition against that of no-uplift condition

S: Subsidence depth at 0 degree

S_r: Distance from the meet point of extensions of the sidewall at 0 and 180 degrees to the bottom plate

T: Tensile axial force per unit width at 180 degrees

T_1: Component of T due to static liquid pressure act on the crescent shaped area

T_2: Component of T due to static liquid pressure act on the annular shaped area

T_{d1}: Component of T due to dynamic liquid pressure act on the crescent shaped area

T_{d2}: Component of T due to dynamic liquid pressure act on the annular shaped area

T_f: Total of tensile force

t_b: Thickness of the bottom plate (annular plate)

t_s: Thickness of bottom of the sidewall

t_{sa}: Average thickness of top and bottom of the sidewall

U: Uplift height at 180 degree

u'_0: Horizontal acceleration

V_0: Force of the bottom plate at the sidewall side

V_1: Force at interface of beams

v_1: Displacement of the bottom plate at uplift part

v_2: Displacement of the bottom plate at supported part

v_3: Bulging displacement of the sidewall

$v(\pi)$: Uplift height of bottom plate due to horizontal displacement of the top of the sidewall at 180 degrees

W: Uplift width of bottom plate

W': Assumed uplift width of bottom plate

W_0: Fundamental uplift width

W_a: Width of the bottom plate effected by annular plate

W_b: Width of the annular plate

w: Effective width of bottom plate

w_b: Unit width of bottom plate

w_{ef}: Coefficient expressing of increase in axial force at the bottom of sidewall

α: Angle indicating location of neutral axis

γ: Force couple of compressive side

γ_1: 1st component of γ

γ_2: 2nd component of γ

δ: Horizontal displacement (difference in diameter from complete round) of the top of the side wall

ε: Strain of circumferential direction of the sidewall

θ_b: Angle from 0 degree to each point of the sidewall

θ_t: Angle from the sidewall at 0 degree to each point of bottom plate

ξ: Angle at the point of intersection of a line drawn as an extension to the sidewall at 180 degrees and a line drawn as an extension of the sidewall at 0 degree

ρ: Fluid density

τ: Force couple of tensile side

τ_1: Component of τ due to liquid pressure act on the crescent shaped area

τ_2: Component of τ due to liquid pressure act on the annular shaped area

ϕ : Angle from acceleration direction

Design procedure quoted in API620 Appendix L (Chapter 1) [1]

D : Diameter of the tank

M : Overturning moment applied to the bottom of the tank shell

W_L : Maximum weight of the tank contents that may be utilized to resist the shell overturning moment

t_b : Thickness of bottom plate under the shell

F_{by} : Minimum specified yield strength of the bottom plate under the shell

G : Design specific gravity of the product to be stored, as specified by the Purchaser.

H : Maximum design product height

b : Maximum longitudinal shell compressive force of shell circumference.

W_t : Weight of the tank shell and the portion of the fixed roof and insulation, if any, supported by the shell of shell circumference.

Design procedure quoted in Eurocode 8 (Chapter 1) [2]

R : Radius of the tank

s : Thickness of the base plate

E : Modulus of elasticity of tank material

p : Pressure on the base

μ : $1\text{-}L/(2R)$

L : Uplifted part of the base

Clough Model (Chapter 2) [3]

R :	Radius of container
r :	Radius of portion remains in contact
h :	Height of F
F :	Effective lateral seismic force
W :	Total weight of shell and contents
W_s :	Reaction at the point of contact between shell and foundation
W_f :	Weight of contents within r
f_{max} :	Peak compressive shell force
k :	Dimensionless constant

Wozniak, Mitchell Model (Chapter 2) [1]

N_{umax}:	The maximum tensile force
N_{cmax}:	The maximum compressive force
β:	The start point of uplifting

Taniguchi, Segawa Model (Chapter 3, 4) [4]

p:	Dynamic pressure
ρ:	Fluid density
$\ddot{\theta}_0$:	Angular acceleration of the sidewall
$2l$:	Tank length (= diameter)
a:	Start point of uplift
h:	Tank height

Beam and Plate model general formula (Chapter 4) [5]

p:	Uniformed distribution load
L_{beam}:	Half length of beam
a:	Radius of ring
b:	Radius of inner edge guide
$\delta_{beam\text{-}Max}$:	Maximum displacement of beam
$\delta_{plate\text{-}Max}$:	Maximum displacement of plate

E_{beam}: Modulus of elasticity of beam
E_{plate}: Modulus of elasticity of ring
v: Poisson's ratio
W_{beam}: Width of beam
t_{br}: Thickness of beam and ring

APPENDIX B

P: Concentrated load
v: Displacement of infinite length elastic bearing beam
k: Reaction of the elastic bearing per unit length
E: Modulus of elasticity of beam
I: Momentum of inertia for rectangular cross section beam

REFERENCES

[1] Wozniak, R. S. and Mitchell, W. W., 1978, "Basis of Seismic Design Provisions for Welded Steel Oil Storage Tanks", API Refining Dept. 43rd Midyear Meeting, Toronto.

[2] Cambra F.J., 1982, "Earthquake response considerations of broad liquid storage tanks" Report EERC 82/25.

[3] Clough, D. P., 1977, "Experimental Evaluation of Seismic Design Methods for Broad Cylindrical Tanks", Univ. of California, EERC Rep., No. UCB/EERC-77/10.

[4] Taniguchi, T. and Segawa, T., 2008, "Fluid Pressure on Rectangular Tank Consisting of Rigid Side Walls and Rectilinearly Deforming Bottom Plate Due to Uplift Motion", PVP2008-61166.

[5] Warren C. Young, 1989, "ROARK'S Formulas for stress & Strain 6th edition", McGraw-Hill Book Company.